KINETICS AND DIFFUSION IN HYDRODEMETALLATION OF NICKEL AND VANADIUM PORPHYRINS

by

RAKESH AGRAWAL

B. Tech., Indian Institute of Technology, Kanpur, INDIA (1975)

M.Ch.E., University of Delaware (1977)

Submitted in partial fulfillment of the
requirements for the degree of
Doctor of Science

at the

Massachusetts Institute of Technology

August, 1980

Signature of Author _____
Department of Chemical Engineering

Certified by _____
Prof. James Wei, Thesis Supervisor

Accepted by _____
Prof. G.C. Williams, Chairman,
Departmental Committee on
Graduate Thesis

KINETICS AND DIFFUSION IN HYDRODEMETALLATION OF NICKEL AND VANADIUM PORPHYRINS

by

RAKESH AGRAWAL

Submitted to the Department of Chemical Engineering on August 5, 1980, in partial fulfillment of the requirements for the Degree of Doctor of Science.

ABSTRACT

Experimental and theoretical studies were performed on the hydrodemetallation of the Nickel (II) and Vanadyl (IV) Etioporphyrin-I in the $CoO-MoO_3/Al_2O_3$ catalyst, with and without the intraparticle transport limitations. The experiments were conducted in a unique high pressure liquid phase flow reactor at the temperatures of 288 to 345°C and hydrogen pressures of 4.1 to 9.7 MPa.

In the initial transient phase of the reaction, the activity of the catalyst first decreases, then increases and finally levels off. The increase in both the hydrogenation and demetallation activities can be attributed to the nickel and vanadium deposition on the catalyst. In this study the maximum metal deposited on the catalyst in any single run was about 10 wt %. Once the catalyst has achieved its steady state activity, it is maintained for the rest of the run time. Therefore, up to 10 wt % metal loading, there is no significant pore blockage.

In the hydrodemetallation of both the metals, three major kinetic steps are involved. The first step is hydrogenation to the reaction intermediate with a first order dependence on the metal etioporphyrin concentration in the solution. The other two steps are dehydrogenation and demetallation of the reaction intermediate, both with first order dependence on he reaction intermediate concentration in the solution. The order of dependence of hydrogenation, dehydrogenation and demetallation rates on the hydrogen pressure are first, zero and second respectively. The activation energies for the hydrogenation, dehydrogenation and demetallation rate constants in case of nickel etioporphyrin-I are 17.1, 22.9 and 32.6 and for vanadyl etioporphyrin-I are 18.3, 16.5 and 24.9 Kcal/g mole respectively. The reaction intermediate for the

nickel etio runs has been isolated and identified to be nickel etio-chlorin.

Metal deposition profiles in 1/16 inch catalyst extrudates, at various reactor bed positions, have been studied. At the entrance of the bed, the maximum in the metal deposition occurs inside the catalyst, so that the metal deposition profiles look like the letter M. In the middle and the exit sections of the bed, the maxima moved to the external surface, and the metal deposition profiles look like the classical U-shaped profiles.

These metal profiles have been successfully simulated by theoretical modelling. It is calculated that both the nickel and vanadyl etioporphyrins and their reaction intermediates have diffusivities of the order of 10^{-6} cm^2/sec. For nickel, both the etio and chlorin have the same diffusivities. For vanadium, depending on the temperature of the operation, the reaction intermediate has 3 to 5 times higher diffusivity than the vanadyl etioporphyrin.

New poisoning models to predict the initial and the long range activity of the unimodal and bimodal catalysts have been proposed. The calculation results show that for hydrodemetallation, bimodal catalyst pellets have much better performance: a higher initial rate, as well as much higher catalyst life time. The bimodal catalyst can tolerate many times more metal loading than the unimodal catalysts without significant activity decline.

Thesis Supervisor:

James Wei
Professor of Chemical Engineering

Department of Chemical Engineering
Massachusetts Institute of Technology
Cambridge, Massachusetts 02139

August 1980

Professor George C. Newton, Jr.
Secretary of the Faculty
Massachusetts Institute of Technology
Cambridge, Massachusetts 02139

Dear Professor Newton,

In accordance with the regulations of the Faculty, I herewith submit a thesis, entitled "Kinetics and Diffusion in Hydrodemetallation of Nickel and Vanadium Porphyrins", in partial fulfillment of the requirements for the degree of Doctor of Science in Chemical Engineering at the Massachusetts Institute of Technology.

Respectfully Submitted

RAKESH AGRAWAL

To the Memory

of

My Brother

RAJIV 'PANKAJ' AGRAWAL

ACKNOWLEDGEMENTS

First, I want to thank my thesis advisor, Prof. James Wei, for his support and especially for the freedom given to me during the course of this investigation.

Special thanks are due to Prof. Stanley I. Sandler, of the University of Delaware, for his continued interest and moral support during my stay in the United States.

Thanks are also due to Prof. Peter Hambright of Howard University for helping out with most of the chemistry of the metalloporphyrins.

I cannot but thank all my colleagues at the University of Delaware, who not only helped me in the early part of this project but have maintained the relationship since I left that place. Specially, I would like to mention Drs. S.M. Bhavaraju, M.V. Bhinde, C.A. Cooper and K.M. Gupte.

I wish to thank my doctoral colleagues S. Gültekin and G. Huff at M.I.T.

There are two people who assisted with the preparation of this thesis. Cathy Stacy, with the excellent typing of the manuscript, made the final stage of this work much easier than expected. Stan Mitchell did a wonderful job with many of the figures.

I would like to specially thank my friend Rajan S. Bawa for sharing rooms, meals and thoughts for the last two years. I wish him luck in his future endeavours and hope we remain close.

I am deeply indebted to my friend Raymond R. Cwiklinski for his friendship. The stimulating and the brain-storming three o'clock coffee sessions with him will always be remembered. I am looking forward to a lifelong friendship with him. I wish him all the success in life.

I wish to express my appreciation to my wife, Manju, for waiting patiently for me to finish this thesis. I am looking forward to much happiness together. I thank my father, Shri G. L. Agarwal, my mother, Mrs. Bimla Agarwal and my sister, Ranjana Agrawal, for their love, encouragement, patience and understanding through all these years. Their stimulation and support have helped make this long educational process both possible and enjoyable.

I would like to dedicate this work to the memory of my brother, Rajiv Agrawal, to whom we called 'Pankaj' with love. His memory and whatever we shared and did together for twenty three years will always be a source of inspiration for me.

TABLE OF CONTENTS

TABLE OF CONTENTS (continued)

TABLE OF CONTENTS (continued)

TABLE OF CONTENTS (continued)

LIST OF FIGURES

LIST OF FIGURES (continued)

LIST OF FIGURES (continued)

LIST OF FIGURES (continued)

LIST OF FIGURES (continued)

LIST OF FIGURES (continued)

LIST OF FIGURES (continued)

LIST OF FIGURES (continued)

LIST OF FIGURES (continued)

LIST OF FIGURES (continued)

LIST OF TABLES

LIST OF TABLES (continued)

CHAPTER - I

SUMMARY

A. General Background: In a typical refinery, one of the first steps in the refining of the crude petroleum is distillation into various fractions (Nelson, 1974). The bottom fraction of the fractionation column, also known as residuum, contains a high proportion of sulfur, nitrogen and metal compounds found in the original crude. As heavier crude oils have to be refined to satisfy the demand for transportation fuels, hydrogen processing of these high molecular weight residues has greatly increased to form gasoline and diesel fuels.

In the crude oils, nearly one half of the elements in the periodic table have been identified as trace elements (Smith et al. - 1959). Of these, the most abundant and problematic metals are vanadium and nickel. Depending on the origin of the crude, the concentration of vanadium may vary from 8 part per million by weight to 1200 ppm, while that of nickel from 4 ppm to 100 ppm. For most of the crudes, vanadium is present in larger quantities than nickel.

In a refinery, the major problems caused by vanadium and nickel compounds are in the hydrodesulfurization and the fluid catalytic cracking units. The most common catalyst for hydrodesulfurization (HDS) is cobalt-molybdenum oxide catalyst, which deteriorates rapidly in the presence

of large V and Ni compounds in the feed (Nelson - 1976). These metal compounds deposit on and deactivate the catalysts, which have to be replaced. The quantity of vanadium loading on the deactivated HDS catalyst varies from 15% - 30% by weight (Hastings et al. - 1975). In the fluid catalytic cracking unit, these metal contaminants change the activity-selectivity rating of the unit's catalyst inventory.

In the recent past, a number of pretreatment processes to remove these metal compounds from the crude residuum have been developed. In almost all the processes developed, the demetallized residuum still has roughly 30 ppm - 100 ppm metal concentration. These metals still poison the HDS catalysts. Thus there has been a strong motivation for the studies on the hydrodemetallation (HDM).

B. LITERATURE REVIEW:

B.1. NATURE OF NICKEL AND VANADIUM COMPOUNDS IN PETROLEUM:

The metals in the crude oil are separated in three fractions: porphyrins, maltenes or resins, and asphaltenes (Dickie et al. - 1968, Filby - 1973). Asphaltenes and resins are known to contain porphyrins as well as non-porphyrin type of metal compounds. Larsen and Beuther (1966) have speculated that the nonporphyrin metals may be similar to metalloporphyrins. Sugihara et al. (1970) and Yen (1975) have concluded that the two most important types of metalloporphyrins found in petroleum are

Deoxophylloerythroetioporphyrin (DPEP) and Etioporphyrin (Etio). As the age of petroleum increases, the petroporphyrin evolve from DPEP to Etio. Saraceno et al. (1961) have pointed out that all the vanadium in crude oil appears in the Vanadyl (+4) state and nickel exclusively in the +2 valence state. In our study we have used Ni-Etioporphyrin (I) and Vanadyl-Etioporphyrin (I) as the model metal compounds, and their structures are shown in fig. I-1.

B.2. KINETICS OF HYDRODEMETALLATION (HDM): Various investigators have studied the kinetics of the metal removal from the major crude oils, in the presence of hydrogen and over typical HDS catalysts which are cobalt oxides and molebdenum oxides ($CoO-MoO_3$) supported on alumina (Al_2O_3). Most of the studies have been done in downflow, cocurrent hydrogen and feed flow, trickle bed reactors.

In the literature, with respect to the total metal concentration in the crude oil, second order (Beuther and Schmid - 1963, Oleck and Sherry - 1977) and first order (Larson and Beuther - 1966, Chang and Silvestri - 1976, Riley - 1978) HDM kinetics have been reported. Cecil et al. (1968) have pointed out that if the total metals content could be considered as constituting of two major fractions reacting with greatly different rates, each following first order kinetics, then the total metal disappearance would look like a second order kinetics.

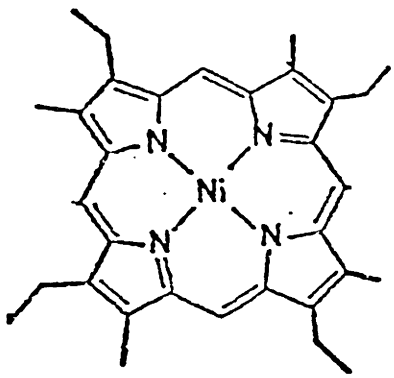

Ni-Etio (I)

$C_{32}N_4H_{36}Ni$
M.W.=535.38

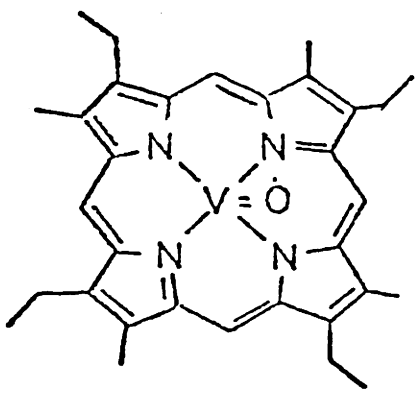

VO-Etio (I)

$C_{32}N_4H_{36}VO$
M.W.= 543.61

^ Ethyl Group
— Methyl Group

Fig. I-1 : Structures of Nickel Etioporphyrin (I) and Vanadyl-Etioporphyrin (I).

Since metal in the crude oil can be divided in porphyrinic and nonporphyrinic metals with wide difference in the reactivity, this hypothesis seems to be a plausible explanation for the observed first and second order HDM kinetics by the various investigators.

However, Van Dongen (1979) speculated that the probable order of the individual vanadium bearing species should be less than 1.0. Indeed, Hung (1979) in his batch autoclave studies of pure nickel and Vanadyl porphyrins observed the fractional order kinetics. The value of the fractional order centered at 0.5 and varied with temperature and pressure of the operation. One of the objectives of this thesis is to remeasure the kinetics in the continuous flow reactor and to explain the observed first and the fractional order HDM kinetics.

B.3. CATALYST DEACTIVATION: Almost every researcher has found that a typical catalyst, in a HDS reactor, deactivates in two steps - first a rapid decline in activity due to coke formation, and then is a slow decline in activity due to metals deposition. It has been reported that with in a short time, carbon attains an equilibrium level of about 10% - 20% by weight on the catalyst (Chang and Silvestri - 1976, Dautzenberg et al. - 1978, Inoguchi et al. - 1971C, and Kwan and Sato - 1970). Unlike coke deposition, metals deposition do not reach a plateau, and the total amounts deposited depend on the duration of the

run and the feed conditions. Oxenreiter et al. (1972) reported the amount of deposited vanadium to be as high as 56 wt% and Nickel 17 wt%. It has been proposed that the pore mouth plugging is the major cause in limiting the total catalyst life (Dautzenberg et al. - 1978, Kwan and Sato - 1970, and Oxenreiter et al. - 1972).

Another important observation is the distribution of the metals profile inside the catalysts at various bed locations. Recent results of Tamm et al. (1979) are plotted in figure I-2. Ni and V depositions show internal maxima at the reactor inlet, and this maxima move to the edge at the reactor outlet. The internal maxima in the metals deposition has also been observed by Audibert and Duhaut (1970), Hardin et al. (1978) and Oxenreiter et al. (1972). There is no explanation for these internal maxima in the metal deposition profiles, and the influence of the location of the catalyst in the beds. Indeed, there is not even any speculation in the literature. One of the objectives of this thesis is to address this question.

B.4. EFFECT OF PORE SIZE DISTRIBUTIONS ON THE CATALYST ACTIVITY AND THE THEORETICAL POISONING MODELS: Hardin et al. (1978), prepared a large number of catalyst with varying pore sizes. Their result for the vanadium and nickel removal activity with respect to median pore diameter is reproduced in fig. I-3. There seems to be an optimum pore size for the maximum initial catalyst

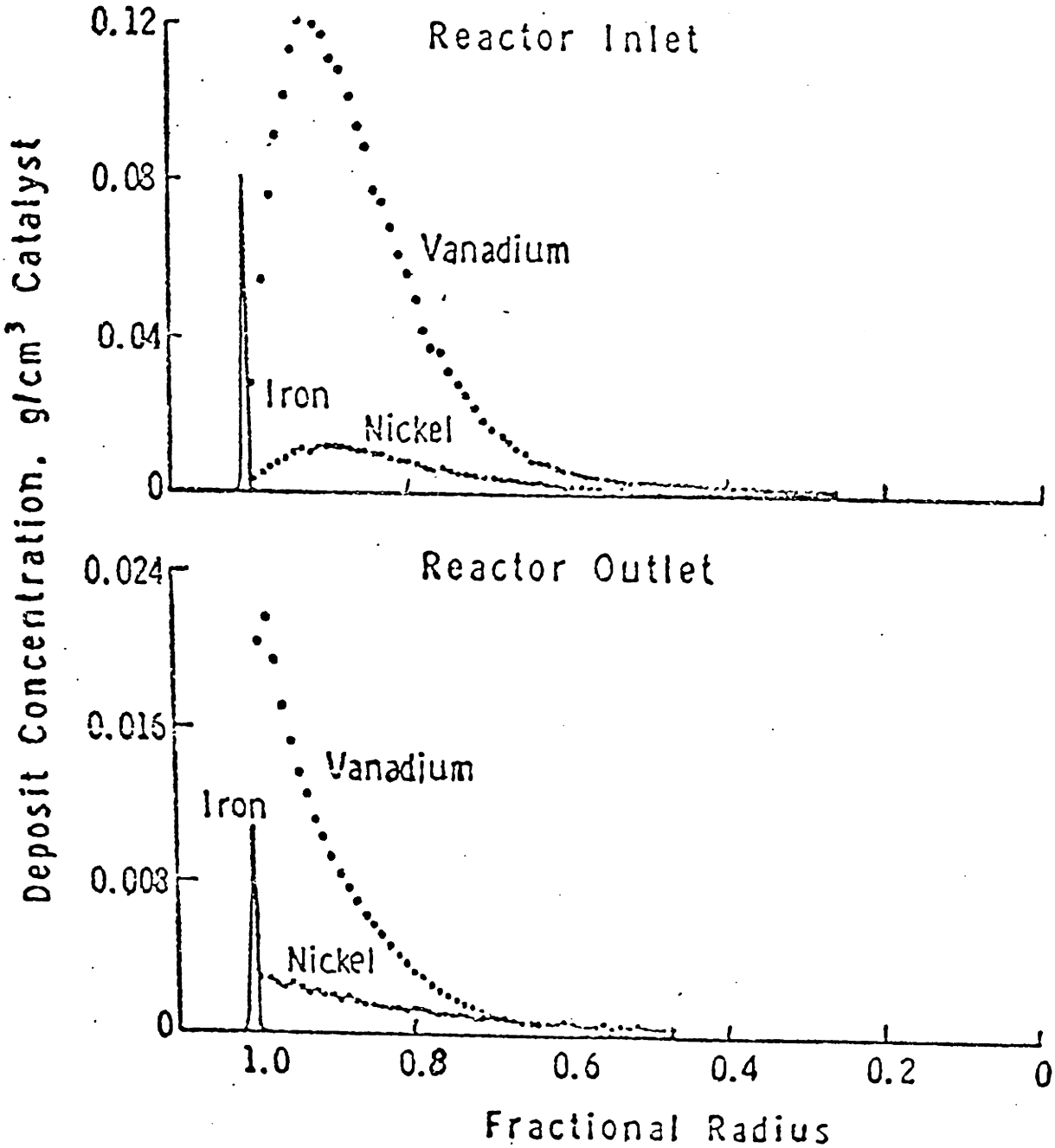

Fig. I-2 : Typical Depositional Patterns for Nickel, Vanadium, and Iron in Residuum Hydroprocessing Catalyst. Arabian Heavy Atmospheric Residuum Reaction Temperature = 700°F Hydrogen Partial Pressure = 1825 psia 1/16 in. Extrudate Catalyst (Tamm et al. - 1979)

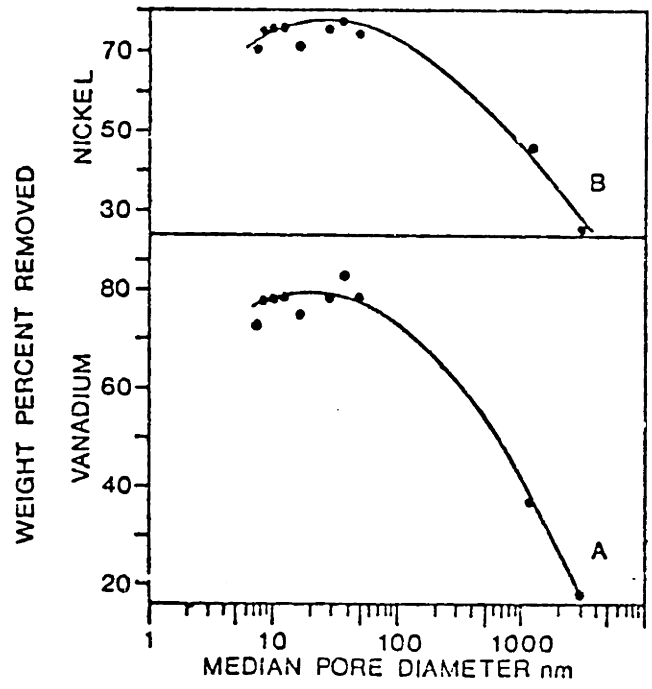

Fig. I-3 : (From Hardin et al. - 1978)

Demetallization of the Athabasca bitumen:

A - Removal of vanadium from a feed of concentration 174 ppm V;

B - Removal of Nickel from a feed of concentration 76 ppm Ni.

activity. For a fixed porosity, the decrease in the pore radius increases the surface area of the catalyst but also decreases the configurational diffusion coefficient. Therefore, for a given molecular size, the maximum in the initial catalyst activity is achieved for a certain intermediate pore size.

Inoguchi et al. (1971b) studied the long run tests of 1,000 to 3,000 hours on catalysts with different physical properties. They found that the catalysts with comparetively small pores had a high initial activity, but the activity fell rapidly with time. On the other hand, in catalysts with comparatively large pore diameters, vanadium deposited in large quantities and maintained its activity for a longer time.

Therefore, there is a need for a pore size distribution which would be a good compromise for both the initial activity and also the long range activity. A suitable catalyst which meets both the needs is the bimodal catalyst.

Newson (1972 and 1975), Dautzenberg et al. (1978) and Rajagopalan and Luss (1979) have developed poisoning models to account for the initial and long range activity of the catalyst. All these investigators assumed that the pore structure could be represented by a set of idealized parallel sided non-intersecting pores of the variable radius, but each of a certain length L. This model is also refered to as 'parallel bundle' model, and it does

not allow for connectivity of the pores. Whereas, the major advantage of the bimodal catalyst lies in the connectivity of the micropores with the macropores. One of the objectives of this thesis is to develop a poisoning model for the bimodal catalyst with the allowance for some connectivity between the micro and macropores.

C. OBJECTIVES: Following are the main objectives of this thesis:

1. To study kinetics more carefully and to identify important kinetic steps in the hydrodemetallation; and thus explain the various inconsistencies in the observed kinetic orders.
2. To study the vanadium and nickel deposition profiles in 1/16 inch catalyst extrudates. The objective is to understand and model the metals deposition profiles at various bed positions, including the internal maxima at the inlet of the reactor, and at various temperatures and pressures of the operation.
3. To develop theoretical poisoning models for the unimodal and the bimodal catalysts. For bimodal catalyst, some allowance for the connectivity between the micro and macropores is made. Through these models, the performance of the unimodal and bimodal catalysts have been compared.

D. APPARATUS AND PROCEDURE: The catalysts used in this research are 1/16 inch CoO - MoO_3/Al_2O_3 extrudates, and are supplied by the American Cynamid Company. Most of the pores of this catalyst are between 59.0 to 88.4 Å and the pore diameter corresponding to 50% of the total pore volume is 80.4 Å. The oil used to dissolve the model metal compounds is a naphthenic type of white oil called Nujol (Plough Inc., Memphis, Tenn.). This oil is free of nitrogen, sulfur and metal compounds. Nickel Etio porphyrin-I (Ni Etio-I) and Vanadyl Etioporphyrin (VO Etio-I) have been used as model metal compounds. Their solubility in Nujol at room temperatures is about 40 ppm.

Most of the hydrodesulfurization reactors used in chemical industry are the trickle bed reactors (Weekman - 1976). As the trickle bed reactors are poorly characterized and suffer severely with complex hydrodynamic effects (Satterfield - 1975), for our lab studies it was decided to use a much more simple and well defined reactor system. The simplified schematic of the reactor system used in this study is shown in fig. I-4. The liquid solution is saturated with hydrogen gas at the room temperature (~25°C) and the desired hydrogen pressure, and is then pumped through the reactor. It has been estimated that under typical operating conditions the approximate ratios of the moles of the dissolved H_2 to the moles of metal would be 200 - 450. This tells us that there is definitely an excess of hydrogen in the reactor. In paraffins and

SIMPLIFIED SCHEMATIC

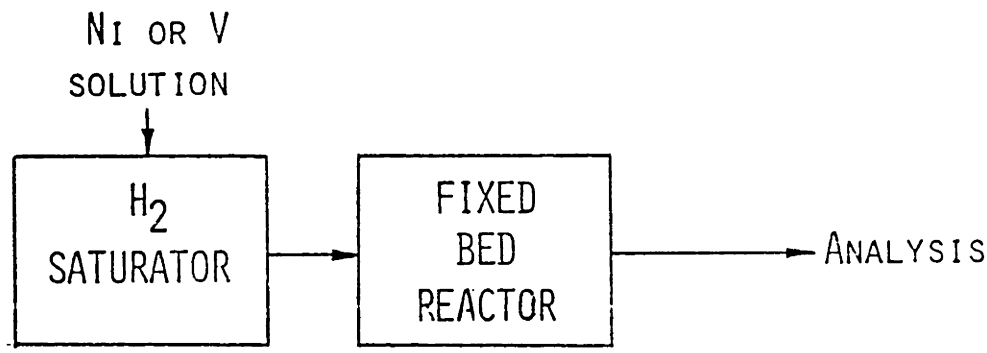

Fig. I-4

Simplified Schematic of the Reactor System

naphthenes, the solubility of hydrogen is known to increase with temperature (Cukor and Prausnitz - 1972, Prather et al. - 1977). It insures that at the reactor temperatures, which are higher than the saturation temperature, no hydrogen gas would leave the solution phase.

The operating conditions for which the apparatus is designed are listed in Table I-1. A schematic flow diagram of the reactor system is given in figure I-5. In this study the catalysts are not presulfided. During the run, liquid samples of about 2 ml volume are periodically collected from the sample valve.

The total metal concentration of the liquid samples is analysed by the atomic absorption spectrophotometry. Both nickel and Vanadyl Etioporphyrins are red in colour and have intensive absorption peaks in the visible band of the spectrophotometer spectrum (fig. I-6). Beer's law and the peaks at 517 and 534 nm are used for the analysis of Ni-Etio and VO-Etio respectively. It is seen that the reactor outlet solution for both VO-Etio and Ni-Etio shows a new peak at 631 and 616 nm respectively (figures I-7a and I-8a). In each case, the new peak corresponds to one major reaction intermediate. By use of the dry column chromatography (Loev and Goodman - 1970), the reaction intermediates could be seperated from the reactor outlet solution. The visible spectra of the reaction intermediates are shown in figures I-7b and I-8b. These compounds are identified to be Chlorins (fig. I-9). Beer's

TABLE I-1

TYPICAL OPERATING CONDITIONS

TEMPERATURE=280-380° C

PRESSURE=600-2000 PSIG

SOLUTION FLOW RATE=2-50 ML/HR.

INLET METAL CONC. =15-30 PPM BY WEIGHT

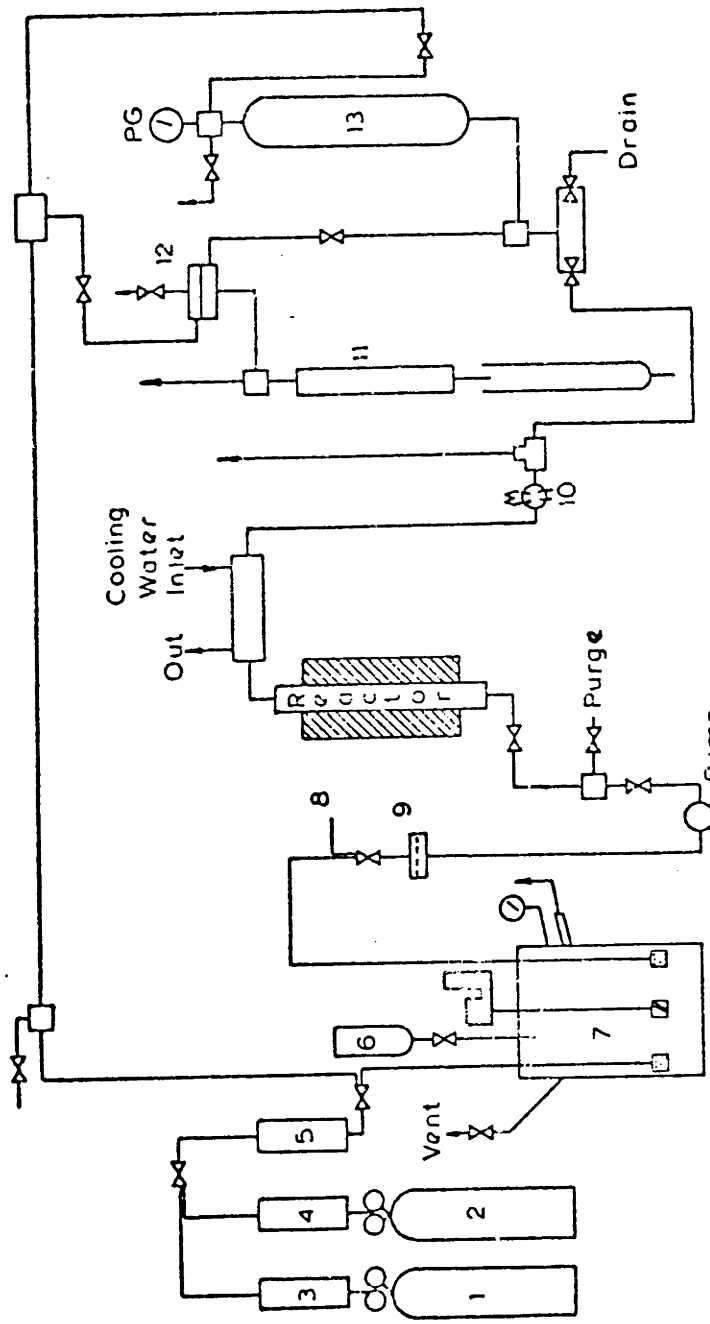

KEY

1 H_2 Cylinder
2 H_2 Cylinder
3 Cu & Zn Oxides
4 Pt / Al_2O_3
5 Molecular Sieves
6 Charging Port
7 Two Litre Autoclave
8 From 1 Litre Autoclave
9 Line Filter
10 Sample Valve
11 Separator
12 Back Pressure Regulator
13 Sample Cylinder

Fig. I-5: FLOW SHEET OF THE REACTOR

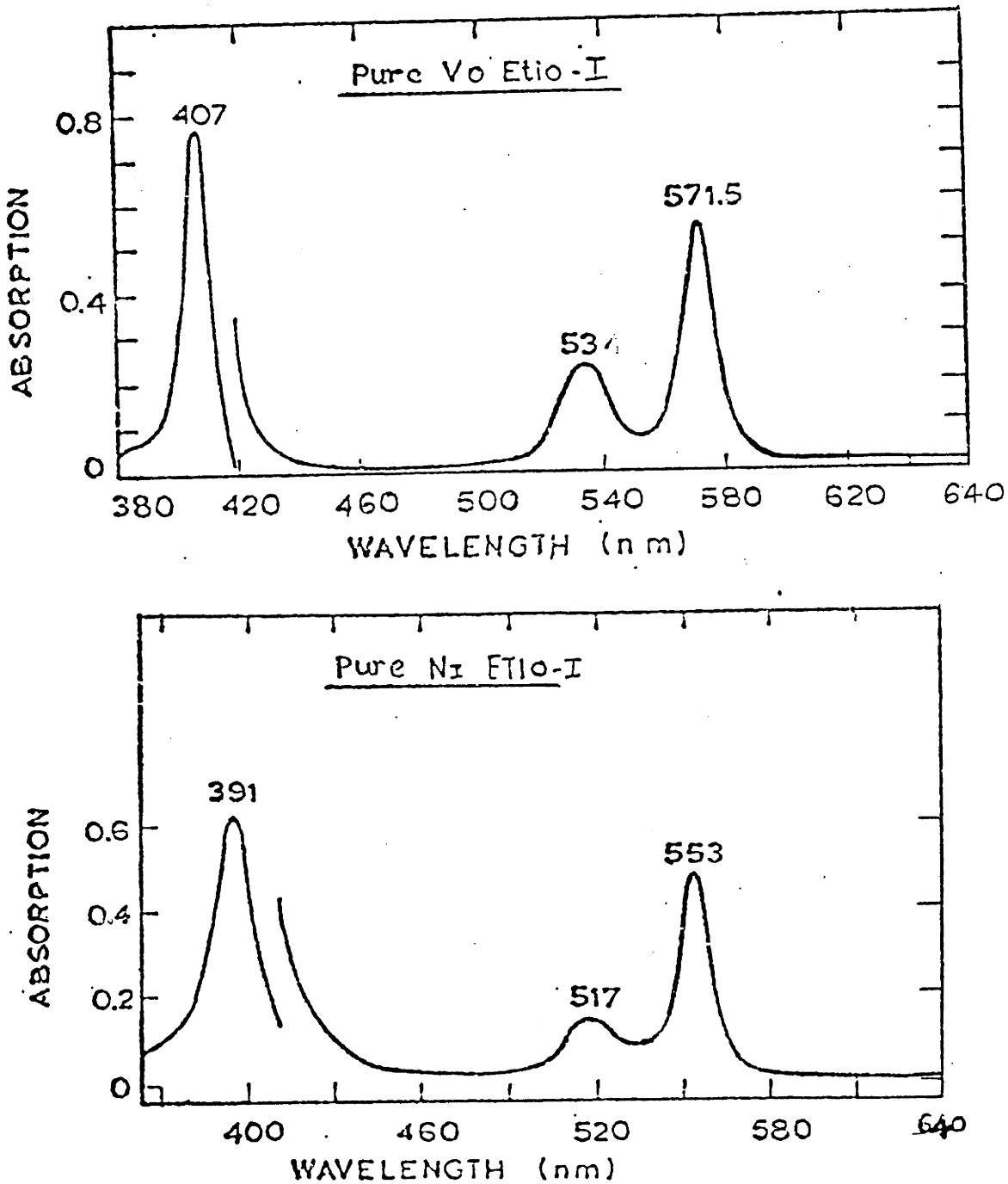

Fig. I-6: Visible Spectra of Vanadyl Etioporphyrin-I and Nickel Etioporphyrin-I in Xylene Solvent.

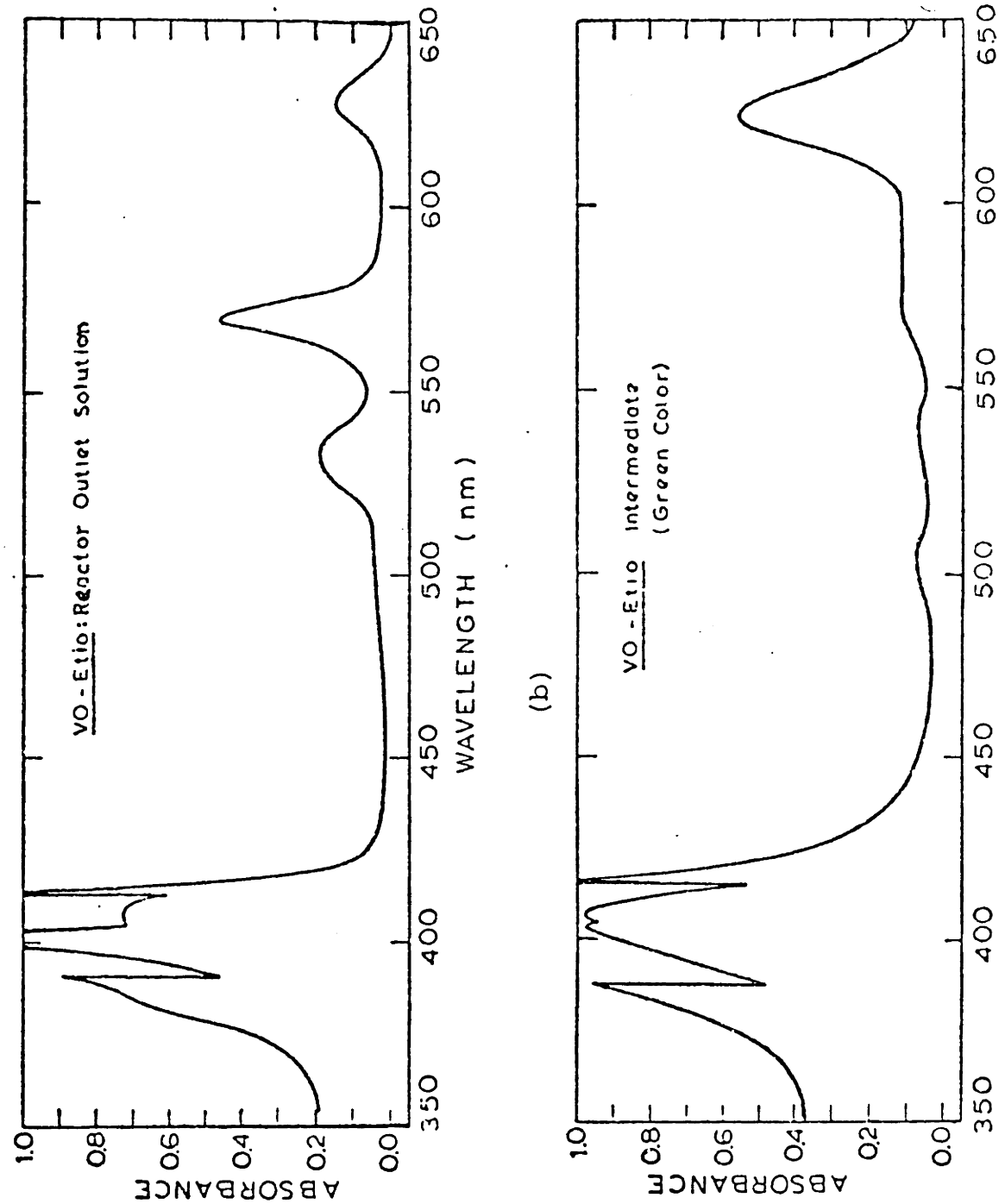

Fig. I-7: Visible Spectra. Solvent: Xylene

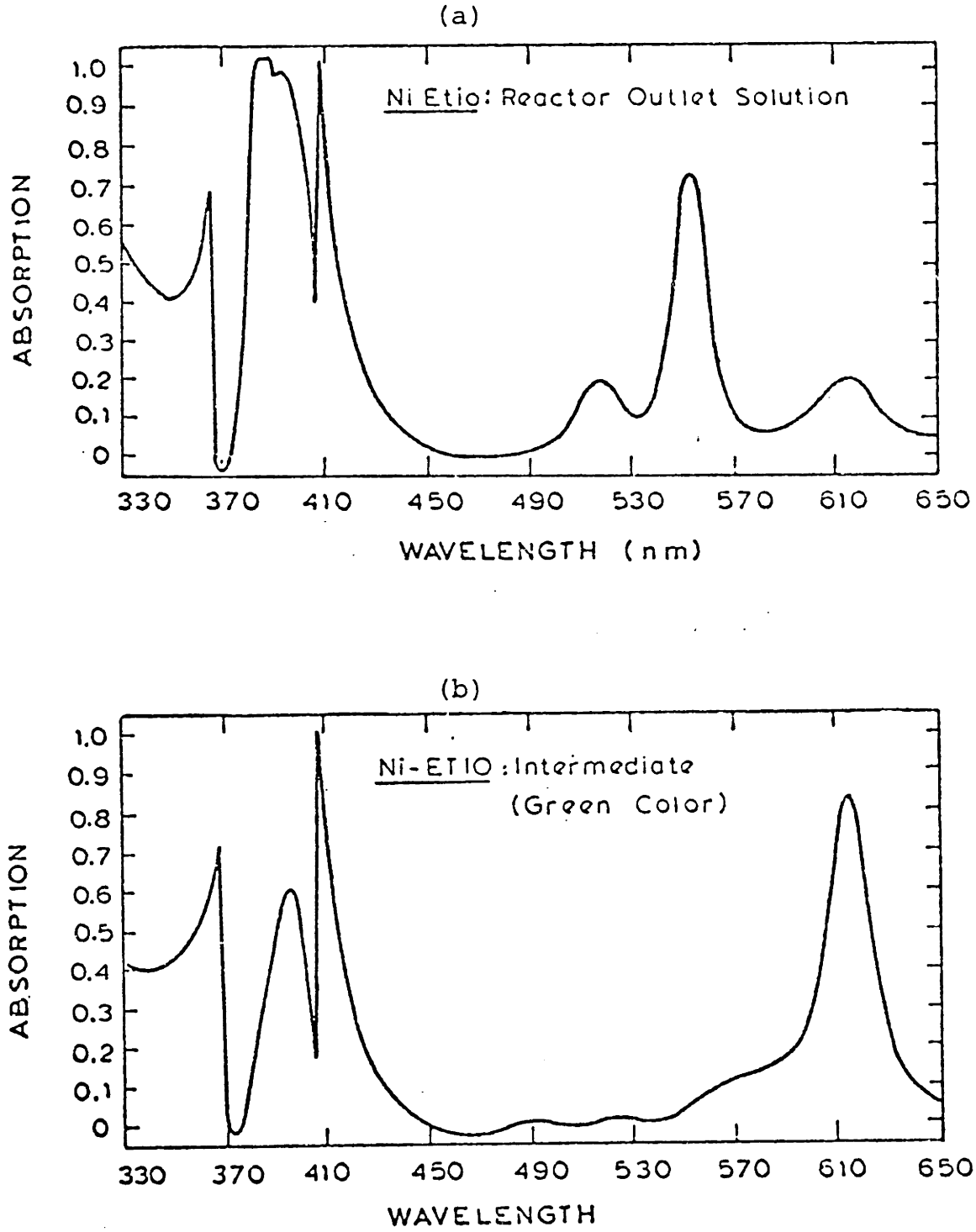

Fig. I-8: Visible Spectra

Solvent: Xylene

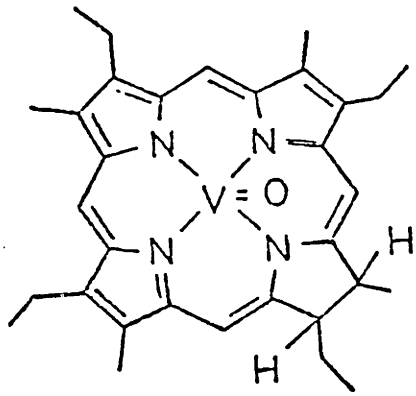

VO-Chlorin (Etio type)

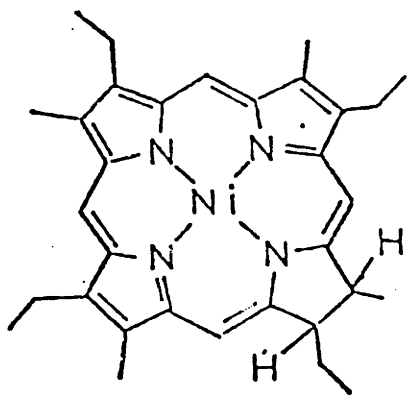

Ni-Chlorin (Etio type)

Fig. I-9 : Structures of Ni and VO Chlorin

law and the peaks at 616 and 631 nm are used for the analysis of Ni-chlorin and VO-chlorin respectively.

The spent catalyst from the reactor was first cleaned free of oil and unreacted metal compounds in a soxhlet extractor for twenty four hours. Chloroform was used as the suitable cleaning solvent. The metal content of the cleaned catalyst was analyzed by the scanning electron X-ray microanalyzer.

E. RESULTS AND DISCUSSION:

E.1. TRANSIENT BEHAVIOUR OF CATALYST: Figure I-10 is a typical plot of the reactor outlet stream concentrations with time on stream. In this figure, throughout the reaction period, the solution flow rate to the reactor has been kept constant. It is seen that at time equal to zero, there is no nickel in the outlet stream. It may be either due to the fact that all the nickel is physically adsorbed on the catalyst surface or the initial activity of the catalyst is too high. After time zero, uptill about 15 hours, a increase in the outlet concentration of the Ni-Etio and the nickel chlorin is observed. This decay in the catalyst activity may be due to the rapid build up of the coke on the catalyst surface.

After about 15 hours and upto 30 hours or so, a decrease in the total metal concentration of the reactor outlet stream is observed. During this period there is no decline in the concentration of the Ni-chlorin; if anything,

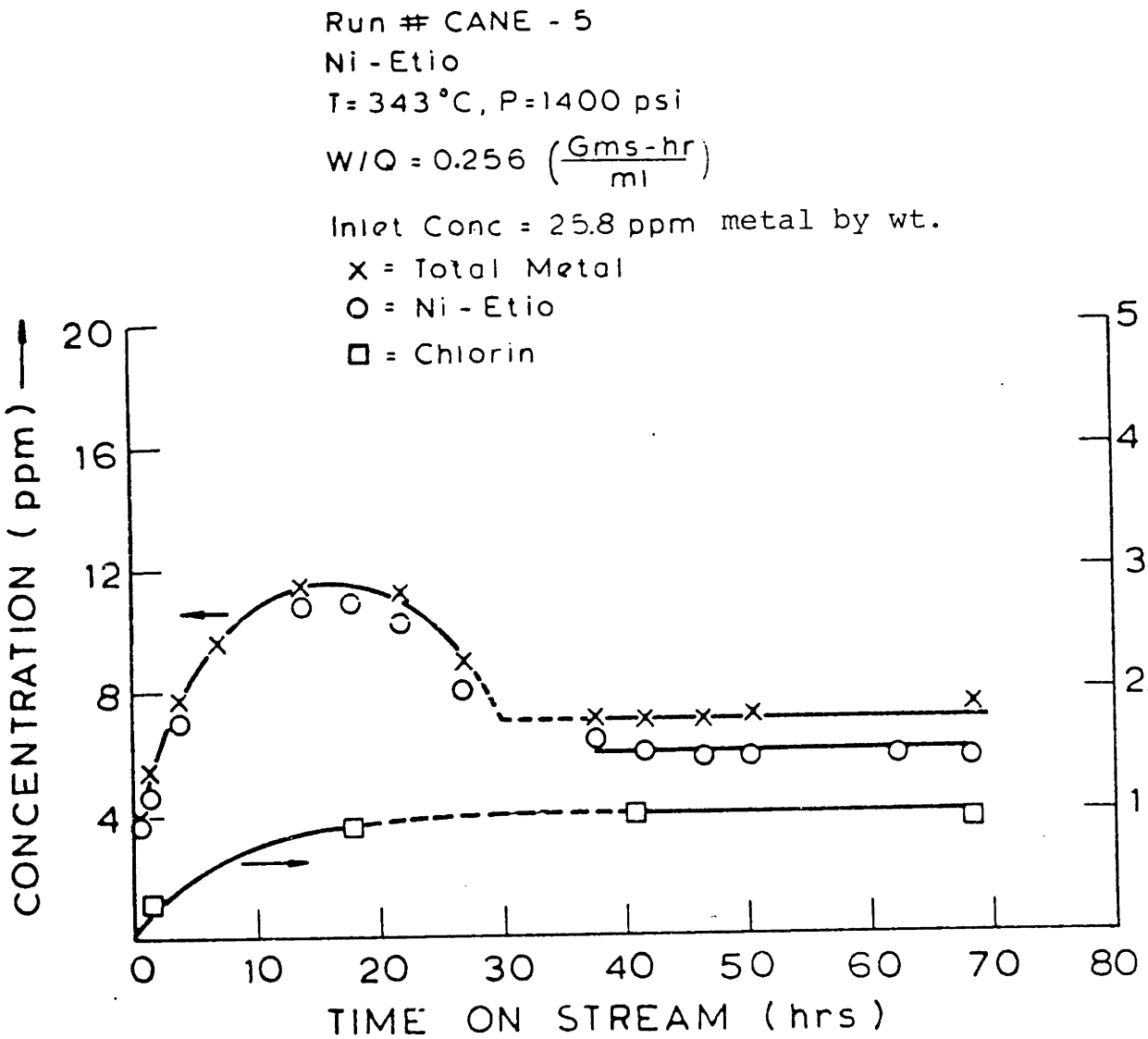

Fig. I-10: Outlet Solution Concentrations vs. time on Stream for a Typical Nickel Etio-I run in one inch Reactor.

it is a mild increase. This increase in the catalytic activity is attributed to the metal deposition on the catalyst surface. Bridge and Green (1979) reported that the metal deposit is catalytically active for hydrogenation and demetallation. Our work further confirms their observation.

After 30-40 hours, there is a long period of constant catalytic activity. Identical transient catalytic behavior is observed for VO Etio-I runs. Similar to fig. I-10, figure I-11 is the plot for a typical vanadium run. In this study the maximum metal deposited on the catalyst in any single run is about 10 wt%. Upto this metal loading no significant change in the catalyst activity is observed. Thus once the catalyst has achieved its steady state activity, it is maintained for fairly long period of time to allow the needed kinetic measurements.

E. 2. HYDRODEMETALLATION KINETICS: The physical dimensions of the catalyst are chosen so that there are no mass and heat transfer limitations. The 1/16 inch $CoO-MoO_3/Al_2O_3$ Catalyst extrudates are crushed to the size range of 170-200 mesh (0.088-0.074 mm). The cross sectional area of the microreactor used is 0.21 cm^2 (I.D. = 0.52 cm). The length of the catalyst bed ranged from 6 cm to 15 cm.

The catalytic runs are made at the pressures of 4.14 MPa (600 psig), 6.89 MPa (1000 psig) and 9.65 MPa (1400 psig); and at temperatures 288°C (550°F), 302°C (575°F), 315°C (600°F), 329°C (625°F) and 343°C (650°F)

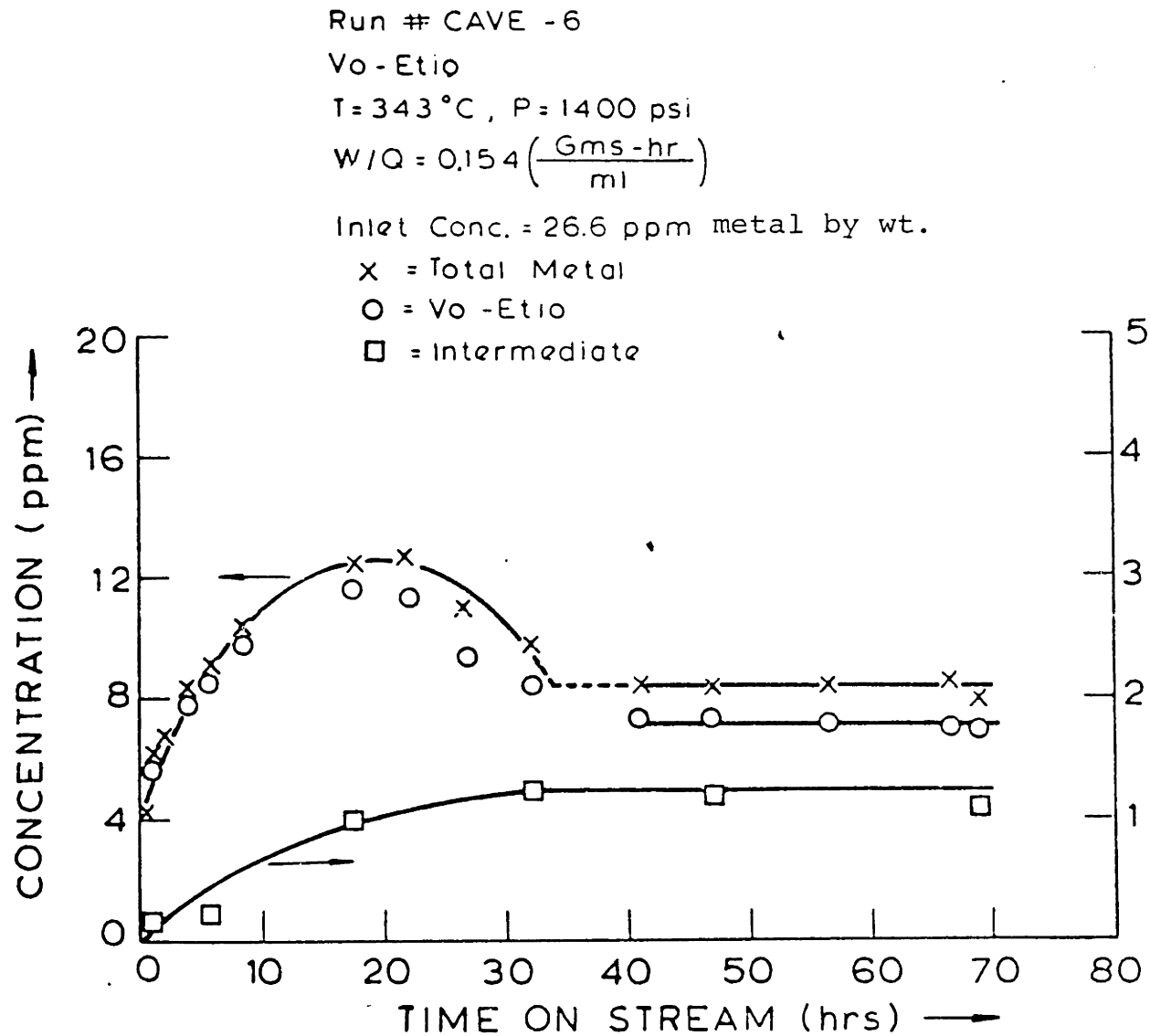

Fig. I-11 : Outlet Solution Concentrations vs. time on Stream for a Typical Vanadyl Etio-I run in one inch Reactor.

and for two different reactor inlet concentrations of about 27 ppm and 15 ppm.

E.2.1. NICKEL ETIOPORPHYRIN-I: Fig. I-12 is a typical plot of the variation of the outlet concentrations as functions of the contact time. It is observed that initially there is a rapid build up of chlorin concentration and during this period decrease in the total metal concentration is not so significant. After this rapid initial build up, the chlorin concentration drops monotonically and the rate of the drop of the total metal concentration also increases.

Uptill now all the investigators of the HDM have modelled the kinetics as the disappearance of the total metal in the solution. So our initial attempt is to neglect the intermediate chlorin concentration and model the kinetics as the function of the total metal concentration only. Of the three different kinetic orders tried, second order did not work at all. The run at 343^{o}C and 9.65 MPa is plotted as first order in fig. I-13 and as half order in fig. I-14. Even though half order fit gives more error than the first order fit, within the experimental error it is difficult to discriminate between the two. It is seen that in both the cases, the magnitude of the error is larger at the higher conversions. Another important observation is that while the best fit line for first order predicts the value of the concentration at zero contact

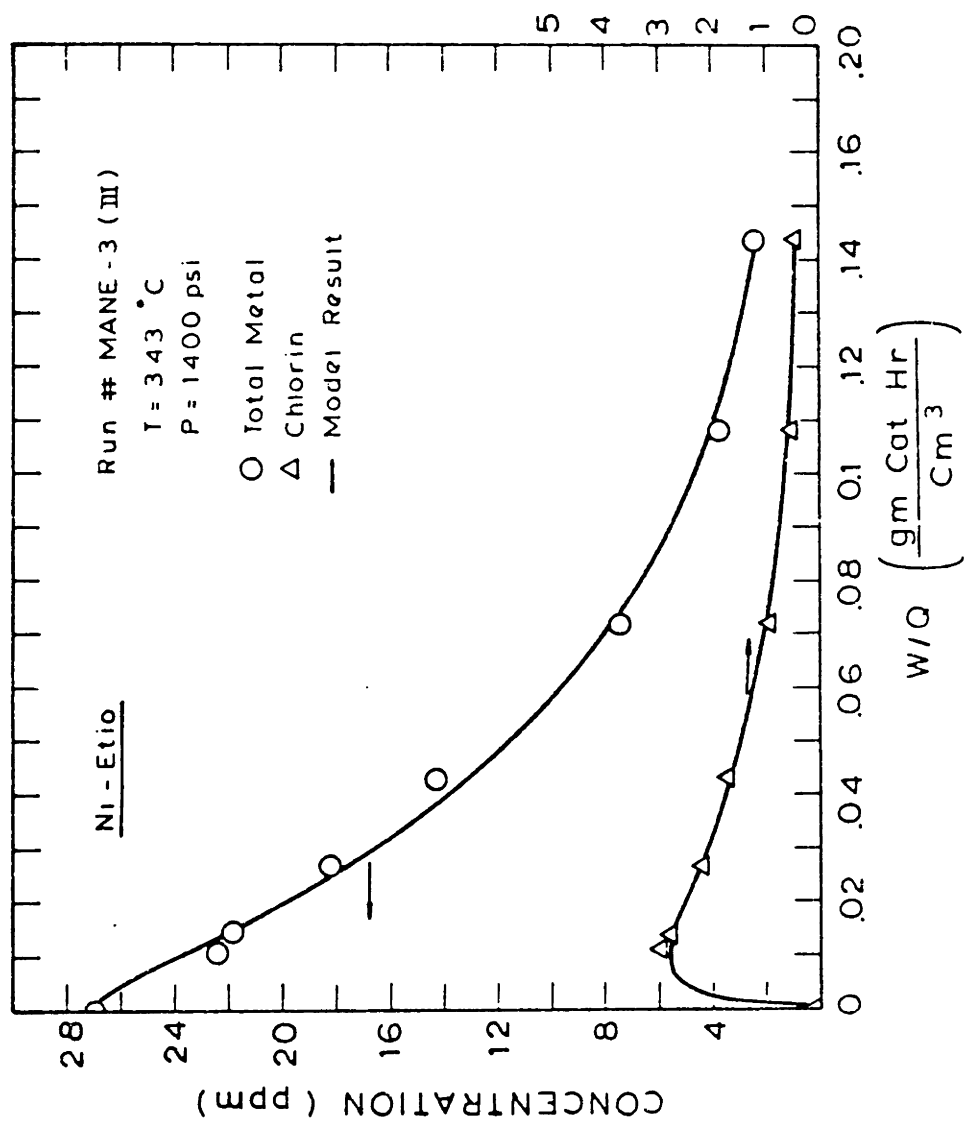

Fig. I-12: Calculation Results of the New Proposed Model and the Experimental Data.

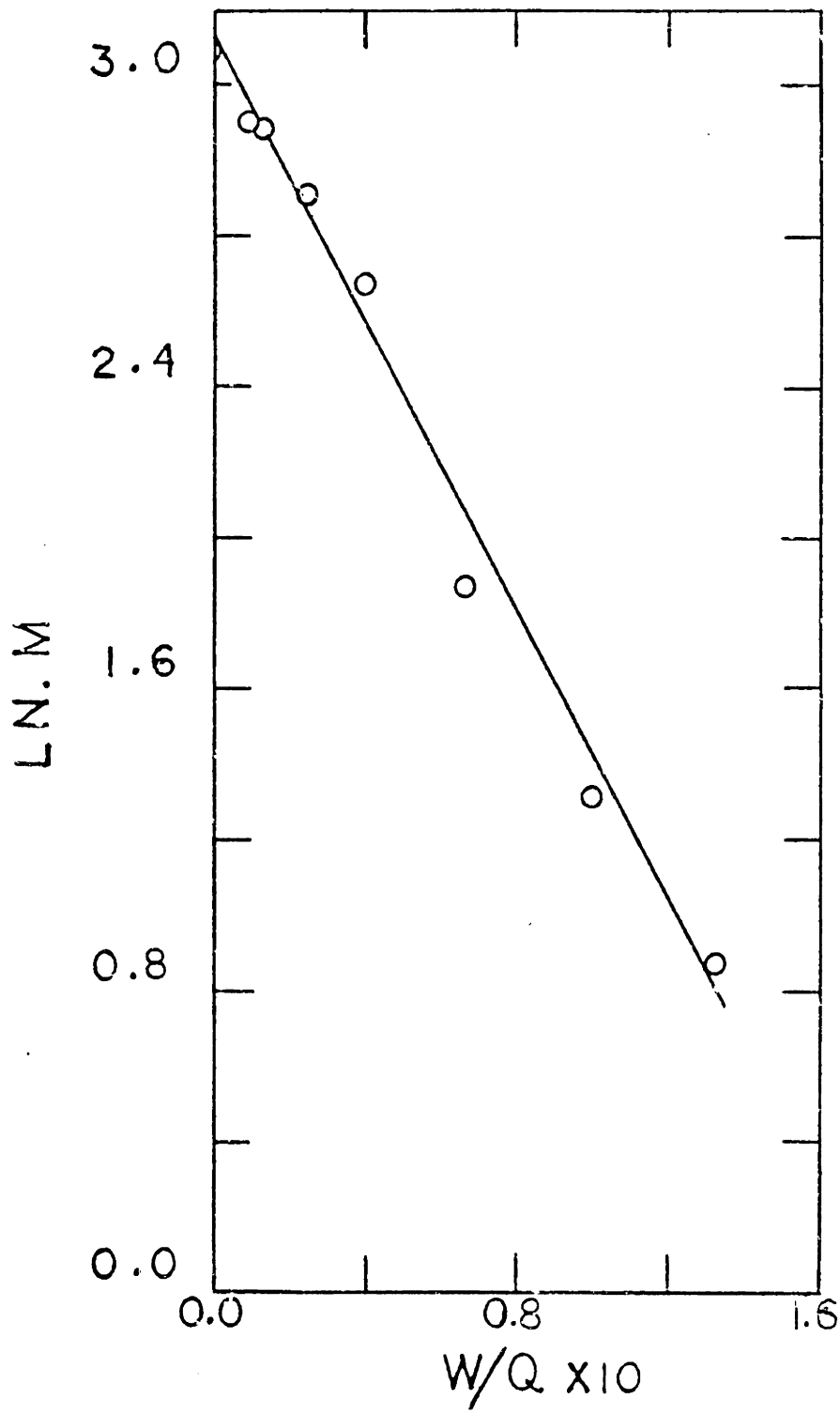

Fig. I-13: First Order Plot for Ni Etio-I at 343°C and P=9.65 MPa. Run # MANE-3 (III). M is in ppm, W in grams and Q in ml/hr.

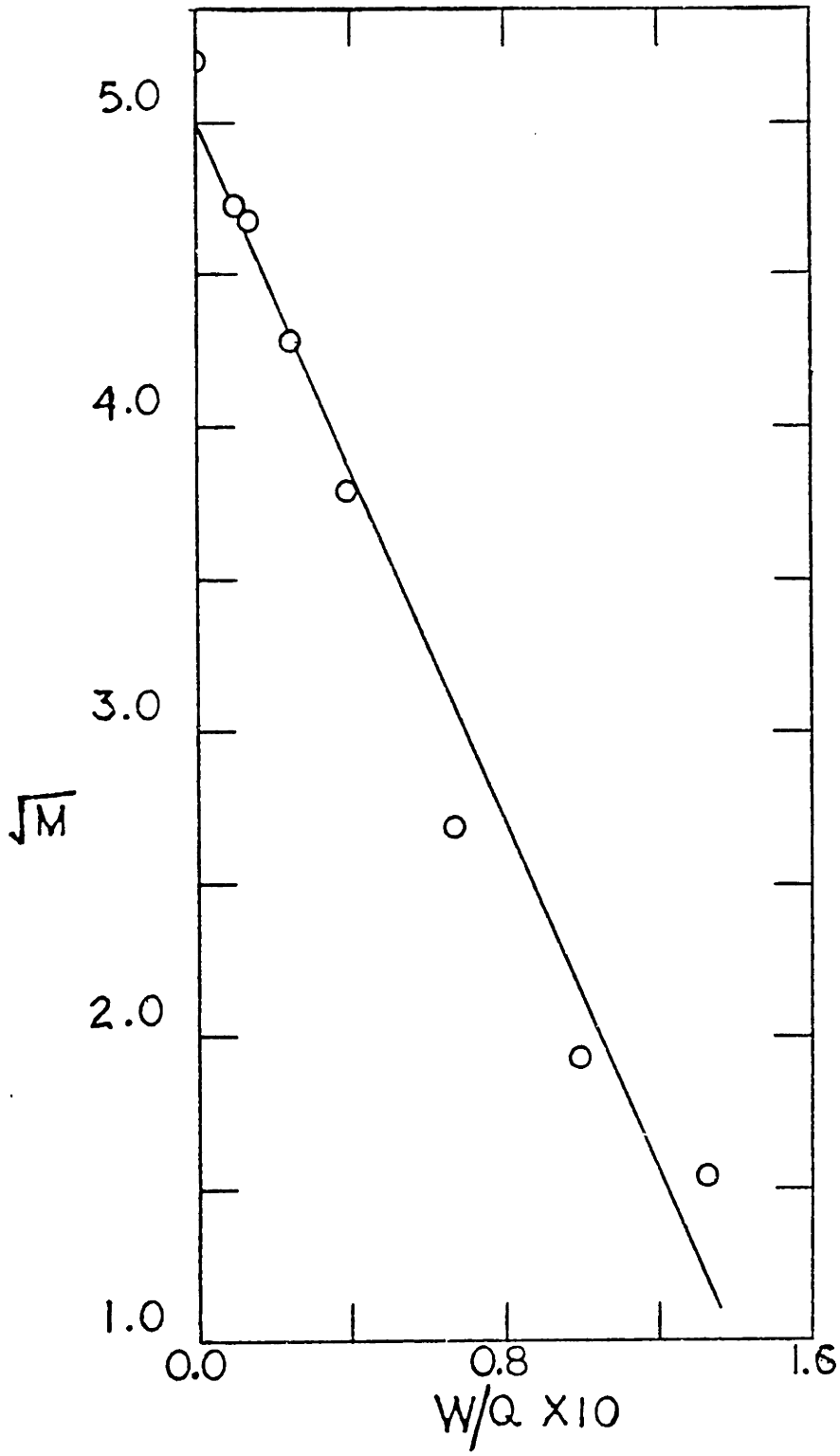

Fig. I-14: Half Order Plot for Ni Etio-I at 343°C, P=9.65 MPa. Run # MANE-3 (III). M is in ppm, W in grams and Q in ml/hr.

time higher than the initial concentration, the half order predicts much lower concentration. All these observations are common to other runs also.

The Arrhenius plot for the first order rate constant is given in figure I-15. The value of the activation energy obtained is 29.1 Kcal/gmole. Fig. I-16 is the plot of the pressure dependence of the first order rate constants at various temperatures. The mean hydrogen pressure dependence is 2.1.

Therefore, the first order global rate seems to do a reasonable job for the total metal disappearance. However it does not take the Ni-Chlorin concentrations into account, and therefore following model is proposed:

$$A \underset{k_2}{\overset{k_1}{\rightleftharpoons}} B \xrightarrow{k_3} \text{Metal Deposition on Catalyst}$$

where A is the original metal Etioporphyrin, B is the reaction intermediate, k_1 is the hydrogenation rate constant, k_2 is the dehydrogenation rate constant and k_3 is the rate constant for the final metal removal step. Prior to the metal deposition on the catalyst, B might go through a sequence of chemical steps, and therefore k_3 might be some sort of lumped rate constant. Whatever may be the sequence of events from B to the final metal deposition, they are so fast that in our experiments they could not be tracked down. All the steps in the model are assumed to be first order in the metal concentrations.

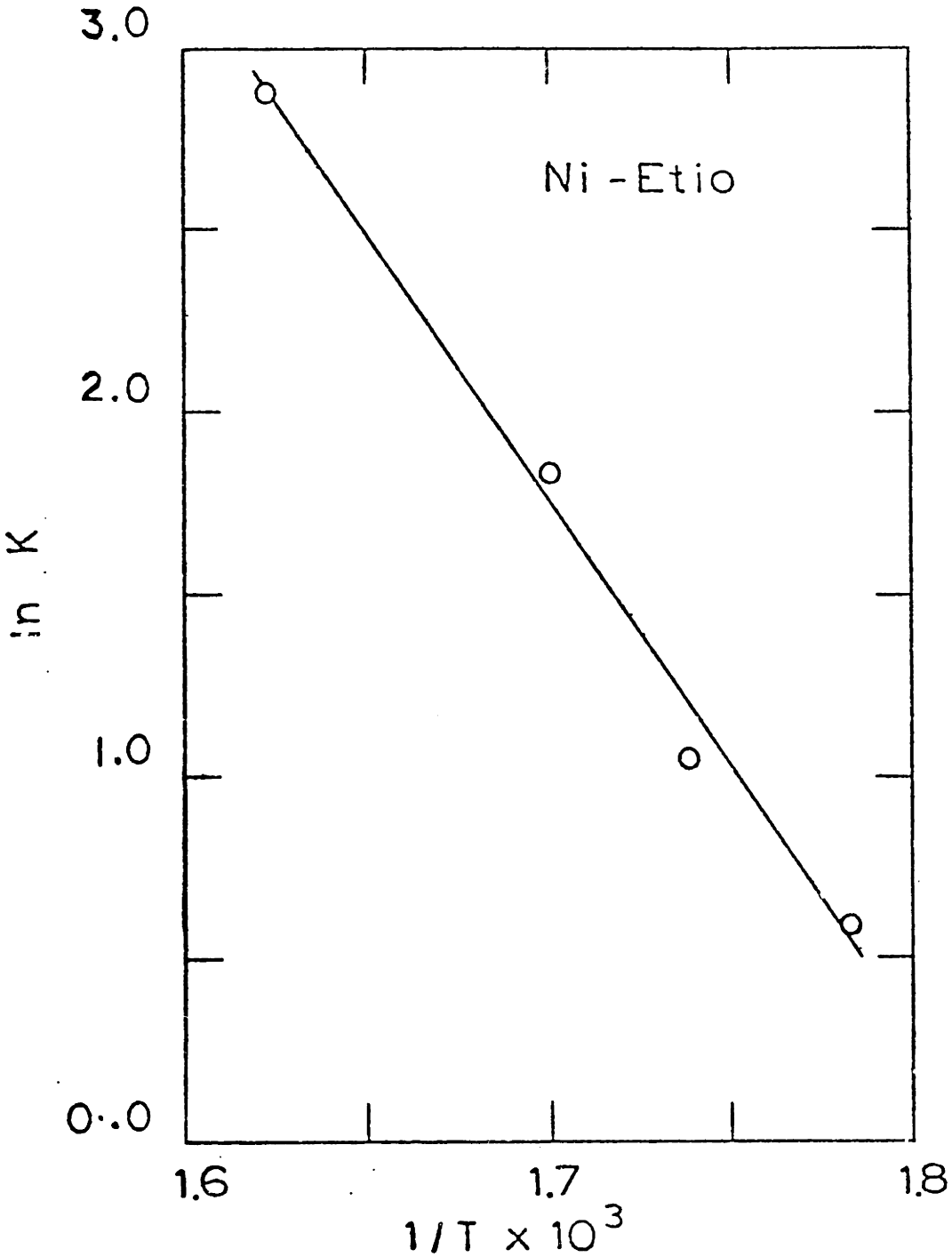

Fig. I-15: Arrhenius Plot for the First Order Rate Constant for Ni-Etio I. Pressure = 9.65 MPa. T is in °K and k in ml/g-hr.

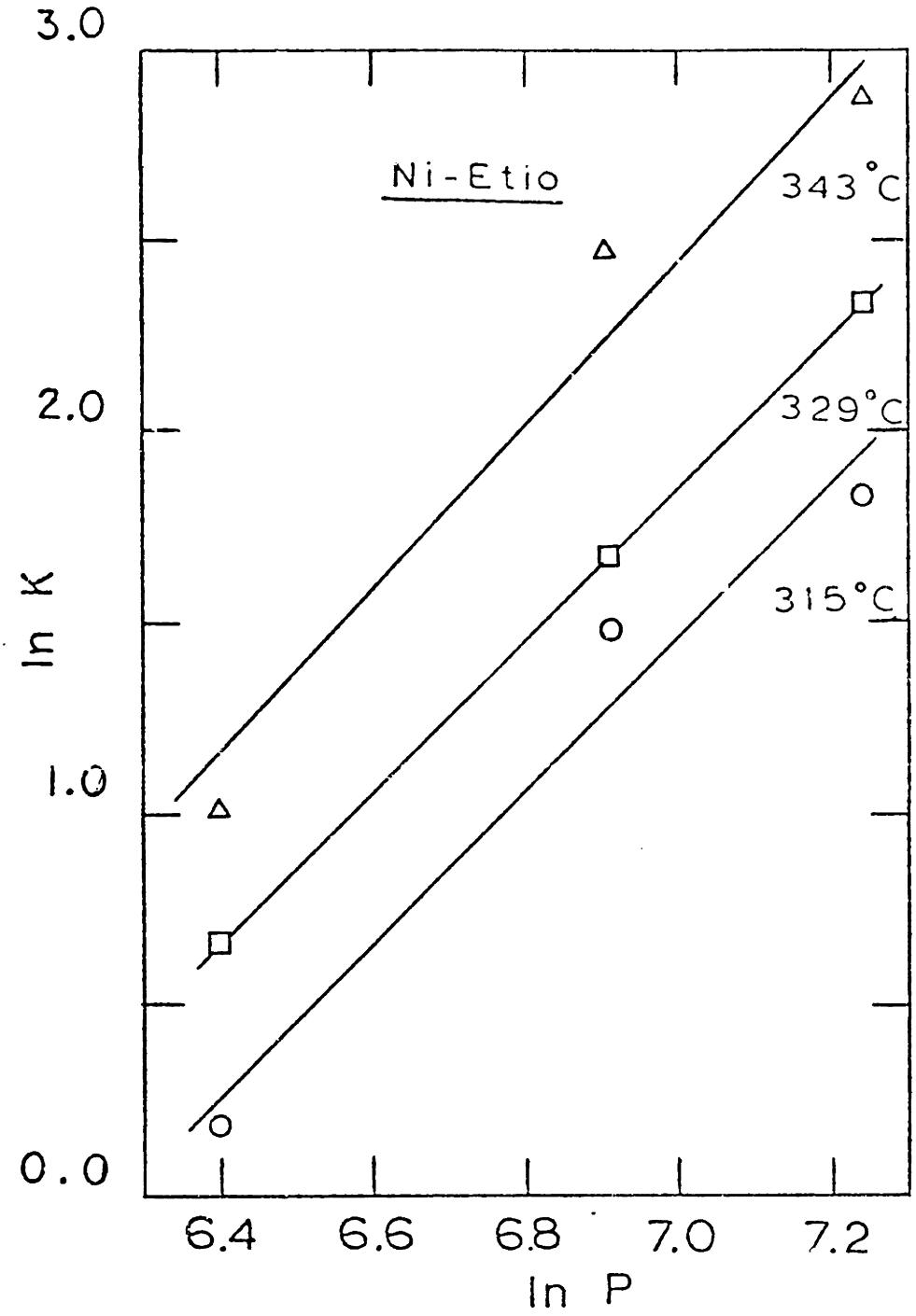

Fig. I-16: Pressure Dependence of the First Order Rate Constants for the Ni Etio-I. P is in psig and k in ml/g-hr.

The rate constants are evaluated by the nonlinear least square and Himmelblau-Jones-Bischoff (HJB-1967) techniques. Both the techniques work reasonably well.

In figure I-12, the solid lines are the calculation results of this model; and the experimental data is same as of figures I-13 and I-14. We see that the new model not only fits the total metal concentration better but also fits the chlorin concentration to a remarkable accuracy. The same observation is made with regards to the other runs. Figures I-17 to I-19 are the Arhenius plots for the rate constants k_1, k_2 and k_3 respectively. Figures I-20 to I-22 are the plots of the dependency of the rate constants k_1, k_2 and k_3 on hydrogen pressure. The results of these figures can be summarized through the following equation:

$$\ln k = \ln k_o - \frac{E}{RT} + n \ln P \qquad \text{I.1}$$

where E is the activation energy in Kcal/gmole, n is the order of dependence on pressure, P is the hydrogen pressure in psig, and k is the first order rate constant in ml of solution/g of cat.-hr. For k_1:

$$n=1,\ E=17.1\ ,\quad \ln k_{10} = 10.4 \pm 0.06$$

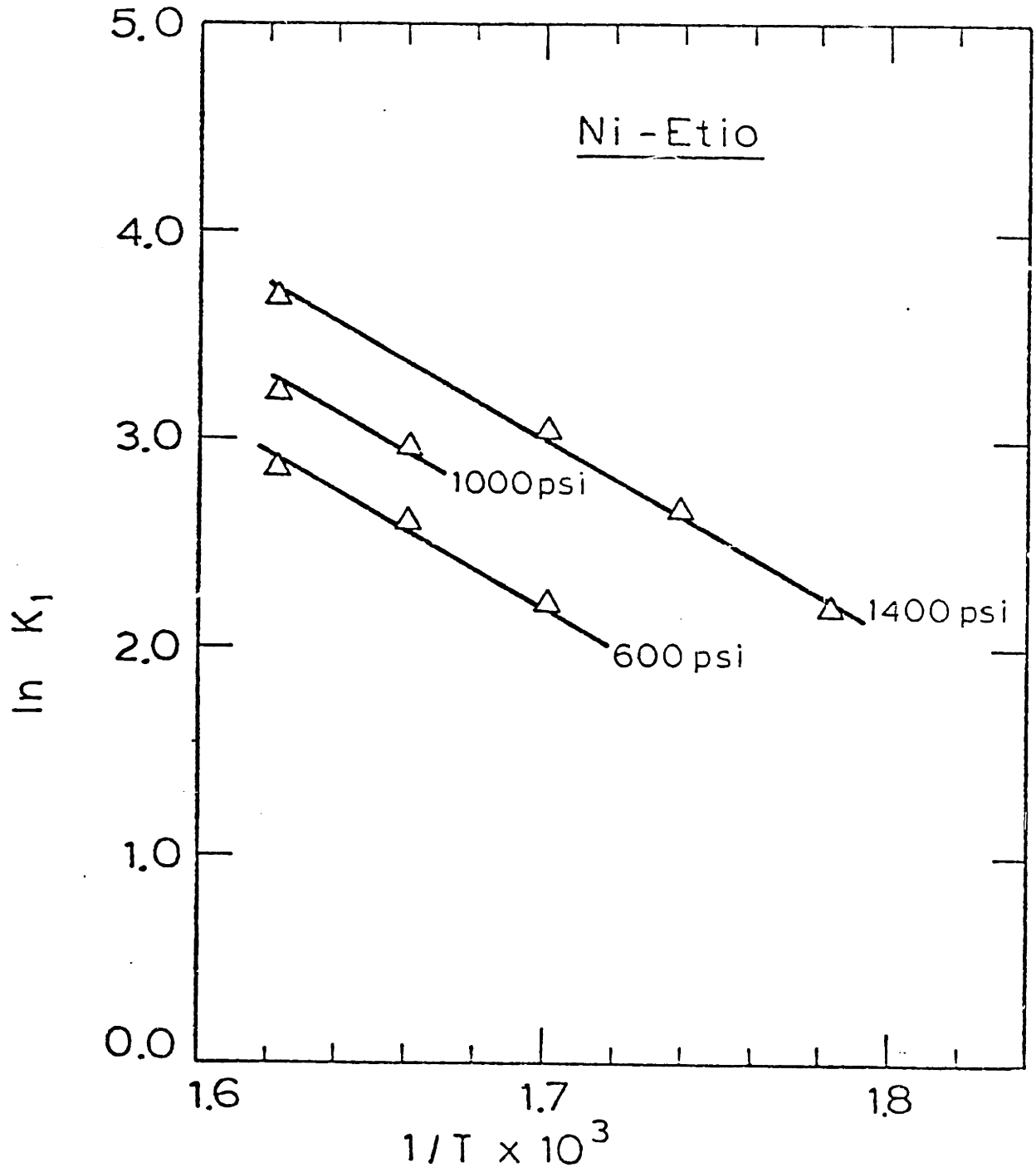

Fig. I-17: Arrhenius Plots for the Hydrogenation Rate Constant k_1 at Various Hydrogen Pressures. T is in °K and k_1 in ml/g-hr.

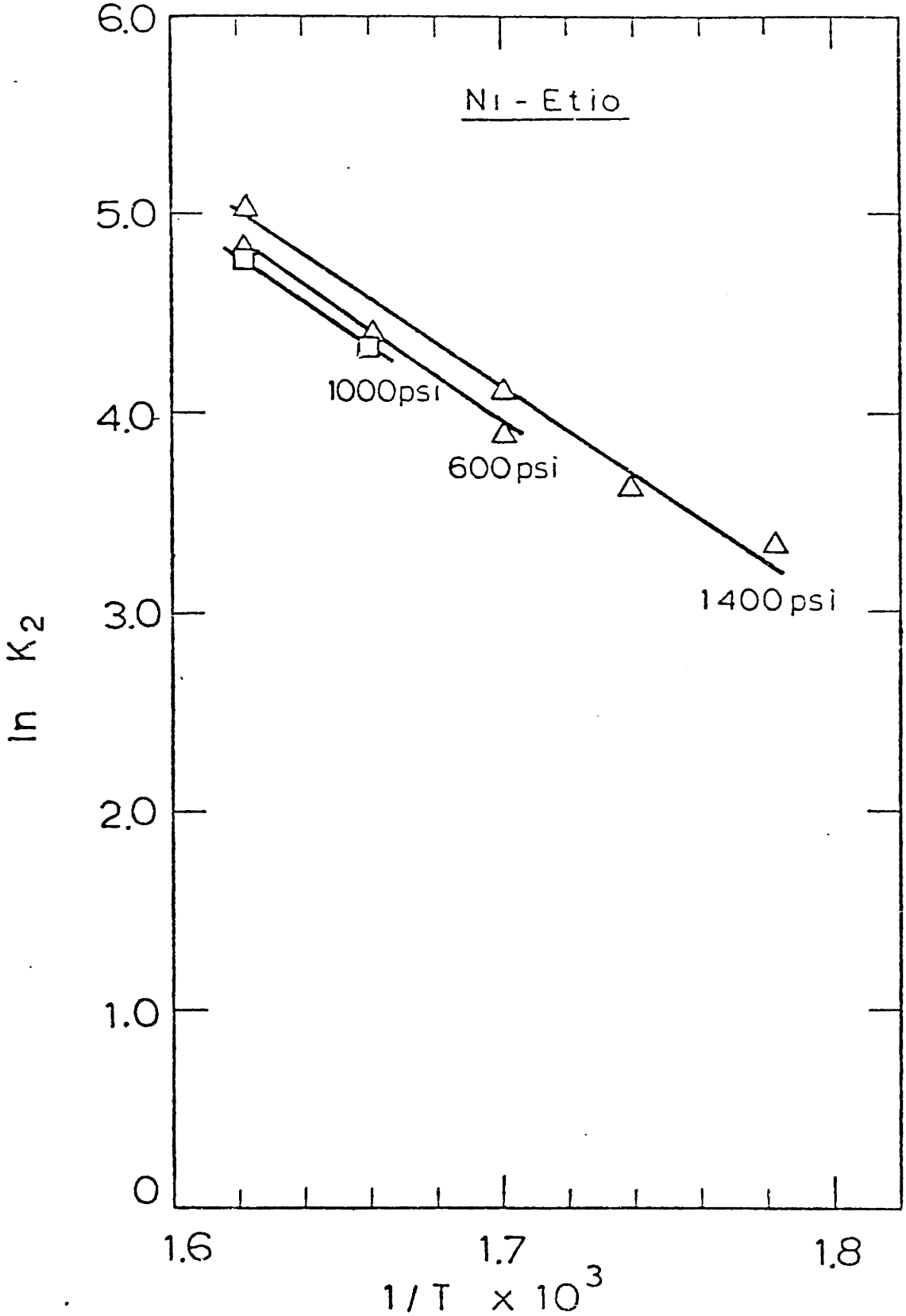

Fig. I-18: Arrhenius Plots for the Dehydrogenation Rate Constant k_2 at Various Pressures. T is in °K and k in ml/g-hr.

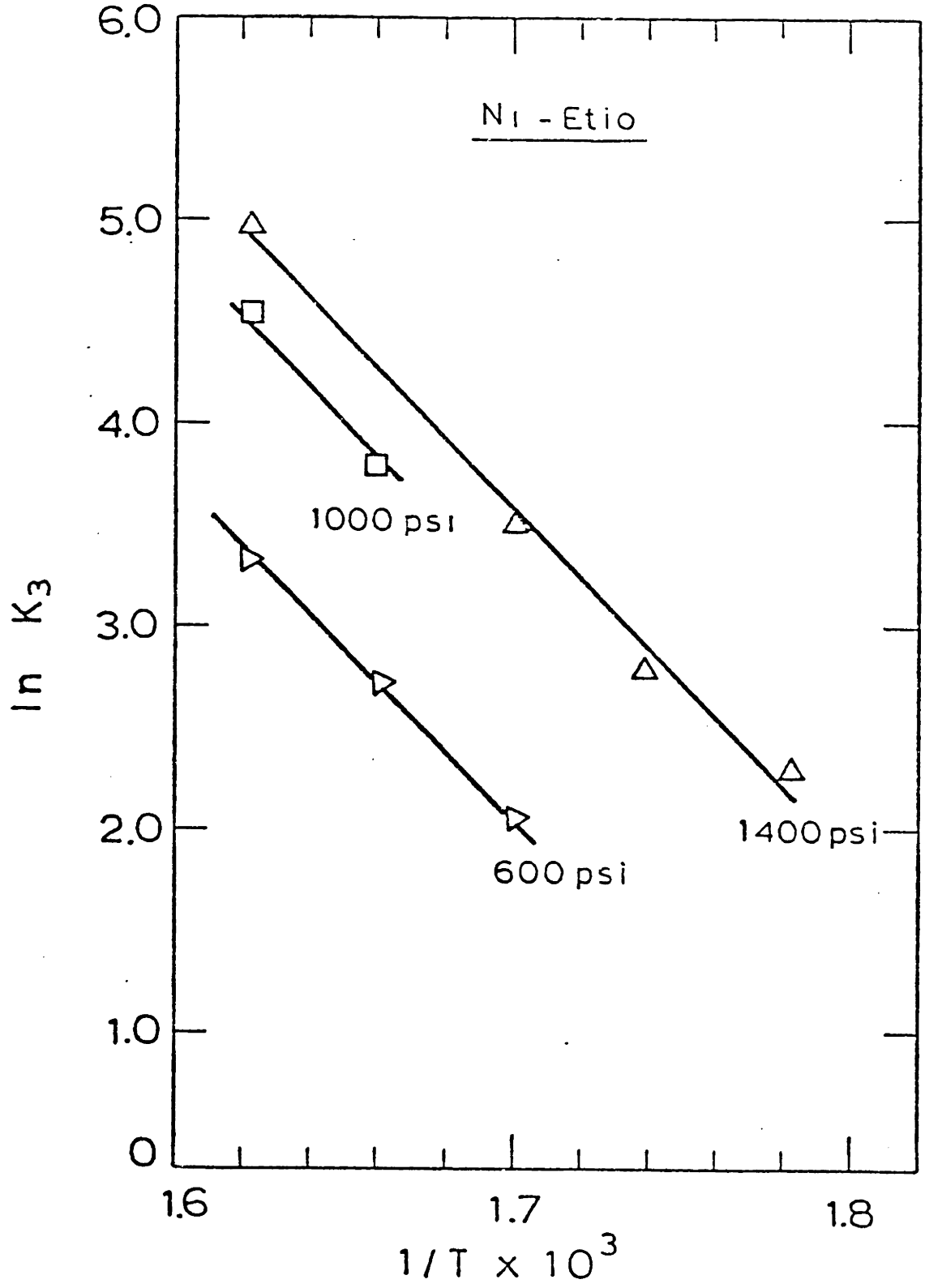

Fig. I-19: Arrhenius Plots for the Rate Constant k_3 at Various Hydrogen Pressures. T is in °K and k_3 in ml/g-hr.

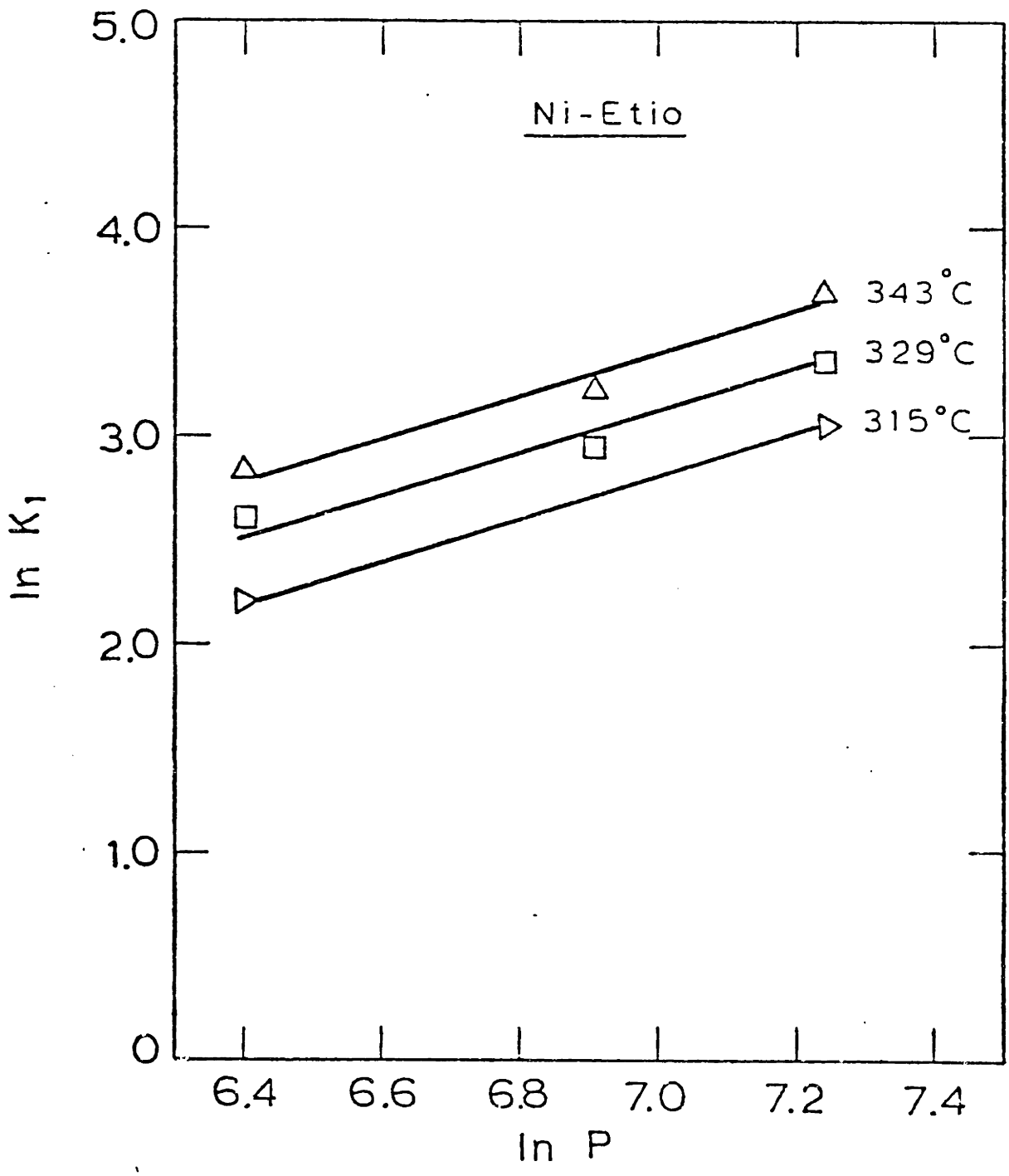

Fig. I-20: Dependence of k_1 on Hydrogen Pressure. P is in psig and k_1 in ml/g-hr.

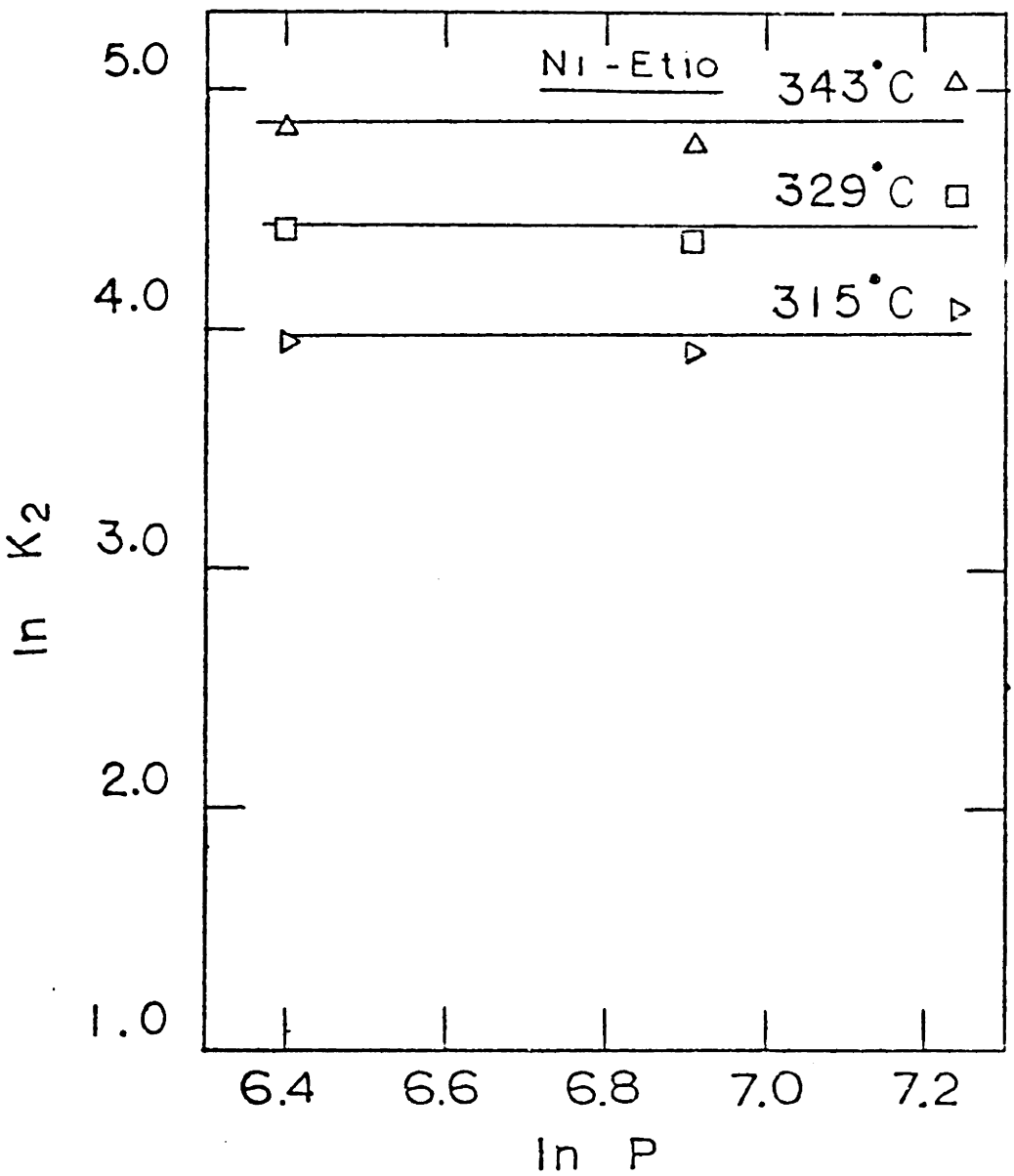

Fig. I-21: Dependence of Rate Constant k_2 on Hydrogen Pressure. P is in psig and k_2 in ml/g-hr.

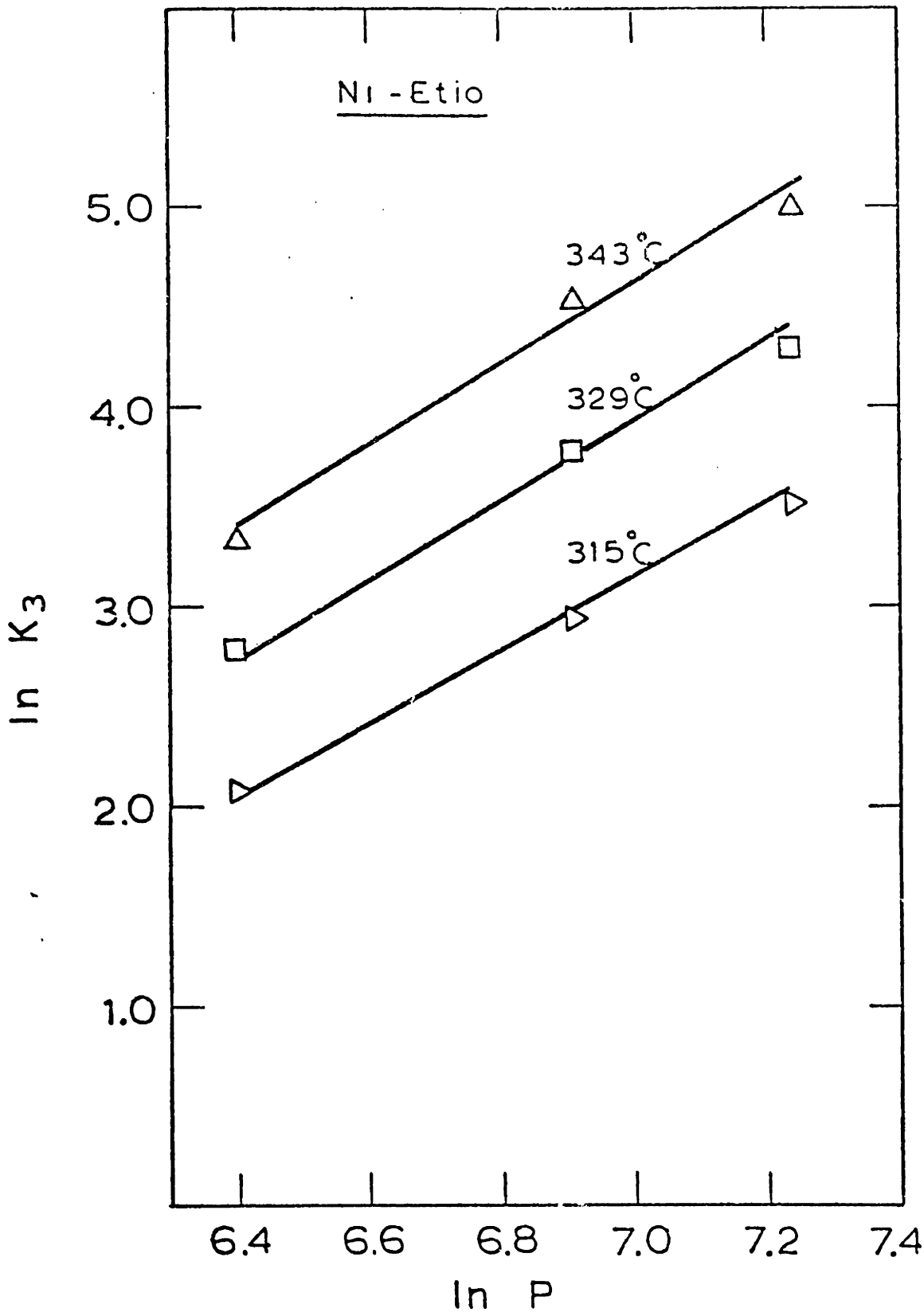

Fig. I-22: Dependence of k_3 on Hydrogen Pressure. P is in psig and k_3 in ml/g-hr.

for k_2:

$n=0$, $E=22.9$, $\ln k_{20} = 23.6 \pm 0.12$

for k_3:

$n=1.83$, $E=32.6$, $\ln k_{30} = 18.3 \pm 0.11$

and for k_3 if the value of n is taken to be 2 then:

$n=2$, $E=32.6$, $\ln k_{30}=17.13 \pm 0.14$

The dependence of k_1 on hydrogen pressure is first order. This is in excellent agreement with our analytical result that B is predominantely chlorin and is formed by the reaction of one hydrogen molecule with metal Etio A.

For all the runs above, the inlet concentration of the solution was maintained at a constant value of 27 ppm. Some runs at the inlet solution of about 15 ppm were also made. Once again the proposed model works extremely well. However, it is found that all the three rate constants are inversely proportional to the inlet solution concentration to the reactor. An attempt to explain this behavior by a Langmuir-Hinshelwood type kinetic expression has been made. This model assumes the adsorption of the final metal-free product molecule. Since the final product has not been identified, the validity of the proposed model could not be checked.

E.2.2. VANADYL ETIOPORPHYRIN - I: Our proposed model of the formation of one dominant intermediate B and then the metal deposition on the catalyst also works well for the vanadium runs. One typical result is plotted in fig. I-23. It must be pointed out that the magnitude of the error involved in the analysis of vanadium solutions at low concentrations is very high. For the solution concentration of about 4 ppm, the uncertainity may be as high as 1.5 ppm.

An attempt to fit half and the first order kinetics to the experimental data has also been made. The results for one of the runs are plotted in figures I-24 and I-25. It is seen from fig. I-24 that the half order kinetics does a fairly poor job. Comparison of figures I-24 and I-25 shows that the first order kinetics again does a better job than the half order kinetics. But unlike nickel, the first order kinetics does not do a reasonable job with the vanadium kinetics data.

Arhenius plots for the rate constants k_1, k_2 and k_3 are given in figure I-26. Dependence of these rate constants on the hydrogen saturation pressure, for the reaction temperature of 343^{o}C, are plotted in fig. I-27. All the three rate constants can be expressed in terms of equation I.1:

for k_1:

$$n=1,\ E=18.3,\quad \ln k_{10}=11.98 \pm 0.03$$

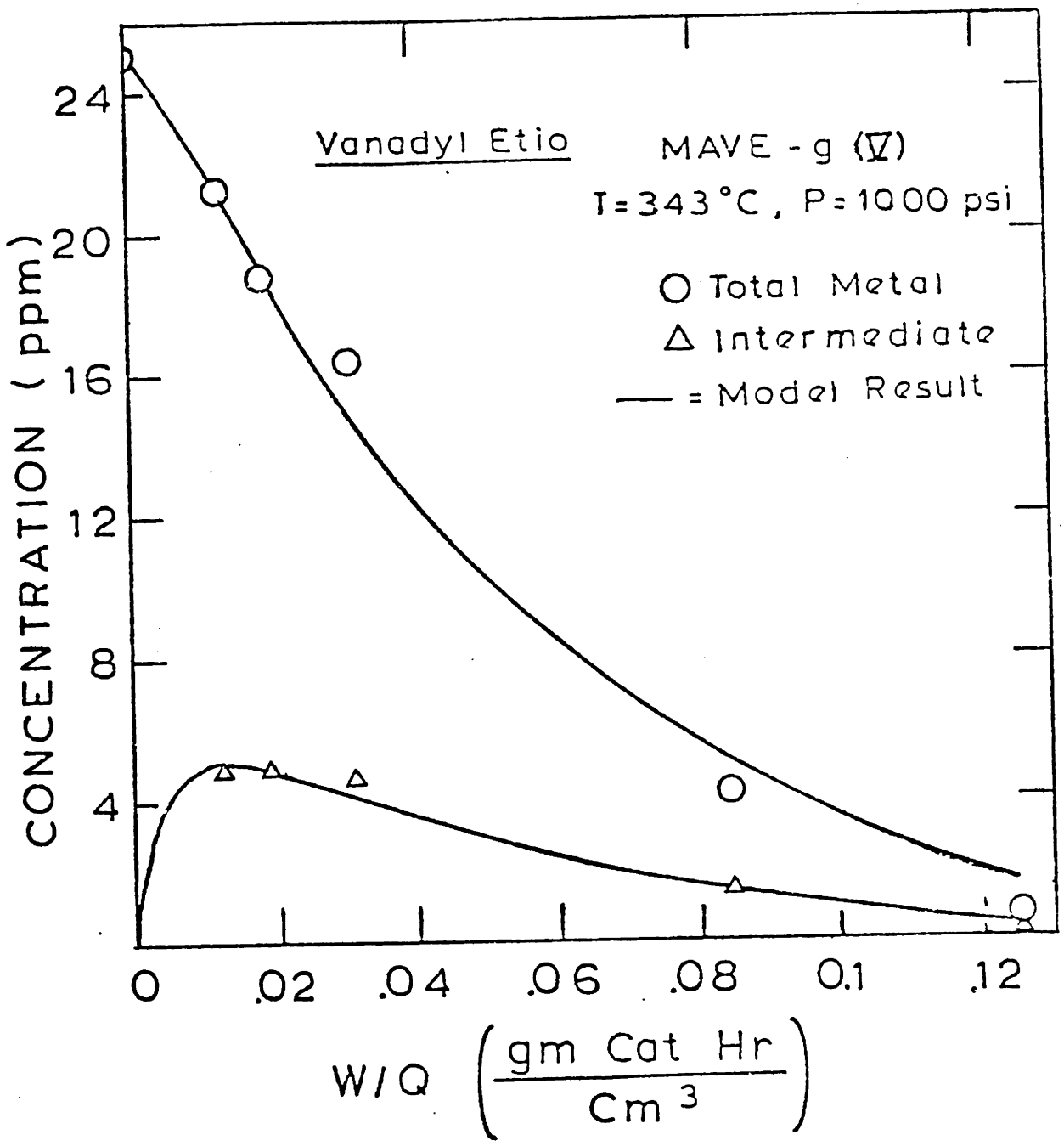

Fig. I-23: Vanadyl Etio-I. Comparison of the Results from the New Model With the Experimental Results.

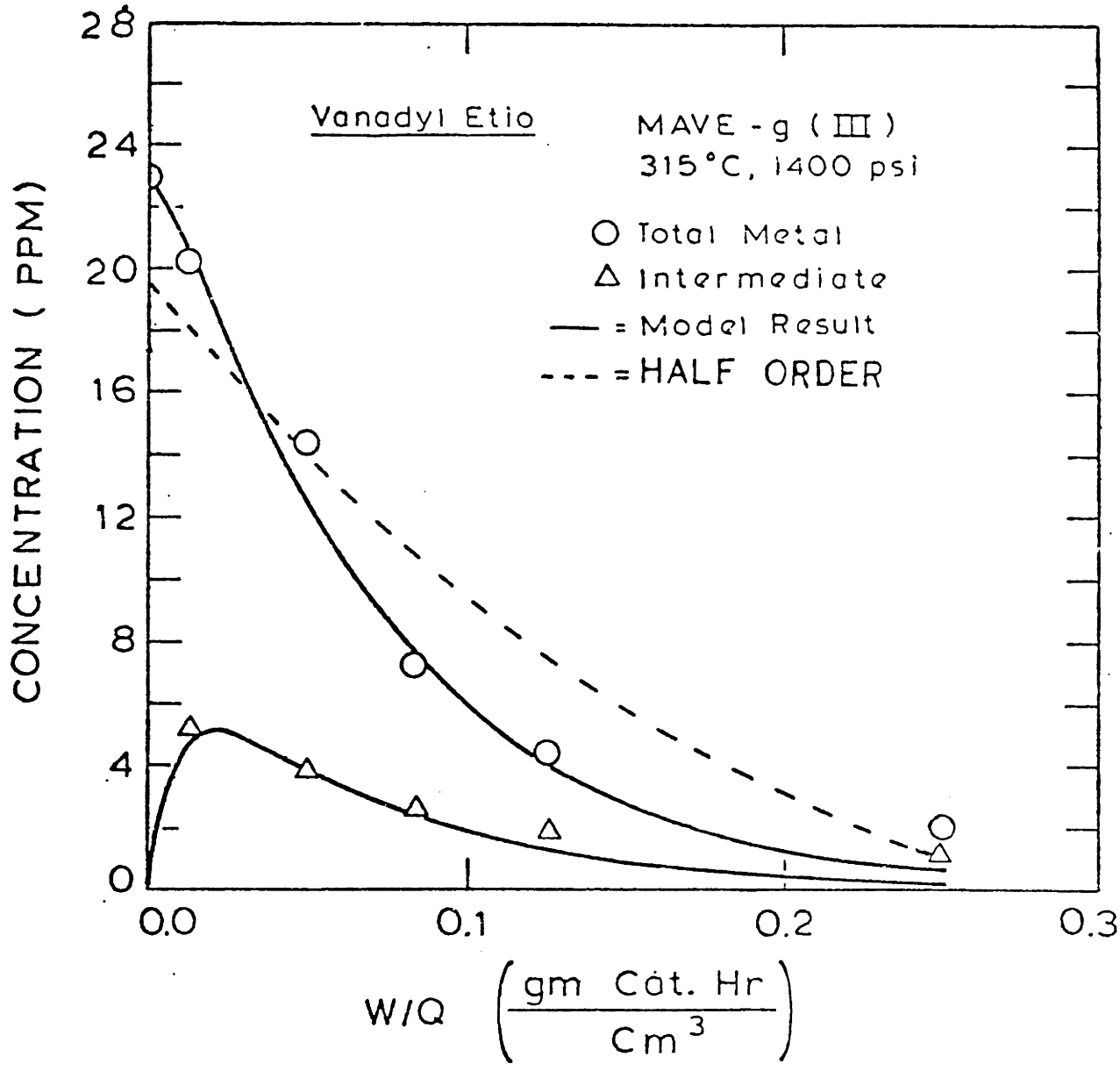

Fig. I-24: Vanadyl Etio-I. Comparison of the New Model and the Half Order Kinetics with the Experimental Results.

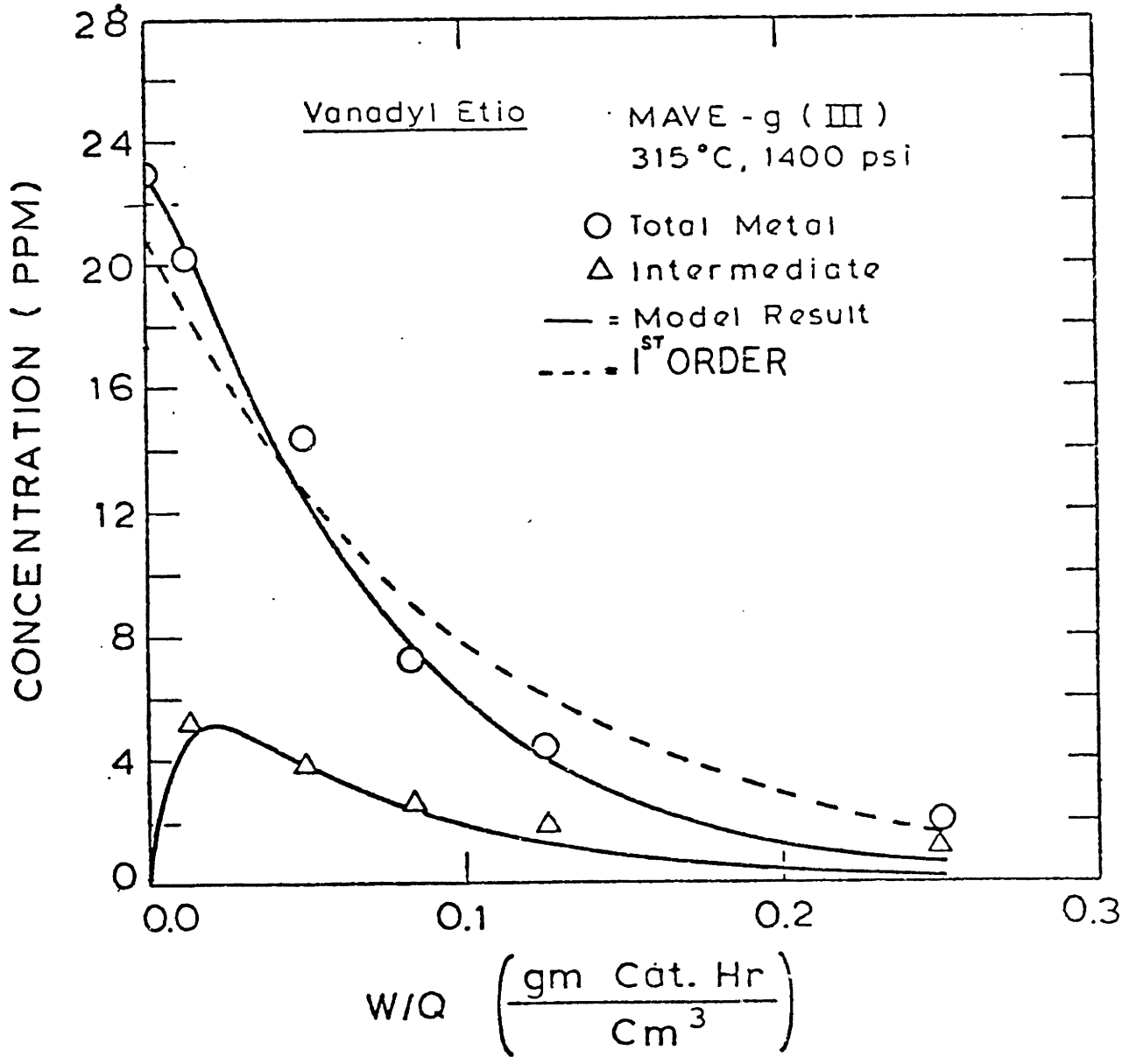

Fig. I-25: Vanadyl Etio-I. Comparison of the New Model and the First Order Kinetics with the Experimental Results.

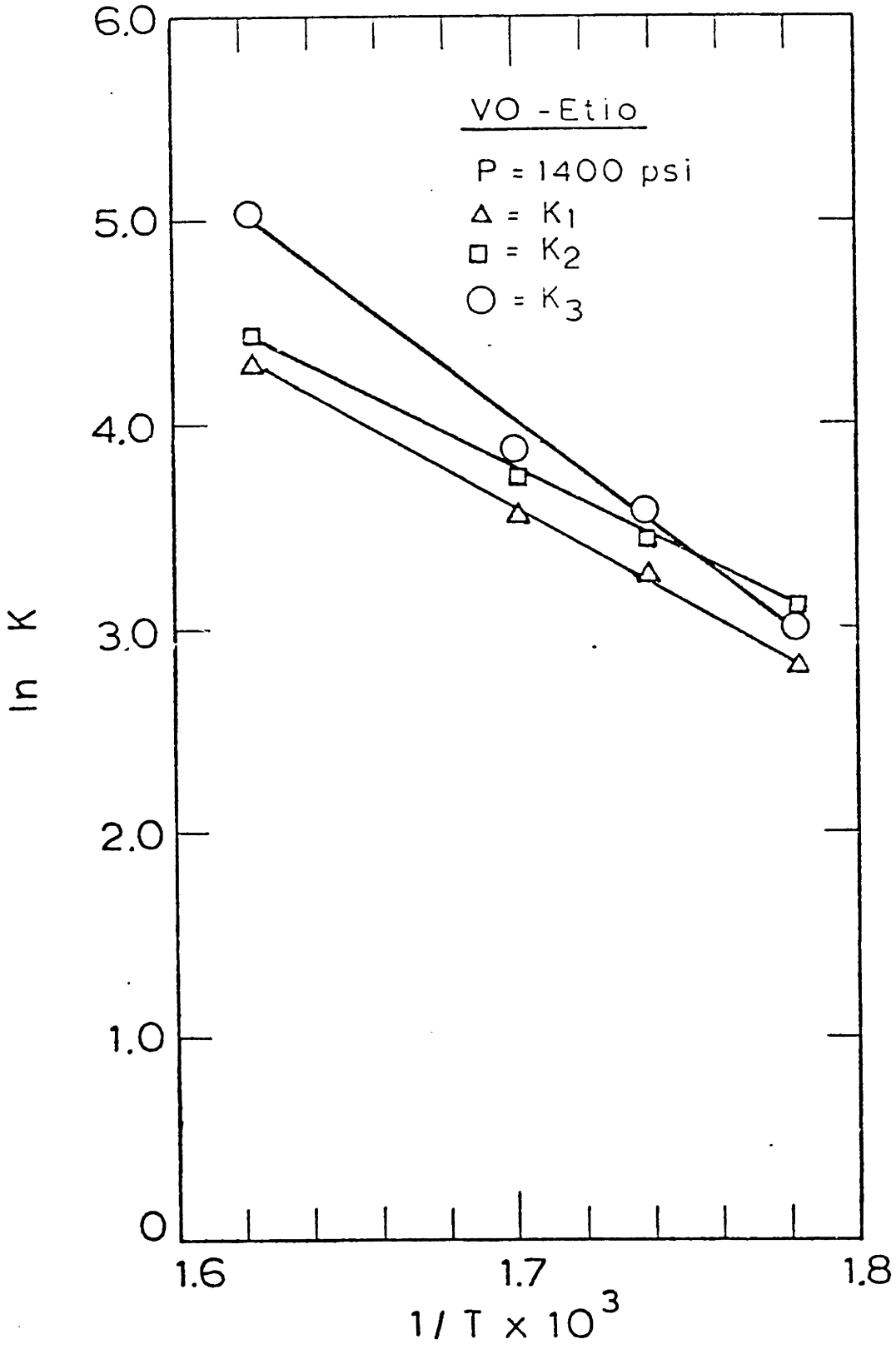

Fig. I-26: Arrhenius Plot for the Rate Constants k_1, k_2 and k_3 at the Hydrogen Pressure of 9.65 MPa. T is in °K and rate Constants are in ml/g-hr.

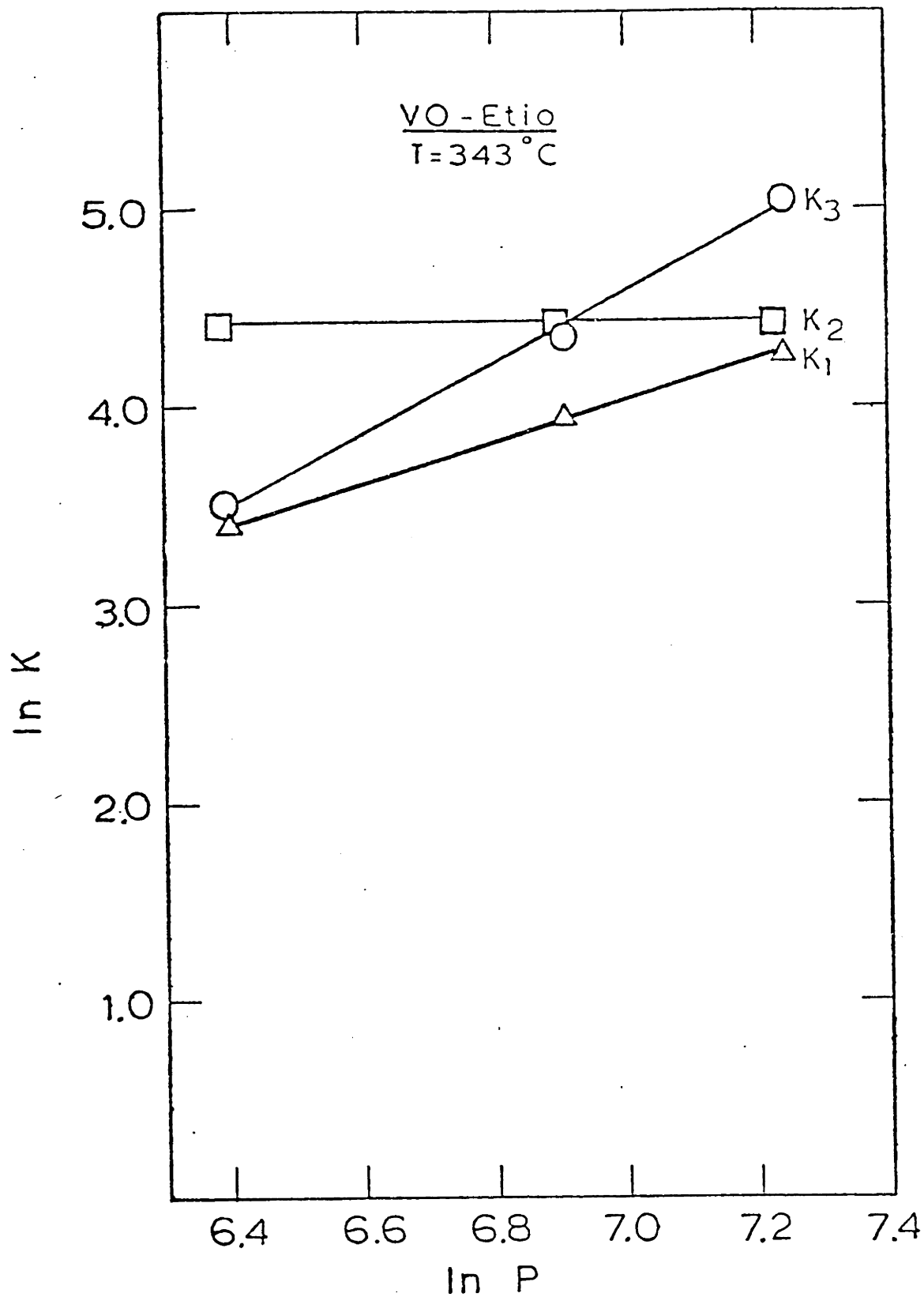

Fig. I-27: Dependence of the Rate Constants k_1, k_2 and k_3 on the Hydrogen Pressure. P is in psig and rate constants are in ml/g-hr.

for k_2:

$n=0$, $E=16.5$, $\ln k_{20}=17.88 \pm 0.02$

for k_3:

$n=1.82$, $E=24.9$, $\ln k_{30}=12.16 \pm 0.08$

and for k_3 if the value of n is taken to be 2 then:

$n=2$, $E=24.9$, $\ln k_{30}=10.89 \pm 0.11$

The last check of the model is to see the effect on the rate constants of the change in the inlet solution concentrations to the reactor. For vanadium it is found that in the concentration range studied, the rate constants are independent of the inlet concentration to the reactor.

Thus we conclude kinetics section with the observation that adequate HDM kinetic models for both vanadium and nickel Etioporphyrin have been developed. It is possible to have the values of the rate constants k_1, k_2 and k_3 such that the total metal disappearance rate may look like a first order or even a fractional order. This explains some of the confusion in the literature.

E.3. SIMULTANEOUS REACTION AND DIFFUSION RESULTS AND THEIR DISCUSSION: In this section the metal deposition profiles inside the 1/16" catalyst extrudates at various reactor positions are discussed.

In a typical run, a one inch O.D. reactor tube was packed with about five grams of 1/16" catalyst extrudates. To insure that there were no cracks in the catalyst extrudates and their ends were not badly broken, each of the catalyst extrudates were carefully handpicked. Also the length of catalyst particles used were controlled within the range of 5mm to 7mm. Through the reactor the metal solution was pumped at the flow rates of 10 ml/hr to 40 ml/hr (0.5-2.0 hr^{-1} L.H.S.V.). In any single run the total amount of the solution pumped was about 1500 ml and the total number of hours on stream were 35-100 hrs. During the run, the liquid samples were collected at various time intervals. At the end of the run, the catalyst from various reactor positions were collected and analyzed for the metal deposition profiles. Calculations of the probable transport limitations for this reactor are done, and it is found that intraparticle mass transfer limitation is the only significant one.

The variation of the reactor outlet solution concentration with time on stream are plotted in figures I-10 and I-11. Similar behaviour is observed for both the vanadium and the nickel runs, and has already been discussed in section E.1.

Vanadium runs at the temperatures of 343, 315, and 288°C; pressures of 1000 and 1400 psig; flow rate of 19.5 and 40 ml/hr; inlet concentrations of 19 ppm and 28 ppm; and also at two different catalyst loadings have been made. Of these runs, the metal deposition profiles for two of the runs are plotted in figures I-28 and I-29. These figures show that at the entrance of the bed, the maximum in the metal deposition occurs inside the catalyst and not at the external surface. In the middle and the top sections of the bed, the maxima moved to the external surface, and the metal deposition profiles look like the classical U shape profiles. At the entrance of the bed, low temperature and low hydrogen pressure lead to inward movement of the maxima in the catalyst.

Results similar to the vanadium are also observed for nickel. The metal deposition profiles for the temperature of 315°C and pressure 1400 psig are plotted in figures I-30.

E.3.1. THEORETICAL MODELING: It is assumed that (i) there are no axial and radial dispersion effects, (ii) the interphase resistance between the catalyst particle and the solution is negligible, (iii) the end effects in the catalyst particle can be neglected and (IV) the diffusivities of A and B inside the catalyst do not change with time. For our runs the metal loadings on the catalyst particles are not large and the last assumption is justified.

Run # CAVE - 4
Vo - Etio
T = 343 °C, P = 1000 psi
W/Q = 0.257 $\frac{gm-hr}{ml}$

x = Cat - 1
o = Cat - 2
--- = $D_A = D_B = 1.6 \times 10^{-6}$ cm²/sec
—— = $D_A = 1.8 \times 10^{-6}$ cm²/sec, $D_B = 0.6 \times 10^{-5}$ cm²/sec

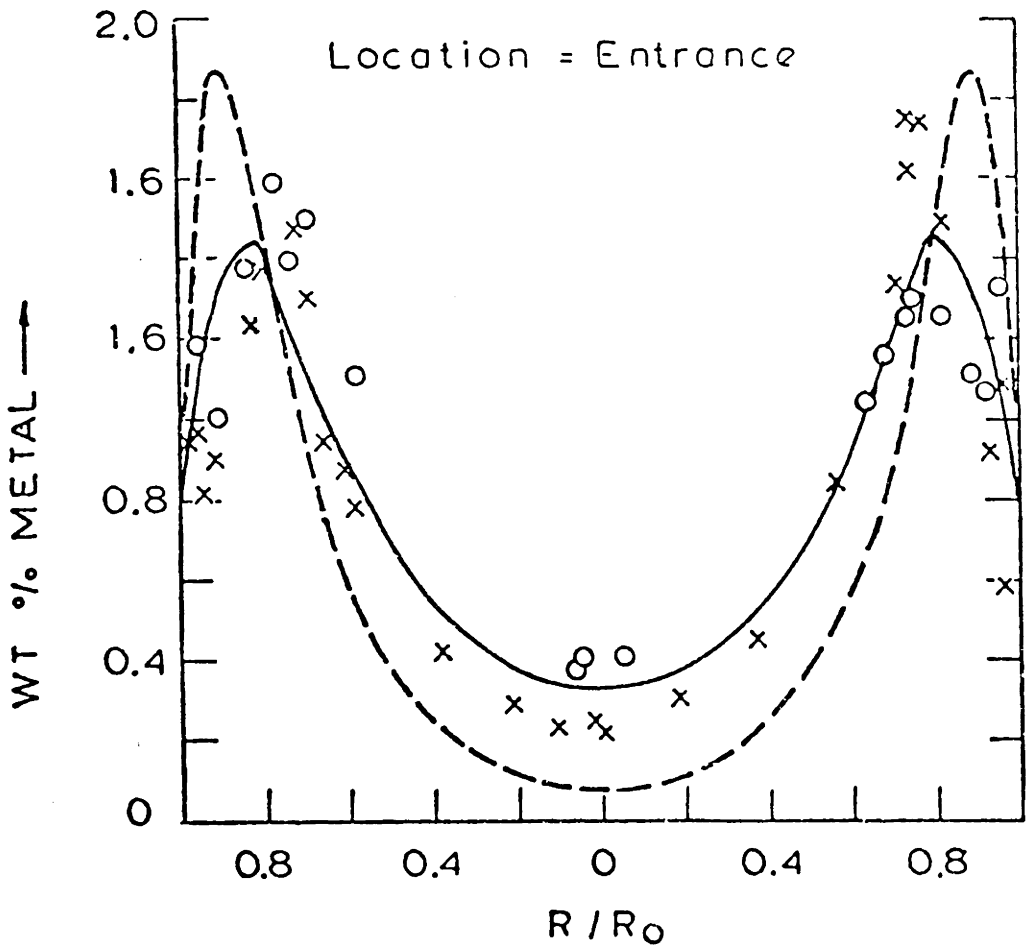

FIGURE I-28a: Vanadium Deposition Profile in the Catalyst

Run # CAVE - 4
Vo - Etio
T = 343°C, P = 1000 psi
$W/Q = 0.257 \frac{gm-hr}{ml}$

x = Cat - 1
o = Cat - 2
Δ = Cat - 3
--- = $D_A = D_B = 1.6 \times 10^{-6}$ cm²/sec
—— = $D_A = 1.8 \times 10^{-6}$ cm²/sec, $D_B = 0.6 \times 10^{-5}$ cm²/sec

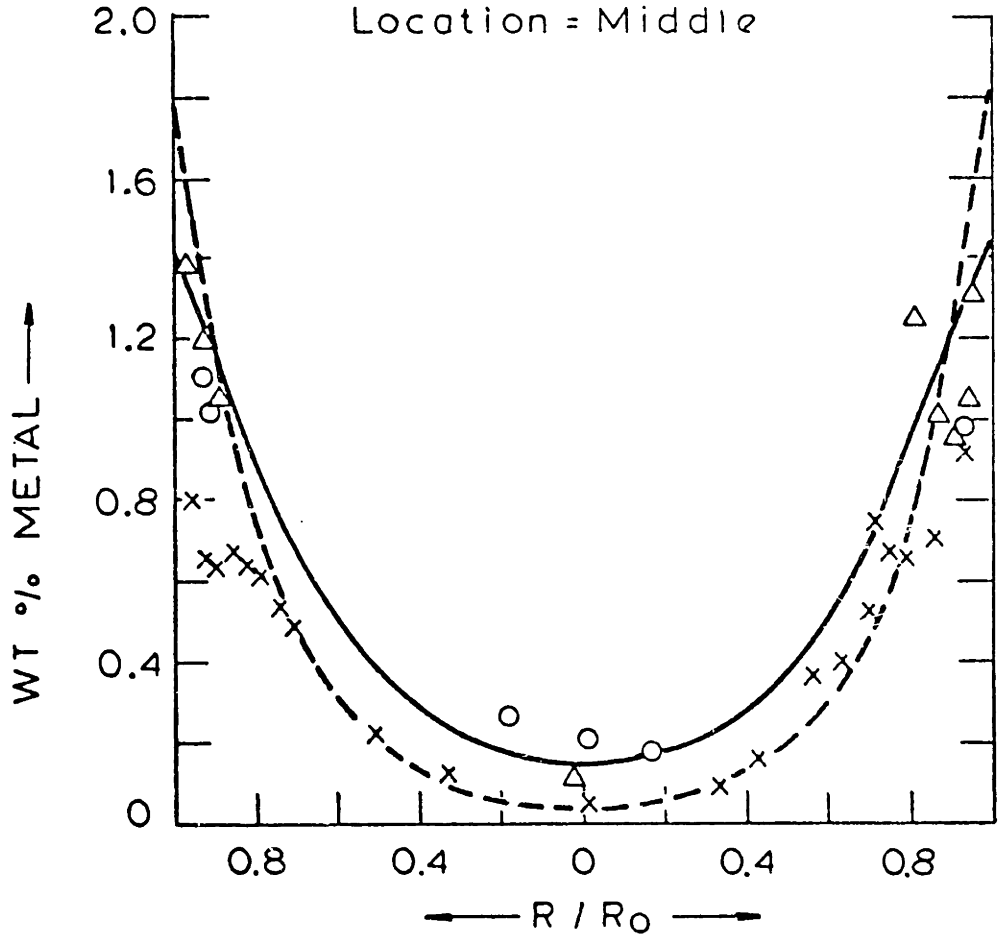

FIGURE I-28b: Vanadium Deposition Profile in the Catalyst

Run # CAVE - 4
Vo -Etio
T = 343 °C, P = 1000 psi
W/Q = 0.257 $\frac{gm-hr}{ml}$

x = Exp Value
--- = $D_A = D_B = 1.6 \times 10^{-6}$ cm²/sec
——— = $D_A = 1.8 \times 10^{-6}$ cm²/sec, $D_B = 0.6 \times 10^{-5}$ cm²/sec

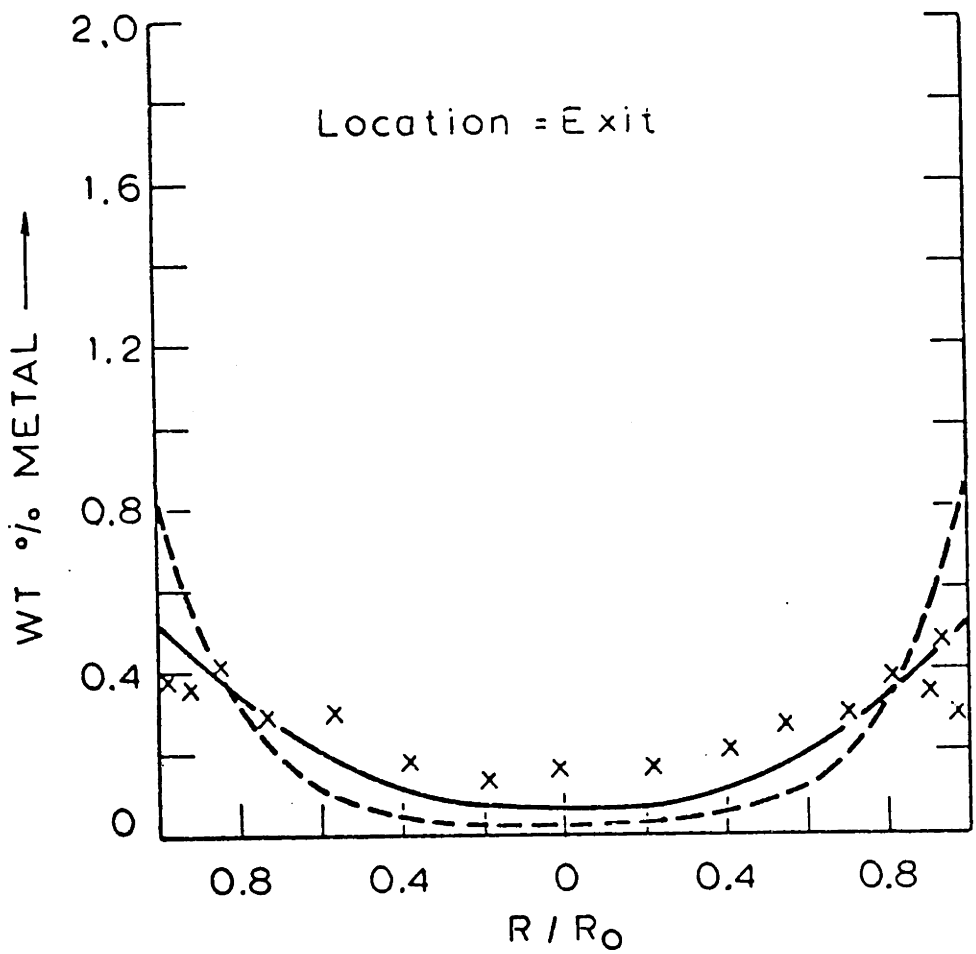

FIGURE I-28c: Vanadium Deposition Profile in the Catalyst

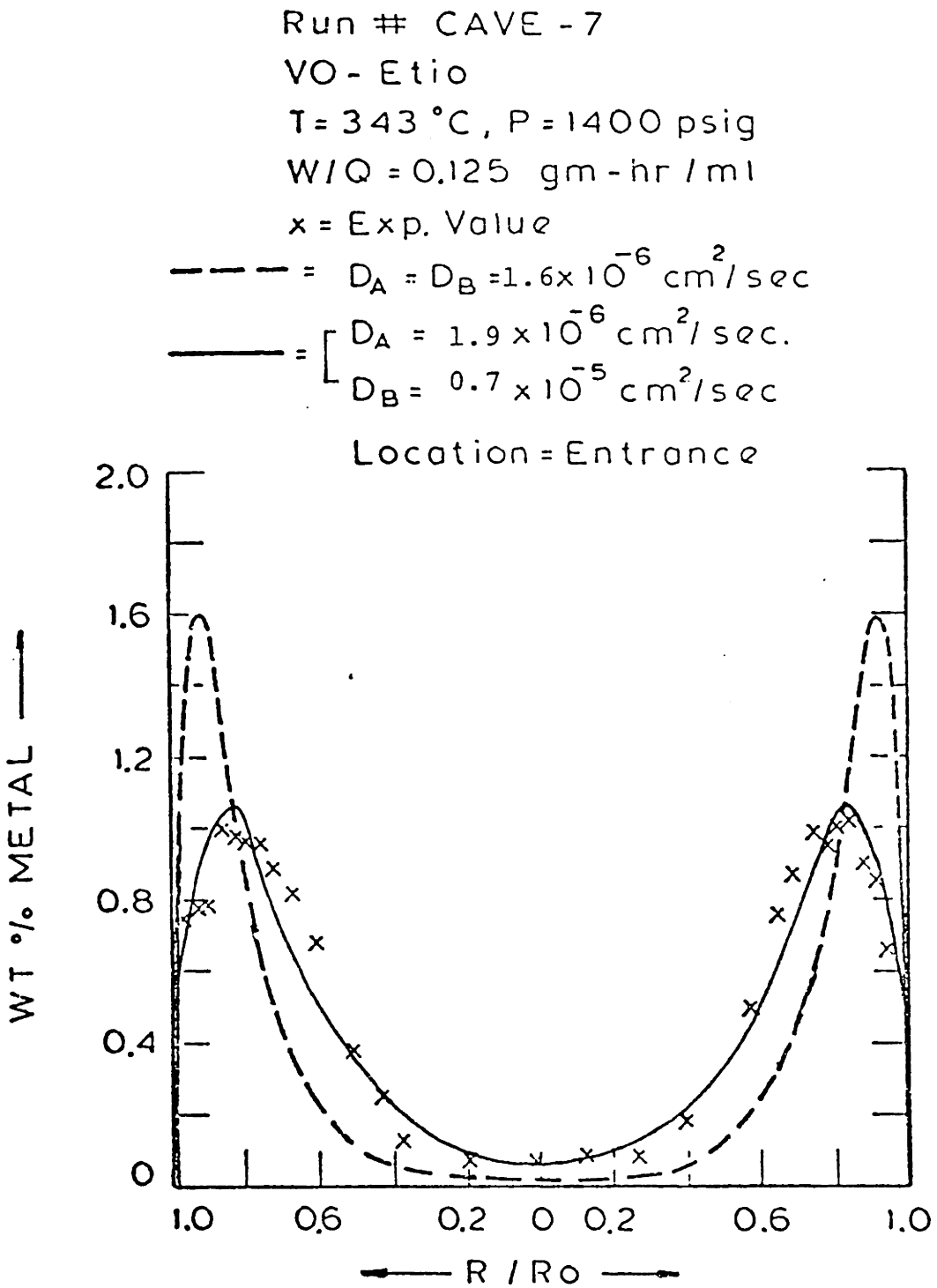

FIGURE I-29a: Vanadium Deposition Profile in the Catalyst

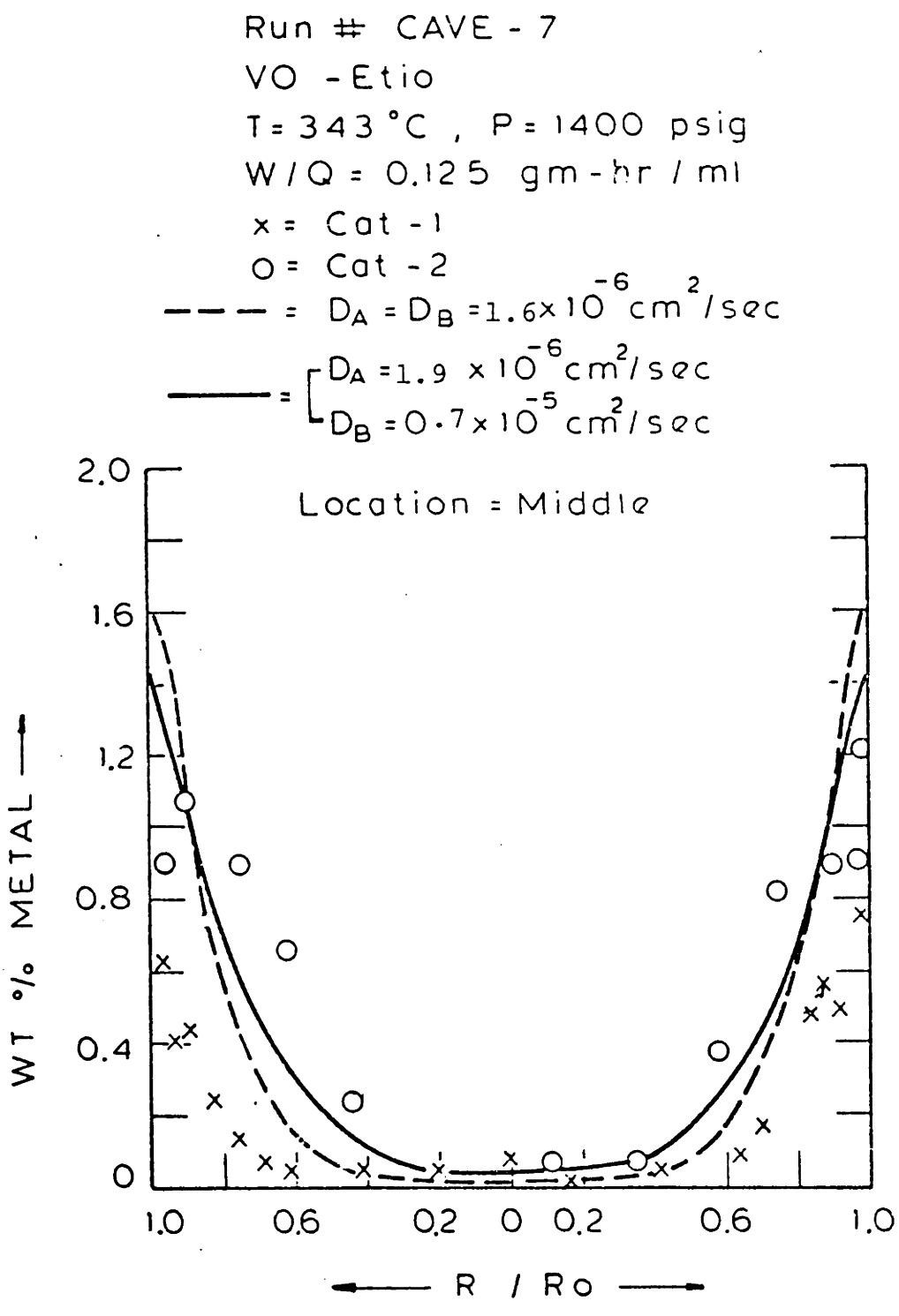

FIGURE I-29b: Vanadium Deposition Profile in the Catalyst

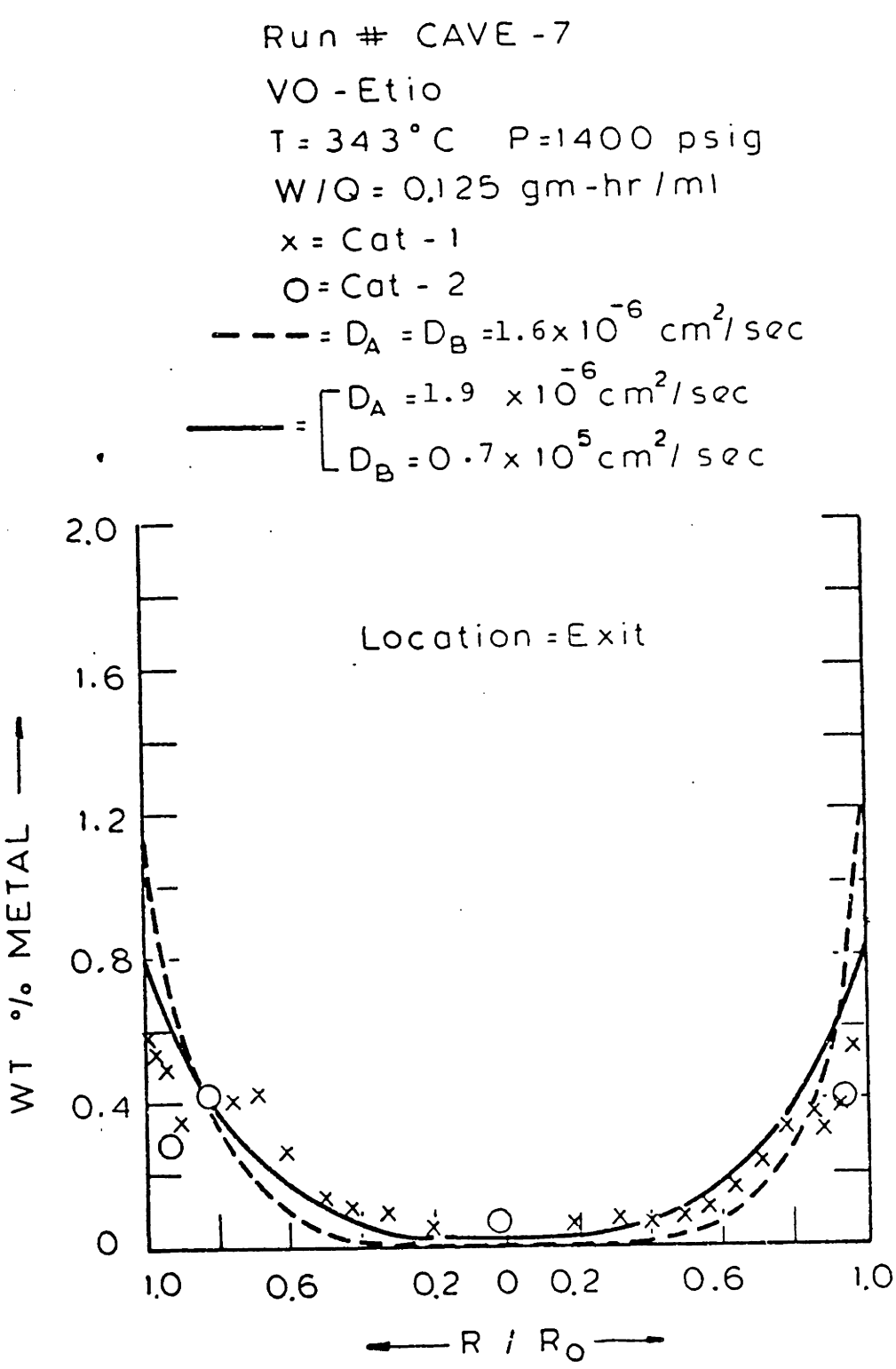

FIGURE I-29c: Vanadium Deposition Profile in the Catalyst

Run # CANE - 8
NI - Etio
T=315 °C, P=1400 psi
$W/Q = 0.256 \frac{gm-hr}{ml}$

O = Exp Value
—— = $D_A = D_B = 2.5 \times 10^{-6} cm^2/sec$

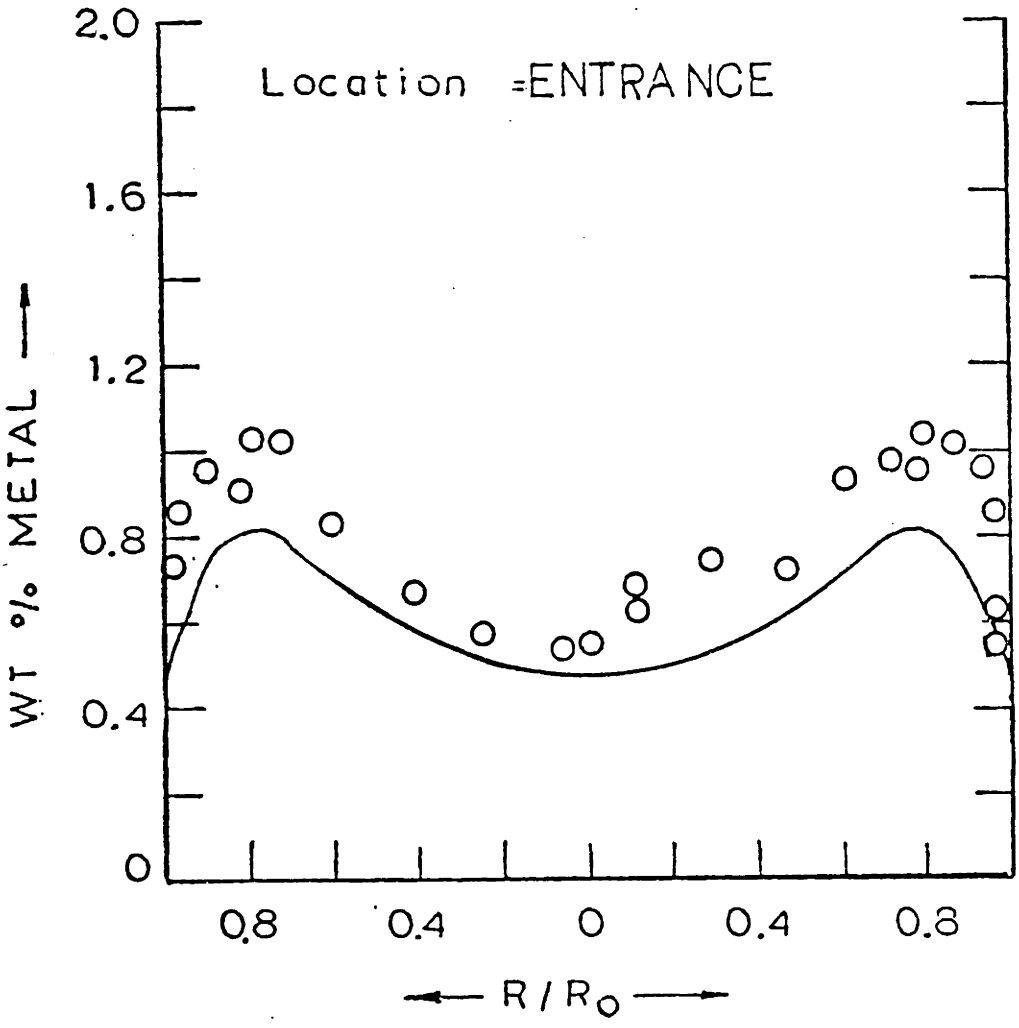

FIGURE I-30a: Nickel Deposition Profile in the Catalyst

Run # CANE - 8
NI - Etio
T = 315°C, P = 1400 psi
$W/Q = 0.256 \frac{gm-hr}{ml}$

O = Exp Value
—— = $D_A = D_B = 2.5 \times 10^{-6} cm^2/sec$

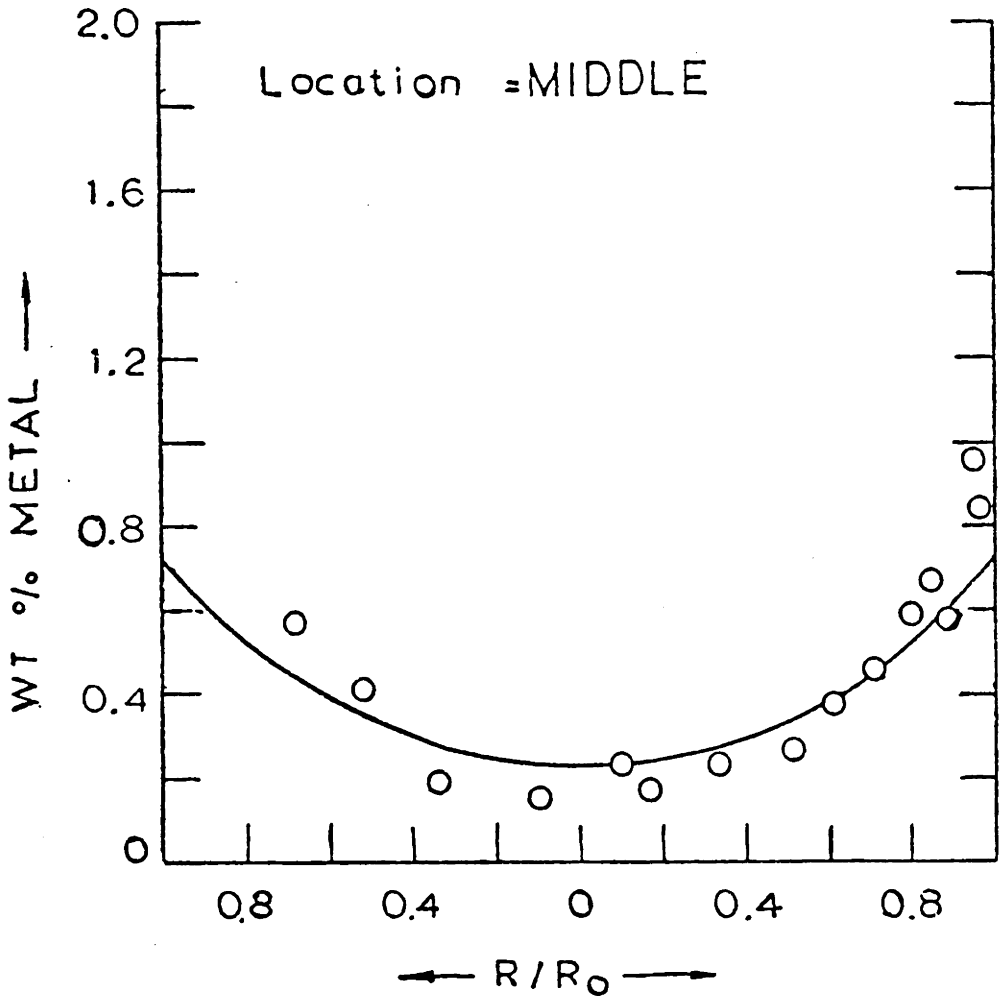

FIGURE I-30b: Nickel Deposition Profile in the Catalyst

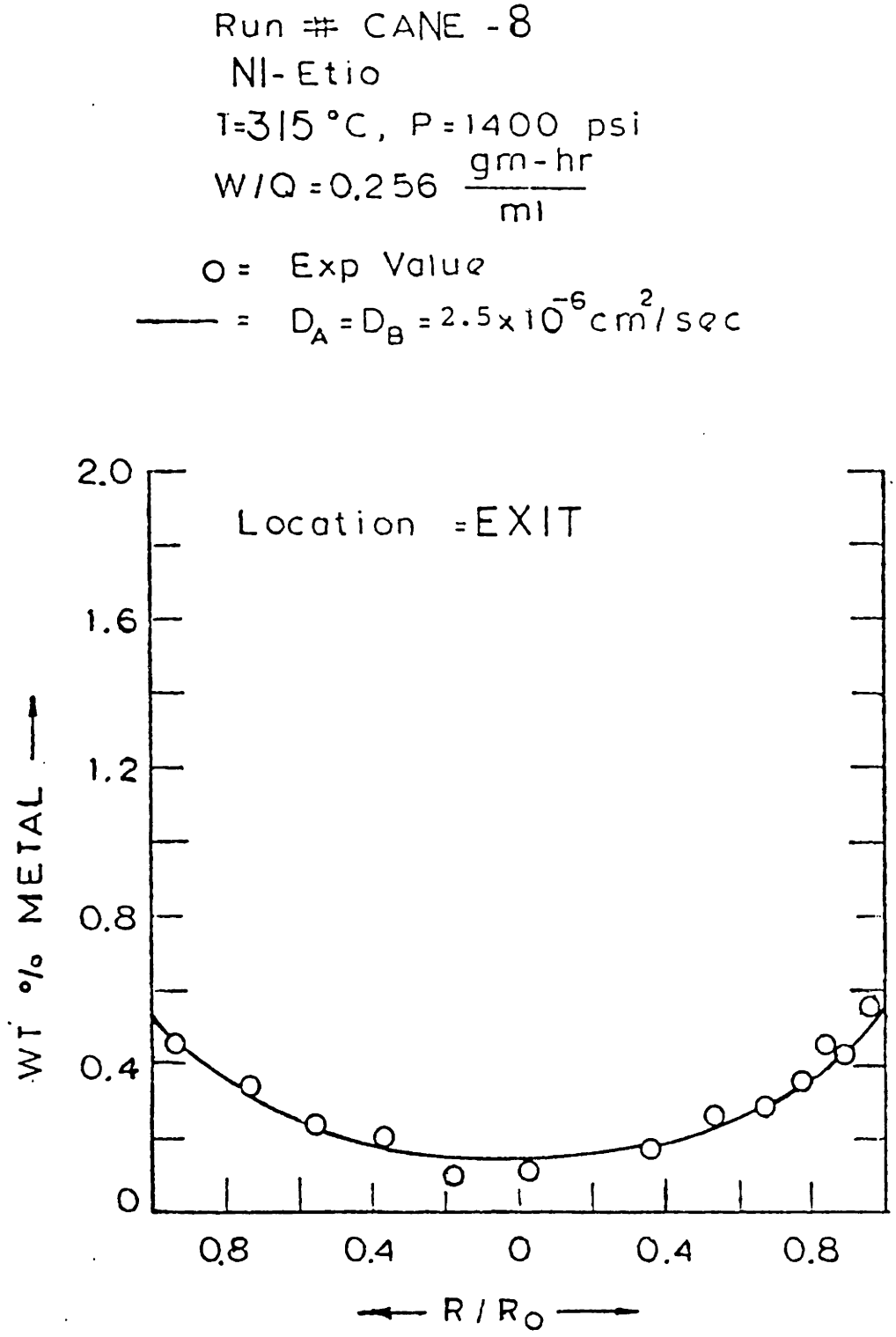

FIGURE I-30c: Nickel Deposition Profile in the Catalyst

First the equations for the flux and the concentration profiles inside a catalyst particle for an arbitrary surface concentrations are developed. Then these equations are integrated over the total bed height to give the exit stream concentrations as a function of the inlet concentrations. The method used for solving the equations has been described by Wei (1962-a,b).

From the Fick's law the steady state diffusion, with the hydrodemetallation reactions inside an infinite cylinder, can be described by the following equations:

$$\frac{-D_A}{\rho_c} \nabla^2 A_c = -k_1 A_c + k_2 B_c \qquad \text{I.2}$$

$$\frac{-D_B}{\rho_c} \nabla^2 A_c = k_1 A_c - k_2 B_c - k_3 B_c \qquad \text{I.3}$$

where ∇^2 is the Laplace operator for the cylinderical coordinates. A_c and B_c are the concentrations of A and B inside the catalyst particle respectively, and ρ_c is the density of the catalyst. The boundary conditions for these two equations are:

$$\text{at } r=0, \quad \frac{\partial A_c}{\partial r} = \frac{\partial B_c}{\partial r} = 0 \qquad \text{I.4}$$

$$\text{at } r=R_c, \quad A_c=A_s \ , \ B_c=B_s \qquad \text{I.5}$$

where A_s and B_s are concentrations in the solution at the outer surface of the catalyst. The above set of equations are readily solved to give diffusion disguised rate parameters k_1^+, k_2^+, k_3^+ and k_4^+. Therefore analytical expressions for the flux and the concentration profiles are known. The mass balance over the differential section dW of the bed gives:

$$-Q \frac{dA_s}{dW} = (k_1^+ + k_4^+) A_s + k_2^+ B_s \qquad \text{I.6}$$

$$-Q \frac{dB_s}{dW} = k_1^+ A_s + (k_2^+ + k_3^+) B_s \qquad \text{I.7}$$

with initial condition:

$$\text{At } W=o,\ A_s=A_o,\ B_s=0 \qquad \text{I.8}$$

where Q is the solution flow rate and dW is the weight of the catalyst in the differential length of the bed. The above set of equations are solved analytically.

For our runs the only unknown parameters were the diffusion coefficients. In order to solve the problem, first a guess of the values of the diffusion coefficients was made. The corresponding diffusion disguised rate parameters were calculated. With these values of the parameters, the reactor exit solution concentrations were calculated by the use of equations I.6 to I.8. If the calculated concentrations matched with the experimental values, the guessed values of the diffusion coefficients

were accepted as the required values. If the concentrations did not agree, then the calculation cycle was repeated with the new guessed values.

In order to calculate the metal deposition profile in the catalyst at a given bed location, the corresponding bulk solution concentrations A_s and B_s were calculated through the equations I.6 to I.8. These values of A_s and B_s were used with equations I.2 to I.5, and the concentration profile B_c in the catalyst was calculated. Finally the metal deposition profile m_d, in time T, in the catalyst was calculated from:

$$m_d = k_3 B_c T \qquad \text{I.9}$$

In order to get a feel of the magnitude of the diffusion coefficient involved, a theoretical estimate of the diffusion coefficient was made. Stokes-Einstein equation, with the configurational correction of Spry and Sawyer (1975) was used. The estimated value of the effective diffusivity at 315^{o}C is 2.5×10^{-6} cm^2/sec.

E.3.2. VANADYL ETIOPORPHYRIN-I: As a first step in the analysis, the diffusion coefficients of the vanadyl Etioporphyrin-I and the reaction intermediate were assumed to be equal. For some of the runs, the experimental and the calculated values of the outlet concentrations are

summarized in Table I-2. It is seen that with the assumption of equal diffusivities, calculated concentrations of the B are on the average 50% higher than the experimental values. The corresponding calculated metal deposition profiles are plotted as dotted curves in figures I-28 and I-29. The assumption of the equal diffusivities gives much higher internal peak near the edge of the catalyst and the lower metal deosition at the center of the catalyst. The calculated values of the diffusion coefficients are listed in Table I-3.

As a next step, the assumption of the equal diffusivities is relaxed. As seen from Table I-2, a better agreement for both the total vanadium and intermediate concentrations are obtained. The corresponding metal deposition profiles are plotted as continuous curves in figures I-28 and I-29. A remarkable agreement between the experimental and the theoretical values are obtained. The calculated values of the diffusion coefficients for the various vanadium runs are tabulated in Table I-3. It turns out that the diffusion coefficient of B is 3 to 5 times higher than A. It is not exactly clear, why the diffusion coefficient for the reaction intermediate should be so much higher than VO-Etioporphyrin.

From the Table I-3 it is observed that for a given temperature, the variations in the (i) inlet solution concentration, (ii) L.H.S.V., (iii) catalyst to inert ratio and (IV) the operating pressure do not change the

TABLE I-2

COMPARISON OF THE EXPERIMENTAL AND THE CALCULATED REACTOR OUTLET SOLUTION CONCENTRATIONS FOR VANADIUM RUNS

Run #	Experimental		Calculated			
			Equal Diffusivity		Unequal Diffusivity	
	M	B	M	B	M	B
CAVE-3	10.8	1.62	9.2	2.63	10.5	1.75
CAVE-4	6.5	1.05	5.9	1.55	5.0	1.04
CAVE-5	16.8	2.82	16.8	4.04	16.5	3.45
CAVE-6	8.4	1.16	7.1	1.76	5.7	1.11
CAVE-7	9.6	1.5	9.6	2.26	8.0	1.45

M = Total metal concentration. It is the sum of the vanadyl etio and the reaction intermediate concentrations (in ppm).

B = Reaction intermediate concentration (in ppm).

TABLE I-3

CALCULATED DIFFUSIVITIES FOR THE VARIOUS VANADIUM RUNS

Run #	T	P	Q	W	A_o	$D_A = D_B$ $D_A X10^6$	$D_A \neq D_B$ $D_A X10^6$	$D_B X10^6$
CAVE-1	343	1400	19.5	4.998	19.1	1.6	1.9	6.0
CAVE-2	343	1400	19.5	4.997	25.7	1.6	1.9	6.0
CAVE-3	315	1400	19.5	5.003	27.1	1.2	0.9	4.5
CAVE-4	343	1000	19.5	5.005	28.4	1.6	1.8	6.0
CAVE-5	288	1400	19.5	4.991	29.3	0.9	0.8	4.2
CAVE-6	343	1400	19.5	2.999	26.6	1.6	1.9	6.0
CAVE-7	343	1400	40	4.999	27.5	1.6	1.9	7.0

Units of diffusion coefficient are cm^2/sec.

T = Temperature in ^oC

P = Pressure in psig

Q = Flow rate of solution in ml/hr.

W = Amount of catalyst in reactor (gms)

A_o = Inlet concentration of vanadyl etioporphyrin (ppm)

Inlet concentration of B is zero.

values of the diffusion coefficients. The values of the diffusivities do increase with the increase of temperature. The calculated values are of the same order of magnitude as the theoretically estimated diffusivity of $2.5X10^{-6}$ cm^2/sec.

E.3.3. NICKEL ETIOPORPHYRIN-I: Calculations similar to vanadium have also been done for the nickel. Unlike vanadium, the assumption of equal diffusivities works very well for the nickel. The calculated values of the diffusion coefficients, along with the calculated reactor outlet concentrations, are listed in Table I-4. The calculated metal deposition profiles at $315^{o}C$ and 1400 psig pressure are plotted in figures I-30. Once again it is observed that for a given temperature, the variations in the inlet solution concentration and the liquid hourly space velocity do not change the values of the diffusion coefficients significantly. The calculated values are also of the same order of magnitude as the theoretically estimated diffusivity of $2.5X10^{-6}$ cm^2/sec.

Finally we finish this section with the conclusion that the second objective of this thesis has been successfully achieved.

TABLE I-4

SUMMARY OF THE CALCULATED AND THE EXPERIMENTAL RESULTS FOR NICKEL

Run #	T	Q	A_o	OUTLET SOLUTION CONC.				$D_A = D_B$
				EXPERIMENTAL		CALCULATED		$D_A X 10^6$
				M	B	M	B	$Cm^2/sec.$
CANE-7	343	30	28.6	11.1	1.33	11.0	1.33	1.6
CANE-6	343	19.5	28.1	7.6	0.93	7.7	0.94	1.2
CANE-9	343	14.7	27.5	5.5	0.97	5.7	0.7	1.0
CANE-10	343	30	16.8	5.1	0.62	5.0	0.62	1.5
						5.1	0.62	2.7*
CANE-4	343	19.5	26.4	7.5	--	7.5	0.92	1.1
CANE-5	343	19.5	25.8	6.9	--	6.8	0.84	1.3
CANE-8	315	19.5	27.2	10.6	1.64	10.6	2.04	2.5

T = Temperature in ^oC

Q = Flow rate of solution in ml./hr.

A_o = Inlet concentration of nickel etioporphyrin (ppm)

M = A+B = sum of the concentrations of the nickel etio and the nickel chlorin.

* These calculations are done with the rate constants which are not corrected for the lower inlet concentration. For all the runs the pressure is 1400 psig and the amount of catalyst in the reactor is about 5 gms.

F. THEORETICAL POISONING STUDIES: The bimodal spherical catalyst is modelled as a spherical macroporous particle consisting of small spherical microporous particles of uniform size called grains; and is shown in figure I-31. It is assumed that the metal deposit does not affect the intrinsic demetallation activity per unit surface area, but it reduces the surface area and may affect the restricted diffusion in the pores. The restricted diffusivity in a pore is written as (Spry and Sawyer-1975):

$$D = D_o \, G(\alpha) \qquad \text{I.10}$$

where D_o in the bulk diffusivity and α is the ratio of the molecular radius R_m to the pore radius R, and

$$G(\alpha) = (1-\alpha)^4 \qquad \text{I.11}$$

The surface area available for the chemical reaction in the macropores is much smaller than the one in microspheres. Therefore the reaction in macropores are neglected. For the qualitative calculation purposes diffusivities of A and B have been assumed to be equal. To describe the demetallation and the diffusion in the catalyst pores, pseudo steady state approximation is used. The conservation equation for A in the macropores is:

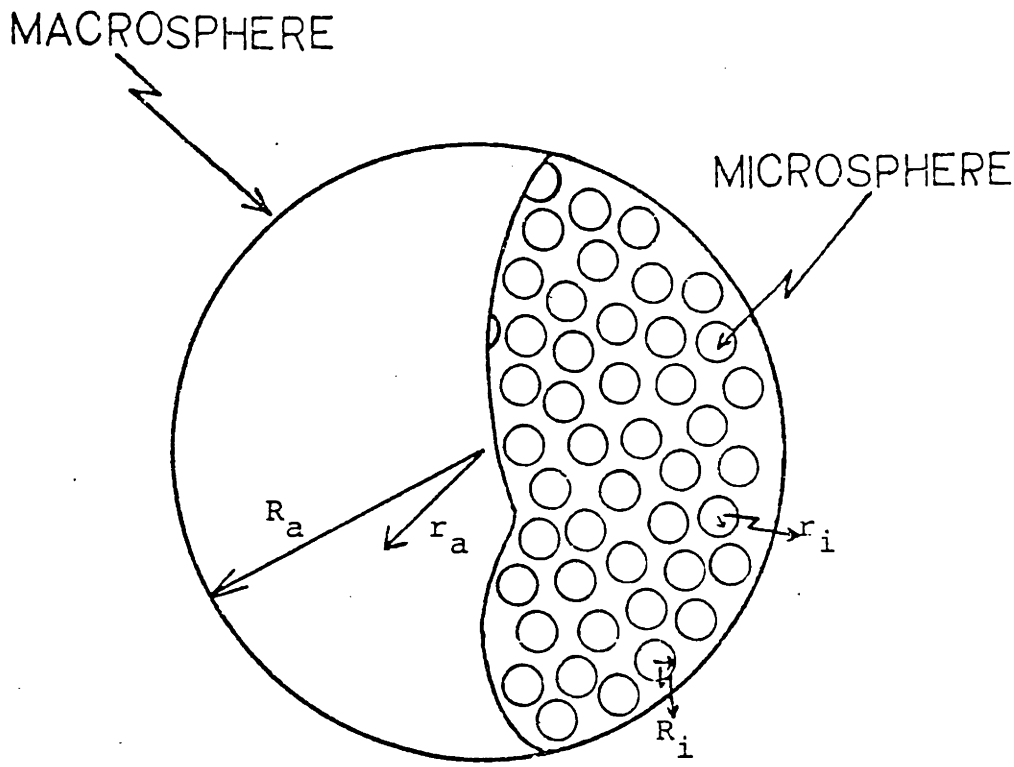

FIGURE I-31: Schematic Sketch of the Grain Model Catalyst.

$$\frac{D_a}{r_a^2}\frac{\partial}{\partial r_a}\left[r_a^2\frac{\partial A_a}{\partial r_a}\right] = n.4\P R_i^2 D_i\left(\frac{\partial A_i}{\partial r_i}\right)_{r_i=R_i} \qquad \text{I.12}$$

An identical equation for B is also written. In the above equation and throughout this chapter, subscripts a and i refer to macrosphere and microspheres (grain) respectively. R_i is the radius of the microsphere. D_a and D_i are effective diffusivities and related to the D of equation I.10 by:

$$D_a = \frac{\varepsilon_a D_o G(\alpha_a)}{\tau_a} \qquad \text{I.13}$$

$$D_i = \frac{\varepsilon_i D_o G(\alpha_i)}{\tau_i}$$

where ε_a and ε_i are the porosities and τ_a and τ_i are tortuosities. For macrospheres $G(\alpha_a)$ is very close to unity. n is the number of microspheres per unit volume of macrosphere and is given by:

$$n = \frac{3(1-\varepsilon_a)}{4\P R_i^3} \qquad \text{I.14}$$

The boundary conditions for equation I.12 are:

$$\text{at } r_a=0\ ,\ \frac{\partial A_a}{\partial r_a} = 0 \text{ and at } r_a=R_a\ ,\ A_a=A_s$$

The pores in the microspheres are idealized as parallel pores. Each of these pores are of same length L and radius R_p:

$$L = \frac{R_i \sqrt{\tau_i}}{3} \qquad \text{I.15}$$

$$N_p = \frac{4\epsilon_i R_i^2}{R_p^2 \sqrt{\tau_i}} \qquad \text{I.16}$$

where N_p is number of idealized micropores in a microsphere. The resulting conservation equations for an idealized pore are:

$$\frac{\partial}{\partial X}\left(R^2 D \frac{\partial A_i}{\partial X}\right) = 2R(K_1 A_i - K_2 B_i) \qquad \text{I.17}$$

$$\frac{\partial}{\partial X}\left(R^2 D \frac{\partial B_i}{\partial X}\right) = 2R(K_3 B_i + K_2 B_i - K_1 A_i) \qquad \text{I.18}$$

with Boundary conditions:

$$\text{at } x = L \text{ , } A_i = A_a \text{ , } B_i = B_a$$

$$x = 0 \text{ , } \frac{\partial A_i}{\partial X} = \frac{\partial B_i}{\partial X} = 0 \qquad \text{I.19}$$

where R is the radius of the pore at any time, D is the diffusivity given by equation I.10, A_i and B_i are concentrations of A and B inside the pore, K_1, K_2 and K_3 are rate constants per unit surface area, and x is the axial length coordinate.

For the given values of the surface concentrations A_s and B_s, the above set of equations are solved numerically. The metal is allowed to deposit for time Δt, and the new values of R for a pore at a point in macrosphere are calculated from:

$$\frac{dR}{dt} = \frac{-10^{-6} K_3}{\rho_m} B_i \qquad \text{I.20}$$

ρ_m is the density of the deposited metal. With the new values of R, the equations are again solved for the concentration profiles. These calculations are repeated till the catalyst is nearly inactive.

In order to simulate the unimodal catalyst, equations for the microspheres (I.15 to I.19) with the radius equal to the catalyst particle are used.

Some of the simulation results on the performance of the unimodal and the bimodal catalysts are plotted in figure I-32. The pertinent parameters used are: K_1 = 0.407, K_2 = 0.467 and K_3 = 0.883 ml/hr-meter^2; radius of the metal porphyrin molecule = 7.1Å, density of

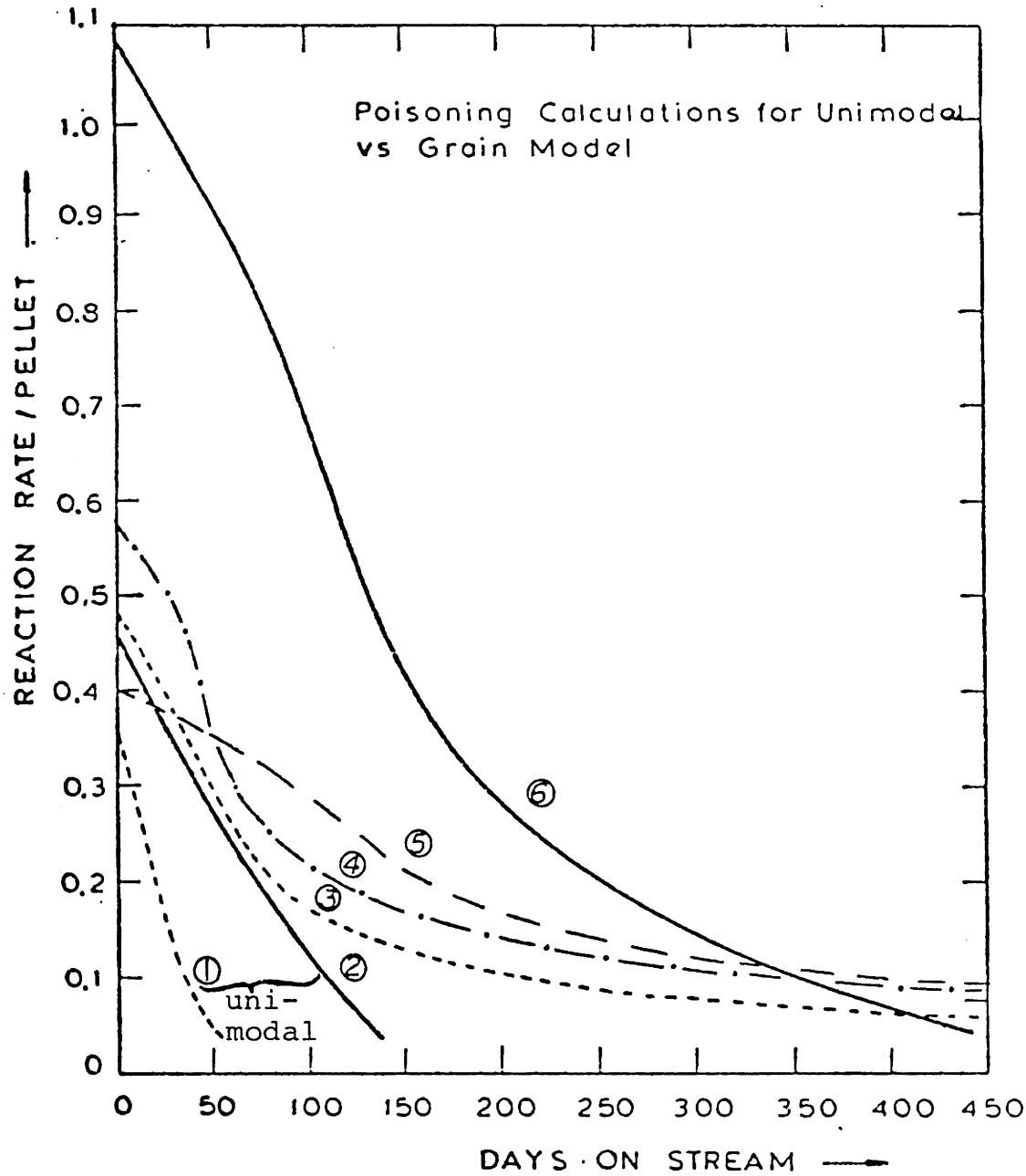

FIGURE I-32: Comparison of the Poisoning Behavior of the Unimodal Model with the Grain model. The Curves are explained in Table I-5.

the deposited metal = 6.1 g/ml, ε_a = 0.26, ε_i = 0.5, $D_o = 1.1X10^{-6}$ cm^2/sec, radius of catalyst particle = 0.079 cm and the concentrations of A and B at the surface of the macrosphere are 50 ppm and 0 ppm respectively. In the computer simulations of the figure I-32, all these parameters are held constant and the effect of the change in micropore radius and the grain size is observed. The pertinent results of the fig. I-32 are summarized in Table I-5.

For the given porosity of 0.5, a unimodal catalyst with the maximum initial activity is designed (curve ② in figure I-32). This catalyst is then crushed and a pellet is made from it. The performance of this new pellet depends on the macropore diffusivities. Curves ⑤ and ⑥ are the results of the two values of macropore diffusivities. For curve ⑥, $D_a \tau_i / \varepsilon_i D_o$ is about 4. It is observed that as compared to the original unimodal catalyst, the initial rate of this catalyst is 2.3 times more and the time on stream is about 3.2 times more (Table I-5). However, more impressive fact is that per unit volume of the catalyst material, this catalyst can take 6.7 times more metal loading than the unimodal catalyst.

The phenomenal increase in the performance of the catalyst of curve ⑥ is attributed to high macropore diffusivity. For the curve ⑤, the tortuosity in the macropore and the micropore are taken to be same, and therfore $D_a \tau_i / \varepsilon_i D_o = 0.52$. This time it is observed that

TABLE I-5

POISONING CALCULATIONS FOR UNIMODAL AND BIMODAL CATALYSTS

Curve #	Model	R_i	R_p	r_p	r_v	$m_p X 10^3$	m_v	T_s
①	U	-	18.0	0.37	179	0.23	0.11	36
②	U	-	35.5	0.46	223	0.80	0.39	110
③	G	42.5	18.0	0.49	321	1.19	0.78	204
④	G	1.0	15.9	0.58	380	1.83	1.20	340
⑤	G	42.5	35.5	0.40	264	2.00	1.31	391
⑥	G	42.5	35.5	1.08	707	3.99	2.61	357

where:

U = Unimodal catalyst model

G = Grain model

R_i = microsphere radius in micron

R_p = micropore radius in Å

r_p = Initial rate/pellet

r_v = Initial rate/volume of catalyst material (when r_p is corrected for the macropore volume r_v is obtained).

m_p = gm of metal deposited/catalyst pellet

m_v = gm of metal deposited/volume of catalyst material

T_s = Days elapsed before the cutoff rate of r_p = 0.1 is achieved.

The value of $D_a \tau_i / \varepsilon_i D_o$ is 3.93 for curve ⑥, and for all others it is 0.52.

the initial rate of the catalyst is about 87% of the unimodal catalyst. But within 20 days of operation the activity of the bimodal catalyst catches up with the original unimodal catalyst, and from then onwards it is always higher. From Table I-5, it is observed that bimodal pellet lasts on stream for 3.6 times more days and the metal loading per unit volume of the catalyst material is 3.4 times more than the unimodal catalyst.

The next question to consider is that whether it is possible with the assumption of tortuosity in macro and micropore same, to get the initial rate of bimodal pellet higher than the most optimum unimodal catalyst pellet. Curves ③ and ④ in figure I-32 are the answers. For catalyst ③, the grain size is the same as that of curves ⑤ and ⑥, but the micropore size has been chosen to be 18.0Å. For curve ④ the pore radius and the grain sizes are 15.9Å and 1.0 micron respectively. Both of these bimodal catalysts show better performance than the most optimum unimodal catalyst ②. It is interesting to observe that if a unimodal catalyst is made of the same pore size as the micropore of bimodal pellet ③, its performance is much worse than catalyst ② (curve ① in fig. I-32).

We conclude this section with the observation that bimodal catalysts are much better for hydrodemetallation.

G. CONCLUSIONS:

1. It is found that in the initial transient phase of the reactor, the activity of the catalyst first decreases, then increases and finally levels off. The increase in the activity is attributed to the nickel and vanadium depcsition on the catalyst. There is an increase in both the hydrogenation and demetallation activities.
2. Prior to the metal removal from the etioporphyrin ring, one major hydrogenated reaction intermediate is formed. For both nickel and vanadium runs, the intermediates have been separated and the corresponding peaks in the visible spectrum have been identified.
3. It is found that in both the nickel and the vanadium hydrodemetallation, three major kinetic steps are involved. The first step is hydrogenation to the reaction intermediate (rate constant k_1). The other two steps are dehydrogenation (rate constant k_2) and the demetallation (rate constant k_3) of the reaction intermediate.
4. For both the metals, hydrogenation step is first order with respect to the metal etioporphyrin concentration in the solution; and dehydrogenation and demetallation rates have first order dependence on the reaction

intermediate concentration in the solution. The order of dependence of hydrogenation, dehydrogenation and demetallation rates on the hydrogen pressure are first, zero and second respectively.

5. Metal deposition profiles in 1/16 inch catalyst extrudates, at various reactor bed positions, have been studied. It is observed that at the entrance of the bed, the maximum in the metal deposition occurs inside the catalyst and not at its external surface. Low temperature and low hydrogen pressure lead to inward movement of the maxima. In the middle and the top sections of the bed, the maxima moved to the external surface, and the metal deposition profiles look like the classical U shape profiles.

6. Theoretical calculations to simulate the continuous reactor with intraparticle mass transport limitations have been done. Both nickel and the vanadyl etio porphyrins show the diffusivities of the order of 10^{-6} cm^2/sec. This order of magnitude agrees with the theoretically estimated value of the diffusion coefficient. It is found that for vanadium, depending on the temperature of the operation, the diffusion coefficients for the reaction intermediate are 3 to 5 times more than the Vanadyletioporphyrin. For nickel both the etio and the chlorin have same values of the diffusivities.

7. Theoretical calculations are not only successful in giving the proper values of the concentrations of the reactor outlet solutions but are also successful in adequately describing the metal deposition profiles in the catalyst particles at various bed locations.
8. Theoretical poisoning models to predict the initial and the long range activity of the unimodal and bimodal catalysts have been proposed. The bimodal model allows for some connectivity between the macro and micropores. The calculation results show that for hydrodemetallation, bimodal catalyst pellets have much better performance. They not only have a higher initial rate, but also much higher catalyst life time. The bimodal catalysts can take many times more metal loading than the unimodal catalysts.

CHAPTER - II

INTRODUCTION

A. General Background: In a typical refinery, one of the first steps in the refining of the crude petroleum is its distillation in various fractions (Nelson - 1974). The bottom fraction of the fractionation column, also known as residuum, contains a high proportion of sulfur, nitrogen and metal compounds found in the original crude (Figure II-1) (Nelson - 1976). The seemingly insatiable demand for transportation fuels has greatly increased the amount of hydrogen processing of these high molecular weight residues to form gasoline and diesel fuels.

In the crude oils, nearly one half of the elements in the periodic table have been identified as trace elements (Smith et al. - 1959). Of these the most abundant and problematic metals are vanadium and nickel. Table II-1 shows the metal contents of some heavy crudes (Yen - 1975). Depending on the origin of the crude, the concentration of vanadium may vary from 8 parts per million (by weight) to 1200 ppm, while that of nickel from 4 ppm to 100 ppm. For most of the crudes, vanadium is present in larger quantities than nickel.

Following are the main problems caused by the presence of these metal compounds:

DISTILLATION OF CRUDE OIL

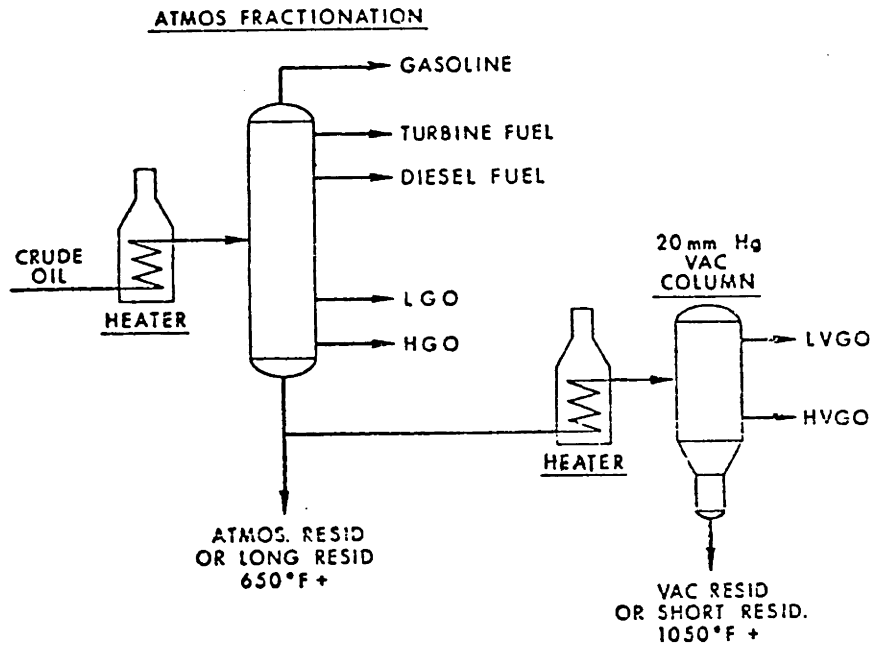

LGO : Light Gas Oil
HGO : Heavy Gas Oil
LVGO: Light Vacuum Gas Oil
HVGO: Heavy Vacuum Gas Oil

Fig. II-1

(From Richardson and Alley - 1975)

TABLE II-1

(From Yen - 1975)

Metal Contents of Some Heavy Crudes (ppm)

Crude Oil	*°API gravity*	*V*	*Ni*
Boscan	10.3	1200	100
Heavy Mara	17.5	961	85.7
Laqunillas	16.3	455	58.3
Taparito	---	393	42
Bachaquero	19.0	355	54.5
Hamaca	6.0	330	83.3
La Canoa	15.2	322	93.5
Cabimas	22.0	280	32
Merey	17.0	205	47
Heavy Orinoco	18.6	199	50.8
Barinas	26.5	158	71
Leona	24.1	126	36
Temblador	20.0	46	43
Baxterville	---	33	15
Kuwait	---	16	4.4
Ragusa	19.9	8.5	68.6
West Texas*	---	4.3	3.3
San Joaquin*		2.8	0.95
Ordovician*		.09	.23

*Actually it is light oil

1. Today, in the western world, it is difficult to find a refinery which does not desulfurize the distillation residues (Riediger - 1976). Desulfurization is done to protect the catalysts further downstream in the refining operations and also to protect the environment from sulfur pollution. The most common catalyst for hydrodesulfurization (HDS) is cobalt-Molybdenum catalyst and it deteriorates rapidly in the presence of large V and Ni compounds in the feed; and also the consumption of the hydrogen goes up (Nelson - 1976). In the direct hydrodesulfurization the deactivated catalyst has to be replaced. Hastings et al. (1975) reported the average catalyst addition cost for Venezuelan medium atmospheric residuum to be 42¢/bbl and for Boscan-high metal crude to be 62¢/bbl. The quantity of Vanadium loading on the deactivated catalyst varied from 15% - 30% by weight. Millensifer (1977) reports that the approximate capacity of catalyst usage for HDS increased from 102,100 barrel per stream day in 1970 to 412,300 b/sd in 1976. Thus V and Ni are hazardous for HDS catalyst.
2. Useful products are obtained by reducing the crudes in the fluid catalytic cracking units. To maintain the proper activity-selectivity rating of the unit's catalyst inventory, it is necessary that the level of metal contaminants on the catalyst be kept under control

(Edison et al. - 1976). Habib et al. (1977) studied the effect over artificially metals-poisoned catalyst, and found that the metals poisoning resulted in a large increase in coke formation and small increases in hydrogen and light gas.

3. If V and Ni are present in the fuel oil, then on burning the fuel oil for power generation, they form oxides. Vanadium oxide corrodes and Nickel oxide errodes the turbine blades and the linings of the furnace (Yen - 1975).
4. The emission of these metal compounds in the enviroment is the health hazard for living beings and plants (Yen - 1975).

Thus in the recent past there has been a great interest in finding the various means to remove these metal compounds from the crude residuum. One of the suggestions have been to use a guard reactor in front of the HDS reactor. The guard reactor would have a relatively cheap and natural catalyst. This catalyst would have a strong selectivity for Hydrodemetallation (Berti et al. - 1975; Hastings et al. - 1975). It has been shown that for feeds having the metal content higher than about 100 ppm such a process is economically beneficial (Hastings et al. - 1975; Nelson - 1976 and 1977). The second suggestion has been to use some extraction techniques. Union Oil Products has

come up with Demex process, where by the use of low molecular weight paraffinic solvents the vacuum residuals are demetallized. Kerr-McGee Refining Corp. demetallizes the residuum by Supercritical Extraction and using Pentane as the solvent. An excellent source for the demetallation processes is "Hydrocarbon Processing", September (1978).

In almost all the processes described above the demetallized residuum still has the metal concentration of roughly 30 ppm - 100 ppm. These metals still poison the HDS catalyst. Thus there has been a strong motivation for studying the hydrodemetallation.

B. LITERATURE REVIEW

B.1. NATURE OF NICKEL AND VANADIUM COMPOUNDS IN PETROLEUM:

The metals in the crude oil are separated in three fractions. The first fraction is methanol soluble, second one is soluble in n-pentane only and the third one is insoluble in both and is called asphaltenes (Dickie et al. - 1968, Filby - 1973). It is believed that methanol soluble fractions are porphyrins, and pentane soluble ones are maltenes or resins. In case of crude oils, asphaltenes are almost without exception, completely soluble in benzene. Asphaltenes and resins fractions together are called asphaltic fraction of petroleum.

There is a lot of literature on porphyrins. The good references are Dolphin (1978), Smith (1975) and Yen (1975). The extractable fossil porphyrins are identified as a series of alkyl homologs of cycloalkanoporphin. Structures of the four basic type of porphyrins are reproduced, from Baker and Palmer (1978), in fig. II-2. In case of Metalloporphyrins, the metal atom is positioned in the center of the porphyrin ring. Fig. II-3, shows Ni-Etioporphyrin (I) and Vanadyl-Etioporphyrin (I). Saraceno et al. (1961) have pointed out that all the vanadium in crude oil appears to be in the vanadyl (+4) state and nickel exclusively in the +2 valence state. Thus vanadium containing molecule is more polar and surface active than nickel containing molecule.

Structure of asphaltenes has been a subject of extensive research. X-ray and chemical analytical techniques have been used. Yen et al. (1961) have proposed that asphaltenes are micellar clusters of true molecules. The proposed schematic view of asphaltene micelles and associated inter-micellar fluid has been reproduced, from Larson and Beuther (1966), in fig. II-4. Maltene like molecules are also called resin like molecules.

Asphaltenes and resins are known to have porphyrin as well as nonporphyrin type of metal compounds. The results of Sugihara, J.M. are reproduced in fig. II-5 (Source: Larson and Beuther - 1966). While nonporphyrin type of

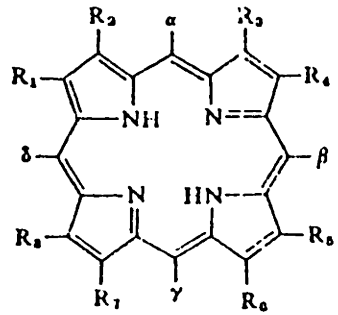

Compound	Substituents[a]												Spectral type
	R_1	R_2	R_3	R_4	R_5	R_6	R_7	R_8	α	β	γ	δ	
Etioporphyrin I	M	E	M	E	M	E	M	E	H	H	H	H	Etio
Etioporphyrin II	M	E	E	M	M	E	E	M	H	H	H	H	Etio
Etioporphyrin III	M	E	M	E	M	E	E	M	H	H	H	H	Etio
Etioporphyrin IV	E	M	M	E	M	E	E	M	H	H	H	H	Etio
γ-Phyllioporphyrin XV	M	E	M	E	M	H	P	M	H	H	M	H	Phyllo
Deuteroetioporphyrin II	M	E	M	H	M	E	M	H	H	H	H	H	Etio
α, γ-Dimethyldeuteroetio-porphyrin II	M	E	M	H	M	E	M	H	M	H	M	H	Phyllo
Rhodoporphyrin XV	M	E	M	E	M	C	P	M	H	H	H	H	Rhodo
Deoxophyllocrythrin methyl ester	M	E	M	E	M	CH_2CH_2	Pme	M	H	H		H	DPEP
Deoxophyllocrythroetio-porphyrin	M	E	M	E	M	CH_2CH_2	E	M	H	H		H	DPEP

[a] M = CH_3; E = CH_2CH_3; P = CH_2CH_2COOH; me = methyl ester; C = COOH.

Fig. II-2: Structures of Selected Porphyrins of the Four Spectral Series (Baker and Palmer - 1979)

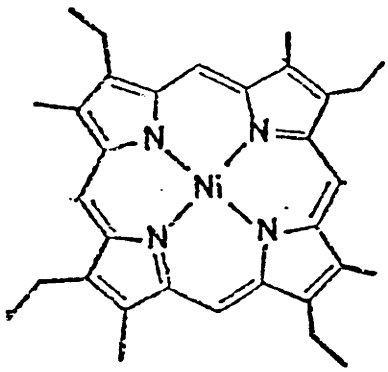

Ni-Etio (I)

$C_{32}N_4H_{36}Ni$
M.W.=535.38

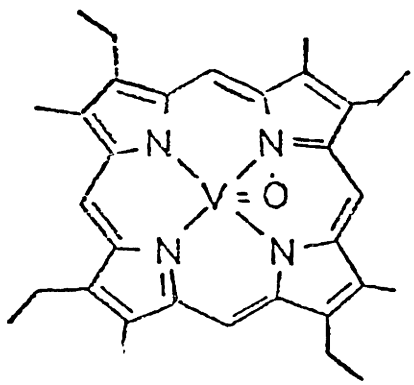

VO-Etio (I)

$C_{32}N_4H_{36}VO$
M.W.= 543.61

Ethyl Group

Methyl Group

Fig. II-3: Structures of Nickel Etioporphyrin (I) and Vanadyl-Etioporphyrin (I).

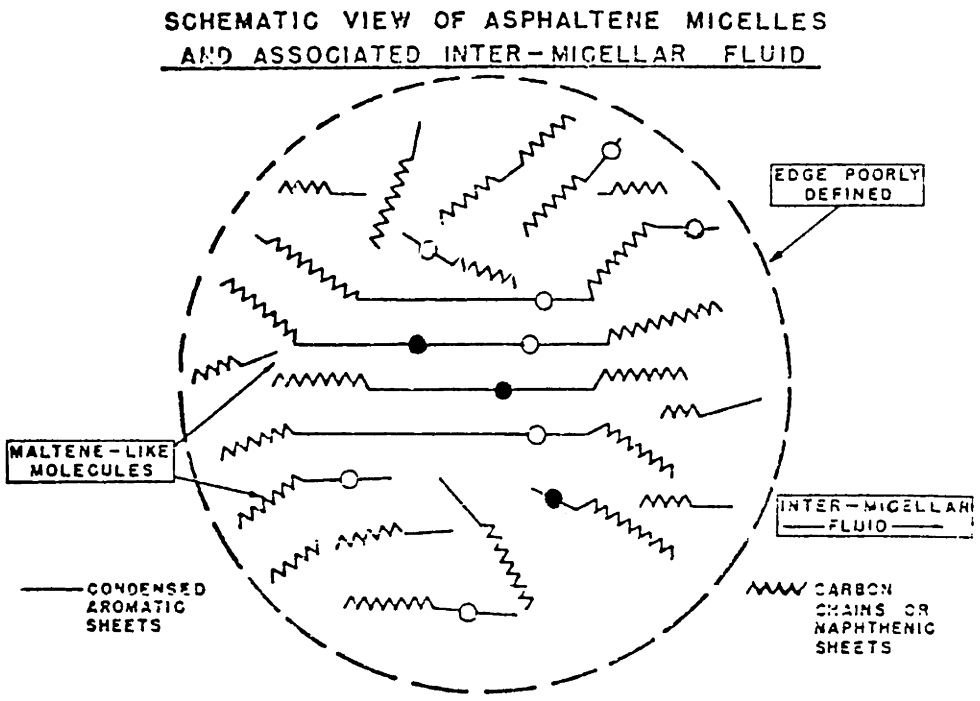

○ VANADIUM

● NICKEL

Fig. II-4

(A Modified Version of Larson and Beuther - 1966)

SCHEMATIC REPRESENTATION OF
LOCATION OF METAL COMPOUNDS IN
COLLOIDAL MICELLES OF ASPHALTENES

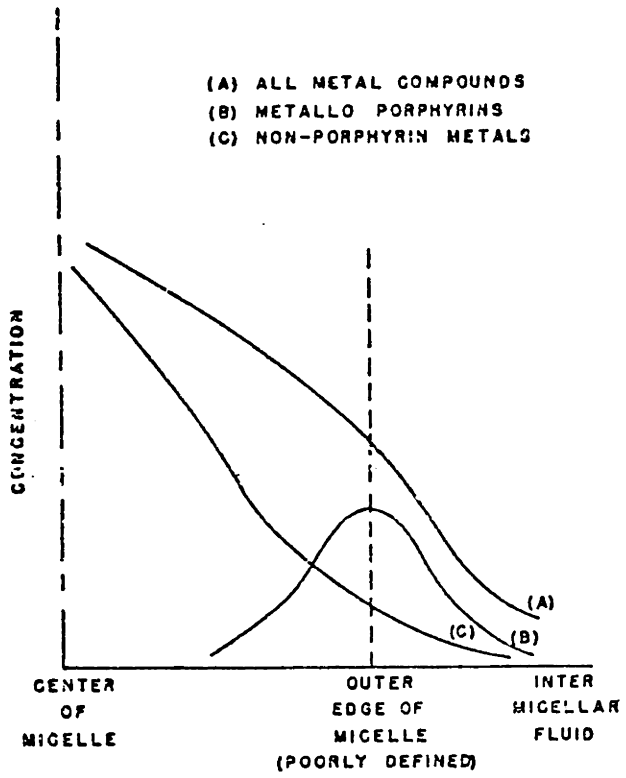

Fig. II-5

(From Larson and Beuther - 1966)

metals are concentrated more at the center of the asphaltene micelle the porphyrin type are near the outer edge of the micelle. Filby (1973) studied the distribution of nickel and nickel porphyrins in the various fractions of the California crude oil. It was found that the proportion of nickel as nickel-porphyrin in methanol soluble, resins and asphaltenes fractions were 100%, 65% and 49.2% respectively; and the rest were non porphyrinic in nature. Yen et al. (1968) concluded that there is enough porphyrin present in asphaltics to account for 1-50% of the combined transition metals, primarily vanadium and nickel. Chelates with ligands, probably of a non-porphyrin nature, account for the remaining 50-99%.

Larsen and Beuther (1966) have speculated that the non-porphyrin metals may be similar to metalloporphyrins. Their speculation is that the nonporphyrin metal complexes of crude oils are simply hetero-atom aromatic ring structures resembling porphyrins except that they contain sulfur and nitrogen in varying proportions. This speculation may be in agreement with the observation, of Sugihara et al. (1970), that crudes with high vanadium content are high in sulfur and crudes with high nickel content are high in nitrogen. It is known that crudes with high metal content are high in asphaltenes and hence high in nonporphyrinic metal. The authors argue that oxovanadium (IV) mostly prefers to coordinate to ligands with oxygen and

then with sulfur and the least with nitrogen; nickel on the contrary prefers nitrogen over oxygen with sulfur occupying the intermediate position.

Some studies have been done to understand the type of porphyrins found in petroleum. Rosscup and Pohlmann (1967), isolated two fractions of vanadyl-porphyrins from the Boscan crude and identified that one of the fraction was probably vanadylrhodoporphyrin while the other was definitely not vanadyletioporphyrin-I. However, Sugihara et al. (1970) and Yen (1975) have concluded that the two most important types of metalloporphyrins found in petroleum are DPEP and Etio type. As the age of petroleum increases, the petroporphyrin proceeds from DPEP to Etio.

Baker and Palmer (1978) have reported that for the free base porphyrins molecular weight range is 394 to 562, and depending on the crude the weight average mass are 420 to 490. Porphyrin dimers and trimers have also been reported (Blumer and Rudrum - 1970). Diameter of the metalloporphyrins are roughly 15Å (Fleischer - 1963). On the other hand asphaltenes have molecular weight ranging from 1000 to 500,000 and the size of a asphaltene cluster may be as high as 400 Å (Bridge and Green - 1979).

As regards the origin of porphyrins in petroleum, Treibs (1936) proposed that they are derived from chlorophylls of aquatic life. The source of metals in porphyrins are debated to be either from the living organisms

(Hodgson et al. - 1967) or the vanadium present in non-porphyrin complexes such as asphaltenes (Sugihara et al. - 1970).

B.2. KINETICS OF HYDRODEMETALLATION (HDM): Various investigators have studied the kinetics of the metal removal from the major crude oils, in presence of hydrogen, and over typical hydrodesulfurization (HDS) catalysts which are cobalt oxides and molybdenum oxides ($CoO-MoO_3$) supported on different forms of alumina (Al_2O_3). Most of the studies have been done in downflow, cocurrent hydrogen and feed flow, trickel bed reactors.

Beuther and Schmid (1963) studied the kinetics of Ni and V removal from both Kuwait atmospheric and vacuum residues over HDS catalysts. They found that the rates of metals removal are less well defined and believed it to be second order. However, Larson and Beuther (1966) found HDM of the Kuwait atmospheric residuum to be first order. Inoguchi et al. (1971-a) reported that the kinetics of the metals removal of the Khafji (Saudi Arabia) and the Kuwait atmospheric residua could be explained equally well by the first order and the second order kinetics. Oleck and Sherry (1977) observed second order HDM kinetics for Lagomedio (Venezuelan) atmospheric residua. Riley (1978) hydrotreated the Safaniya atmospheric Residuum so that the hydrotreated product retained the large fraction of the

total asphaltene fraction and hence the large portion of the total contaminants. This hydrotreated Safaniya atmospheric residuum showed first order HDM kinetics.

Apart from the above authors who did their studies with various HDS catalysts (differing in Co-Mo loading and structure of alumina support) there have been studies with cheaper substances like manganese nodules and activated bauxite (Porocel). The motivation for these studies comes from the fact that the residuum can be first passed through a guard reactor packed with these cheap substances but having a high HDM activity and then through the HDS unit. This would enhance the life of the catalysts in HDS units and therefore lower the processing cost considerably. Chang and Silvestri (1974) studied the HDM kinetics of topped Agha Jari Crude over Atlantic Ocean, Pacific Ocean and Lake Michigan manganese nodules. They found that the two ocean nodule catalysts which contain substantial amounts of Ni, Co and Mo, metals normally associated with hydrogenation and hydrodesulfurization activity, were less active than the fresh water nodules which contain only very low levels of these metals. Same authors in a later study (Chang and Silvestri - 1976) reported that HDM kinetics of V and Ni removal over Lake Michigan manganese nodules (LMN), Co-MO/Al_2O_3 catalyst and Porocel catalysts obey first order kinetics. However, Oleck and Sherry (1977) reported second order kinetics for Lagomedio atmospheric residuum over LMN and HDS catalysts.

It has been speculated (Beuther and Schmid - 1963, Cecil et al. - 1968, Inoguchi et al. - 1971-a, Kurito et al. - 1971, Mosby et al. - 1973, Oleck and Sherry - 1977 and Riley - 1978) that the apparent second order HDM kinetics may be attributed to the presence of more than one kind of metal compounds with varying kinetic activities; where each individual species follow first order kinetics. Inoguchi et al. (1971-c) observed that nickel and vanadium existing in the form of micelle combined with asphaltene molecules were more unstable and easily decomposed by contact with catalysts, whereas vanadyl and nickel porphyrins were more stable. Kwan and Sato (1970) also divided the total metal present in the Khafji heavy oil in to vanadyl-vanadium and non-vanadyl-vanadium and observed that vanadyl-vanadium is not as readily removed and as readily deposited as non-vanadyl-vanadium. Oxenreiter et al. (1972) report that for both Khafji and Gach Saran residuum, resin fraction of the metals show faster demetallation than the asphaltene fraction. Riley (1978) argues that his first order observed kinetics is due to the uniform chemical enviroment of the metal species. As pointed out by Cecil et al. (1968); if the total metals content could be considered as constituting of two major fractions reacting with greatly different rates each following first order kinetics, then the total metals disappearance would look like a second order kinetics. Bridge and Green (1979) have shown concern that catalyst

wetting may be incomplete under small scale trickle flow conditions and that the second order effects may be an artifact of this problem. Thus there seems to be a plausible explanation for the observed first and second order HDM kinetics by various workers.

However, the kinetic orders different from first and second have also been observed. Van Dongen (1979) studied the vanadium kinetics over HDS catalyst in a simulated continuous stirred tank reactor and also in a simulated co-current moving-bed reactor. The observed order for the co-current moving-bed reactor was 1.5 and for the continuous stirred tank reactor 1. The author attributed this anomaly to the multicomponential nature of petroleum fractions. Also the speculation of an exponential distribution in activity, with the probable order of the individual vanadium bearing species to be less than 1.0 has been made. Indeed, Hung (1979) in the batch autoclave studies of pure nickel and vanadyl porphyrins observed the fractional order kinetics. The fractional order centered at 0.5 and varied with temperature and pressure of the operation. One of the objectives of this thesis is to explain this fractional order behavior and is discussed in the kinetic result section.

One important feature of the HDM kinetics, as observed by almost all of the above authors and also by others (Arey et al. - 1967, Audibert and Duhaut - 1970 and Shah

and Paraskos - 1975) is that vanadium has a higher reactivity than nickel. Beuther and Schmid (1963) give two reasons for it. 1.- All the vanadium in Kuwait crude exists in +4 valence while the nickel in +2 valence state. As the net effect vanadium, just like vanadium in vanadium porphyrin complexes, does not have its valences satisfied in the coordinating plane, but is bound to an oxygen atom or to a sulfur atom perpendicular to the planar structure of the remainder of the molecule. This tendency of atoms to project from the plane for vanadium complexes may make the vanadium atom more accessible to the catalyst through the projecting hetero atom. While on the other hand, Nickel has its valences satisfied with in the plane and would be a less polar compound. 2.- Even though the micellar nature of asphaltenes may not persist under reaction conditions, the authors postulated that nickel concentrates on the interior of the micelles, while vanadium concentrates on the exterior of the micelles (fig. II-6). Thus, vanadium's polarity and easy accessibility at the periphery of the asphaltene molecule or micelle, may be responsible for its easy removal relative to nickel. This line of thought has been accepted by almost all the workers.

Another important feature observed by nearly all the authors is that there exists a relationship between HDM and sulfur removal. Massagutov et al. (1967) emperically

A. Before HDS

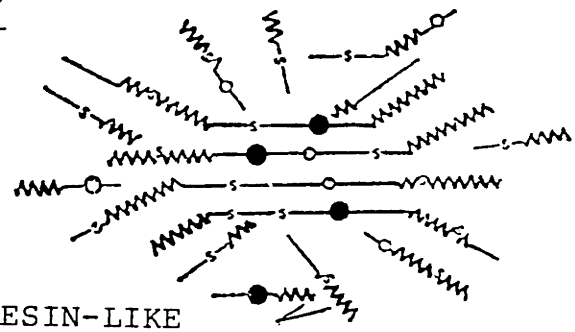

B. After HDS

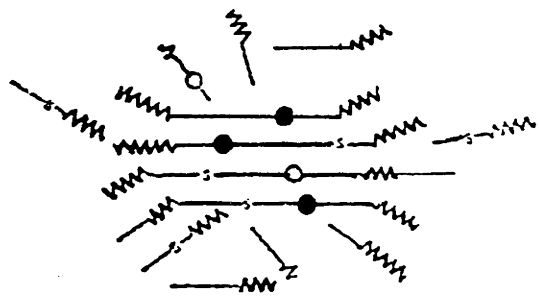

S = Sulfur
o = Vanadium
● = Nickel
— = Aromatic Rings
WV = Naphthenic Rings

Fig. II-6: Qualitative Changes in Asphaltenes and Surrounding Resins During HDS Processing (Beuther and Schmid - 1963)

correlated the amount of metal removal with the amount of sulfur removal. They were successful in correlating a large number of data on different crudes. Their correlations are gives as:

Nickel removal, %

$$Y_1 = \frac{X}{0.456 + 0.00522X}$$

Vanadium removal, %

$$Y_2 = 1.055\ X$$

where X is % sulfur removed. The linear relation between vanadium and sulfur removal and the nonlinear between nickel and sulfur removal may be explained on the basis of the figure suggested by Beuther and Schmid (1963) (fig. II-6). The model given in figure II-6 shows that most of the sulfur atoms are removed from the exterior fragments of the asphaltene molecules than from the interior aromatic sheets. Since a significant portion of the vanadium atoms are on the exterior of the micelles and are also removed more easily, one sees a linear relation between sulfur and vanadium removal. On the other hand, most of the Nickel are concentrated in the interior of the micelles and are not that easily removed, and therefore, show a nonlinear relation with sulfur removal.

A good review on hydrodesulfurization is by Schuit and Gates (1973). Even though there is no literature showing the relation between HDM and hydrodenitrogenation, a possible correlation between the two cannot be denied. The good references for hydrodenitrogenation are Bhinde (1979) and Gultekin (1980).

Now the only thing left to be discussed about HDM kinetics is its dependence on hydrogen pressure. For HDS catalyst, Audibert and Duhaut (1970) report first order dependence; while Chang and Silvestri (1976) and Oleck and Sherry (1977) report dependence to be greater than first order. However, for manganese nodules and porocel, Chang and Silvestri (1976) and Oleck and Sherry (1977) report order with respect to hydrogen to be less than one.

Costantinides et al. (1963), Fischer et al. (1976), Hodgson and Baker (1957) and Rosscup and Bowman (1967) have also reported thermal demetallation or nonhydrogenative demetallation. They all have reported a first order kinetics with activation energy about 40-60 Kcal/g mole. However, as pointed out by Chang and Silvestri (1976), the thermal demetallation rate is atleast two order of magnitude less than the hydrodemetallation. Therefore, the assumption of various workers that thermal demetallation as compared to HDM can be neglected is justified.

B.3. CATALYST DEACTIVATION: Almost every researcher has found that a typical catalyst, in a HDS reactor, deactivates in two steps - first step is a rapid decline in activity due to coke formation and the second one is a slow decline in activity due to metals deposition.

B.3.a. COKE DEPOSITION: Beuther and Schmid (1963) observed that of the total carbon deposited on the HDS catalyst in 16 days of operation, one half deposited in the first 12 hours. Kwan and Sato (1970) found that there was virtually no change in carbon deposition from 50 hours of operation to 1000 hours of operation. Similar establishment of equilibrium level of carbon in a short time on the catalyst is reported by Chang and Silvestri (1976), Dautzenberg et al. (1978) and Inoguchi et al. (1971-c). The level of coke deposition is normally 10% - 20% by weight on the catalyst.

Beuther and Schmid (1963) observed that their coke containing catalysts had surface areas and pore volumes only about one-third of the original catalysts. Further, the average pore radius reduced only slightly and the pore size distribution from the coke saturated catalysts retained their original identification by maintaining approximately the same percent distribution as of the original fresh catalyst. However, Richardson and Alley (1975) found that along with the reduction in the total surface areas and pore volumes there was a significant alteration

in the pore size distributions due to the coke deposition on the catalysts. Riley (1978), from his studies, concluded that the coking tendency of resid HDS catalysts is controlled by intrinsic surface properties rather than the initial pore size distribution of the catalysts. Beuther and Schmid (1963) also concluded that the initial high depositions of the coke on the catalyst are not the result of a hydrogen deficiency nor from the presence of large, highly condensed asphaltenes.

The upper saturated value of the deposited coke on the catalyst is explained by some sort of dynamic equilibrium between the hydrocracking rate and the hydrogenation rate on the catalysts surface (Beuther and Schmid - 1963, Kwan and Sato - 1970).

B.3.b. METALS DEPOSITION: Arey et al. (1967), Audibert and Duhaut (1970), Kwan and Sato (1970), Oxenrieter et al. (1972) and Sato et al. (1971) studied the metals deposition on the catalyst by scanning electron X-ray microanalyzer. All these investigators found that vanadium deposits in a outer thin shell of the catalyst whereas nickel tends to be uniformly distributed along the diameter of the catalyst. Fig. II-7 shows the results of Sato et al. (1971). In the figure vanadium is shown to have a U shape, while nickel is uniformly distributed. The authors did the classical diffusion treatment of the metals deposition and

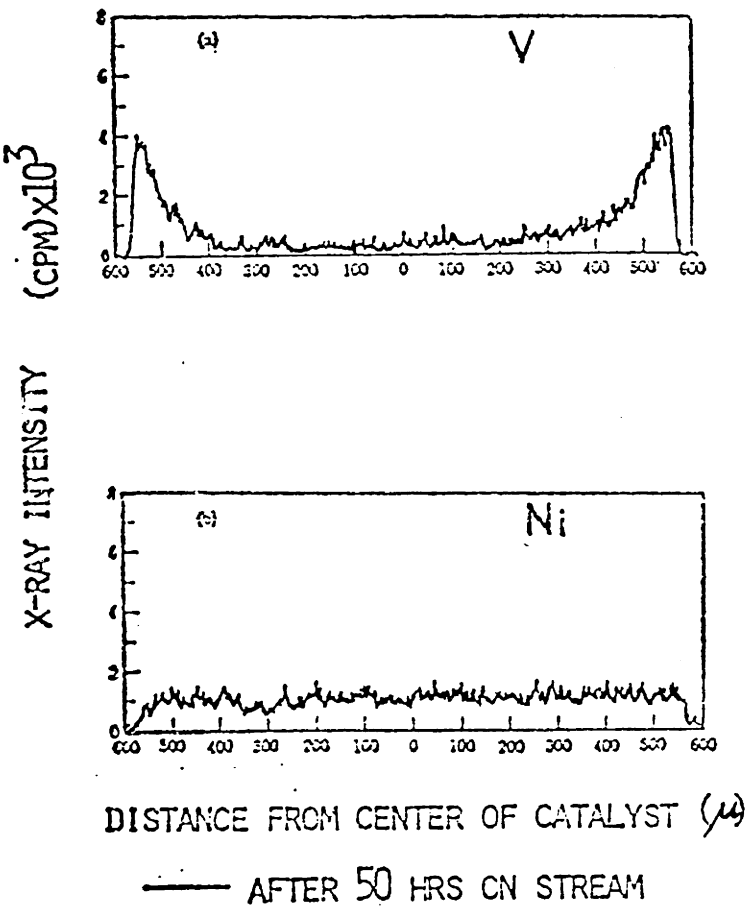

Fig. II-7: Concentration Profile of Vanadium (Top) and Nickel (down) deposition on the HDS Catalyst after 50 hours of Reaction. (Sato et al. - 1971)

concluded that the effective diffusivity for vanadium has to be less than 10% of nickel, which seems to be unreasonable. However, the important effect of the relative adsorption of vanadium and nickel compounds were not taken into consideration. As pointed out by Larson and Beuther (1966), vanadium compounds adsorb more strongly on the catalytic surfaces than nickel. It is very much possible that near the edge of the catalyst where vanadium concentration in the solution phase is highest, nickel could not absorb in sufficient quantities on the catalyst surface to give high deposition rate. Once, sufficiently inside the catalyst the vanadium concentration would drop rapidly while nickel concentration would be still higher and therefore nickel deposition rate would be sufficiently high. Thus, relative adsorption on the catalyst surface may be the cause for the more uniform distribution of Nickel. This hypothesis can be easily tested by running pure nickel and vanadium compounds separately and then together; and studying the metal deposition profiles in each case.

However, Todo et al. (1971) reported that the concentration profiles for both nickel and vanadium were U shaped. This contradiction with respect to that of other investigators may be due to the difference in pore size distribution of the catalysts.

Unlike coke deposition, metals deposition do not have any upper limit (only limited by the physical void volume available), and the total amounts deposited depend on the duration of the run and the feed conditions. Oxenreiter et al. (1972) reported the amount of deposited vanadium to be as high as 56 wt % and Nickel 17 wt %. They further speculated that pore mouth plugging was the most probable cause for plugging. Dautzenberg et al. (1978) and Kwan and Sato (1970) also proposed that pore mouth plugging is the major cause in limiting the total catalyst life. Brunn et al. (1975) reported that the ultimate life of the catalyst depends on its maximum capacity for metals deposition which could be function of the feedstocks and the severity of operation.

Almost all the investigators agree that the metals deposit on the surface as their sulfides (Newson-1975).

B.4. CATALYST DEACTIVATION ALONG THE BED LENGTH: Inoguchi et al. (1971-c), Kwan and Sato (1970), Oxenreiter et al. (1972) and Sato et al. (1970) have investigated the metals and coke deposition profiles along the length of the reactor. All the investigators have observed that the maximum deposition of the metals occured at the inlet of the reactor and it decreased in somewhat linear fashion towards the reactor outlet. On the other hand coke formation on the catalysts increased linearly from the inlet to the outlet. The results of Sato et al. (1970) are

plotted in Fig. II-8. The additional information from this figure is that the amount of coke deposited from 50 hours to 1000 hours remained unchanged, whereas the quantity of metals increased considerably. This is in agreement with our discussions in the earlier two sections.

Another important observation is the distribution of the metals profile inside the catalysts at various bed locations. Recent results of Tamm et al. (1979) are plotted in figure II-9. Nickel and Vanadium deposition show internal maxima at the inlet and this maxima moves to the edge at the reactor outlet. The internal maxima in the metals deposition has also been observed by Hardin et al. (1978) and Oxenreiter et al. (1972). Audibert and Duhaut (1970) observed more than one internal maxima for the Nickel deposition in the catalyst. There is no explanation for these internal maxima in the metal deposition profiles; and the effect of the location of the catalyst in bed on them. Indeed, there is even no speculation in the literature. One of the objectives of this thesis is to adress this question.

Since vanadium, from the feed solution, is removed faster than the nickel, the ratio of Nickel to vanadium in the solution phase has been observed to increase from the reactor inlet to outlet (Kwan and Sato-1970).

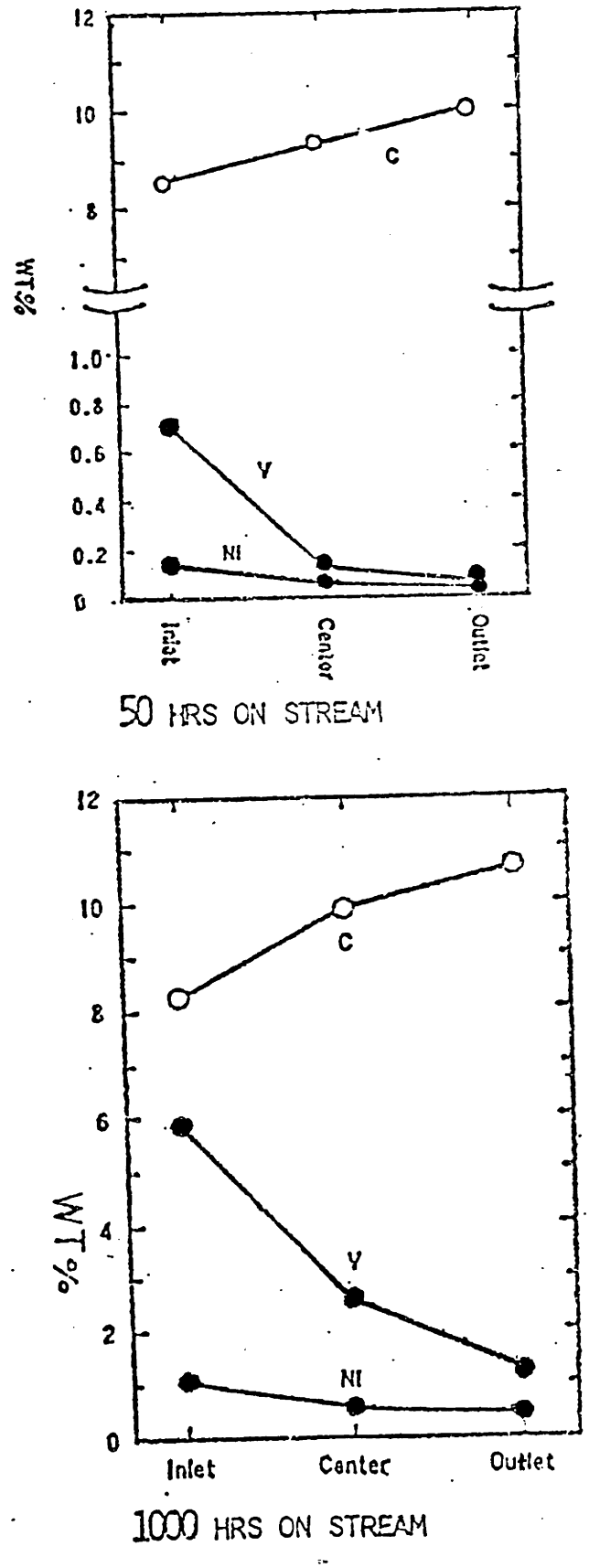

Fig. II-8: Concentration Profile of Carbon, Vanadium, and Nickel Deposition Along the Reactor Bed. (Sato et al. - 1970)

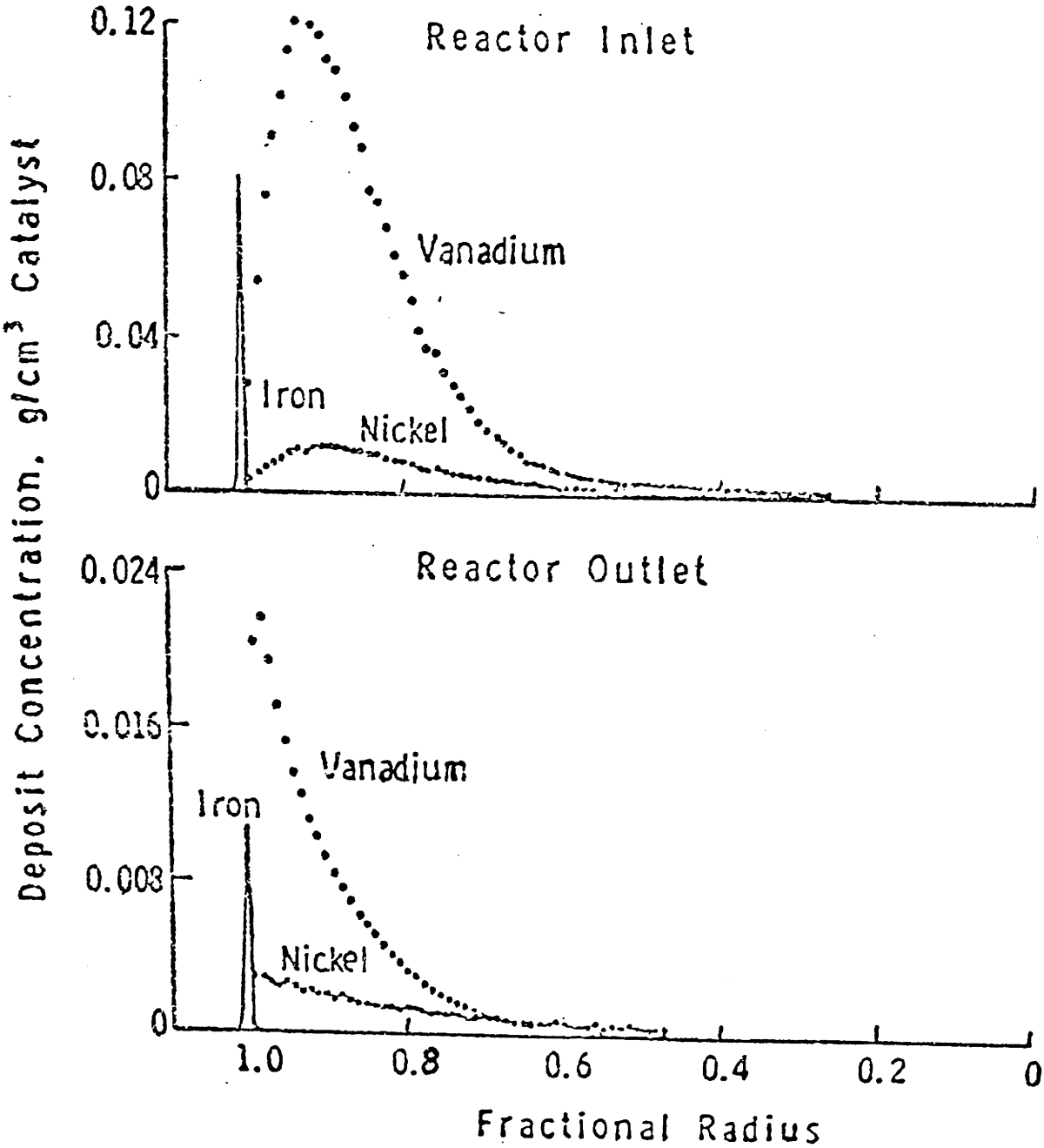

Fig. II-9: Typical Depositional Patterns for Nickel, Vanadium, and Iron in Residuum Hydroprocessing Catalyst. Arabian Heavy Atmospheric Residuum
Reaction Temperature = 700°F
Hydrogen Partial Pressure = 1825 psia
1/16 in. Extrudate Catalyst (Tamm et al. - 1979)

B.5. EFFECT OF PORE SIZE DISTRIBUTIONS ON THE CATALYST ACTIVITY AND THE THEORETICAL POISONING MODELS: Shah and Paraskos (1975) have reported the intraparticle diffusivity for vanadium and nickel compounds in the reduced Kuwait crude to be $7X10^{-8}$ cm^2/sec and $3X10^{-8}$ cm^2/sec respectively. Since catalysts have pores ranging in size from 25 to greater than 1000 Å, and asphaltenes range in size from 25 to greater than 100 Å in molecular diameter; intraparticle diffusion may be very important. Spry and Sawyer (1975) reported that the diffusion of 100 Å particles will be hindered in their diffusion in pores up to 1000 Å in diameter and estimated the diff ity to be of the order of $3X10^{-8}$ cm^2/sec.

Tamm et al. (1979) studied the effect of mean pore size on the metals deposition on the catalyst. They found that increasing the pore size increased the depth of metals deposition in the catalyst. Riley (1978) has investigated the vanadium and nickel removal activity from the hydrotreated Safaniya atmospheric residuum with respect to mean pore diameter of the catalyst, and found that in the pore size range studied the metals removal rate increased with increasing pore diameter.

Hardin et al. (1978), prepared a large number of catalysts with varying pore sizes. Their pore system could be described as having two regimes a) The large, interparticle pores corresponding mainly to intergranular

voids greater than 30,000 Å (3μ); and b) the intraparticle pore system usually in the range below 500 Å. Their result for the vanadium and nickel removal activity with respect to median pore diameter is reproduced in fig. II-10. There seems to be an optimum pore size for the maximum catalyst activity. This behavior can be easily understood if it is assumed that the catalyst activity is directly proportional to the active surface area available. As pore diameter decreases the surface area increases but the configurational diffusional resistance increases; on the other hand increase in pore diameter decreases the surface and also the configurational diffusional resistance. There is a compromise between the increase in activity due to the increase in surface area and the decrease due to the increase in the configurational diffusional resistance; and hence an optimum pore size.

However, as discussed earlier, asphaltenes in the residuum have a molecular size distribution. Bridge and Green (1979) and Richardson and Alley (1975) used gel permeation chromatography (GPC) to get the molecular size distribution in the residuum before and after the reaction over the catalyst. Both observed that even the asphaltene molecules with diameters larger than the pore diameter showed reasonable activity. They concluded that the molecules are considerably smaller at the reaction conditions than at GPC conditions. The speculation of the thermal depolymerization mechanism was made. Since big asphaltene

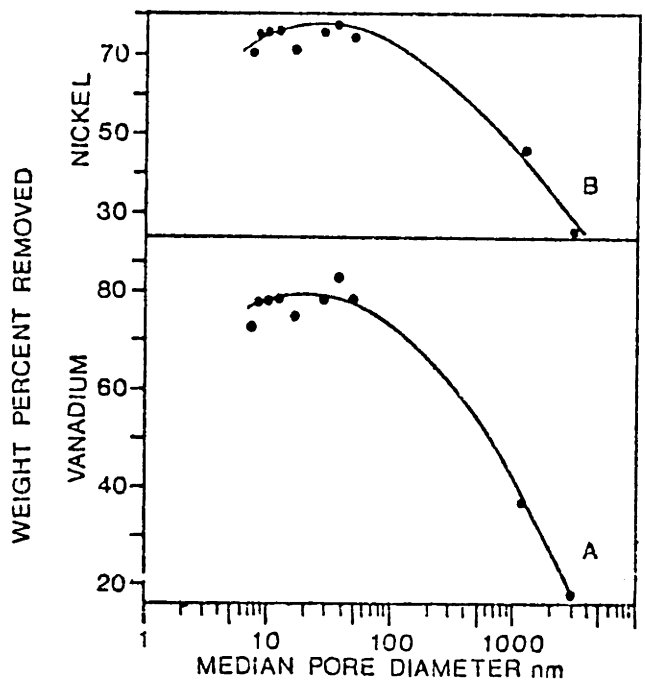

Fig. II-10: (From Hardin et al. - 1978)

Demetallization of the Athabasca bitumen:

A - Removal of vanadium from a feed of concentration 174 ppm V;

B - Removal of Nickel from a feed of concentration 76 ppm Ni.

molecules cannot diffuse easily in the catalysts with smaller pore diameters, both group of investigators suggested that catalysts should have some macropores. However, Hardin et al. (1978) observed that the quality and quantity of coke on the small pore catalysts would be preferable, and emphasized the compromise between the small pores and large macropores in the catalyst.

Bridge and Green (1979) also stated that the gross vanadium removal rates were consistent with pore diffusion theory. Thus by pore diffusion theory, they studied the effect of pore size and the catalyst size on the HDM. They concluded that for a given size of the molecule, a decrease in the particle size leads to decrease in the optimum pore diameter and vice versa. This is due to the fact that when particle size is decreased one can tolerate a higher intraparticle diffusional resistance; and hence can increase the total surface area per unit volume of catalyst by decreasing the pore diameter. Thus as particle size is reduced one can get with optimal pore size a higher catalytic activity. However, due to the practical considerations, the size of the catalyst particles in a reactor, cannot be reduced indefinitely.

Spry and Sawyer (1975) developed a model, which can take into account the configurational diffusional resistance of the asphaltenes with molecular size distributions, in the catalysts with pore size distributions. Thus they suggested that optimum catalyst pore size for a given molecular size distribution can be calculated.

Uptill now, in this section, we have discussed the effect of the pore size distribution and the size of catalyst particle on the initial rate of HDM. But, for longer reaction times, the metals deposit on the catalyst and change its pore size distribution. Inoguchi et al. (1971-b) studied the long run tests of 1,000 to 3,000 hours on some of the catalysts, which had different physical properties. They found that catalysts with comparetively small pores had a high initial activity, but the activity fell rapidly with time. On the other hand, in case of catalysts, with comparatively large pore diameters, vanadium deposited in large quantities and maintained its activity for a longer time. Physical considerations clearly show, if the void fraction of the catalyst is not changed significantly and the pore diameter is increased, then prior to the total hinderance of the diffusing metal molecules more metals per unit volume of the catalyst would deposit. Thus one has to compromise between the high initial rate and the total life of the catalyst.

A few attempts have been made to model the initial and long run activity of the catalyst. Newson (1972 and 1975) modelled the pore plugging due to deposition of metal sulfides and coke. Dautzenberg et al. (1978) developed a two parameter model describing the deactivation behavior due to metals deposition. However, the above investigators neglected the change in the restricted diffusion with

decreasing pore size. Rajagopalan and Luss (1979) considered this effect and developed a model to predict the optimal initial activity and the optimal pore size for the metals deposition only. All these investigators assumed that the pore structure could be represented by a set of idealized parallel sided non intersecting pores of the variable radius, but each of a certain length L. This model is also referred as 'parallel bundle' model. From such a model, Rajagopalan and Luss (1979) proved that among all catalysts with the same surface area and porosity, the largest initial activity is attained for pellets with a uniform pore size. One of the objectives of this thesis is to develop a new poisoning model for a bimodal type of catalyst which would give higher initial activity and longer lifetime activity than predicted by any of the above poisoning models.

C. OBJECTIVES: Following are the main objectives of this thesis:

1. In the literature, kinetics of HDM has been observed as fractional, first and second order. The first objective is to study kinetics more carefully and to identify important kinetic steps in the hydrodemetallation; and thus explain the various inconsistencies in the observed kinetic orders.

2. To study the vanadium and nickel deposition profiles in 1/16 inch catalyst extrudates. The objective is to understand and model the metals deposition profiles at various bed positions, including the internal maxima at the inlet of the reactor, and at various temperatures and pressures of the operation.
3. To suggest a better catalyst and propose a theoretical poisoning model for it. A catalyst, which would take advantage of the large surface area of the small particles, and still have the convenience of big geometrical size. Theoretical poisoning model to predict the optimal pore size and particle size for optimum initial activity and life time is to be proposed. The kinetic rate expression used will be the one found in the kinetic studies.

CHAPTER-III

APPARATUS AND PROCEDURE

Crude oils are very complex in nature; they contain many metal compounds and all of them are not very well characterized. Besides metal compounds there are many sulfur and nitrogen compounds and these compounds do interact with metal compounds. Thus, if crude oil were to run directly through the reactor, it would be difficult to uncouple the hydrodemetallation effect from the rest of the complex chemical and physical phenomenons. Therefore, in this scientific study, it is decided to use model metal compounds which are typical representative of the metal compounds found in the crude oil, and dissolve them in model clean oil free of sulfur and nitrogen compounds. The choice of catalyst, oil and model metal compounds are discussed below:

A. THE CATALYST: Since hydrodemetallation reactions occur mainly in hydrodesulfurization reactors, it was decided to use a HDS catalyst. In a typical HDS catalyst cobalt oxides and molybdenum oxides are supported on a high surface area alumina ($CoO-MoO_3/Al_2O_3$). The alumina is normally gamma phase; but delta, theta and eta phases or their combinations have also been used (Fischer

and Milstein - 1977). There have been a lot of work to suggest an optimal combination of transition metal oxides on alumina oxides (Chervenak et al. - 1975 and 1976, and Rovesti and Wolk - 1973).

The second criterion for the choice of the catalyst was that it should have a well defined geometrical shape. This is necessary, for minimizing the uncertainties due to the geometrical shape of the catalysts, in the modelling of the metals deposition profiles. Differential equations are relatively easier to handle for the spherical shapes and hence spherical shape would be the most desirable. On the other hand pellets would be most complex to handle. Long extrudates, with the assumption that the diffusion from the ends could be neglected, would have the simplicity of the cylindrical geometry in modeling.

The third criterion was that the pore size distribution should be as narrow as possible (unimodal catalyst). This is needed to avoid the usage of micropore and macropore diffusivities. It is necessary to keep the rate parameters to the minimum possible number. Since pellets are made from pelletizing and invariably have macropore and micropores, they are not considered.

With the above considerations in mind, various catalyst manufacturers were contacted. Most of the spherical catalysts were bimodal. This is basically due to the fact that they were probably prepared by letting a nucleus roll and grow in the catalyst powder. By the oil drop method it is

possible to get nearly uniform pore size spherical catalysts. However, these catalyst are not perfectly spherical and are of the drop shape with a tail at the end and also there is a wide distribution in the size of the catalysts. Union Oil Products manufactures such a catalyst called RCD-5 catalyst. But due to proprietary nature of this catalyst it could not be considered for this research.

The catalyst used in this research is AERO® HDS-16A supplied by American Cynamid Company, Linden, New Jersey (Lot #MTG-S-0573). It is the $CoO-MoO_3/Al_2O_3$ catalyst and is supplied as 1/16" extrudates. This catalyst meets the criterion that the pore size distribution is relatively narrow (fig. III-1). The pore diameter corresponding to 50% of the total pore volume is 80.4 Å, and when calculated by dividing the Pore volume (Hg) by the total surface area and multiplying it by 4 it is 97.7 Å. It is clear from fig. III-1 that most of the pores are between 59.0 Å to 88.4 Å, and 80.4 Å would be a better number to characterize the pore size.

Chemical and physical properties of the catalyst are listed in table III-1. The procedure used to measure the pore volume of table III-1 is (i) Dry the catalyst in oven at 440°C for a couple of hours to remove the adsorbed water, (ii) Quickly weigh some quantity of the dried catalyst, (iii) Transfer the dried catalyst in distilled water and soak it for couple of hours, (IV) Remove the water from the external surface area of the soaked catalyst by quickly

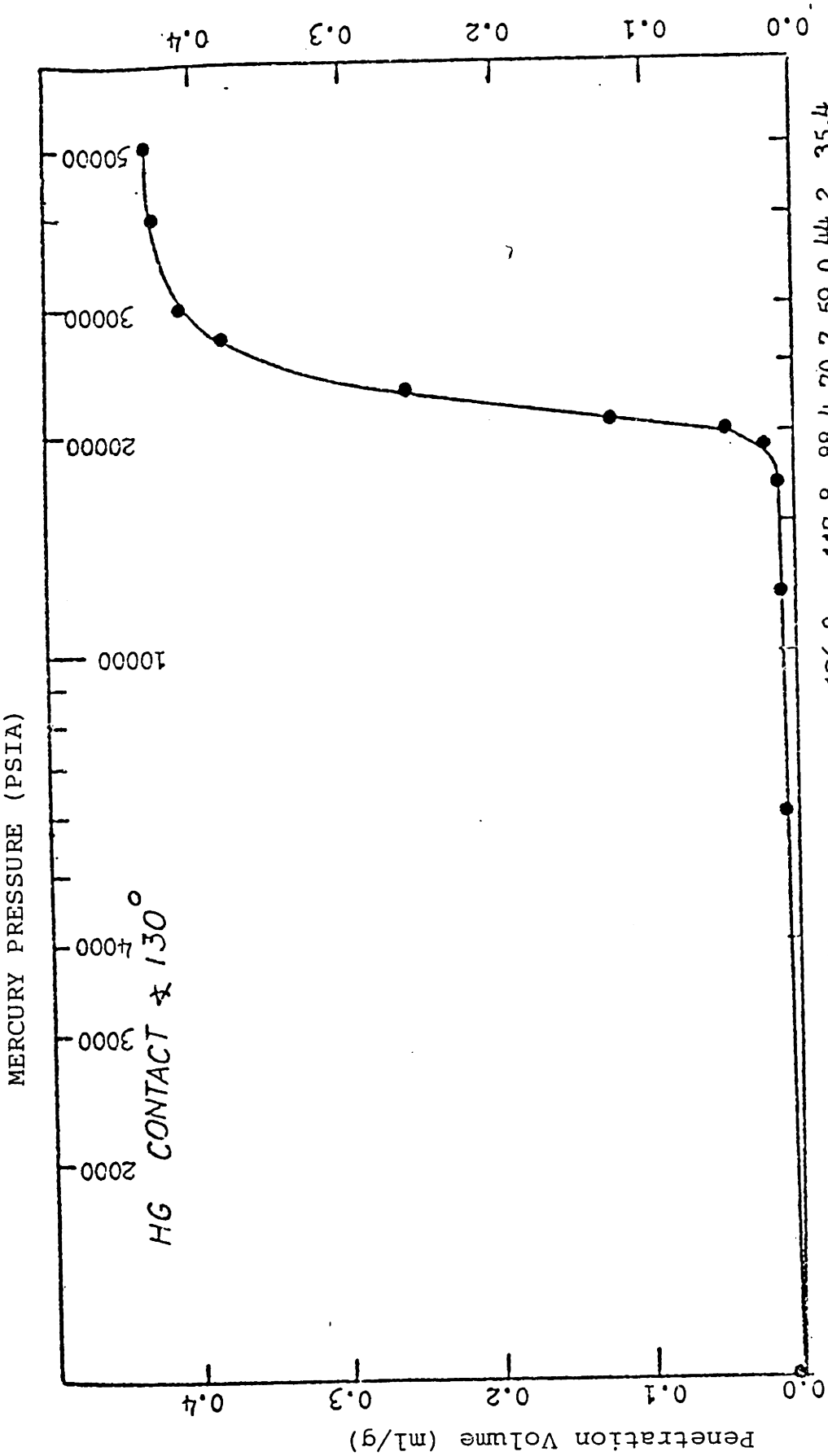

Fig. III-1: Pore Size Distribution of AERO® HDS-16A Catalyst Extrudates
(Courtesy: American Cynamid Company)

TABLE III-1

CHEMICAL AND PHYSICAL PROPERTIES OF THE HDS-16A CATALYST

(Courtesy - American Cynamid Company)

(1) Chemicals, wt. % dry basis:

CoO	: 5.7
MoO_3	: 12.2
Na_2O	: 0.03
Fe	: 0.04
Base	: ALUMINA

(2) Physicals:

Apparent bulk density (poured), g/ml	: 0.737
Average diameter, cm	: 0.152 (1/16 inch)
Average length, cm	: 0.432
Average Crush Strength, g	: 6350.4
Fines, wt %	: 0.2 (-16 mesh)
Pore volume (H_2O), ml/g	: 0.4331 $\pm$ 0.0044
Pore volume (Nujol), ml/g	: 0.4389 $\pm$ 0.0060
Pore volume (Hg), ml/g	: 0.43
Surface area, m^2/g	: 176
Density of a particle, g/ml	: 1.49
Pore diameter corresponding to 50% of the total pore volume, Angstron	: 80.4

rolling it over Kimwipes (a kind of blotting paper) (V) Reweigh the Catalyst (VI) By difference in the weight, and from the density of the water the pore volume is calculated (Weisz - 1966). To see the effect of drying, the catalysts were dried for 12 hours and 24 hours; to study the soaking time effect, catalysts were soaked for 24 hours and 1 hour; and finally more than one kind of blotting paper were used. All the results agreed fairly well. This whole procedure relies on the fact that blotting papers have pore sizes much larger than the pore size of the catalyst and hence do not suck the water out of the catalyst pores by capillary action. Using the same procedure, the pore volume is measured for Nujol which is a white oil (discussed in the next section). The agreement between the pore volumes measured by the water, Nujol and mercury is excellent.

B. THE OIL: The oil used as solvent for the metal compounds should be (i) nitrogen and sulfur free, (ii) sufficiently high in viscosity, (iii) liquid at room temperatures, (IV) high in boiling point so that at the reaction temperatures of about 350^{o}C, the amount of oil in the vapor phase may be negligible, (V) and finally it should not crack significantly at the reaction conditions.

It has been reported that in catalytic cracking, stability increases in the order: (1) olefins (2) aromatics with C_3 or larger substituent groups, (3) naphthenes,

(4) polymethyl aromatics, (5) paraffins, (6) unsubstituted aromatics (Greensfelder et al. - 1945, Haensel, V. - 1951). High carbon aromatics would tend to saturate and would increase the hydrogen consumption; moreover naphthalene which has only 10 carbons is solid at room temperature. α -Methyl naphthalene ($C_{10}H_7CH_3$) is liquid at room temperatures but its boiling point is only 245°C. Among the paraffins, anything above hexadecane ($CH_3(CH_2)_{14}CH_3$) is solid at room temperatures, even hexadecane tends to solidify at 18.5°C. Hexadecane is also not very high in viscosity and boils at 287.5°C. The oils satisfying all of the criteria reasonably well are white oils also called the mineral oils.

White oils are mixture of naphthenes, paraffins and isoparaffins (Fiero - 1965, Franks - 1964-a and 1964-b, Meyer - 1968 and Steenbergen - 1974). They are free of sulfur, nitrogen and any metal compounds; and also have relatively high viscosity and boiling point range. Some white oils maybe more naphthenic while others more paraffinic. Naphthenic type have about 40% carbon in naphthene rings and the rest in paraffinic structure; and the average number of naphthene rings are about three.

In the early part of the research, catalytic cracking activity of the three mineral oils were tested - Drakeol - 35 and 4434 mineral oils, both supplied by Penreco, (Butler, PA); and Nujol from Plough Inc., (Memphis, Tenn.). To test an oil, it was placed in a one litre autoclave

with about 2 grams of HDS-16A catalyst. It was purged with helium and then pressurized with hydrogen to about 6900 KPascals (1000 psi). The temperature of the autoclave was increased till the significant cracking was observed. When the colour of the sample collected from the autoclave became yellow it was thought that the molecules of the oil had undergone severe changes. It was found that while the two mineral oils, supplied by Penreco, heavily cracked at about 325°C-350°C, Nujol showed mild cracking activity at about 375°C-400°C.

Thus, in the whole research, Nujol has been used as the suitable solvent. The typical properties of the Nujol, as supplied by the manufacturer, are listed in Table III-2. Nujol is a mixture of liquid hydrocarbons obtained from petroleum and is naphthenic type of white oil.

C. SELECTION OF MODEL METAL COMPOUNDS: Costantinides and Arich (1963) studied nine different crudes and reported that the percentage of the total vanadium and nickel as porphyrins varied from about 12% to 44%. Dean and Whitehead (1963) also found that for several crudes the percentage of metals as metalloporphyrins ranged from 5% to 34%. Since some of the pure metalloporphyrins can be now synthesized in the lab, and unlike asphaltics these are well characterized, for the present investigation it was decided to use them.

TABLE III-2

NUJOL SPECIFICATIONS

(Courtesy: Plough Inc., Memphis, Tenn.)

Specific gravity @ 25°C	: 0.8750 to 0.8850
Viscosity @ 37.8°C	: 360 tc 390 SSU
Viscosity @ 100°C	: 54 SSU (Typical)
Flash point, Pensky-Martin open cup	: 216°C (Typical)
Pour point	: -32°C (Typical)
Refractive Index @ 20°C	: 1.48 (Typical)
Net Optical Density	: 0.100 maximum
U.V. absorption at - (Typical):	
275 mμ	: 0.075
295/299 mμ	: 0.150
299 mμ up	: 0.100
Distillation at atmospheric Pressure (Typical):	
IBP	: 358°C
50%	: 429°C
90%	: 470°C
95%	: 484°C
FBP	: 497°C

TABLE III-2 (continued)

Distillation at 10 mm Pressure (Typical):	
IBP	: 208°C
5%	: 240°C
10%	: 252°C
50%	: 274°C
90%	: 305°C
95%	: 317°C
FBP	: 329°C
Range of carbon atoms	: $C_{18} \sim C_{36}$
Average Formula	: $C_{30}H_{57}$
Average Molecular weight	: 417
Description, solubility, Acidity or alkalinity, readily carbonizable substances, solid paraffin, sulfur compounds, and cloud point	: all passes U.S.P. test.

Pure porphyrins as well as metalloporphyrins are fine solid powder at room temperatures. In order to dissolve them in Nujol, the mixture of the two have to be heated to about 200 - 300°C. It became clear in the early stage of the research that most of the porphyrins and metalloporphyrins are hardly soluble in Nujol. Thus a systematic approach to find the suitable metalloporphyrins was undertaken.

The solubility of a number of porphyrins and metalloporphyrins have been tried. All of these compounds were purchased from Man-Win Chemicals, Washington, D.C.. Prof. Peter Hambright of Howard University, Washington, D.C. has been of immense help in suggesting and providing the various type of porphyrins.

The maximum solubility of Nickel Tetraphenylporphine (Ni(II)TPP) in Nujol is 35 parts per million (ppm by weight) of nickel in the solution. However, the solubility of vandyl tetraphenylporphine (VO (IV) TPP) is only 15 ppm; even with such low concentrations it precipitates inside the tubes upstream of the reactor. Tetraphenylporphine (TPP) has four  groups. The solubility of PARA-CH_3-TPP  has also been tried and is found to be very low. But it is suggested that Meso-CH_3-TPP 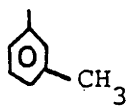 may be more soluble and should be given a try (Hambright - 1978). Solubility check of Nickel and Vanadyl TPP in a aromatic like α-methyl naphthalene also failed. As discussed in sec. II-B.1., the two most important types of

metalloporphyrins found in petroleum are DPEP and Etio type, therefore the work with TPP was not persued further.

Metal free Hematoporphyrin Dimethyl Ester (HPDME), a natural porphyrin derivative, also has low solubility. Again it is speculated that Hematoporphyrin-IX-Dimethylester should be more soluble (Hambright - 1978) but was not checked. Solubility of nickel Protoporphyrin Dimethylester (Ni(II)-PPDME) is also found to be very low. It is found that solubility of Vanadyl mesoporphyrin Dimethylester (VO(IV)MPDME) is sufficiently high, but the cost is prohibitive to allow its usage. Solubility of Octaethylporphine (OEP) in the form of magnesium-OEP was also tried and is found to be low.

Finally, it is found that the concentrations of metals obtained in the solutions of Nickel-Etioporphyrin-I(Ni (II)-Etio I) and Vanadyl-Etioporphyrin-I (VO(IV)-Etio I) may be as high as forty ppm. Solution of Ni-Etio I is more stable than Vandyl Etio I. When Vanadyl Etio I solutions of vanadium concentrations higher than 30 ppm are allowed to stand for a couple of days the vanadium concentration invariably falls to about 25 ppm. However, of all the porphyrins tried Ni-Etio I and VO-Etio I seems to be the most optimal ones and have been used as model metal compounds for this research. The structures of Ni-Etio I and Vanadyl Etio I are shown in fig. II-3.

Now we have the metal compounds, the suitable solvent and also the catalyst and it is time to look at the reactor.

D. REACTOR DESIGN CONSIDERATIONS: Most of the hydrodesulfurization reactors used in chemical industry are trickle bed reactors (Weekman - 1976). In typical trickle bed reactors the gas and liquid phases flow concurrently downwards (Satterfield - 1975). Upflow reactors have also been commercially employed (Kubo, 1975).

However, the operation of trickle bed reactors are not very well understood. Hydrodynamic effects are poorly defined. Considerable controversy over the characterization of the contact efficiencies of gas liquid and solid exists. Dudukovic and Mills (1978) observed that the catalyst effectiveness factor in trickle bed reactors is a function of the Thiele modulus, incomplete external wetting, and fractional pore fill up; it is precisely these last two which are very poorly understood. It has also been observed that in some cases one gets almost twice the global reaction rate in the larger pilot plant compared to the bench unit (Weekman - 1976). The cause for the increase in global reaction rate with the increase of reactor size has been attributed to increased efficiency. The efficiency depends on the liquid holdup (Goto et al. - 1975, Schwartz et al. - 1976), mass transfer effects (Specchia et al. - 1978, Sylvester et al. - 1975), axial dispersion (Mears - 1971, Shah et al. - 1978), catalyst wetting (Purnanik an Vogelpohl - 1974), and also on the uneven flow distribution or channeling (Herskowitz and Smith - 1978).

Since the appearance of the excellent review by Satterfield (1975) the state of the art on trickle bed reactors has not changed significantly. As the trickle bed reactors are poorly characterized and suffer severely with complex hydrodynamic effects, it was decided to use a much more simple and well defined reactor system in our lab studies.

The simplified schematic of the reactor system used in this study is shown in fig. III-2. It is a continuous flow reactor where only the liquid solution without any gas stream is pumped through the reactor packed with the catalyst. The liquid solution is saturated with hydrogen gas at the room temperature ($\sim 25^{o}C$) and the desired hydrogen pressure, and is then pumped through the reactor. This makes the reactor system much more simple . However, the question of the availability of enough hydrogen for the reaction in the reactor needs some consideration.

Data on the solubility of hydrogen in a number of organic solvents at various temperatures and hydrogen pressures have been reported (Cukor and Prausnitz - 1972, Grayson and Streed - 1963, Prather et al. - 1977, Simnick et al. - 1978, and Sokolov and Polyakov - 1977). However, there is no data available on the solubility of the hydrogen in the Nujol. Thus, to make an engineering approximation, the solubility of hydrogen in Hexadecane is considered. Fig. III-3 is a plot of H_2 mole fraction vs. saturation pressure for two saturation temperatures, i.e., 26.9 and $76.0^{o}C$. The calculations were done by

SIMPLIFIED SCHEMATIC

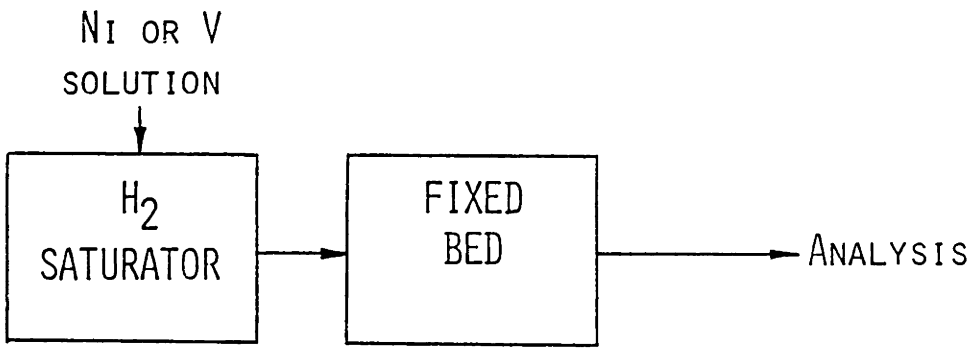

Fig. III-2

Simplified Schematic of the Reactor System

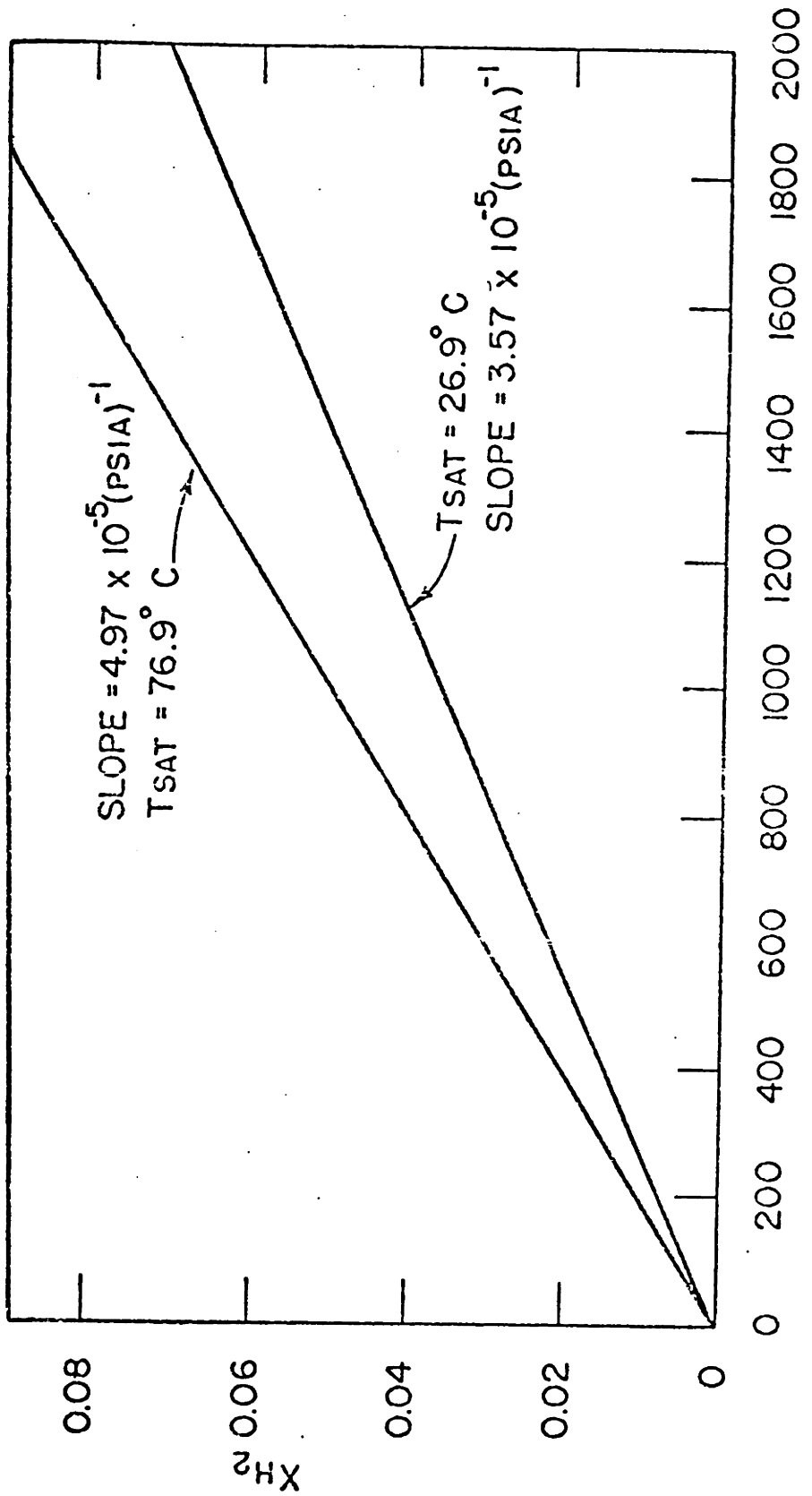

Fig. III-3: Calculated Molefraction of Hydrogen Dissolved in n-hexadecane at 26.9°C and at 76.9°C. (Courtesy: Dr. M.V. Bhinde).

the Chao-Seader correlation (Chao and Seader - 1961). It is seen from the figure that for the metal concentration of 30 ppm in the solution, the approximate ratios of the moles of H_2 to moles of metal (Ni or V) at 26.9°C and hydrogen pressures of 600, 1000 and 1500 psig would be 190, 300 and 450 respectively. This tells us that we will definitely have excess of hydrogen in the reactor. Excess of hydrogen does not necessarily mean that the rate constants would be independent of hydrogen pressure, but it insures that the change in the concentration of hydrogen from the inlet of the reactor to the exit of the reactor would be negligible. However, whatever we have discussed is for n-Hexadecane and is hoped that it would be applicable for Nujol. Indeed, later on in our experiments we did confirm that we have excess of hydrogen.

Another important property observed from fig. III-3, and also true for all the paraffins, naphthenes, olefins and aeromatics studied, is that the solubility of hydrogen increases with temperature (Cukor and Prausnitz - 1972, Prather et al. - 1977). This is to our advantage, as it insures that at reactor temperatures which are higher than the saturation temperature, no H_2 gas would leave the solution phase.

In the early stage of the project the idea of adding the good hydrogen donor solvents like Tetralin, Dihydronaphthalene, octaline and Cyclohexylbenzene was also considered (Doyle - 1976). But later on during the

experimentation it was found that we have more than enough hydrogen and there was no need to use a hydrogen donor solvent.

In the present study no carbon disulfide or any other sulfur compound is used in the feed solution, but if they were to be used the demand on hydrogen dissolved in the solution phase would increase (Broderick - 1979). If hydrogen sulfide were to be also dissolved in the solution, a good reference may be Tremper and Prausnitz (1976).

One of the central problem in the design of the laboratory reactors is to insure that the data is free from the influence of the unwanted transport effects (Anderson - 1968; Doraiswamy and Tajbl - 1974). In order to insure that channeling and wall heat transfer effects are not limiting, the radial aspect ratio (ratio of the bed diameter to the catalyst particle diameter) should be greater than four to five (Doraiswamy and Tajbl - 1974). This criterion assumes that the catalyst are spherical, but we are using catalyst extrudates which are cylinders. Therefore, the equivalent spherical diameter is calculated by the formula (Mears - 1971):

$$d_s = (d_c l_c + d_c^2/2)^{1/2}$$

where: d_c = diameter of the extrudate catalyst

l_c = length of the extrudate catalyst

d_s = equivalent spherical diameter

For the cylindrical catalyst of diameter 0.152 cm and length 0.432 cm (Table III-1) the value of d_s is 0.28 cm. In order to satisfy the above criterion of Doraiswamy and Tajble the internal diameter of the reactor should be greater than 1.4 cm.

Doraiswamy and Tajbl (1974) have also suggested that if axial aspect ratio is greater than 30 then axial dispersion and axial heat conduction effects can be neglected. For our system it implies that the length of the catlayst bed should be greater than 8.4 cm.

A reactor tube of internal diameter 1.75 cm (0.688 inch) outer diameter 2.54 cm (1 inch) and length 30.5 cm (12 inch) is chosen. It satisfies both the radial and axial aspect ratios.

E. REACTOR SYSTEM: Reactor system is designed on the basis of the information supplied by Eliezer et al. (1977). Dr. Manoj V. Bhinde (of Sun Oil Company, Marcus Hook, PA.) has been of immense help in the design and construction of the apparatus.

The operating conditions for which the apparatus is designed are listed in the Table III-3. A schematic flow diagram of the reactor system is given in figure III-4.

Since the reactor is designed to work up to 13.8 MPa ($\sim$2000 psi) of hydrogen pressure and 375-400^{o}C temperatures, the safety is of paramount concern. The whole equipment is mounted at the back of a portable strainless

TABLE III-3

TYPICAL OPERATING CONDITIONS

TEMPERATURE=280-380° C

PRESSURE=600-2000 PSIG

SOLUTION FLOW RATE=2-50 ML/HR.

INLET METAL CONC. =15-30 PPM BY WEIGHT

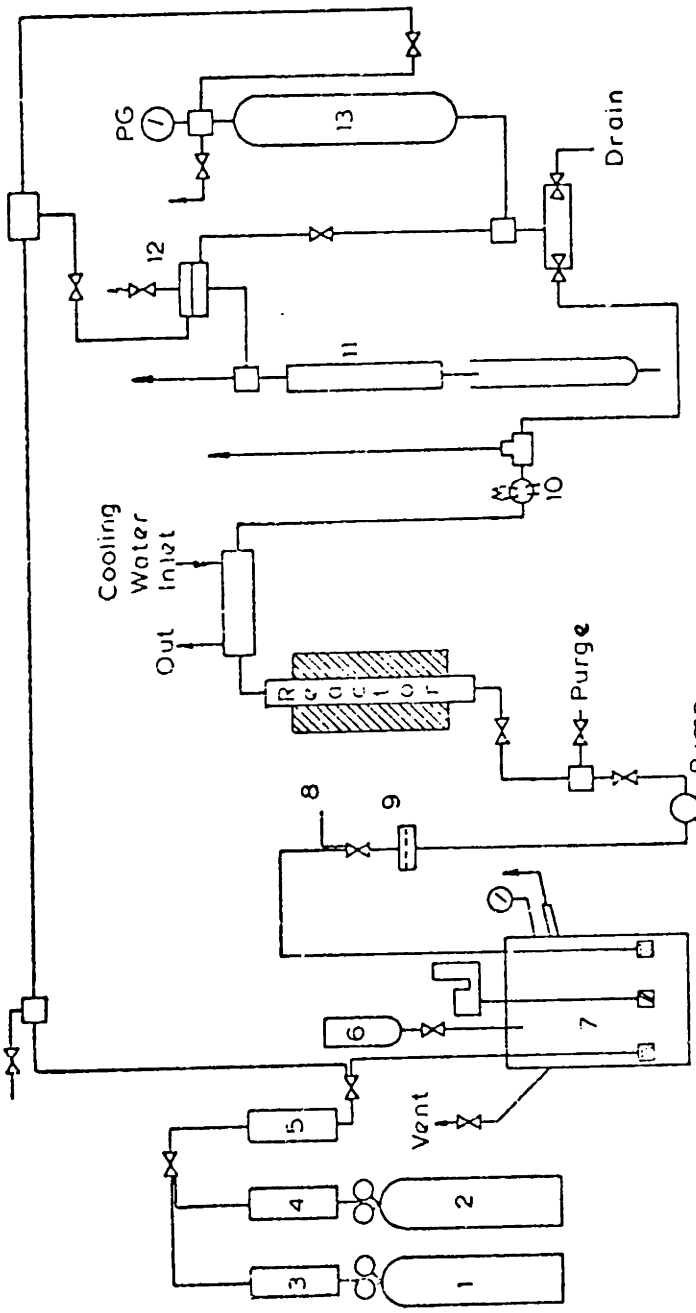

KEY

1 He Cylinder
2 H_2 Cylinder
3 Cu & Zn Oxides
4 Pt / Al_2O_3
5 Molecular Sieves
6 Charging Port
7 Two Litre Autoclave
8 From 1 Litre Autoclave
9 Line Filter
10 Sample Valve
11 Separator
12 Back Pressure Regulator
13 Sample Cylinder

Fig. III-4: FLOW SHEET OF THE REACTOR

steel barricade (fig. III-5). The thickness of the stainless steel sheets is 0.32 cm (1/8 inch). The back of the barricade is closed by a thin flexible sheet; this is done so that in an event of a mishap most of the pressure would be released from the back. Moreover, the whole barricade is connected to an exhaust, such that the mean residence time of the circulating air inside is less than 15 seconds; in case of a less severe leak of H_2 this will help to keep its concentration lower than the lower ignition limit of 4 percent by volume in air (upper limit being 75 percent of volume in air). The total dimensions of the barricade cart are 1.14X0.61X1.9 meter (3.75X2X6.25 ft); out of this only the top portion of 1.14X0.61X0.9 m (3.75X2X3 ft) is the stainless steel baricade and is used for mounting the equipment.

The main components of the reactor flow sheet are (1) Gas cylinders and the autoclave, (2) line filter and the pump, (3) furnace and the reactors, (4) cooler and the sampling value and (5) rupture disk, back pressure regulator and the separator. Each one of these are discussed below:

(1) Gas cylinders and the autoclave: A 2-litre autoclave (Autoclave Engineers, Erie, PA., Model AFP-2005) is used as the saturator. The gases are supplied to the autoclave through a filter (Water Associates, Milford, MA.) which acts as a sparger. Ultra high purity hydrogen, in 2200 psig cylinders, with concentration of oxygen less than 3

Fig. III-5: Front view of the portable stainless steel barricade. The whole equipment is mounted at the back of the barricade.

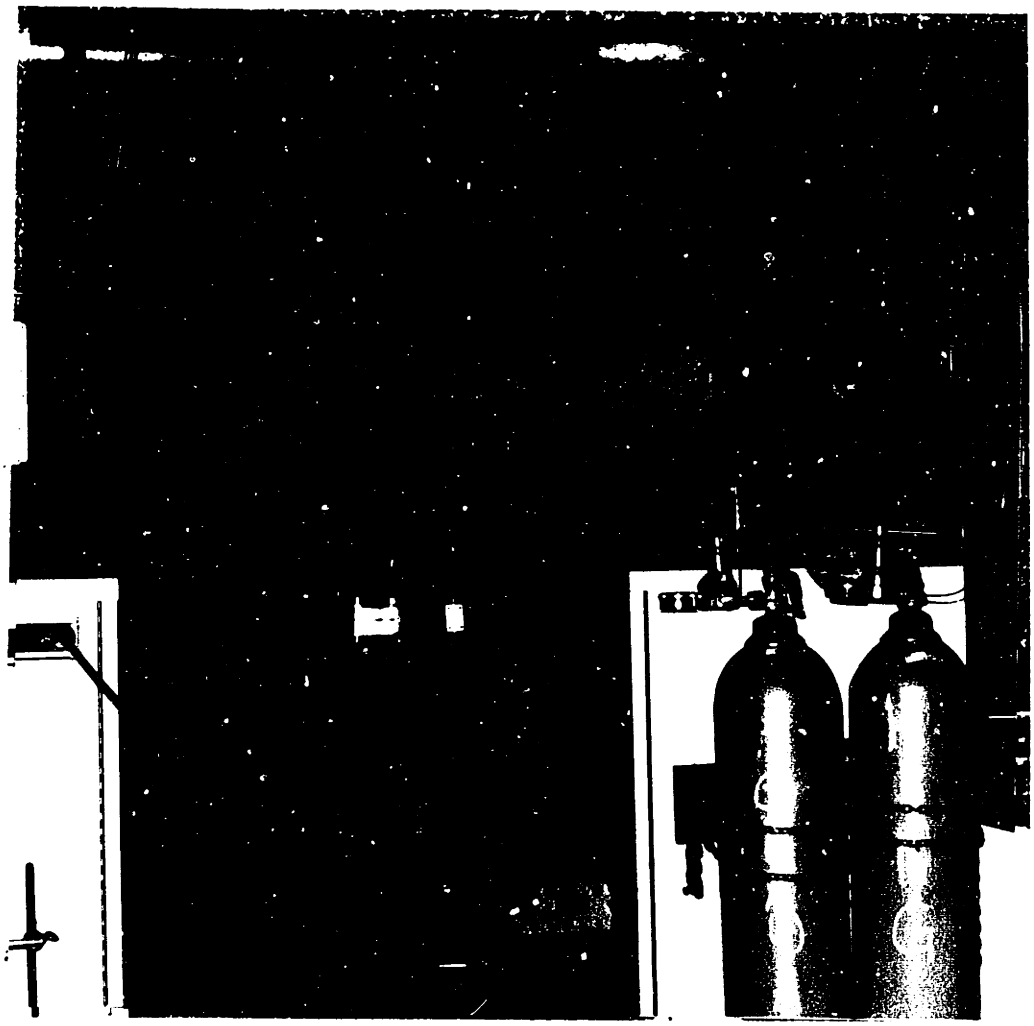

Fig. III-5: Front view of the portable stainless steel barricade. The whole equipment is mounted at the back of the barricade.

ppm and of hydrogen at least 99.999% is used. Helium, in 3500 psig cylinders, of 99.995% purity is used. Both the gases are purchased from Matheson Gas Products (Gloucester, MA.). The oxygen in hydrogen is converted to water by passing it through a column packed with 0.5 wt% Pt on alumina, 1/8 inch pellets type M Catalyst (Engelhard Industries, Newark, N.J.). In order to remove oxygen, helium is passed through a column packed with a mixture of nearly equal quantities of Copper catalyst, with 10% CuO on alumina (Cu-0803 T 1/8 inch) and Zinc catalyst, 100% ZnO (Zn - 0401E 3/16 inch); both of these were supplied by Harshaw Chemical Co. (Cleveland, Ohio). Molecular Sieves, Linde 4A (Union Carbide Corporation, Linde Division, South Plainfield, N.J.) are used to remove the water from both the gas streams. These molecular sieves are regularly generated by purging with helium at temperatures 425-450^{o}F for 2 hours at the flow rate of 800 standard cu cm/min; this roughly gives the adsorption capacity of 8% by weight. All the three catalysts are packed in Stainless Steel 316 column of 1/2 inch outer diameter (O.D.) and 16" in length (columns 3, 4, and 5 in Fig. III-4).

There is also a one litre autoclave, shown by point 8 in fig. III-4, which is connected to the apparatus. Two autoclaves give much more flexibility in varying the solution feed conditions to the reactor and also remove the time limitation; as when one autoclave is about to get

empty the flow can be switched to the another one. The one litre autoclave is very similar to the two litre autoclave described above, however for more details see Hung (1979).

(2) Line filter and the pump: The saturated feed from the autoclave is filtered through a 0.5 micron filter (high pressure stainless steel line filter, 25 mm, model # xx45-02500; manufacturer: Millipore Corp., Bedford, MA.) and supplied to a high pressure feed delivery pump.

The pump is a 6000 A solvent delivery pump (Water Associates Inc., Milford, MA.). The pump as supplied can deliver the feed at the rate of 6-600 cm^3/hour in the step increaments of 6 cm^3/hour up to the pressure of 41MPa ($\sim$6000 Psi). However, for our kinetic studies we need the flow rate as low as 1-2 cm^3/hour and should be able to vary the flow rate with in 0.1 cm^3/hour step sizes. To achieve this, a frequency synthesizer (Model 171, Wavetek, San Diego, CA.) is connected to the control unit of the pump. The synthesizer gives precision (0.005%) frequency from 1.000 HZ to 1.9999 MHZ in six discrete ranges. Frequency synthesizer's 50 ohm output with DC square wave and the attenuation of 20 dB is used. Amplitude and DC offset knobs are set in 1 and 2:30 clock positions respectively. Now by varying the frequency input to the pump the frequency of the reciprocating pistons is changed and hence

the flow rate from the pump can be varied. Within the experimental error the following equation adequately describes the calibration curve for the flow rate vs. frequency:

Flow rate (gms/hour) = 0.2420 frequency (HZ) -0.05

In an ideal case the intercept should be zero and a non-zero value reflects the experimental error. To get the flow rate in ml/hr, the density of the solution used is 0.8752 gms/ml. Thus now we have a large flexibility in the flow rates.

The pump also has a pressure transducer at its outlet, which sends the signal in the range of 0-10 mv. In the range of 0-6000 Psig the signal is directly proportional to the operating pressure. This signal is fed to an on/off control device (Model No. 0303-x, LFE Corp., Process Control Division, Waltham, MA.). The maximum tolerable pressure for any given run is set on the on/off controller and the reactor pressure signal from the pump is always fed to it. In case, the operating pressure is equal to the set pressure, the pump would stop pumping the solution. This safety device is not only for the reactor but also to save the pump from any damage.

The pump cannot take any fine particles in the solution, but in three to four days the solution in the autoclave starts forming a very small amount of precipitate of the metal compounds, and therefore upstream of the pump a

line filter is provided. In any event, if the pump malfunctions due to the metal porphyrin deposition inside, the run has to be stopped. The pump is cleaned by first pumping chloroform and then xylenes (both reagent grade). In most cases it makes the pump operational again. But if this cleaning is not sufficient, more solvents are pumped in the order-acetone, distilled water, 6N nitric acid, a lot of distilled water, acetone and finally Xylenes. If pump is still not operational the manufacturer has to be contacted.

(3) Furnace and the reactors: In our study we need two kinds of reactors; one for the kinetic data collection and the other for the reaction limited by the intraparticle mass transport. In the preceding section we have already discussed the use of an one inch O.D. tube as the reactor for the study of intraparticle limited reactions; in the rest of this thesis we will refer this reactor as one inch reactor. The dimensions of the reactor used for kinetic rate measurements are 0.95 cm O.D. X 0.52 cm I.D. (3/8"X0.203"); since this dimension is much less than the dimensions of the one inch reactor we will refer it as micro reactor. The design considerations for the choice of the dimensions of the microreactor are discussed in the next chapter. Our reactors are upflow reactors.

A schematic sketch of the 1" reactor is given in fig. III-6. About 12 cm ($\sim$5 inch) of the preheating zone to heat the solution to the desired reaction temperature is

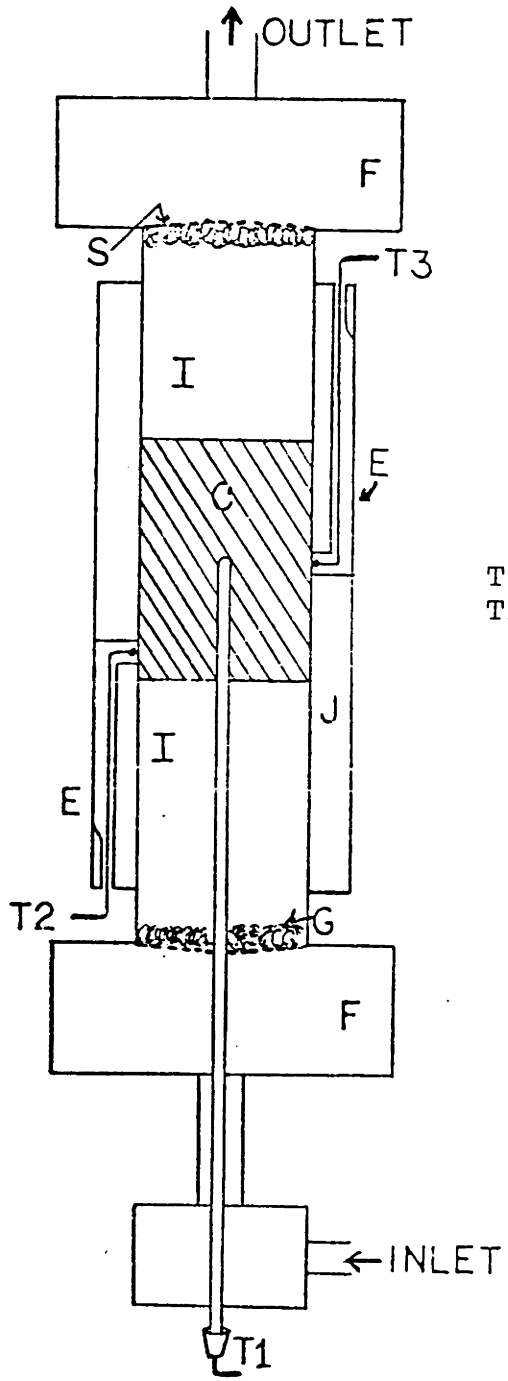

C = Catalyst bed
E = Sealing Cement
F = Fittings
G = Pyrex Glass Wool
I = Inert Packing
J = Outer Jacket
S = 5 Micron Wire Cloth
T1 = 1/16" Thermocouple
T2,T3 = 1/32" Thermocouples

Fig. III-6: Schematic Sketch of the One Inch Reactor

needed. Since at the outlet of the reactor there are heat losses due to the conduction and radiation, therefore in order to have nearly a uniform axial temperature along the length of the catalyst bed it is necessary to povide approximately 8 cms (∿3 inches) of postheating zone. As discussed in the preceeding section the length of the catalyst bed should be about 10 cm (∿4 inches); and hence the total length of the reactor tube heated is 30 cm (∿12 inches).

Fittings at the ends of the reactor also take up some length of the tube and it turns out that the exact length of the tube used is 45.1 cm (17 3/4"). Thus a stainless steel -316 tube of dimensions 1" O.D.X0.688"I.D.X17 3/4" length is purchased from Autoclave Engineers (Erie, PA) and is used as the reactor tube. This reactor tube is rated for 69 MPa at 38^{o}C (10,000 psi at 100^{o}F) and about 55 MPa at 540^{o}C (8,000 psi at 1000^{o}F). With respect to the pressure rating it should be noted that, beyond 1000^{o}F, it drops rapidly for stainless steel-316.

The inert packings in the preheating and post heating zones are 3 mm diameter pyrex glass beeds. The catalyst bed consists of 0.152 cm extrudates diluted with about 2 mm diameter pyrex cylinders broken to about same length as that of the extrudates. Normally the dilution ratio by volume of the inert: catalyst used is 2.5:1; the justification for this is treated in chapter V. In order to support the catalysts and the inerts, both the ends of the

tube are packed with a small quantity of glass wool and plugged with a stainless steel-304 wire cloth of 5 micron openings (Part # CX-2300, Small Parts Inc., Miami, Florida).

The whole reactor tube is placed snugly in an 316 SS tube of 3.2 cm (1 1/4") O.D. The purpose of this tube is two fold a) to provide uniform heat distribution to the reactor tube; b) to hold two thermocouples against the external surface of the reactor tube. These two thermocouples are chromel-alumel with 0.79 mm (1/32") diameter 304 S.S. sheath and are held at different places on the tube by sealing cement (Powder # 33, Sauereisen Cements Company, Pittsburg, PA.). There is also a chromel-alumel thermocouple with 1.59 mm (1/16") diameter 304 S.S. sheath located inside the reactor tube in the catalyst bed. All the three thermocouples are purchased from Omega Engineering, Inc. (Stamford, Conn.) and provide information on the radial and axial temperature distributions in the catalyst bed.

The reactor tube along with its external jacket tube is mounted inside a Lindberg compact tube furnace (CAT. NO. F8408-1, Scientific Products, Columbia, MD). The dimensions of the heating chamber are 3.175 cm I.D. X 30.5 cm length (1 1/4" X 12") and is designed for the maximum temperature of 1010^{o}C. In order to get a better temperature control of the furnace, the original furnace controller is replaced by a Thermo Electric temperature

controller (Model No. 32402, Saddle Brook, N.J.) This temperature controller gets its signal input from an iron constantan thermocouple located in the furnace heating chamber. Since there exists a finite possibility of the failure of the controller thermocouple, an additional on-off controller (Model # 3234211005, Thermo Electric) which gets its signal from an independent chromel-alumel located on the external jacket of the reactor tube is used. In case the temperature of the reactor exceeds the set temperature, on-off controller would shut the power supply to the furnace.

All the thermocouples from the reactor are connected to a digital temperature indicator (Model 2170A, Omega Engineering Inc., Stamford, Conn.).

The most of the details of the microreactor are the same as of the one inch reactor. It is a stainless steel -316 tube of dimensions 3/8" O.D.X0.203"I.D.X17 3/4" length, and is purchased from the Autoclave Engineers. This reactor tube again fits snugly in an 1 1/4" O.D. and 316-S.S. tube. This time the outer jacket tube is fairly thick and provides the thermal inertia to the reactor tube and insures a better temperature distribution in the radial direction. Again the outer jacket tube has two thermo-couples mounted on it. This time the reactor has a very low internal diameter and there is a fear that if a thermo-couple were to be placed inside it would disturb the flow

pattern and hence no thermocouple was placed. The rest of the details are same as for the one inch reactor.

(4) Cooler and the sampling valve: The solution coming out of the reactor is passed through a cooling jacket, and is cooled to near room temperature by a cold water stream. This serves two fold purpose (i) saves the sampling valve downstream from being exposed to temperatures higher than 75°C; and (ii) samples collected from the sampling valve are low in temperature and hence unwanted possible reactions with the oxygen in air are avoided.

The sampling valve is a chromatographic valve (Model No. CV-6-UHPa, Valco Instruments, Houston, Texas). Its dead volume is nearly zero and is rated up to 7000 psig pressure and 75°C temperature. Sampling valve is drawn in fig. III-7. In our lab we have found that the volume of the sample needed is less than 2 ml and therefore the sample loop volume of 2 ml is sufficient.

The solution from the reactor outlet always flows through the sample loop (fig. III-7a). In order to collect the sample, the handle is turned clockwise and the piston of the 10 ml syringe (B-D multifit syringe, Becton-Dickinson, Rutherford, NJ) is pressed (fig. III-7b). In this position of the handle the sample loop is disconnected from the reactor tube. The air in the syring forces the liquid out of the sample loop in to a sample vial. Now the syringe is disconnected, filled with Xylene, and is connected back. The sample loop is now filled with Xylene

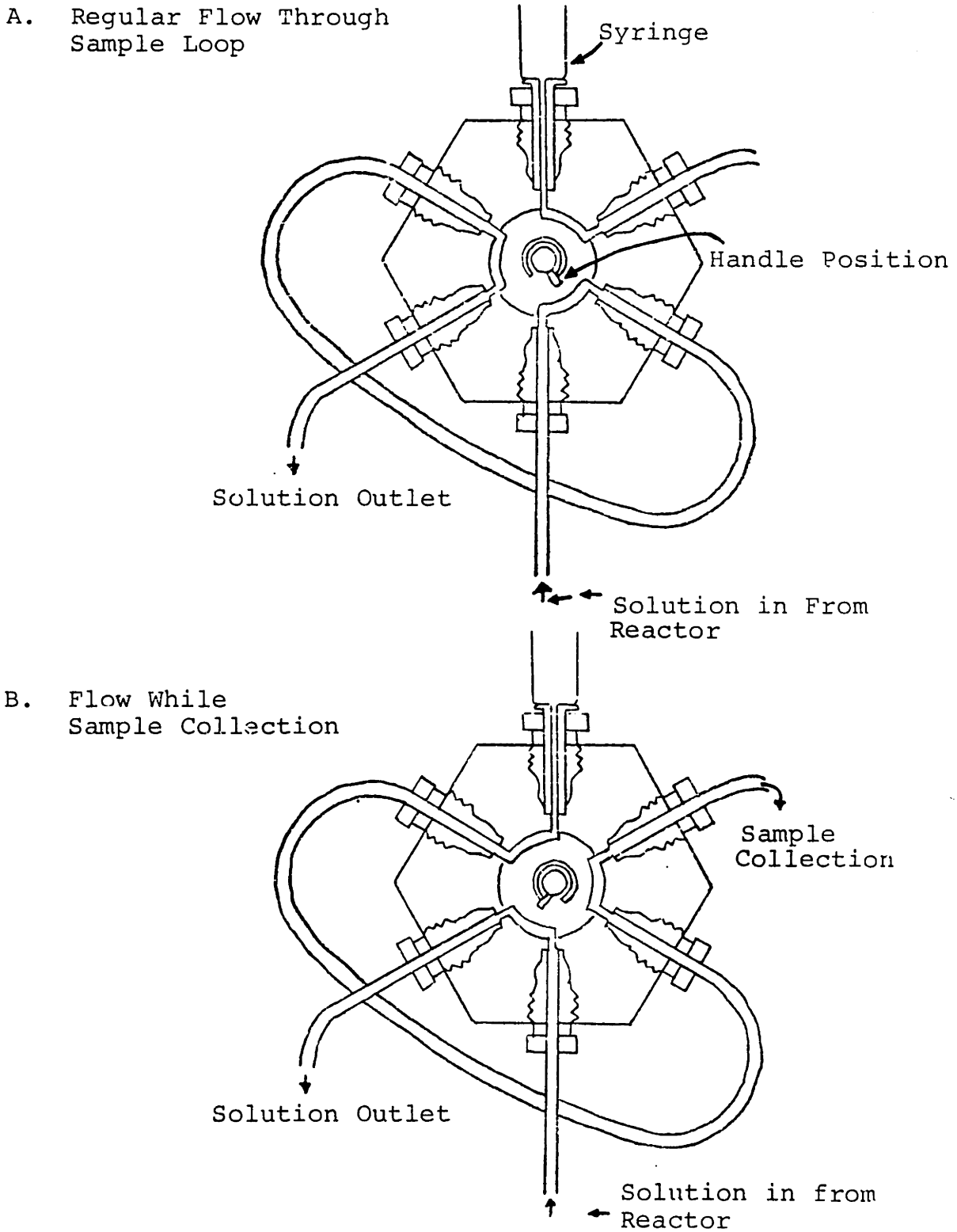

Fig. III-7: Flow Through Sample Valve. While A. Regular Flow; B. Sample Collection

and the handle is turned counterclockwise to its original position. It is necessary to fill the sample loop with Xylene to avoid introduction of any oxygen in the reactor system. Left over Xylene in the syringe is purged with acetone and then dried by blowing a little air through it. Now before the next sample collection one has to make sure that at least 6-8 ml of solution has been fed through the sample loop.

In order to reduce the dead volume between the reactor outlet to the sample valve, 1.59 mm O.D.(1/16") stainless steel 316 tubing has been used.

(5) Rupture disk, back pressure regulator and the Separator: As a safety precaution the stream from the sample valve goes through a rupture disc of rating 2500 psig. Finally, the solution goes through a back pressure regulator to the separator and then collects in the buret. The dome of the back pressure regulator is pressurized with helium to the desired reaction pressure and thus the pressure in the reactor is maintained at the required level. The back pressure regulator (Model 91W, Douglas Sales Co., Woburn, MA.) is rated up to 2000 psi. In the seperator, dissolved gases are separated. The graduations on the buret help to monitor the flow rate of the solution. One litre sample cylinder is connected in parallel to the back pressure regulator; it acts as a large dead volume and dampens any minor fluctuations in the pressure of the system.

A photographic view of all the pieces mounted at the back of the barricade is given in fig. III-8.

F. REACTOR OPERATING PROCEDURE: The required reactor tube is packed with the inerts and the catalysts. While packing it is tapped regularly to insure the reproducibility of the packing. Then the reactor is mounted in the furnace and is pressure tested with helium for at least 500-1000 psi above the operating pressure. Normally the pressurized reactor is left overnight and the pressure gauge over the sample cylinder is monitored. This confirms the absence of even a minor leak in the reactor system.

At the same time two litre autoclave is also pressure tested for the desired pressure and is then depressurized and charged with 1750 ml of the metal solution. With the stirrer speed around 200-300 rpm, for the first forty-five minutes helium at the pressure of about 300 psig is purged through the solution at the rate of around 5 litre/min; for the next forty-five minutes hydrogen at the same pressure and rate is purged. This is done to make sure that the solution in the autoclave is totally free of dissolved air. Now the pressure of the hydrogen in the autoclave is raised to the reaction pressure. This autoclave is kept stirred for another two to three hours. It is believed that the typical saturation time is less than two hours. The unstirred solution is allowed to stand overnight. This makes the solution fed to the reactor free of any hydrogen bubbles.

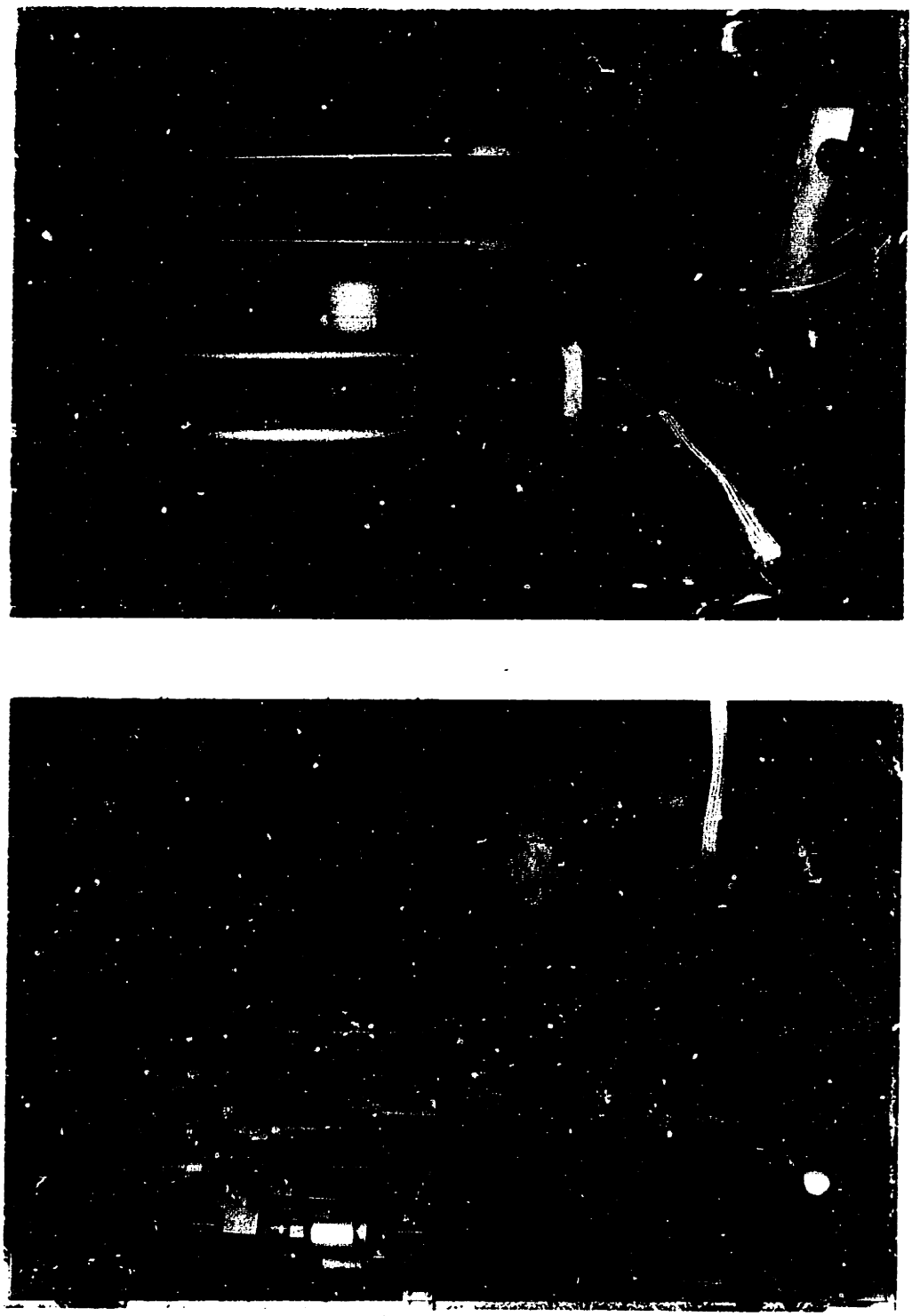

Fig. III-8: A photographic view of all the equipment pieces mounted at the back of the barricade.

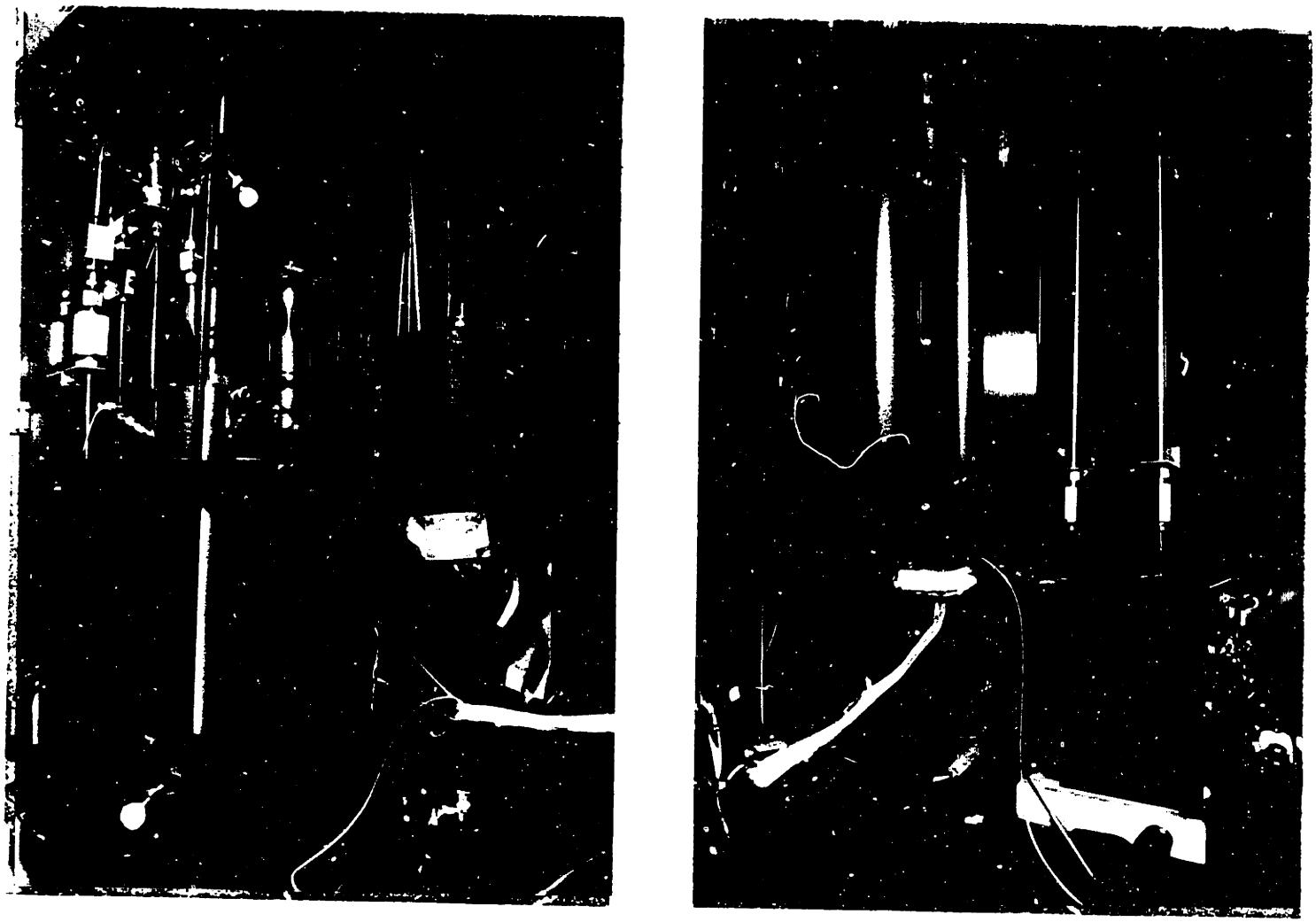

Fig. III-8: A photographic view of all the equipment pieces mounted at the back of the barricade.

Once the reactor is leak tight it is heated in three hours with a step increase of about 60-80^{o}C per thirty minutes to a temperature of 370-390^{o}C. The helium in the sample cylinder is released through the purge line and the pressure of the system is brought down to about 300 psig. The dome of the back pressure regulator is pressurized with helium to the required reaction pressure. For the next three hours reactor is purged with helium at the rate of 2.5 litre/min. Again the purpose of helium purging is two-fold (i) to remove all the air from the reactor system; (ii) to remove the moisture of the catalyst. Adams et al. (1974) observed that even out of a soaked gamma-alumina, at 350^{o}C, most of the moisture can be removed in less than one hour. Therefore a period of three hours with He flowing over the catalyst at 370-390^{o}C should be a sufficient time.

Once the reactor has been purged, the pressure of helium in the reactor is increased to the reaction pressure. The setting on the temperature controller is decreased to bring the temperature of the reactor to the reaction temperature. The supply of solution from the autoclave to the pump is opened. About 20 ml of solution is pumped through the reference valve of the pump and then about 3 ml of solution is collected in the sample vial. Then for about five minutes the solution is pumped through the purge and sample is collected in another sample vial. These two samples would tell us the concentration of the

metal in the solution at the reactor inlet. Now purge valve is closed and the valve to the reactor is opened. The solution is allowed to flow to the reactor, till the catalyst in the reactor are covered with the solution. For one inch reactor at the solution flow rate of about 69 ml/hr (250 HZ frequency) it takes about 25 minutes; and for microreactor at the feed flow rate of 10 ml/hr (36.60 HZ frequency) it takes 15 minutes. Next step is to stop the pump and vent the helium from the reactor system till the pressure drops to some low valve (say~20 psig). Now the reactor is pressurized back to the required level with hydrogen and pump is started to feed the solution to the reactor. The reactor is now on stream. It has a great deal of flexibility and allows the operator to change the operating conditions when desired.

Once the run is completed, pump and the temperature control units are shut off. The liquid from the sample cylinder is drained off, and the liquid in the reactor is taken out through the purge line. Then the reactor is cooled down rapidly by allowing hydrogen and helium to flow from the reactor to the purge. Once cooled, the reactor can be disconnected to be cleaned and packed for the next run.

G. ANALYSIS OF LIQUID SAMPLES: The oil samples collected from the reactor are too viscous and high in metal concentration to render to any conventional analysis. Therefore a weighed quantity (0.3-0.75 g) of solution is transferred in a 10 ml volumetric flask and Xylene (ΔX-5-S, ACS certified, Fischer Scientific, Fair Lawns, N.J.) is added to bring the total volume to 10 ml.

Two techniques of analysis- atomic absorption spectrophotometry and the visible spectrophotometery have been used.

(i) Atomic Absorption Spectrophotometry: The solution is burnt in a suitable flame and the metal atoms are ionized. Thus atomic absorption, irrespective of what chemical form metal exists in the solution phase, gives the total metal concentration (Hofstader et al. - 1976).

We used Perkin Elmer-403 (Norwalk, Conn.) atomic absorption spectrophotometer. The standard solutions of 5000 ppm of Nickel or Vanadium dissolved in paraffinic hydrocarbons (21 cst viscosity at 100°F and 400°F flash point) were purchased from Conostan Division, Continental Oil Company, Ponca City, Oklahoma. Standard solutions of about 150 ppm are prepared by diluting the 5000 ppm Conostan standard with Nujol. Even though the required amount of Conostan Stabilizer is added to this 150 ppm standard solution, it is not stable for more than one month. Each time for our analysis, the 150 ppm standard

solution was further diluted with Xylene to get approximately 5 ppm standard solution, which was then used to analyse the concentrations in the samples by the method of standard addition (Trent and Slavin - 1964).

For nickel analysis air-acetylene flame is used (Kerber - 1966, Moore et al. - 1966, Trent and Slavin - 1964). In our analysis the lower detection limit for nickel is about 0.05 ppm and the caliration curve is linear up to 1.5 ppm.

Vanadium analysis uses nitrous oxide - acetylene flame, and due to the reducing conditions of the flame the analysis is relatively more difficult and less accurate than nickel (Lang et al. - 1975, Manning - 1965, Smith et al. - 1973). The lower detection limit for vanadium is about 0.1 ppm and the calibration curve is linear up to 1.5 ppm.

(ii) Visible Spectrophotometry: Both nickel and Vanadyl etioporphyrins are red in colour and have intensive absorption peaks in the visible band. The spectra of Ni and Vanadyl etio were scanned in the visible range on the Cary-14 spectrophotometer and are given in fig. III-9. In both the figures, the break in the curve around 420 nm is due to change of zero on the absorbance scale. Both the spectra have a high absorbance peak, called the Soret band, around 400 nm. Porphyrin macrocycle is highly conjugated and Soret band is the result of this resonance (Smith - 1975). Two other peaks in the spectra are characteristic

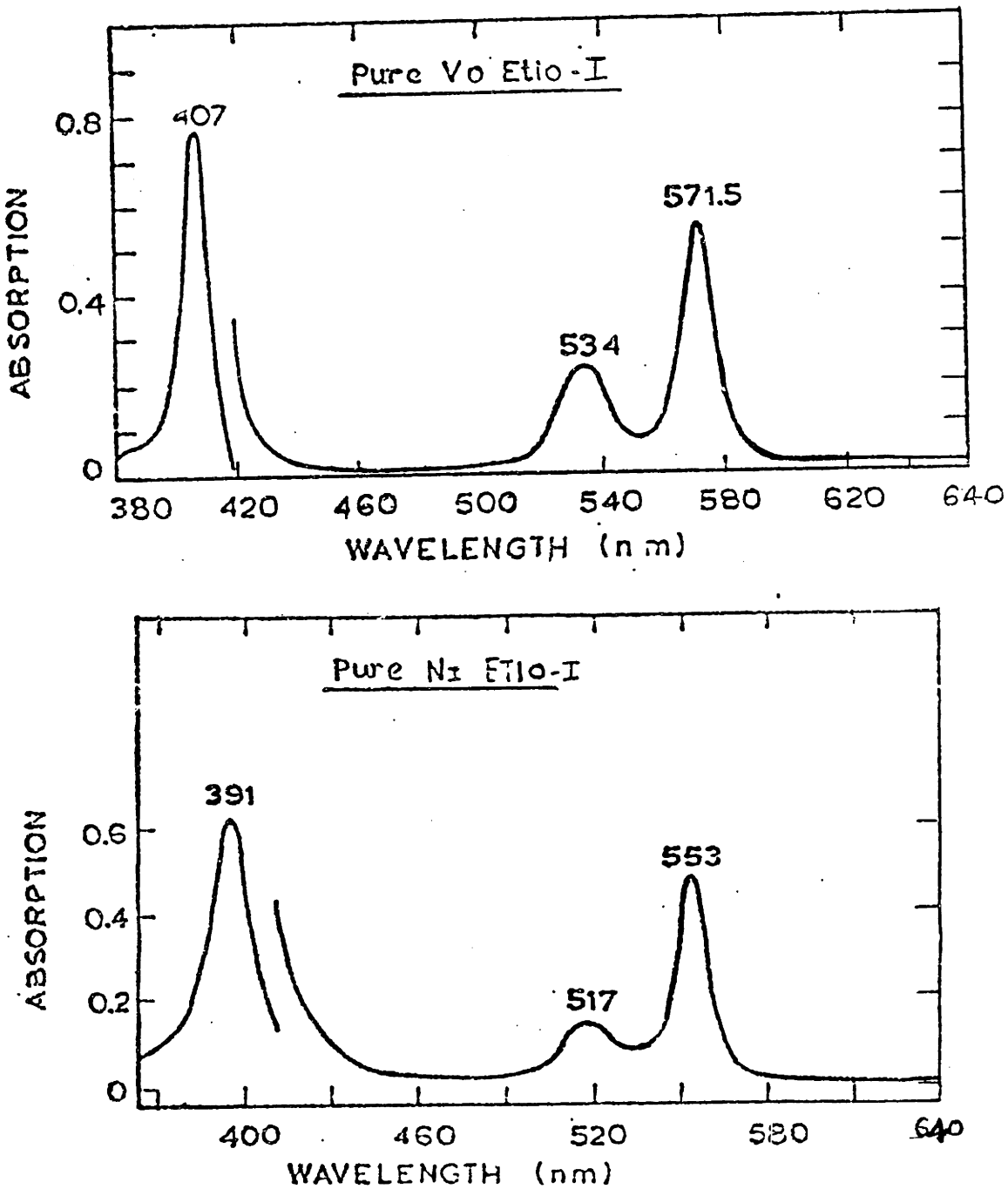

Fig. III-9: Visible Spectra of Vanadyl Etioporphyrin-I and Nickel Etioporphyrin-I in Xylene Solvent.

of the side chains. Either of these two peaks can be chosen and by the Beer's law the concentration of the metal porphyrin can be find out.

The solutions prepared for the atomic absorption are also used for the visible spectrophotometery. Coleman 111 (Perkin-Elmer) visible spectrophotometer is used for the quantitative analysis. For Ni-Etio and VO-Etio analysis peaks at 517 and 534 nm are chosen respectively. In order to draw a calibration curve, the pure metal-Etio solution in Xylene is prepared and its total metal concentration is measured by atomic absorption and finally the absorbance at the desired wave length is noted on the visible spectrophotometer. It has been found that for the Ni-Etio and VO-Etio at their respective wavelengths of 517 and 534 nm the absorption constant (absorbance/ppm metal) is about 0.18 ± 0.2 and 0.26 ± 0.3 respectively.

Therefore, while atomic absorption spectrophotometry gives us the total metal concentration, the visible spectrophotometry gives us concentration of the original metal-Etioporphyrin in the solution. For the visible spectrophotometer it is seen that (i) the absorption constant varies a great deal, (ii) for background absorbance pure Xylene is used which may not be identical to the sample collected from the reactor and (iii) the effects of any structural change in the side chains of metallo-porphyrin ring are not known. Therefore the

magnitude of the errors involved in the visible spectrophotometer analysis are fairly large and the reliability of the calculated concentrations low.

H. PREPARATION OF NICKEL AND VANADYL ETIO-I SOLUTIONS IN THE WHITE OIL: Both nickel and vanadyl etioporphyrins are powder at room temperatures and in order to dissolve them in Nujol the mixture of the two has to be heated to about 200°C. It is found that if the mixture is heated in an open pyrex beaker for about five hours, the concentration of the metal in the resulting solution as given by atomic absorption is about 25-30 percent higher than the one given by visible spectrometer. It implies that the 25-30% of the total metal present in the solution is not metallo-etioporphyrin any more. Heating the mixture in a stainless steel beaker, teflon bottle and a closed pyrex glass bottle gave similar results. About 50 ml of the mixture, in a pyrex glass flask, was purged with helium at the pressure of about 10 psig for about 15-20 minutes and heated under the helium atmosphere. It was found that still 10-15 percent of the total metal present in the resulting solution was nonporphyrinic. Since the nonporphyrinic metal decreaed, it was clear that the dissolved oxygen in the Nujol was culprit and purging with helium at a low pressure helped but could not remove all the dissolved air.

A better system to remove all the dissolved air in the Nujol is developed. The oil is filtered through a 5 micron filter paper under vacuum. Since the oil drops are very fine, due to the surface tension effects almost all the dissolved air is pumped out. The filtered oil with the required quantity of porphyrin is heated for about one hour under vacuum and at the temperature of about 80°C. Any left over dissolved gases would be removed now. At the end of one hour, vacuum pump is disconnected, and helium at about 10 psig is introduced in the flask. Under this inert environment, the solution is heated at 300°C for four hours and is then left under the helium environment to cool down to the room temperature. The cooled solution is filtered through a 0.5 micron filter paper to remove all the undissolved metal porphyrin. In this filtered solution the total metal and the metalloporphyrin concentrations, with in the experimental error of the analysis, agree reasonably well.

It is observed that if a small quantity of metal-porphyrin solution is placed in an oven at 80-100°C, with in twelve hours the dark red coloured solution is converted to light yellow colour. This further proves that at moderate temperatures metal-porphyrins used are highly reactive to oxygen (when heated in nitrogen, no reaction is observed).

In any one batch about 1300 ml of solution is prepared in a two litre Erlenmeyer flask fitted with a 24/40 joint at its opening. The pyrex glass filter (Model No. xx1004700), 5 micron filter paper (FHUP04700) and 0.5 micron filter paper (LSWP 04700) are purchased from Millipore Corporation, Bedford, MA.

Finally, as stated in the sec. III.C., the solubility limit of both Ni(II)-Etio I and VO(IV)-Etio I is about forty ppm.

I. SEPARATION AND IDENTIFICATION OF REACTION INTERMEDIATES: The visible spectra of the samples collected from the reactor outlet for VO-Etio and Ni-Etio are given in figures III-10 and III-11 respectively. When these spectra are compared with the ones shown in fig. III-9, it is seen that for both VO-Etio and Ni-Etio there is a new peak at 631 and 616 nm respectively. It is further observed that in most of the solution product samples the concentrations of the total metal are higher than the metal-Etioporphyrin concentrations by 10-30%. Thus, for both the compounds we have the formation of at least one important reaction intermediate.

It can be argued that if we assume the formation of only one important reaction intermediate, its concentration can be found by the difference in the concentrations given by atomic absorption spectrophotometry and visible spectrophotometry. Since we are dealing with low metal

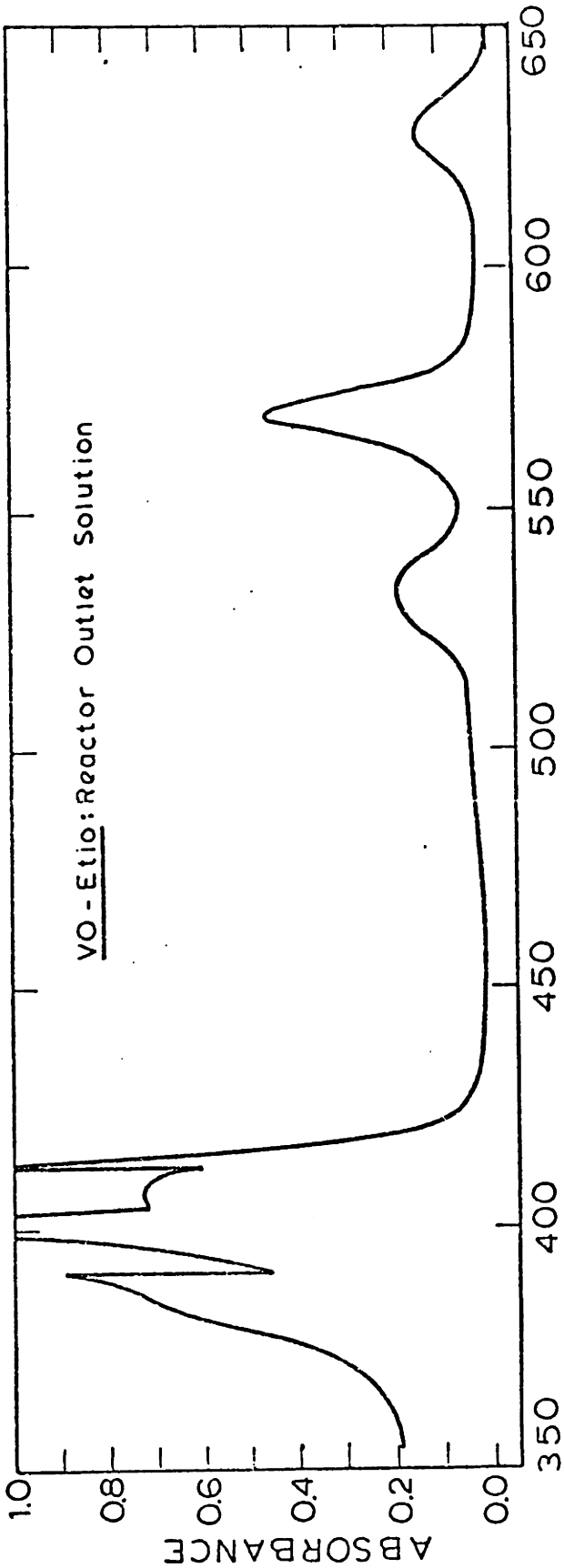

Fig. III-10: Typical Visible Spectra of the Sample Collected From the Reactor for the Vanadyl Etio (I) run. Solvent: Xylene

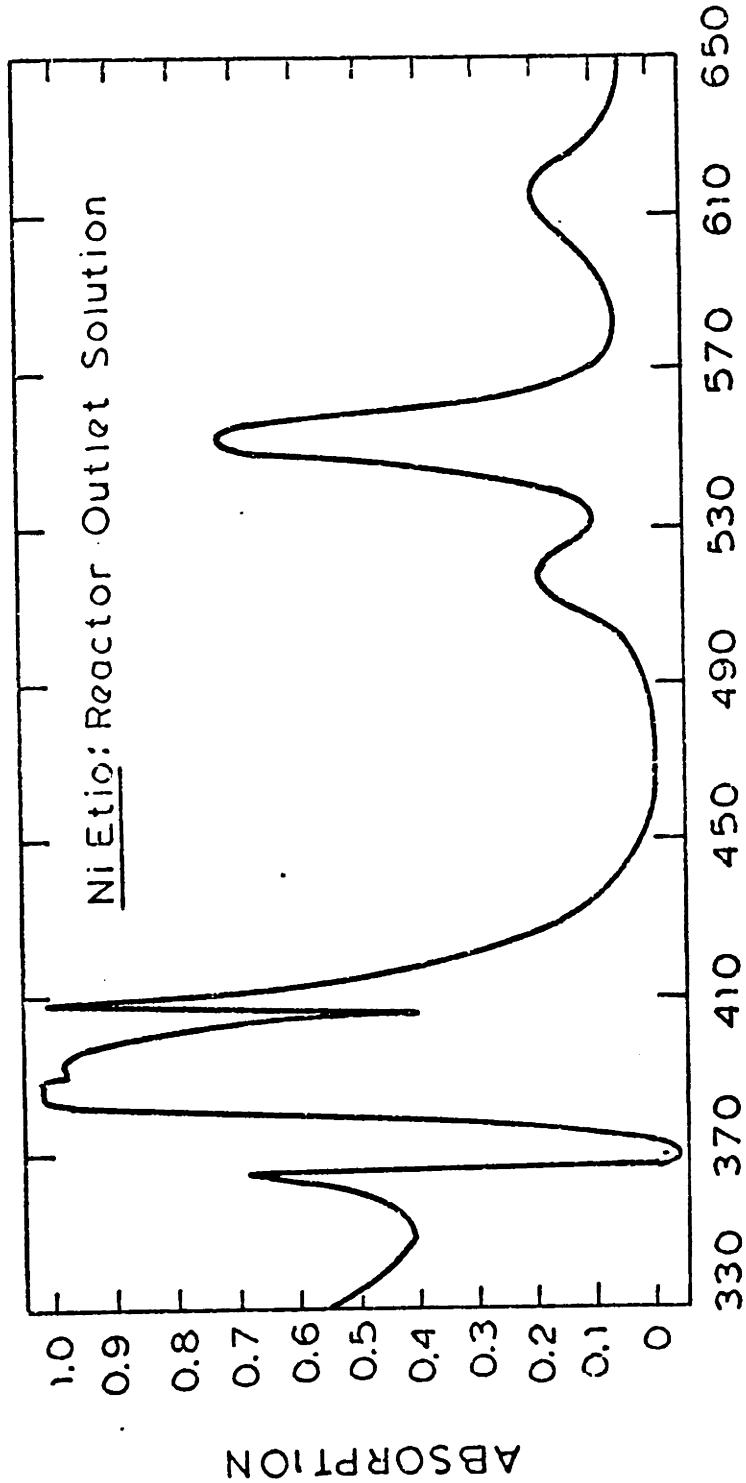

Fig. III-11: Typical Visible Spectra of the Sample Collected from the Reactor for the Nickel Etio (I) run. Solvent: Xylene

concentrations, the range of the concentration values for the intermediate are 0-5 ppm with the typical values around 2-3 ppm. As discussed at the end of sec. III.G the concentration values of metal-Etioporphyrins found from the visible spectrophotometer are a great deal in error ($\pm$1.5-2 ppm) and therefore precludes the possibility of the calculation of the concentration of the intermediate from the difference of the two concentrations.

The first guess would be that the reaction intermediates may be hydrogenated product of the pure metal Etioporphyrins and by comparing the visible spectra of these with that of the reaction product the intermediates could be identified. Unfortunately none of the possible hydrogenated forms of either VO-Etio or Ni-Etio are commercially available. Therefore, it is necessary to separate the intermediates from the reaction product, identify and measure their concentration by an independent technique.

(i) Separation: The technique used for the separation is "Dry Column" chromatography (Loev and Goodman - 1970). A 1" diameter pyrex glass tube, fitted with a fritted disk at the bottom, is packed up to about 3 inch height with A-540 adsorption alumina (Fisher Scientific) of the size 80-200 mesh. 200 ml of the liquid product from the reactor is diluted with 200 ml of Xylenes (ΔX-5-S, ACS certified, Fisher Scientific, Fair Lawns, N.J.) and is allowed to trickle down the alumina column. As the liquid trickles

down, the metal compounds are adsorbed at various heights and a colourless metal free solution comes out of the column. The result for the VO-Etio product is shown in fig. III-12. The unreacted VO-Etio is adsorbed as a dark red colour band while the green colour band is due to the reaction intermediates. The appearance of the green colour is not surprising. Since in fig. III-10 we saw a strong peak at 631 nm and the complimentary wave length of the light for the wave lengths greater than 600 nm is around 490 nm which is green in colour (Evans - 1948). Similar results are obtained for the nickel.

The adsorbed column of the alumina is taken out of the pyrex glass tube and the green band is separated. The glass tube is again packed with four inches of pure alumina and the green adsorbed alumina is placed at its top. About 200 ml of pure Xylene is allowed to trickle down. The adsorbed red coloured porphyrins remains at the top and a more pure green colour band travels down. The other advantage is that the alumina is cleaned of adsorbed oil. The bottom green coloured alumina is taken out and with the help of the reagent grade chloroform (#4441, Mallinckrodt Inc., St. Louis, Missouri) all the adsorbed porphyrins are extracted. The chloroform is evaporated under vacuum and one is left with the green coloured compound. The visible spectra of the green coloured compound is scanned and if it shows any peaks corresponding to the original metal etioporphyrin the purification step with

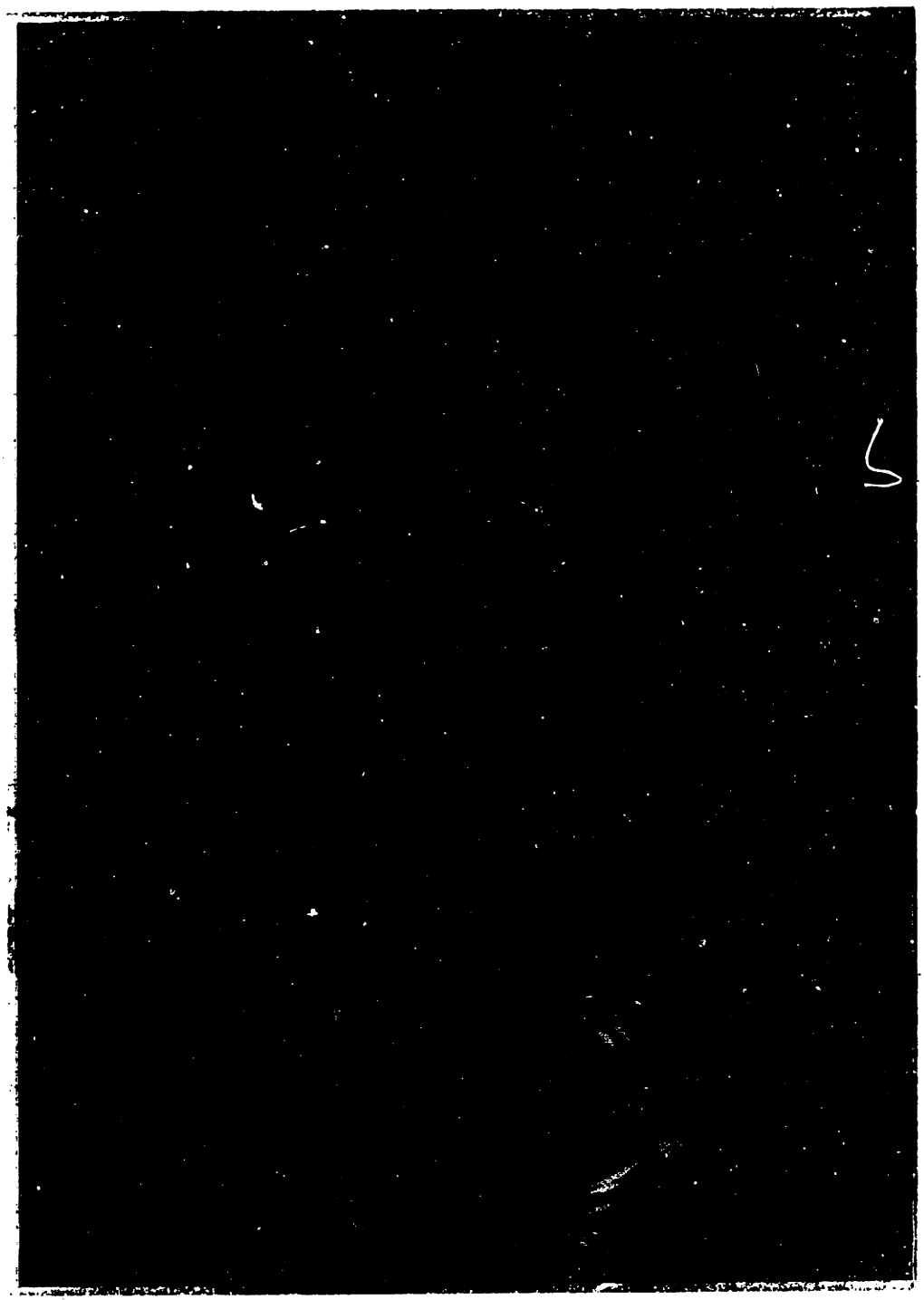

Fig. III-12: Separation of reaction intermediate for Vanadyl Etioporphyrin (I) run by dry column chromatography.

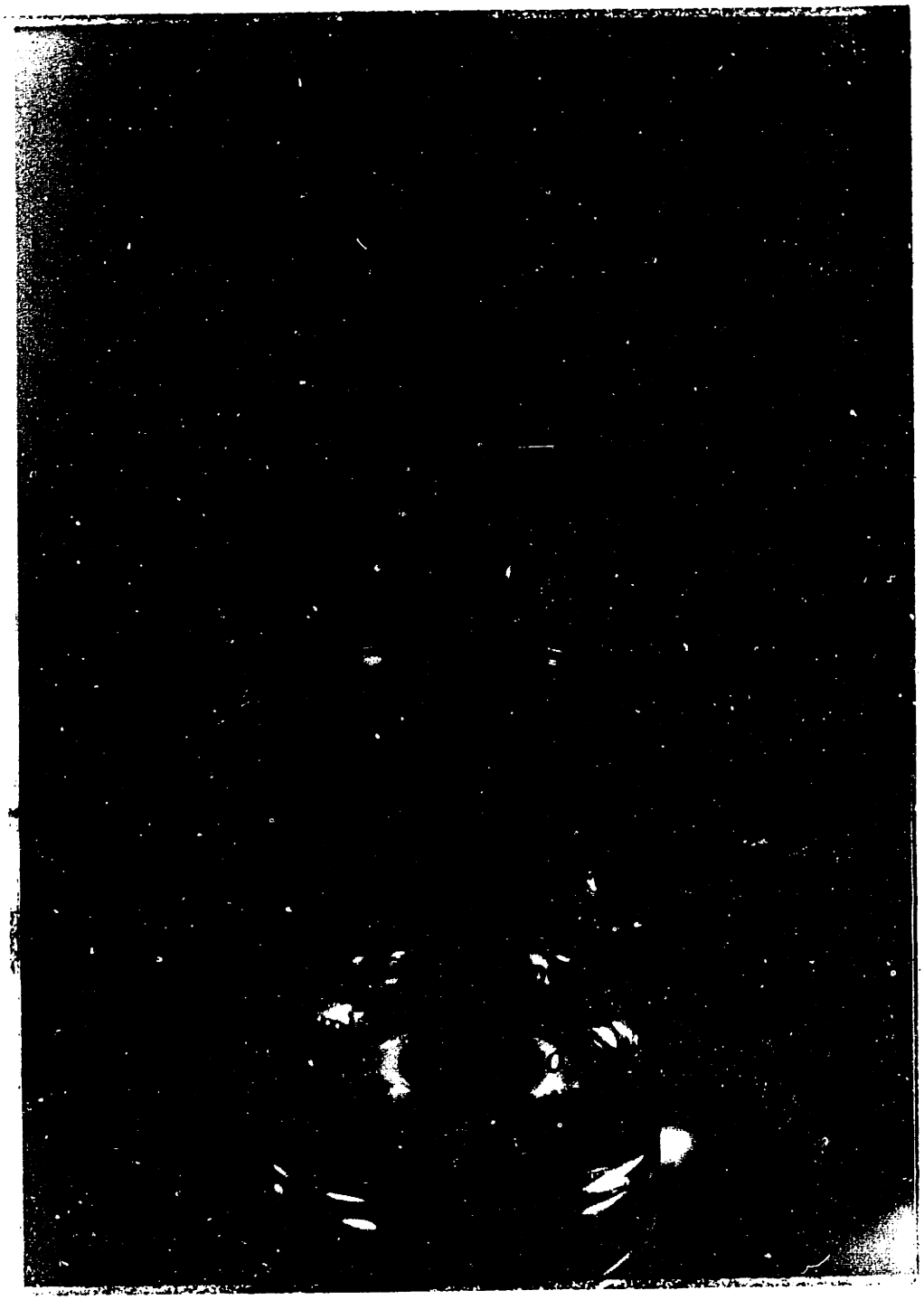

Fig. III-12: Separation of reaction intermediate for Vanadyl Etioporphyrin (I) run by dry column chromatography.

Xylenes is repeated. In separation methods of this kind there is always a danger of unwanted side reactions and therefore the contact time between alumina and the solution was minimized to the lowest possible value of about 8 hours.

The visible spectra of the seperated green compounds for VO-Etio and Ni-Etio are shown in figures III-13 and III-14 respectively. In these figures, the spectra of the original reaction products are also plotted. On comparing the two it is clear that we have been successful in separating the intermediates in relatively pure form and they show some new peaks. While the peak locations for pure VO-Etio-I are 407, 534 and 571.5 nm the separated compound shows peaks at 405.4, 409.5, 506, 543, 575 and 627.5 nm with relative absorbance of 23, 25.7, 1, 1, 1.5 and 5.6 respectively. Similiarly pure Ni-Etio-I has peaks at 391, 517 and 553 nm whereas green compound has peaks at 397, 490, 523 and 616 nm with relative absorbance of 161, 1, 1.5 and 83.5 respectively. For VO-Etio intermediate we see that during the process of separation the peak at 631 nm has shifted to 627.5 nm. It may be that the correct location of the peak is at 627.5 nm and the reactor sample shows it at 631 nm due to matrix interference, or the right location is at 631 nm and during the separation some minor structural change has taken place. The shift due to matrix interferance is more likely. For example Vandyl Etio is known to give a peak at 531 nm in neutral solvents, whereas

(a)

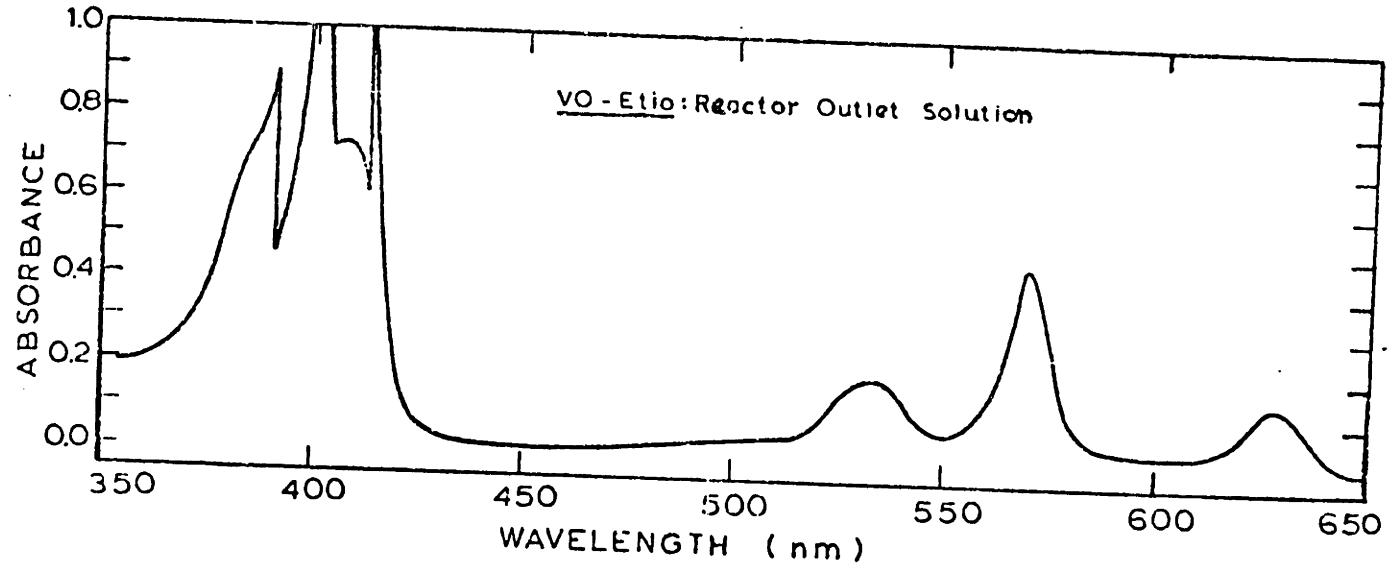

(b)

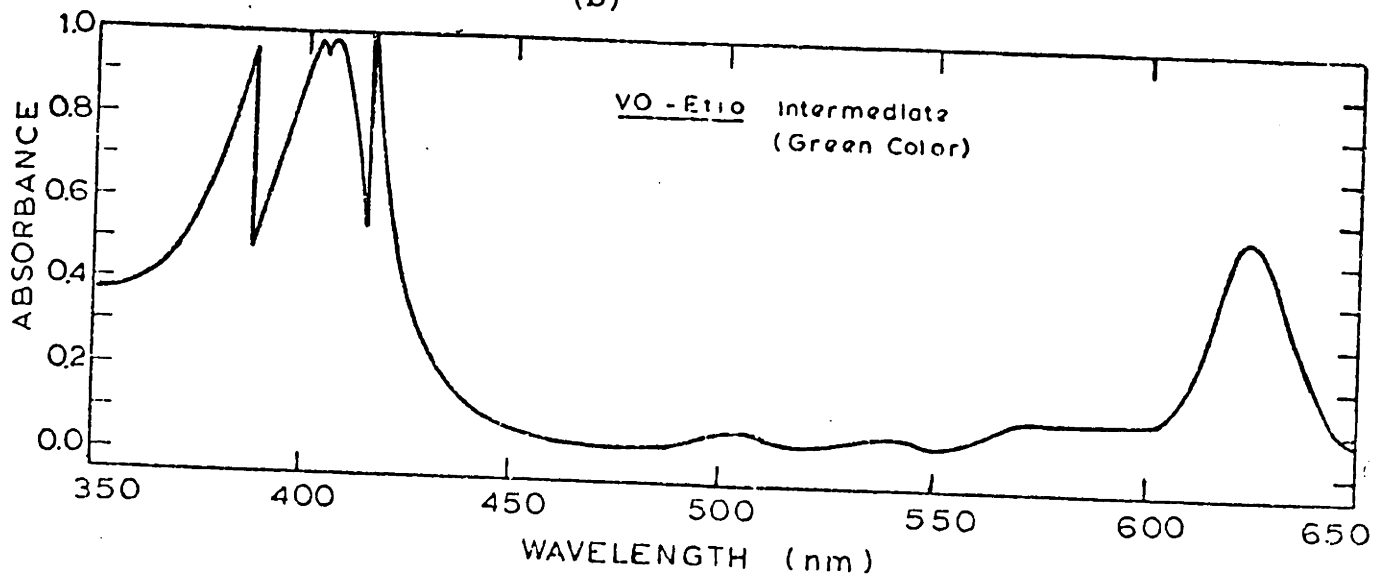

Fig. III-13: Visible Spectra. Solvent: Xylene

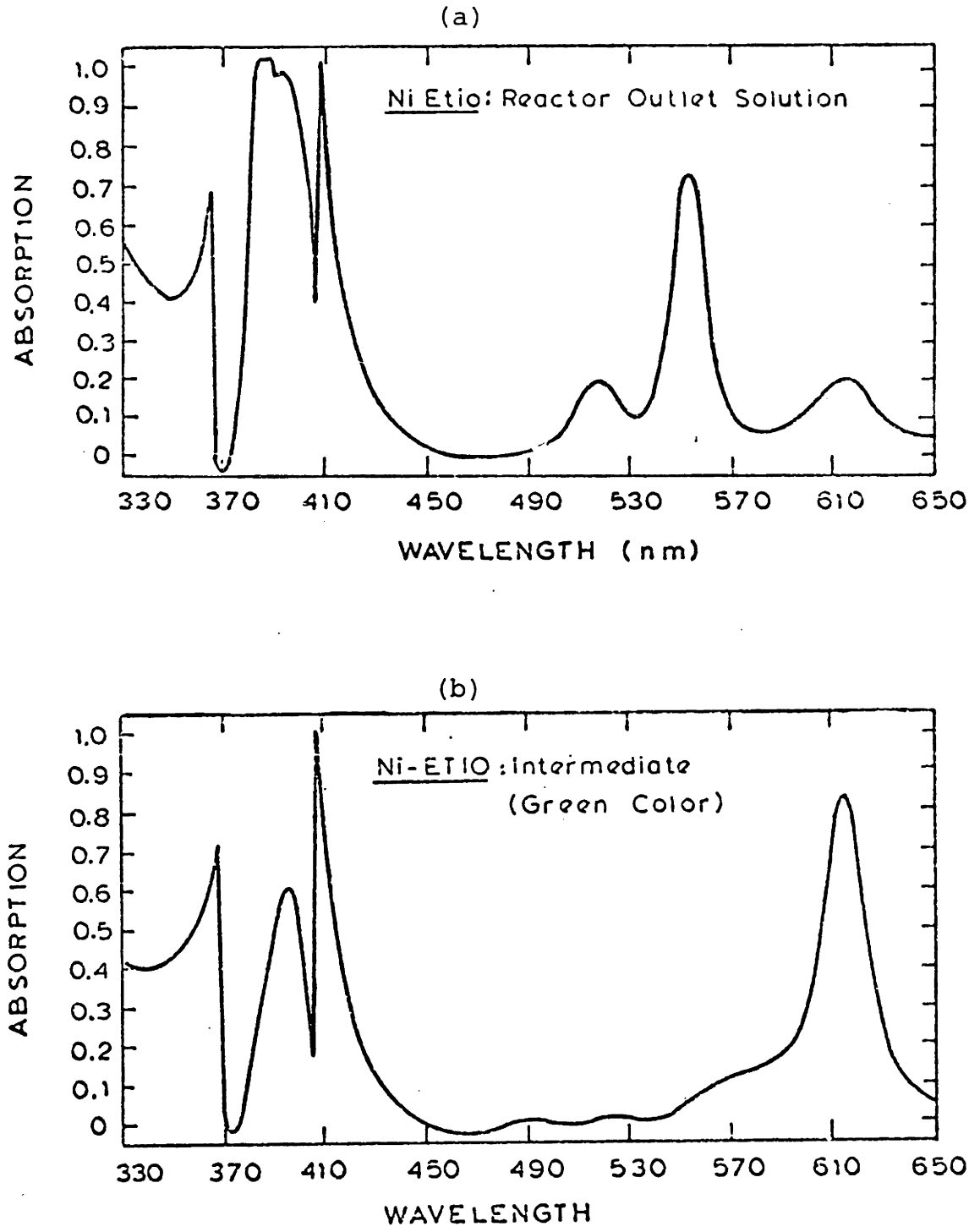

Fig. III-14: Visible Spectra

Solvent: Xylene

in our xylene solution it is at 534 nm. Similary it is possible that the separation of some of the hydrocarbons formed during the reaction might have led to the shift from 631 to 627.5 nm. In any event the peak is not very sharp and the absorbance at 631 nm is about 95% of the absorbance at 627.5. It should also be pointed out that for VO-Etio the ratio of absorbance at 571.5 nm to 534 nm is 2 while for the intermediate compound the corresponding ratio at 575 nm to 543 nm is 1.5. Similiarly for Ni-Etio the ratio of absorbance at 553 nm to 517 nm is about 3 and the corresponding ratio for the intermediate compound at 523 nm to 490 nm is only 1.5. This proves that we definitely do not have any parent metal etioporphyrin in the separated solution and the above peaks are not an artifect of the shift.

Along with the one major peak, the presence of other minor peaks in the spectra of the compound seperated raises possibility of the presence of more than one intermediate. Indeed it is observed that if the separation over alumina with xylene is repeated a couple of times the solution can be separated in to two major fractions - one being yellowish green while the other is bluish green. For these two fractions the ratio of the absorbance at various peaks are a little different from each other. Even though the presence of more than one reaction intermediate is confirmed, there is only one which is dominant, and a further separation for each species was not pursued.

(ii) Identification: An attempt to identify the nickel intermediates by mass spectrometry was made (Baker - 1966, Baker et al. - 1967). As the temperature of the mass spectrometer chamber was raised, a lot of compounds desorbed at various temperatures. However, all the compounds could not be exposed to the various photographic plates. From the exposed plates it was seen that Ni-Etio chlorin, which is formed by the addition of two hydrogen atoms to the porphyrin ring, is the dominant intermediate compound (fig. III-15). Even though higher hydrogenated products were not observed their presence cannot be totally ruled out. The details about the higher hydrogenated compounds can be found in Yen et al. (1969). If it is desired to identify all the reaction intermediates, thin layer chromatography in conjunction with the mass spectrometry should be used.

The fact that nickel etio chlorin is the dominant reaction intermediate is also confirmed from the work of Fuhrhop (1970). The author synthesised nickel octaethyl chlorin and found that the ratio of the absorbance of the Soret peak to the major peak (395 nm to 613 nm) is 2. The difference between the nickel octaethyl chlorin and nickel Etio chlorin is that the former has eight ethyl groups while the later has four ethyl and four methyl groups. Substitution of four methyl groups for the four ethyl groups would not alter the visible spectra significantly

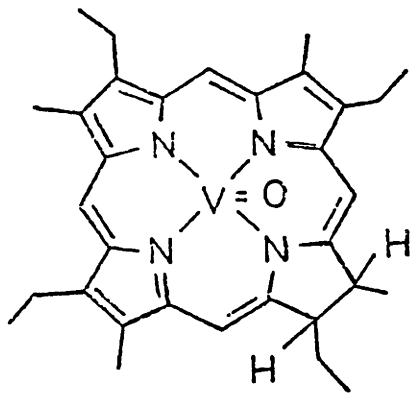

VO-Chlorin (Etio type)

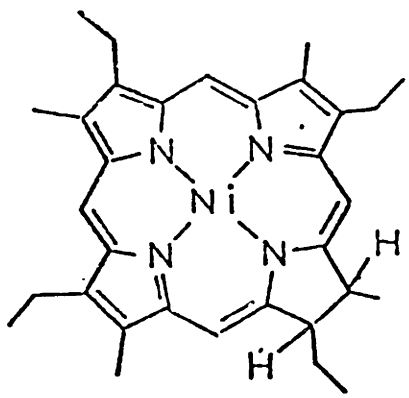

Ni-Chlorin (Etio type)

Fig. III-15: Structures of Ni and VO Chlorin

(Hambright). Indeed, we see that for our intermediate compound the ratio of the absorbance at the soret band (397 nm) and the absorbance at 616 nm is about 2.

Unfortunately it is observed that the vandium intermediate solution is highly unstable and in about twelve to twenty-four hours becomes more or less colourless. This did not allow the sufficient time to run the sample on the mass spectrometer. However it is speculated that most likely the dominant intermediate is again vanadyl Etio chlorin. Its structure is given in figure III-15.

(iii) Concentration Measurement: For the quantitative analysis of VO-Etio and Ni-Etio intermediates, respective visible spectral peaks at 631 and 616 are used. Total metal concentration of the separated green coloured solution is found by the atomic absorption spectrophotometry and is correlated with the corresponding absorbance at the proper wave length on the visible spectrophotometer. The absorption constants (absorbance/metal concentration in ppm) for vanadium and nickel are 0.61 and 0.72 respectively.

Even though throughout the whole thesis the concentration of the reaction intermediates, thus measured, would be referred as the concentration of the VO-Etio Chlorin and Ni-Etio chlorin, it should be pointed out that these may not be the concentration of pure chlorins but some sort of lumped reaction intermediate concentrations with chlorin as the major component.

J. ANALYSIS OF THE USED CATALYST: The spent catalyst from the reactor is first cleaned free of oil and the unreacted metal compounds in a soxhlet extractor for twenty-four hours. In the early stage of the research Xylene was used as the solvent in the soxhlet extractor. Later on it was found, that with chloroform, one could still extract a miniscule amount of the unreacted metal compound from the Xylene cleaned catalyst. Even though it had a negligible impact on the ultimate analytical results, it was decided to use chloroform as the solvent.

The cleaned catalyst is dried in vacuum for 12 hours. A proper epoxy mixture of 1 part by weight Epon Z hardner (brown) and 5 parts Epon 828 resin (clear) is prepared and the catalyst is mounted on a 1" diameter phenolic resin disk (Miller Stephenson Chemical Co. Inc., Danbury, Conn.). The catalyst is mounted such that its major axis (the longitudnal one) is parallel to the plane of the disk. The epoxy on the mounted disk is cured for four hours at about 100^{o}C. The epoxy and the catalyst is now grinded on 240 grit sand paper (Buehler LTD., Evanston, Ill.). Grinding is continued till nearly half of the catalyst is left and the major surface along the diameter of the catalyst is exposed. The size of the scratchs on the surface is reduced by successive minor grinding on 320, 400 and 600 grit sand papers. Since the diameter of the scanning electron beam is about 3 micron, it is necessary that all the scratches on the catalyst surface be much less than

this dimension. Therefore the catalyst surface is further polished on a 8" diameter Met-X polishing cloth with polishing alumina powders of 1 and 0.3 micron sizes succesively (Mark V laboratory Inc., East Granby, Conn.). Finally this polished catalyst is cleaned with plenty of water, dried and coated with carbon to increase the conductivity of the surface. Scanning electron x-ray microanalyzer (ETEC(MAC) Model 5 Electron Microprobe Computer Automation, Hayward, CA.) is used to scan the concentration of deposited vanadium or nickel on the catalyst. The instrument is run at 15 kilo volts and 30 nanoamps current.

For carbon, nitrogen, hydrogen and nickel analysis, a few cleaned catalyst samples were sent to Galbraith Laboratories (Knoxville, Tenn.).

CHAPTER-IV

KINETIC RESULTS AND THEIR DISCUSSION

For the hydrodemetallation kinetics of nickel and vanadyl etio (I) porphyrins a microreactor has been used. Following are the major advantages of the micro reactor (Difford and Spencer - 1974):

1. The amounts of catalyst and feedstock needed are small. The cost of model metal porphyrins are very high and limits the quantity of the solution used.
2. It is simpler to get isothermal operation.
3. A very wide range of the space velocities can be used and hence the kinetic information over a wide range of conversions are feasible.
4. Unlike the batch operation the change in catalyst activity with time can be observed and taken into modelling account.
5. Last but not the least important, the high pressure operation is safe enough for the Laboratory bench.

The physical dimensions of the reactor and the catalyst are chosen so that there are no mass and heat transfer limitations. The details of the calculation are given in Appendix-I. The cross sectional area of the micro reactor used is 0.21 cm^2 (internal diameter = 0.52 cm). The 1/16 inch $CoO-MoO_3/Al_2O_3$ catalyst extrudates are crushed to the size range of 170-200 mesh (0.088-0.074 mm). This

size of the catalyst eliminates the effect of heat transfer resistance at the wall of the reactor and also the intra-particle heat and mass transfer limitations. For the axial dispersion effects not to be important, it is required that the length of the catalyst bed should be greater than 1.2 cm. The length of the catalyst bed used range from 6 cm to 15 cm. These lengths of the bed insure that the operation of the bed is like a plug flow reactor.

The catalyst bed should be diluted with some inert to avoid the radial temperature gradient. The lower and the upper values of the ratio of diluent to catalyst volume are 1 and 5.5 respectively. We have used crushed pyrex glass of the size 170-200 mesh. The typical values of the ratio of the diluent to catalyst volume used are 1 to 2. The amount of catalyst used varied from 0.3 g to 1.5 g.

Calculations in the Appendix-I also show that, from liquid to solid, we do not have any heat or mass transfer limitations. Thus the real kinetics would not be disguised by any transport limitations.

It must be emphasized once again that in our study we have not sulfided the catalyst.

A. TRANSIENT BEHAVIOUR OF CATALYST: In most of the hydro-processing units, fresh catalysts before a stable operating activity, go through a transient activity period. Fig. IV-1 is a typical plot of the reactor outlet stream concentrations with time on stream. This plot is actually from

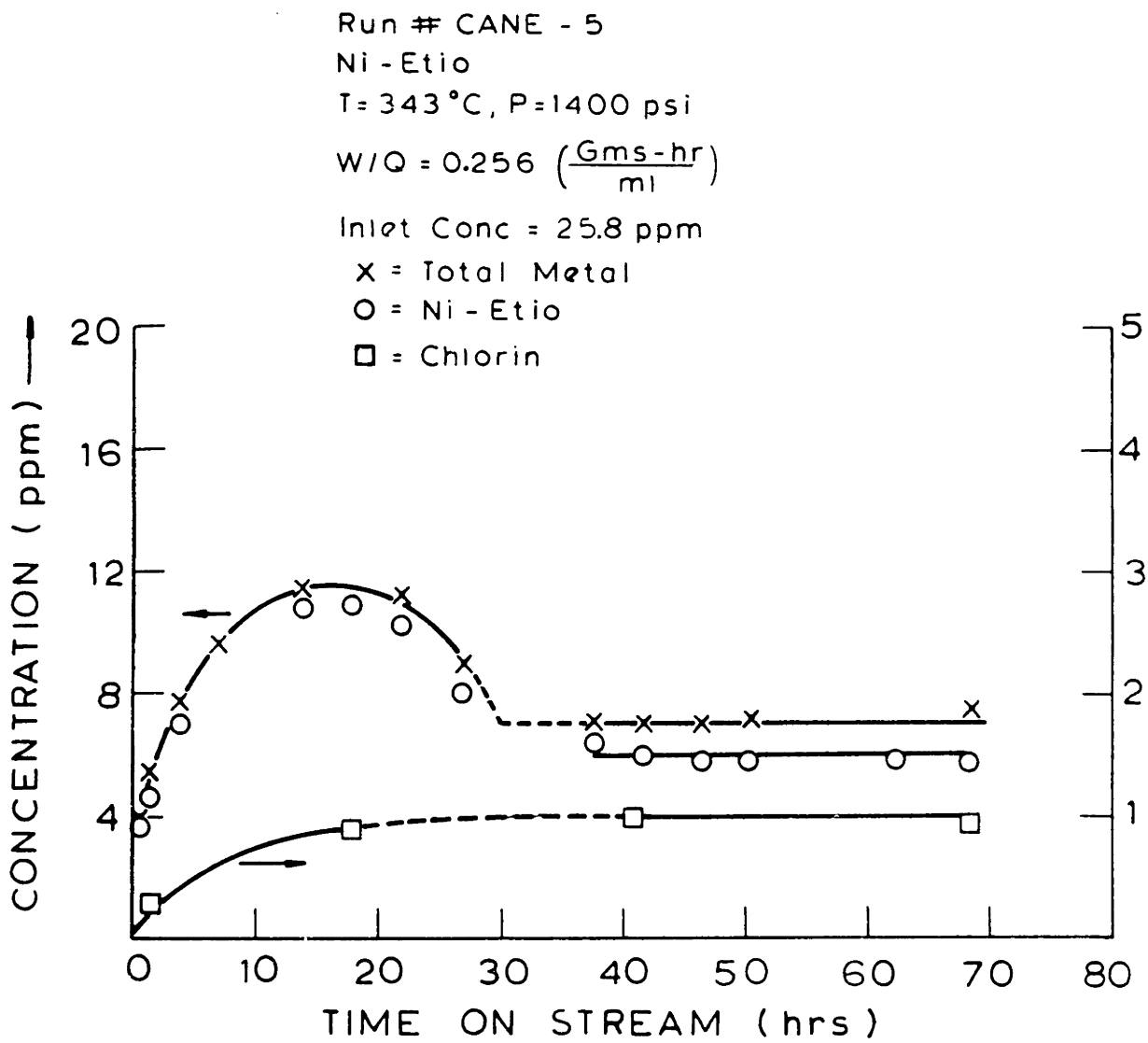

Fig. IV-1: Outlet Solution Concentrations vs. time on Stream for a Typical Nickel Etio-I run in one inch Reactor.

the one inch reactor operation and is described in the next chapter, but here it serves the useful purpose of qualitatively depicting the change in the activity of the catalyst with the operating time.

In fig. IV-1, throughout the reaction period, the solution flow rate to the reactor has been kept constant. At various time intervals, the reactor samples have been collected and analysed and are plotted in fig. IV-1. It is seen that at time equal to zero, there is no nickel in the outlet stream. It may be either due to the fact that all the nickel is physically adsorbed on the catalyst surface or the initial activity of the catalyst is too high. After time zero, uptill about 15 hours, a increase in the outlet concentration of the Ni-Etio and the nickel-chlorin is observed. This decay in the catalyst activity is believed to be the outcome of the classical decrease in the initial active sites of the catalyst. This behaviour is observed in almost all the hydroprocessing units. In our case it may be due to the rapid build up of the coke on the catalyst surface. A time period of 15 hours may be sufficient to build up almost all the coke formed during the total course of the reactor operation. As discussed in Sec. II.B.3.a., such rapid coke formations are feasible. Beuther and Schmid (1963) observed that of the total carbon deposited on the HDS catalyst in 16 days of operation, one half deposited in the first 12 hours.

After about 15 hours and upto 30 hours or so, one observes a decrease in the total metal concentration of the reactor outlet stream. During this period there is no decline in the concentration of the Ni-chlorin; if anything, it is a mild increase. This is a little unusual behaviour. After 30-40 hours, there is a long period of constant catalytic activity.

Figure IV-2 shows the typical transient activity of the catalyst during a microreactor run. In this run the flow-rate through the reactor is not kept constant. By varying the flow rate through the reactor, an attempt is made to learn about the conversions at various contact times during the transient period. In this figure the very initial period of the decline in the catalyst activity is not plotted.

In fig. IV-2 it is observed that as reaction time progresses, there is a drop in the solution concentrations of the total metal at various contact times but an increase in the concentrations of the nickel chlorin. From this observation it is clear that both the hydrogenation and the total metal removal activity of the catalyst increases and ultimately reaches to the constant value. It may be possible that the initial metal deposition on the catalyst surface causes an increase in hydrogenation activity of the surface; and after some metal has deposited there is no

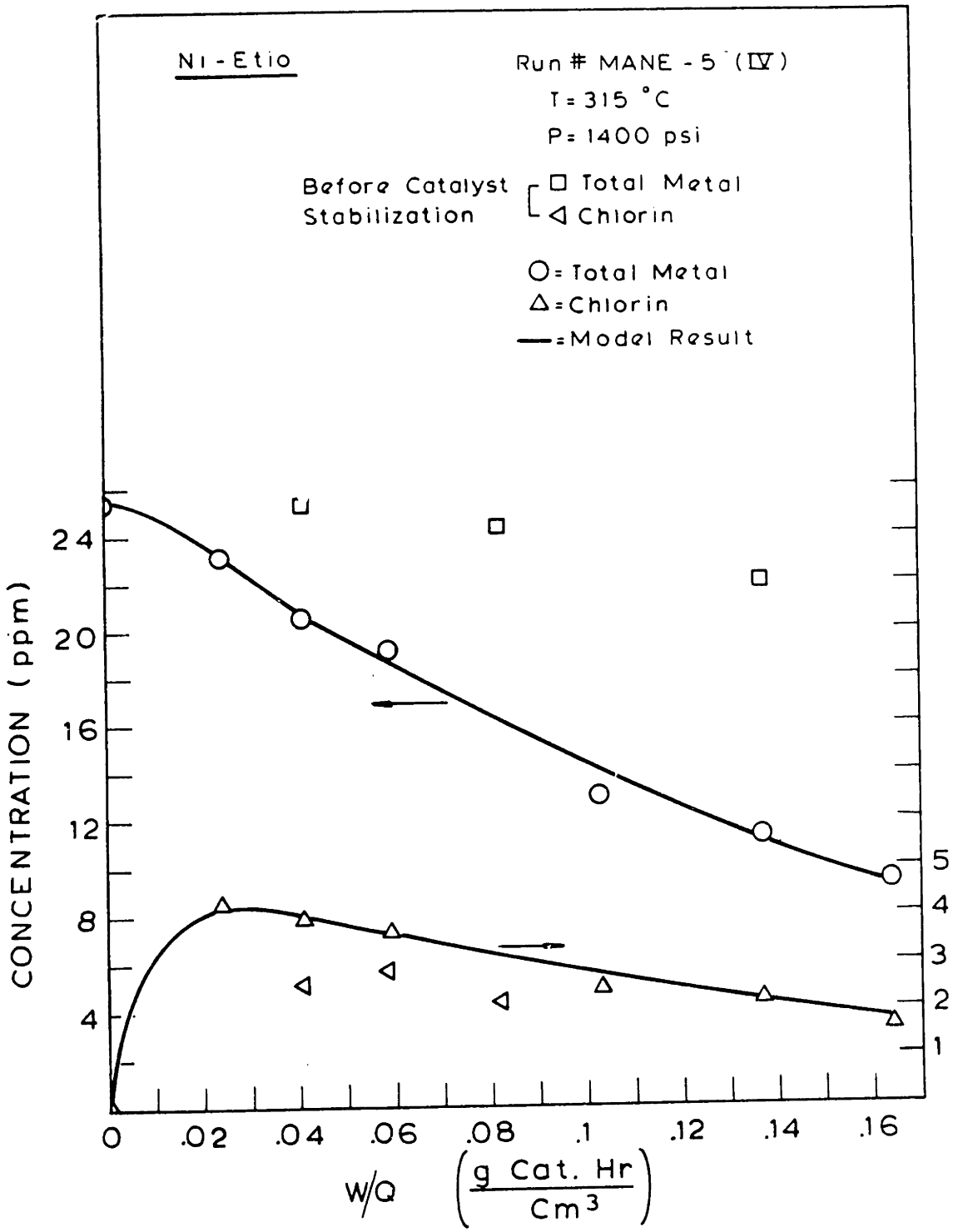

Fig. IV-2: A Typical Microreactor run, depicting the Transient Activity of the Catalyst.

more increase in the activity due to the further deposition. Later on in this chapter, once a suitable kinetic model has been proposed, a more detailed discussion on these changes in the activity would be taken up.

Identical transient catalytic behaviour is observed for VO-Etio-I runs. Similar to fig. IV-1, figure IV-3 is the plot for a typical vanadium run.

All the kinetic analysis is done for the stable catalyst operation. The time taken by the catalyst to reach the stable operation depends on the temperature and pressure of the operation. One would tend to think that a particular metal deposition would be needed before the catalyst achieves its stable activity; however it is found that depending on the operating conditions the metal deposited varied from 0.2 to 0.5 wt %. One sure and quick way, to get to the stable activity of the catalyst, used in this study is to pump about 400 ml of the solution over a period of about 50 hours at 315^{o}C and then change to a low flow rate of about 4 ml/hr at 288^{o}C for twelve hours or so and ultimately bring the temperature and flow rate to the desired operation values. This method ensured that any further change in the reactor temperature and pressure did not alter the catalyst activity.

In this study the maximum metal deposited on the catalyst in any single run is about 10 wt %, and up to this loading no significant change in the catalyst activity is

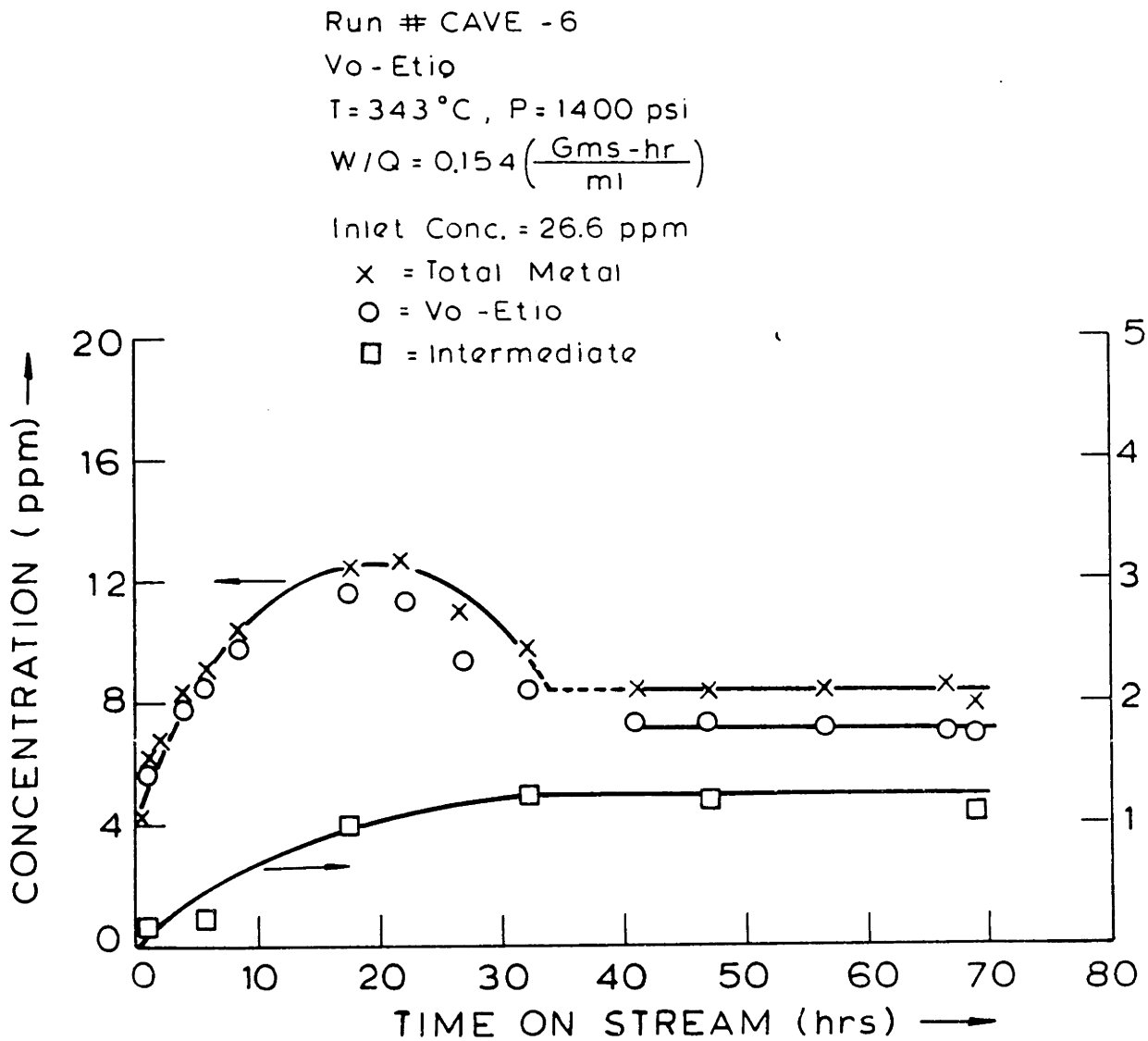

Fig. IV-3: Outlet Solution Concentrations vs. time on Stream for a Typical Vanadyl Etio-I run in one inch Reactor.

observed. Thus once the catalyst has achieved its steady state activity, it is maintained for fairly long period of time to allow the needed kinetic measurements.

B. NICKEL ETIOPORPHYRIN-I: In the very first run, the reactor was packed with the pyrex glass only. The run was made at temperature and hydrogen pressure of 343^{o}C and 9.65 MPa (1400 Psig) respectively. The reactor outlet concentration was monitored over a period of eighteen hours. There was no difference between the inlet and the outlet solution concentrations. This proved that the crushed pyrex glass is suitable as an inert.

The catalytic runs are made at the pressures of 4.14 MPa (600 psig), 6.89 MPa (1000 psig) and 9.65 MPa (1400 psig); and at temperatures 288^{o}C (550^{o}F), 302^{o}C (575^{o}F), 315^{o}C (600^{o}F), 329^{o}C (625^{o}F) and 343^{o}C (650^{o}F) and for two different reactor inlet concentrations of about 27 ppm and 15 ppm. The pertinent details of all the runs are given in Appendix-III.

B.1. GENERAL OBSERVATIONS: In fig. IV.2 we have a typical plot of the variation of the outlet concentrations as functions of the contact time. We have to focus our attention on the curves corresponding to the stable activity of the catalyst (circles for the total metal concentration and vertical triangles for the chlorin concentration). It is observed that initially in a very short time there is a

build up of chlorin concentration and during this period decrease in the total metal concentration is not so significant. After this rapid initial build up, the chlorin concentration drops monotonically and the rate of the drop of the total metal concentration also increases.

The second important observation comes through the figure IV-4. This figure is a plot of the ratio of the chlorin and the total metal concentrations of fig. IV-2 vs. the contact time. Since there is no chlorin in the feed the initial ratio is zero, but it rapidly builds up and then remains nearly constant for the total course of the reaction. This behavior is observed for all our runs. The natural question to ask is that do we have a thermodynamic or a dynamic equilibrium. This question is answered later on with respect to our final kinetic model.

Uptill now all the investigators of the HDM have modelled the kinetics as the disappearance of the total metal in the solution. So our initial attempt is to neglect the intermediate chlorin concentration and model the kinetics as the function of the total metal concentration only.

We vary the contact time by changing the flow rate, Q, therefore the differential equation governing a first, second or fractional order kinetics is:

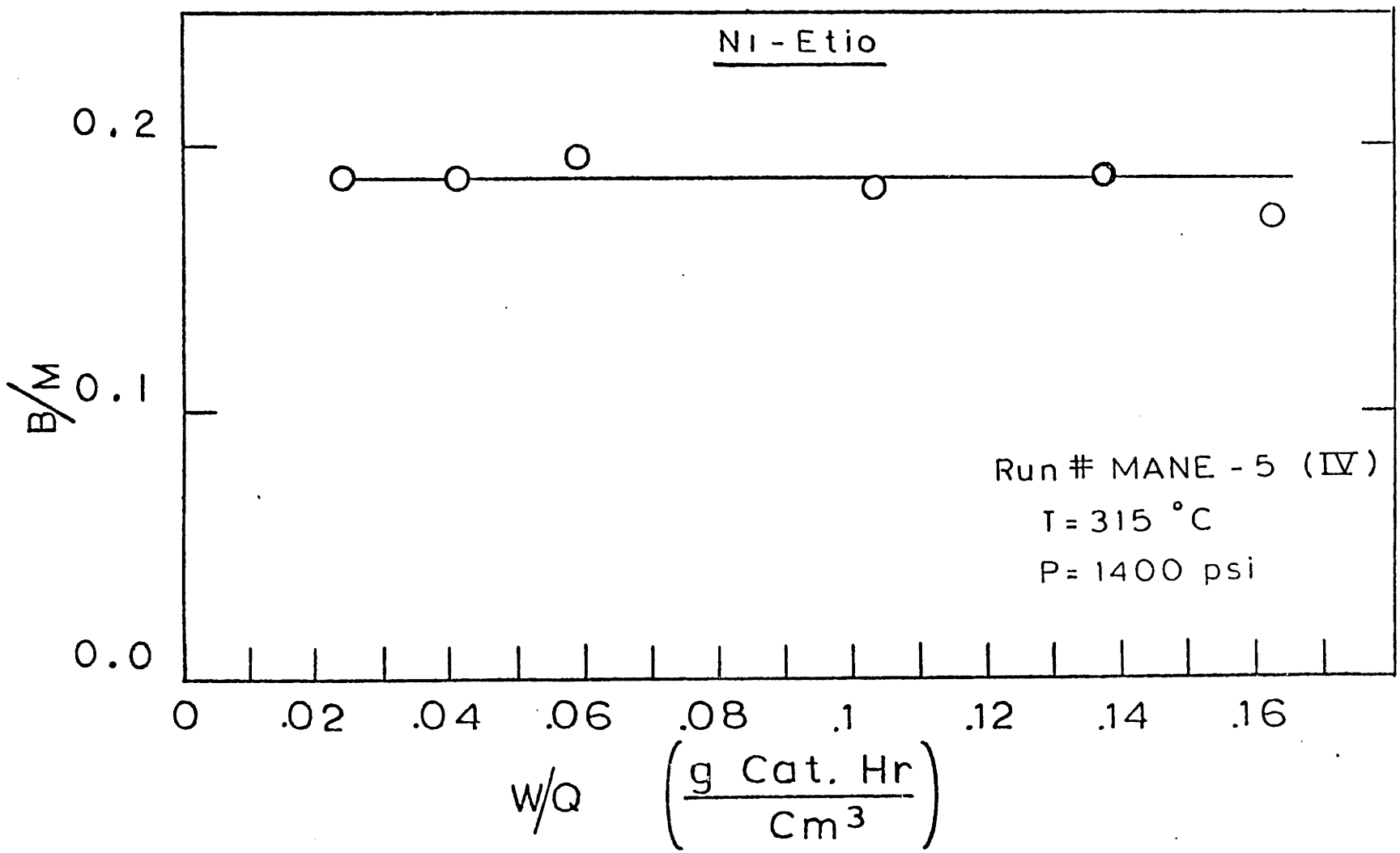

Fig. IV-4: Ratio of the Metal Chlorin and the Total Metal Concentration vs. contact time.

$$\frac{-dM}{d(W/Q)} = \frac{k''}{\rho} \text{ (concentration function)} \qquad \text{IV.1}$$

$$k \equiv \frac{k''}{\rho} \qquad \text{IV.2}$$

where M = total metal concentration, W = weight of catalyst, k" = rate constant, ρ = density of the solution, and concentration function depends on the order of the kinetics assumed. Since ρ for the solution is not precisely known, in this thesis instead of k", k is used as the rate constant.

Of the three different kinetic orders tried, second order did not work at all. The run at 343°C and 9.65 MPa is plotted as first order in fig. IV-5 and as half order in fig. IV-6. Even though half order fit gives more error than the first order fit; within the experimental error it is difficult to discriminate between the two. It is seen that in both the cases the magnitude of the error is larger at the higher conversions. Another important observation is that while the best fit line for first order predicts the value of the concentration at zero contact time higher than the initial concentration, the half order predicts much lower concentration. All these observations are common to other runs also. Therefore, it is concluded that the first order kinetics does the better job. The question of over prediction of initial concentration by

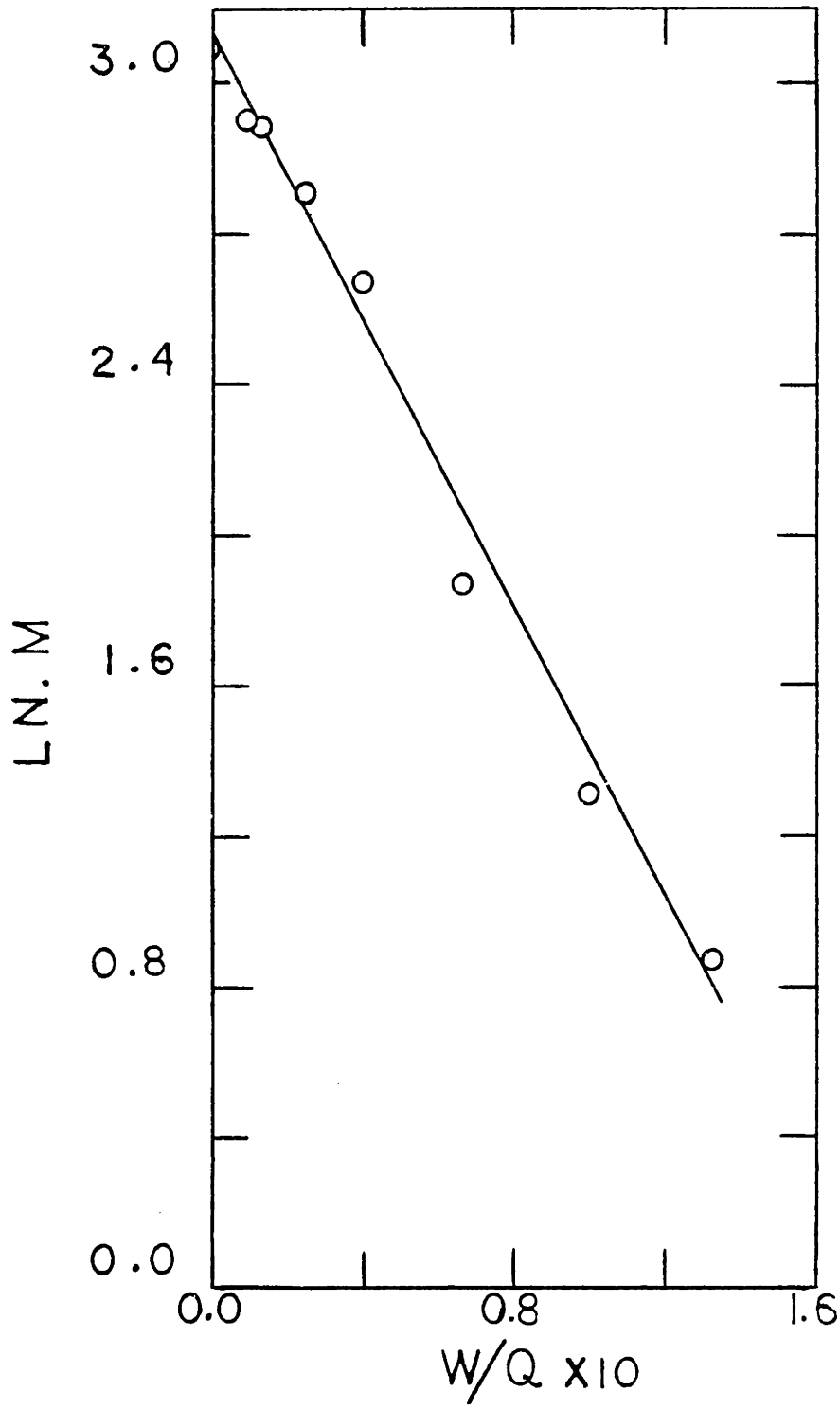

Fig. IV-5: First Order Plot for Ni Etio-I at 343°C and P=9.65 MPa. Run # MANE-3 (III). M is in ppm, W in grams and Q in ml/hr.

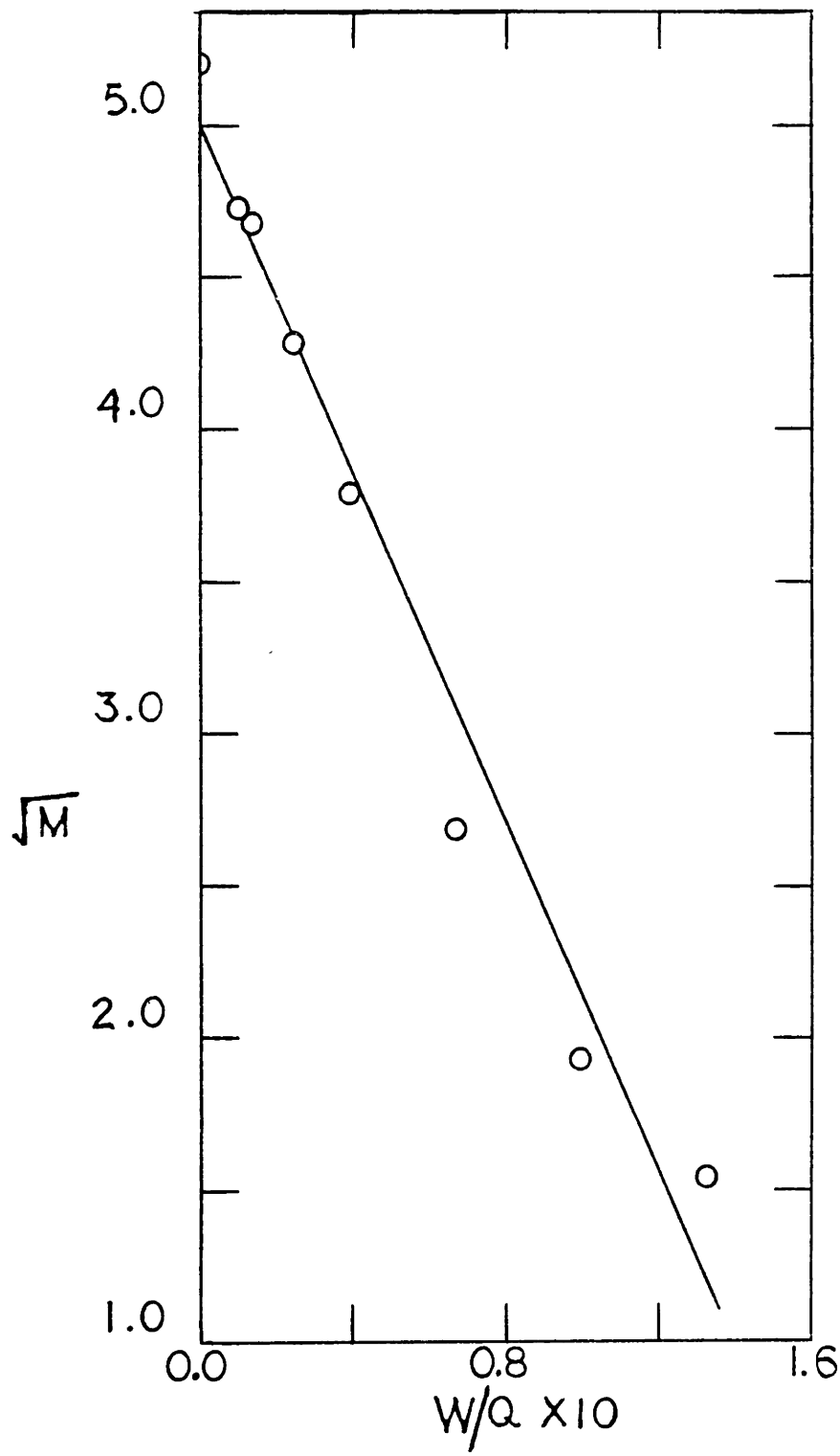

Fig. IV-6: Half Order Plot for Ni Etio-I at 343°C, P=9.65 MPa. Run # MANE-3 (III). M is in ppm, W in grams and Q in ml/hr.

first order and the under prediction by half order will be easily explained with reference to the final kinetic model in the next section.

The Arhenius plot for the first order rate constant is given in figure IV-7. The value of the activation energy obtained is 29.1 Kcal/gmole. Figure IV-8 is the plot of the pressure dependence of the first order rate constants at various temperatures. There is a little scatter in the figure. The slopes of the lines at temperatures 315, 329 and 343°C are 1.996, 1.986 and 2.251 respectively. The mean hydrogen pressure dependence is 2.08.

Therefore, the first order global rate seems to do a reasonable job for the total metal disappearance. However it does not take the intermediate concentrations into account and hence cannot explain fig. IV-4.

B.2. THE FINAL MODEL: The successful model considered is:

$$A \underset{k_2}{\overset{k_1}{\rightleftharpoons}} B \xrightarrow{k_3} \text{Metal Deposition on Catalyst}$$

where A is the original metal Etioporphyrin, B is the reaction intermediate, k_1 is the hydrogenation rate constant, k_2 is the dehydrogenation rate constant and k_3 is the rate constant for the final metal removal step. Prior to the metal deposition on the catalyst, B might go through a sequence of chemical steps and therefore k_3 might be some sort of lumped rate constant.

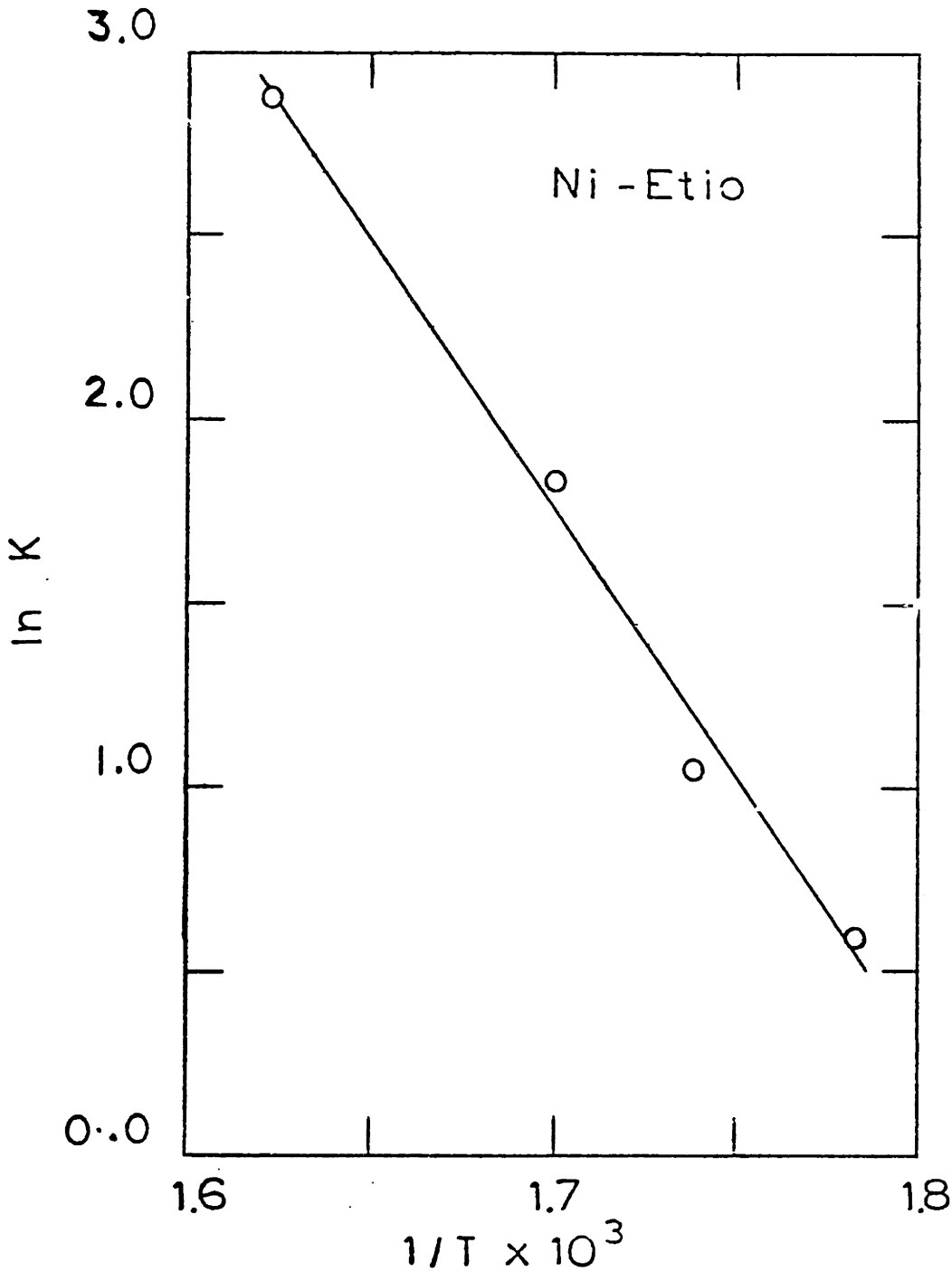

Fig. IV-7: Arrhenius Plot for the First Order Rate Constant for Ni-Etio I. Pressure = 9.65 MPa. T is in °K and k in ml/g-hr.

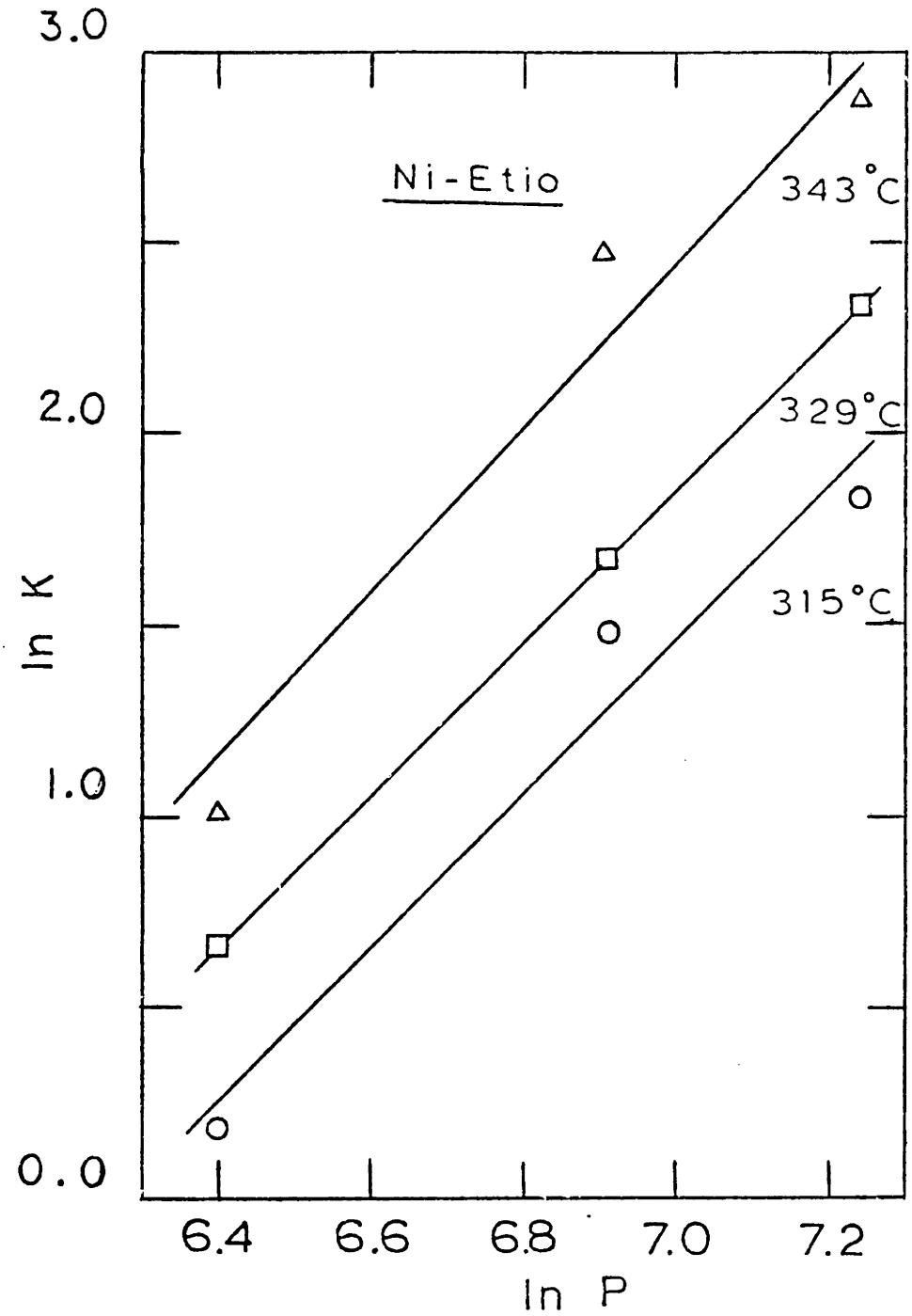

Fig. IV-8: Pressure Dependence of the First Order Rate Constants for the Ni Etio-I. P is in psig and k in ml/g-hr.

Whatever may be the sequence of events from B to the final metal deposition, they are so fast that in our experiments they could not be tracked down.

All the steps in the model are assumed to be first order in the metal concentrations. The rate expressions for this model are solved in Appendix-II. The rate constants are evaluated by the nonlinear least square and Himmelblau-Jones-Bischoff (HJB - 1967) techniques. Both the techniques work reasonably well. The computer programs written are listed in Appendix-IV.

In figure IV-2, the solid lines are the calculation results of this model. Figure IV-9 shows the model results for the run shown in figures IV-5 and IV-6. We see that the new model not only fits the total metal concentration better but also fits the chlorin concentration to a remarkable accuracy. The same observation is made with regards to the other runs.

Figures IV-10, IV-11 and IV-12 are the Arhenius plots for the rate constants k_1, k_2 and k_3 respectively. Excellent straight lines are obtained in all the three figures and at all the operating hydrogen pressures.

The values of the activation energies for k_1 at the pressures of 4.14, 6.89 and 9.65 MPa are 16.2, 16.8 and 18.3 Kcal/gmole respectively. Thus mean activation energy is 17.1 Kcal/gmole. This value is in agreement with the hydrogenation activation energies reported in the literature (Gultekin - 1980).

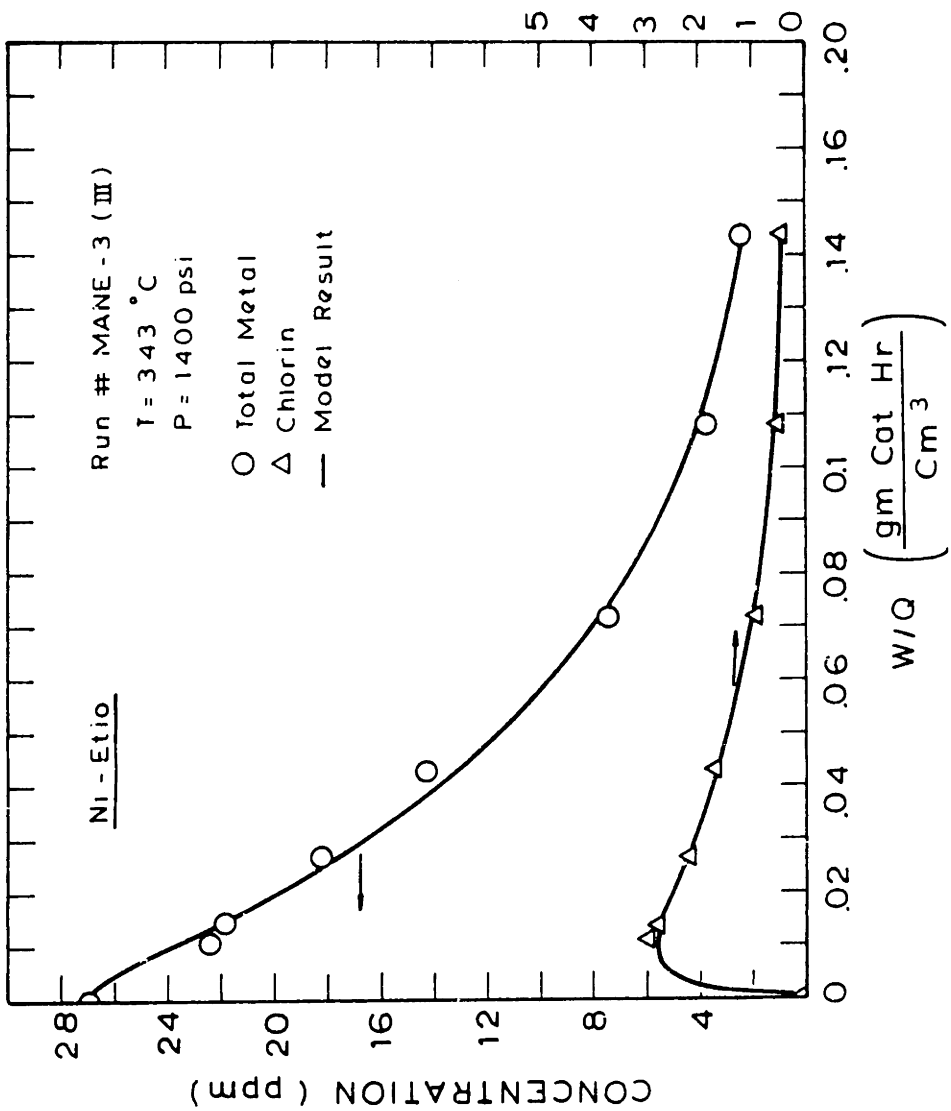

Fig. IV-9: Calculation Results of the New Proposed Model and the Experimental Data.

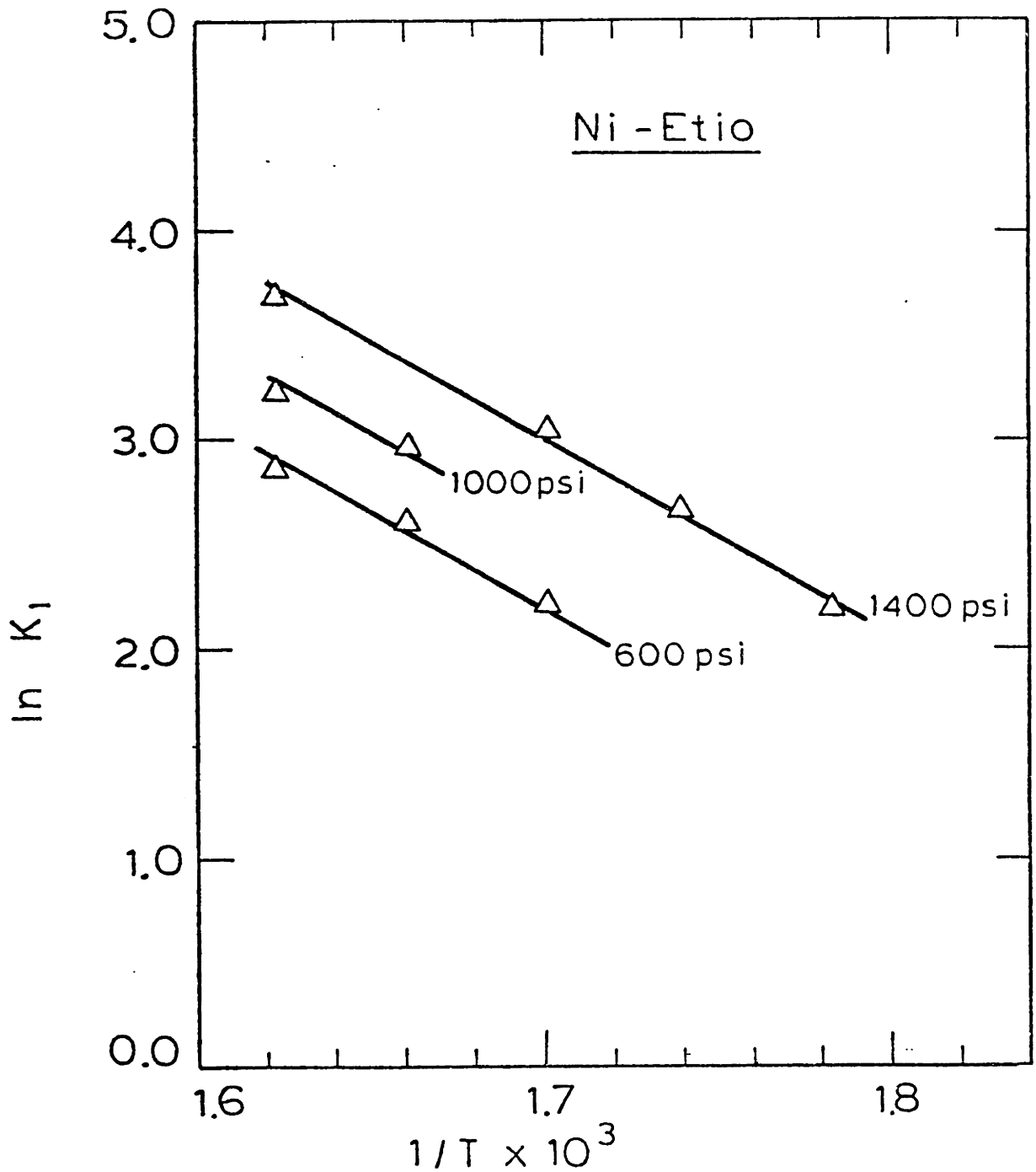

Fig. IV-10: Arrhenius Plots for the Hydrogenation Rate Constant k_1 at Various Hydrogen Pressures. T is in °K and k_1 in ml/g-hr.

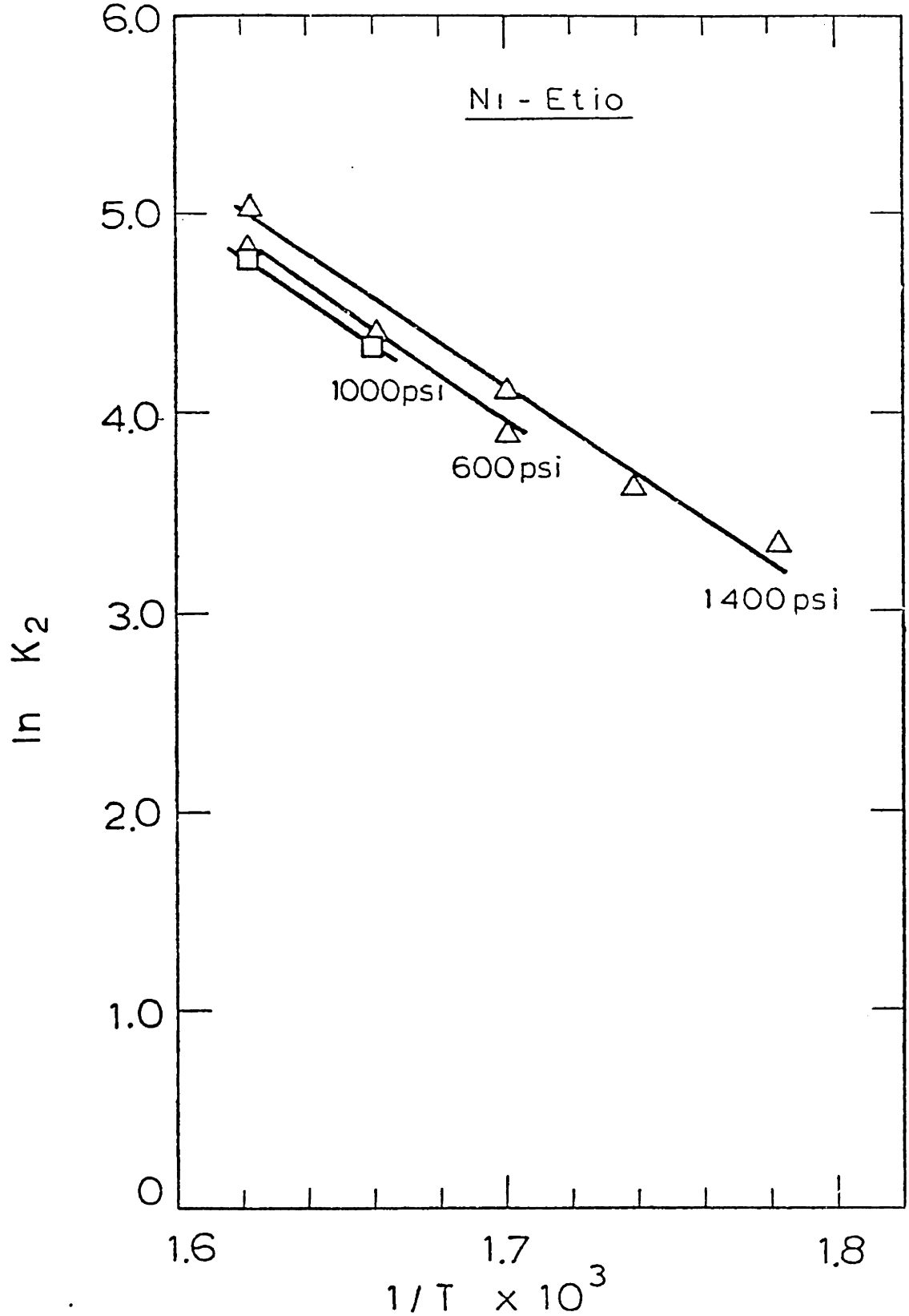

Fig. IV-11: Arrhenius Plots for the Dehydrogenation Rate Constant k_2 at Various Pressures. T is in °K and k in ml/g-hr.

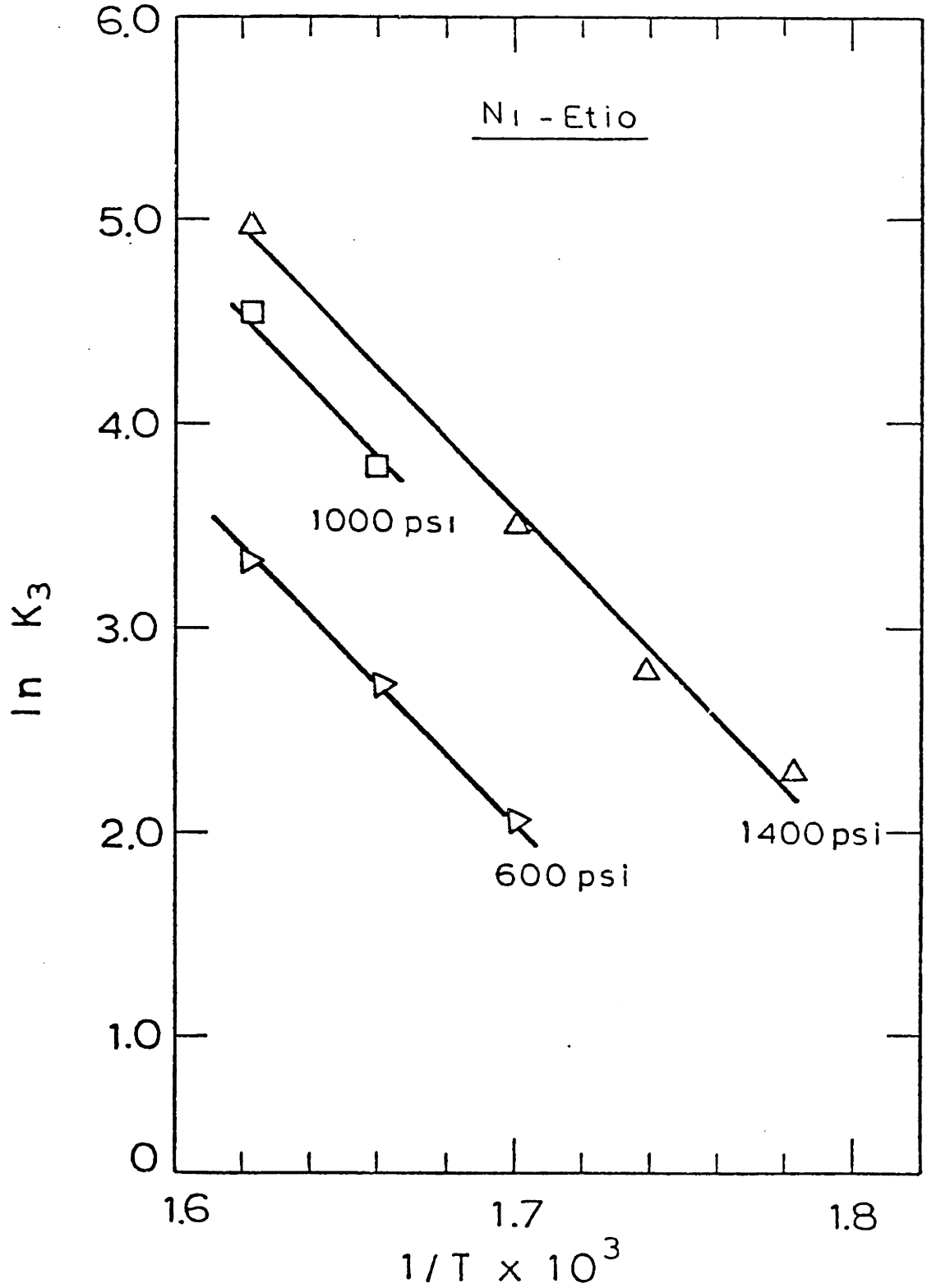

Fig. IV-12: Arrhenius Plots for the Rate Constant k_3 at Various Hydrogen Pressures. T is in °K and k_3 in ml/g-hr.

The values of the activation energies for k_2 at the pressures of 4.14, 6.89 and 9.65 MPa are 24.2, 22.8 and 21.7 Kcal/gmole respectively. The mean activation energy is 22.9 Kcal/gmole. This value is again in agreement with the dehydrogenation activation energies found in the literature.

The values of the activation energies for k_3 at the pressures of 4.14, 6.89 and 9.65 MPa are 31.1, 41.4 and 34.1 Kcal/gmole respectively. As seen from fig. IV-12, at the pressure of 6.89 MPa, there are only two data points and therefore the value of 41.4 is not considered in the averaging of the activation energy values. Thus mean activation energy is 32.6 Kcal/gmole. Since k_3 may be either hydrogenation or hydrogenolysis or the combination of both, it is not clear whether we can make any judgement on the order of magnitude of the activation energy.

Figures IV-13, IV-14 and IV-15 are the plots of the dependency of the rate constants k_1, k_2 and k_3 on the hydrogen pressure respectively. From figure IV-13 it is seen that k_1 dependence on hydrogen pressure at 315, 329 and 343^{o}C are 1.0, 0.87 and 0.99 respectively. Thus dependence of k_1 on hydrogen pressure is first order. This is in excellent agreement with our analytical result that B is predominantely chlorin and is formed by the reaction of one hydrogen molecule with metal Etio(I) A. From figure IV-14 it is seen that due to the scatter in the data it is difficult to draw the definite conclusion.

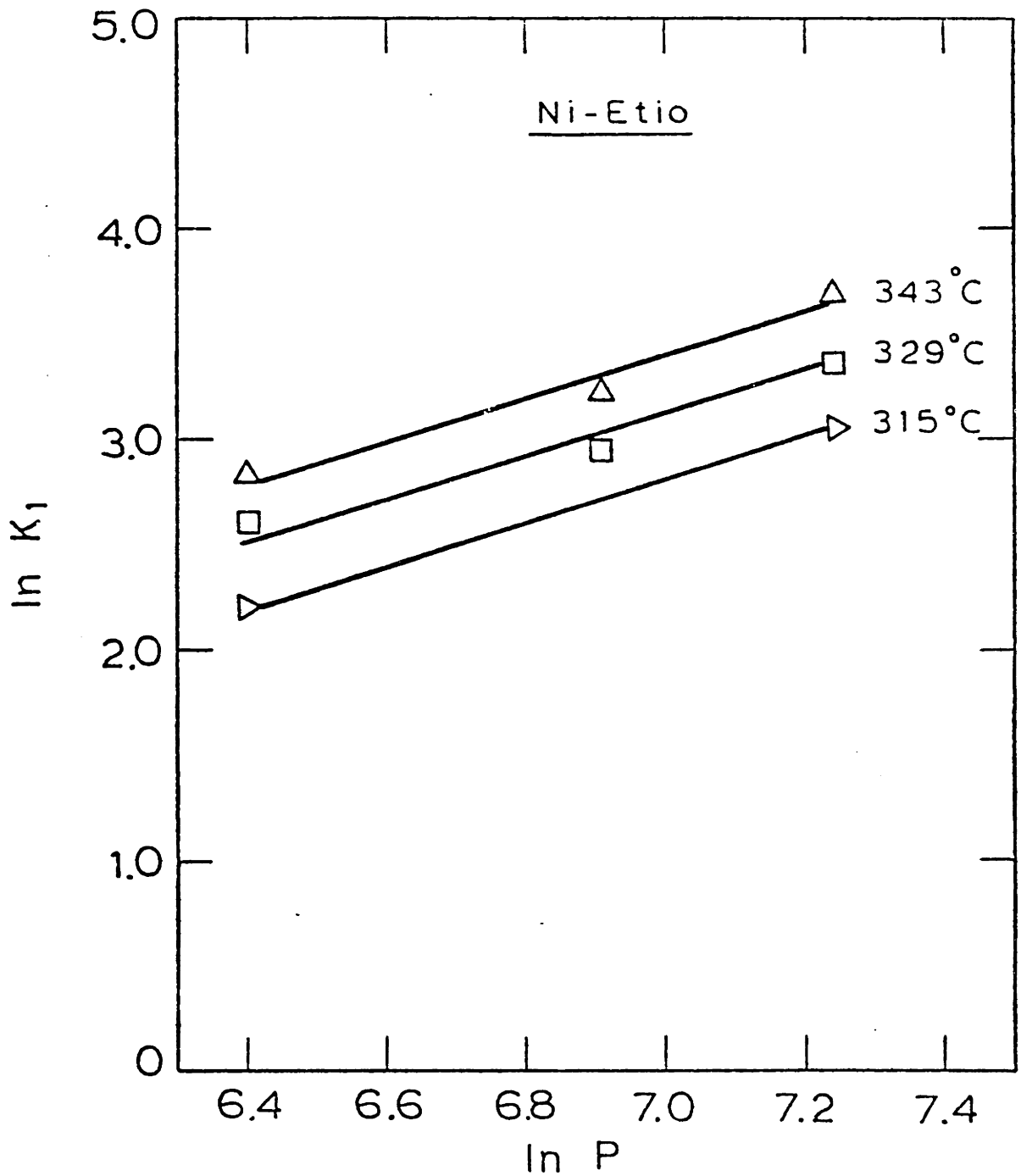

Fig. IV-13: Dependence of k_1 on Hydrogen Pressure. P is in psig and k_1 in ml/g-hr.

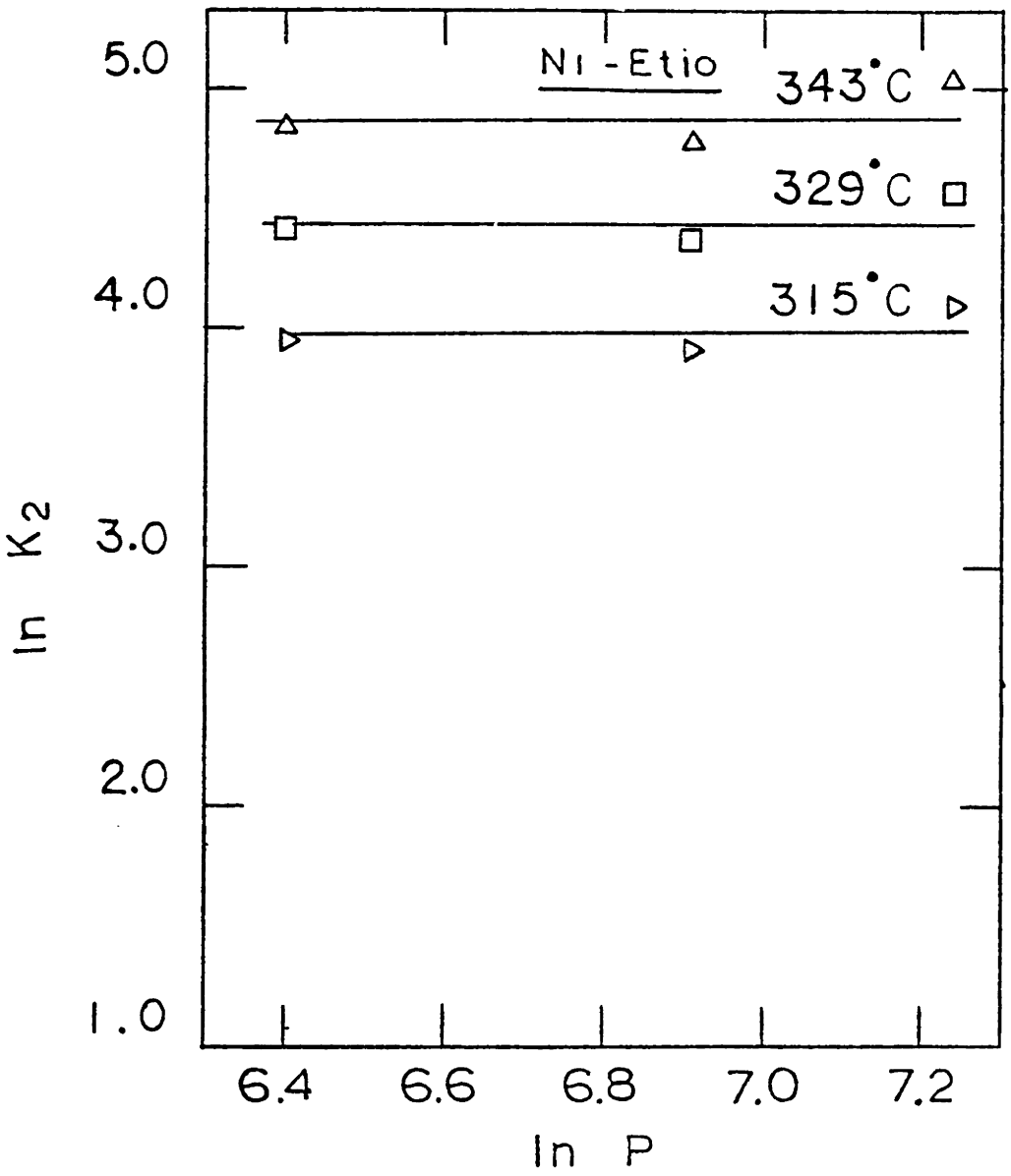

Fig. IV-14: Dependence of Rate Constant k_2 on Hydrogen Pressure. P is in psig and k_2 in ml/g-hr.

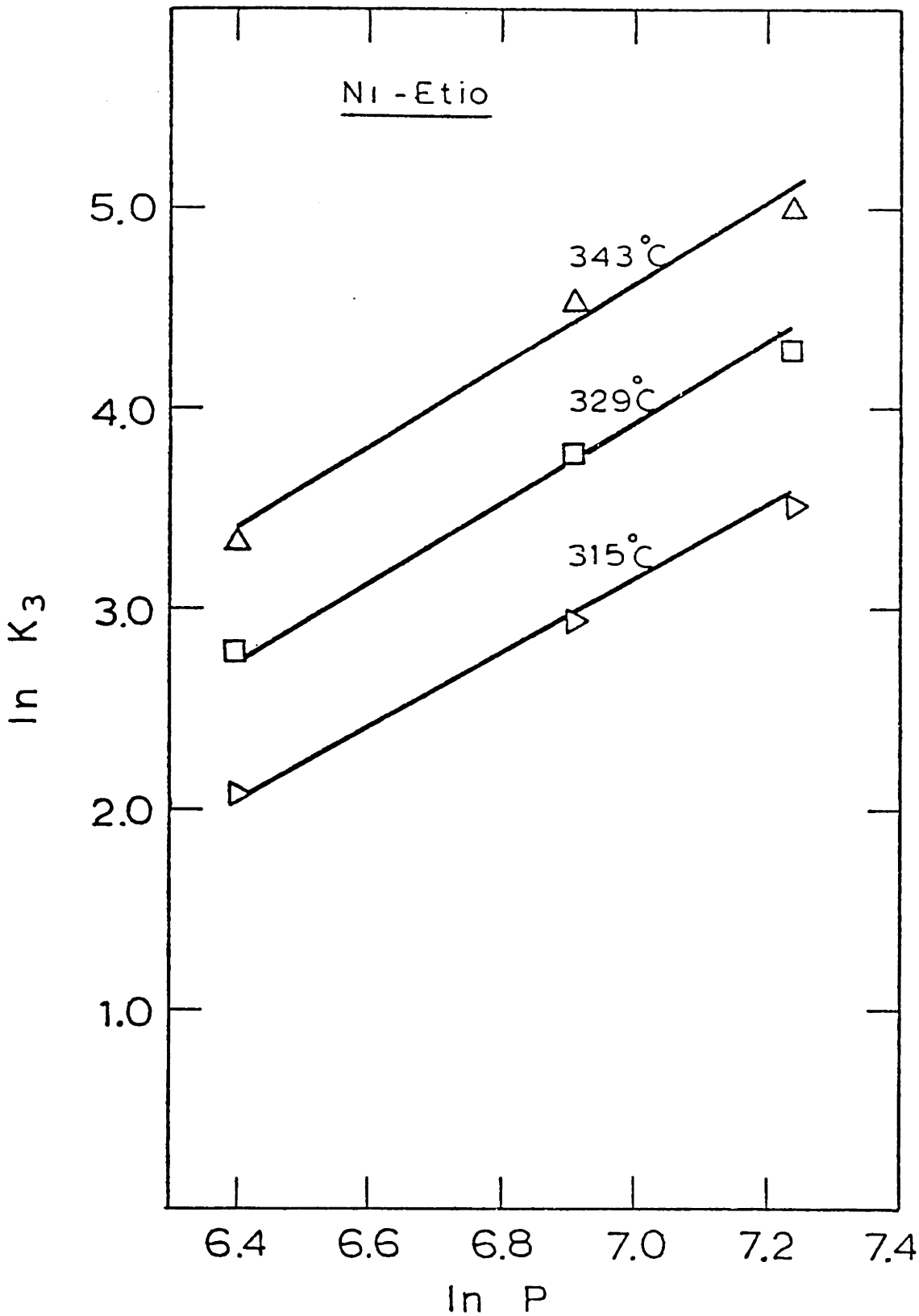

Fig. IV-15: Dependence of k_3 on Hydrogen Pressure. P is in psig and k_3 in ml/g-hr.

However, one would expect k_2 to be independent of hydrogen pressure and the mean lines are plotted in the figure IV-14. From fig. IV-15 it is seen that k_2 dependence on the hydrogen pressure at 315, 329 and 343°C are 1.7, 1.8 and 2.0 respectively. The mean dependence on the hydrogen pressure is 1.83. It may be concluded that the dependence of k_1, k_2 and k_3 on the hydrogen pressure are first, zero and second order respectively.

In order to summarize let us write the rate constant k as:

$$\ln k = \ln k_o - \frac{E}{RT} + n \ln P \qquad \text{IV.3}$$

where E is the activation energy in Kcal/gmole, n is order of dependence on pressure, P is the hydrogen pressure in psig, and k is the first order rate constant in ml of solution/g of cat. - hr. Thus for k_1:

$$\left.\begin{array}{l} n = 1,\ E = 17.1 \quad ,\ \ln k_{10} = 10.4 \pm 0.06 \\ \text{for } k_2: \\ n = 0,\ E = 22.9 \quad ,\ \ln k_{20} = 23.6 \pm 0.12 \end{array}\right\} \qquad \text{IV.4}$$

for k_3:

$$n = 1.83,\ E = 32.6\ ,\ \ln k_{30} = 18.3 \pm 0.11$$

and for k_3, if the value of n is taken to be 2 then: IV.4

$$n = 2,\ E = 32.6\ ,\ \ln k_{30} = 17.13 \pm 0.14$$

Once we have a suitable kinetic model, we can address the question of constant ratio of chlorin to total metal concentration shown in figure IV-4. As shown in appendix-II, there are three ways in which we can calculate the ration B/M; (i) at large contact times one has:

$$\lim_{t\to\infty} \left[\frac{B}{M}\right]_1 = \frac{-\lambda_+}{k_3} \qquad \text{A.II.11}$$

where $\lambda+$ is the larger of the two eigen values of the $\underline{\underline{K}}$ matrix, (ii) if it is assumed that $\frac{dB}{dt} = 0$, i.e. the rate of change of B is negligible then:

$$\left[\frac{B}{M}\right]_2 = \frac{k_1}{k_1+k_2+k_3} \qquad \text{A.II.12}$$

and (iii) for the thermodynamic equilibrium:

$$\left[\frac{B}{M}\right]_3 = \frac{k_1}{k_1+k_2} \qquad \text{A.II.13}$$

Calculations of B/M by all the three methods have been done, and along with the experimental values are summarized in Table IV-1. It is immediately observed that there is no agreement between the experimental values and the ones calculated from the equation A.II.13. This clearly shows that the constant ratios observed are not the consequence of the thermodynamic equilibrium.

In the derivation of equation A.II.11 there is no other assumption than that the two eigen values of the $\underline{\underline{K}}$ matrix are unequal. Since this assumption holds for all the runs reported in Table IV-1, it is natural that the values of $[B/M]_1$ agree reasonably well with the experimental values.

However it is a little surprise that the values calculated from the equation A.II.12 also agree well with the experimental values. It is the result of the fact that, even though B builds upto as large a value as 5 ppm, which is about 30% of the total metal concentration, and then diminishes to nearly zero concentration; its rate of decay is very small.

It is concluded that at short contact times the concentration of chlorin builds up rapidly and then attains a dynamic equilibrium with respect to the total metal concentration. Since in our study, apart from chlorin the other form of the metal in the solution is Nickel Etioporphyrin, the chlorin also attains the dynamic equilibrium with respect to Ni-Etioporphyrin. We can summarize the final model as:

TABLE IV-1

Ni Etio-I. Ratio of Chlorin to Total Metal Concentrations

T(^{o}C)	P(MPa)	$[B/M]_{exp}$	$[B/M]_1$	$[B/M]_2$	$[B/M]_3$
343	9.65	0.127	0.124	0.117	0.219
315	9.65	0.187	0.195	0.184	0.243
302	9.65	0.218	0.224	0.212	0.255
288	9.65	0.193	0.226	0.215	0.269
343	6.89	0.119	0.111	0.106	0.177
329	6.89	0.138	0.145	0.139	0.201
343	4.14	0.118	0.102	0.101	0.120
329	4.14	0.122	0.125	0.123	0.144
315	4.14	0.123	0.140	0.138	0.157

$[B/M]_{Exp}$: Experimental value

$[B/M]_1$: Calculated from equation A.II.11

$[B/M]_2$: Calculated from equation A.II.12

$[B/M]_3$: Calculated from equation A.II.13

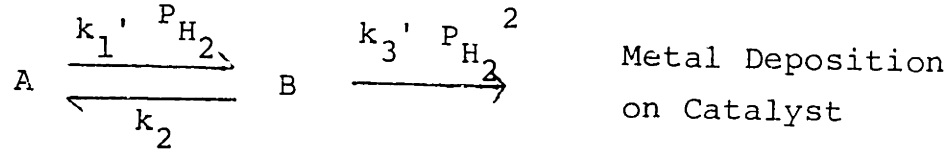

For all the runs discussed above, the inlet concentration of the solution was maintained to a constant value of about 27 ppm. Some runs at the inlet solution concentration of about 15 ppm were also made. Once again the proposed model works extremely well. However, the values of the rate constants calculated at these low inlet concentrations are larger than those calculated at the higher inlet concentrations. The desirable situation would be to be able to make a lot of runs at different inlet solution concentrations. But on the upper side we are limited by the solubility limits, and on the lower side analytical errors become large at low concentrations. Thus no more runs at the different inlet concentrations were made.

The rate constants for two different inlet concentrations and at temperatures of 343, 329 and 315°C and pressure of 6.89 MPa are summarized in Table IV-2. It is interesting to note that at all the three temperatures, all the three rate constants have increased by the same proportionality of two. The average ratio of two inlet concentrations is 1.8. Therefore it can be concluded that as the inlet concentration is reduced to half, the net rate of metal removal doubles up. This conclusion is in agreement with the observation made by Hung (1979) in his batch autoclave studies. On the basis of these two work,

TABLE IV-2

Ni-Etio-I. Comparison of the rate constants for the two different inlet solution concentrations of about 27 ppm and 15 ppm at 6.89 MPa

	M_o	k_1	k_2	k_3
$T = 343^oC$				
	27.8	25.4	118	95.1
	16.3	57.7	228	201.8
Ratio:	1.71	2.27	1.93	2.12
$T = 329^oC$				
	26.0	19.2	76.3	43.1
	15.0	39.4	159.8	99.7
Ratio:	1.73	2.05	2.09	2.31
$T = 315^oC$				
	27.0	14.0	45.6	21.7*
	14.5	27.8	91.9	51.0
Ratio:	1.86	1.99	2.02	2.35
Average				
Ratio:	1.8	2.1	2.0	2.2

* These rate constants are the estimated values.

and the new observation that all the three rate constants change by roughly the same proportion, the following adhoc model is suggested:

The assumptions invoked are -

(i) All three, the metal Etioporphyrin, the chlorin and the final product after the metal removal are adsorbed on the catalyst active sites. For each of these compounds. the surface concentration is in equilibrium with the concentration in the solution.

(ii) Hydrogen is either not adsorbed on the catalyst surface, or if adsorbed it does on the sites where none of the other porphyrin related compounds are adsorbed. This assumption has been invoked by many investigators in the related studies (Gultekin - 1980).

(iii) Kinetic steps are the rate controlling steps.

(IV) Sites where metal has deposited are either still active or the metal deposition does not change the total number of sites involved in the chemical reaction significantly.

For this model the derivation of the bulk rate constants in terms of the surface rate constants are given in Appendix-II. If it is assumed that the adsorption constants for all three, Ni-Etio(I), Ni-chlorin and the final metal free product are about equal then eq. A.II.17 gives:

$$[S] = \frac{S_o}{1+k_A M_o} \qquad \text{A.II.17}$$

where [S] = occupied active sites, S_o = total number of active sites, k_A = adsorption constant for A and M_o = inlet concentration of the nickel to the reactor. It is further assumed that in our concentration range studied, $k_A M_o >> 1$:

$$[S] = \frac{S_o}{k_A M_o} \qquad \text{A.II.18}$$

when this equation is substituted in equation A.II.20:

$$k_1 = \frac{k_{1s} S_o}{M_o} \; P_{H_2}$$

$$k_2 = \frac{k_{2s} S_o}{M_o} \qquad \text{IV.5}$$

$$k_3 = \frac{k_{3s} S_o}{M_o} \; P_{H_2}^2$$

In the above equations all the three rate constants are inversely proportional to the inlet concentrations. If the value of M_o is reduced to half, the values of all the three rate constants would double up and therefore the total rate will also increase by a factor of two. This explains our observations of the Table IV-2 and also the increase in the total rate observed by Hung (1979). However, it must be pointed out that equations IV.5 have to

be subjected to some more critical testing. The most important assumption invoked is about the adsorptivity of the final metal free product formed in the reaction. One way to test would be to add this compound in the inlet solution to the reactor and observe its impact on all the three rate constants. But unfortunately we have been unable to identify this final metal free reaction product and therefore the validity of equations IV.5 remain a little uncertain.

C. VANADYL ETIOPORPHYRIN-I:

Just like the nickel runs, Vanadyl Etio(I) runs are made at the pressures of 4.14 MPa, 6.89 MPa and 9.65 MPa and at temperatures 288, 302, 315, 329 and 343^{o}C, and for two different reactor inlet concentrations. The details of all the runs are given in appendix-III.

Our proposed model of the formation of one dominant intermediate B and then the metal deposition on the catalyst also works well for the vanadium runs. One typical result is plotted in figure IV-16. It must be pointed out that the magnitude of the error involved in the analysis of vanadium solutions at low concentrations is very high. For the solution concentration of about 4 ppm the uncertainity may be as high as 1.5 ppm. This uncertainity is reflected in the relatively poor fit at the high conversions.

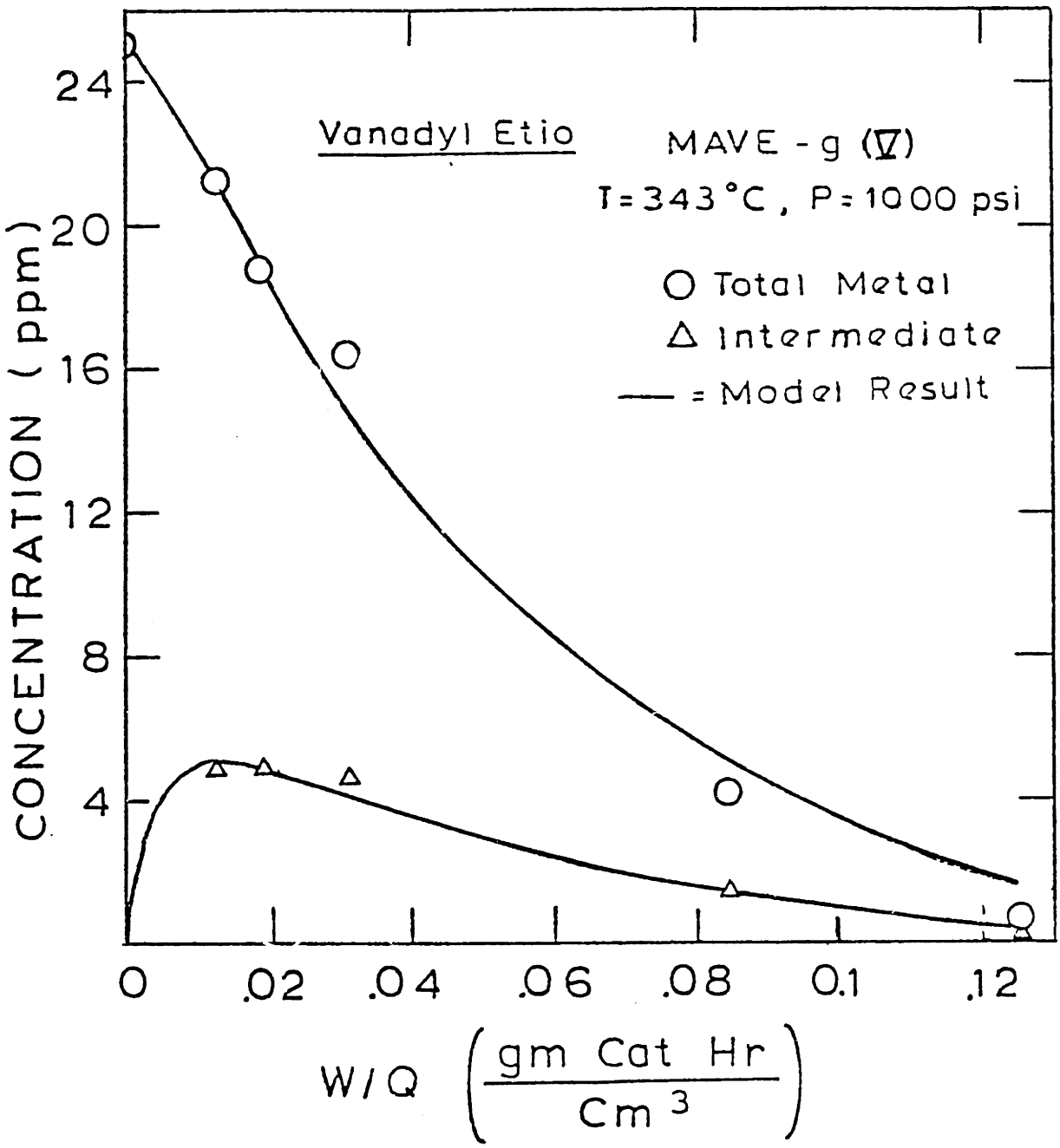

Fig. IV-16: Vanadyl Etio-I. Comparison of the Results from the New Model With the Experimental Results.

An attempt to fit half and the first order kinetics to the experimental data has also been made. The results for one of the runs are plotted in figures IV-17 and IV-18. It is seen from fig. IV-17 that the half order kinetics does a fairly poor job. Comparison of the figures IV-17 and IV-18 shows that the first order kinetics again does a better job than the half order kinetics. But unlike nickel, the first order kinetics does not do a reasonable job with the vanadium kinetics data.

Arhenius plots for the rate constants k_1, k_2 and k_3 are given in figure IV-19. It is seen that all the three rate constants give excellent straight lines on the Arhenius plot. It is found that the activation energies for the rate constants k_1, k_2 and k_3 are 18.3, 16.5 and 24.9 kcal/gmole respectively. Once again, the activation energies for the hydrogenation and dehydrogenation steps fall in the range of the reported hydrogenation and dehydrogenation energies in the literature (Bhinde - 1979 and Gultekin - 1980).

Dependence of the rate constants k_1, k_2 and k_3 on the hydrogen saturation pressure, for the reaction temperature of 343°C, are plotted in figure IV-20. As expected, k_1 and k_2 have the order of dependence of one and zero respectively. k_3 shows the order to be 1.82 which is again close to two.

Now we can express all the three rate constants in terms of equation IV.3:

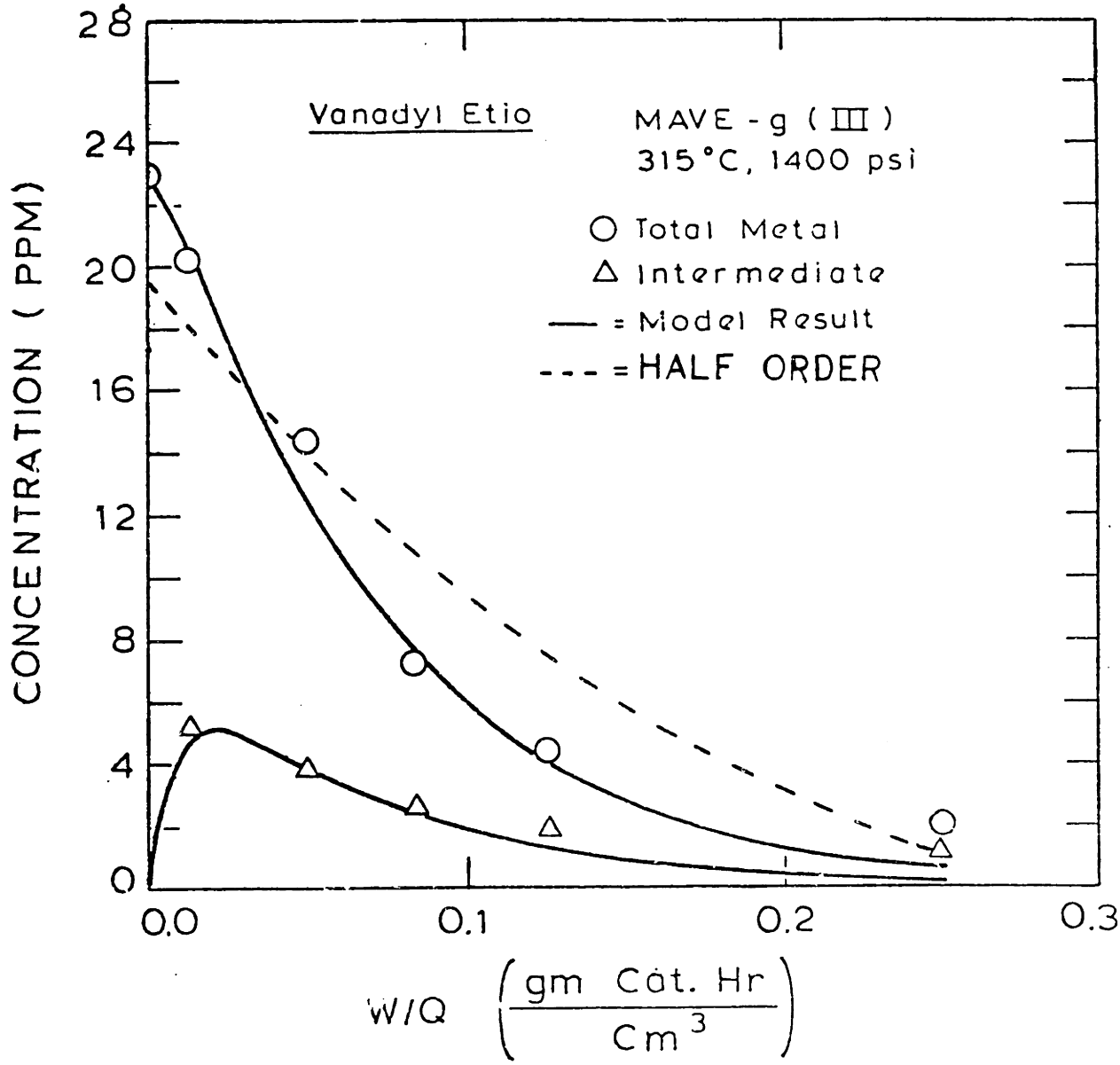

Fig. IV-17: Vanadyl Etio-I. Comparison of the New Model and the Half Order Kinetics With the Experimental Results.

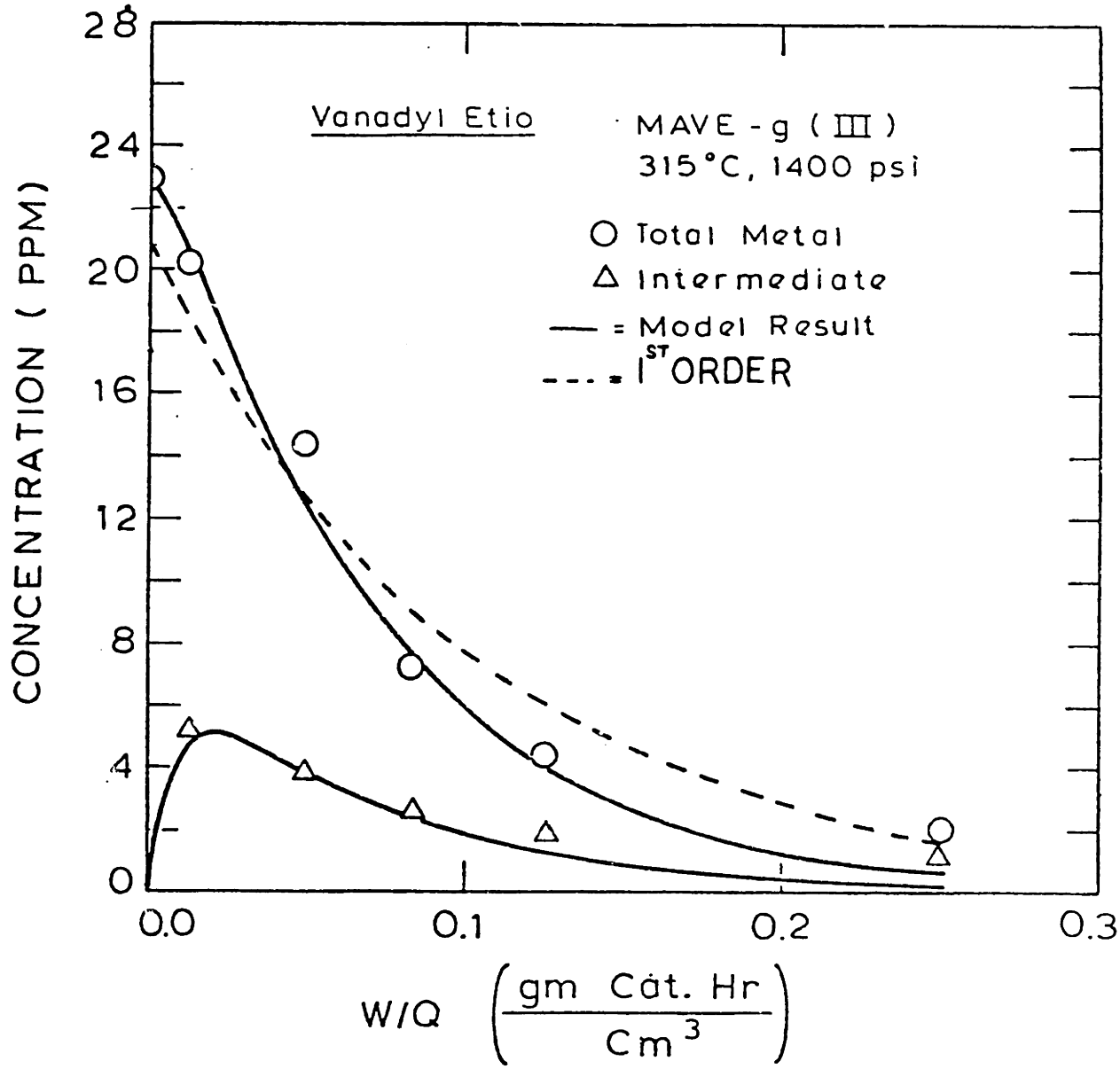

Fig. IV-18: Vanadyl Etio-I. Comparison of the New Model and the First Order Kinetics With the Experimental Results.

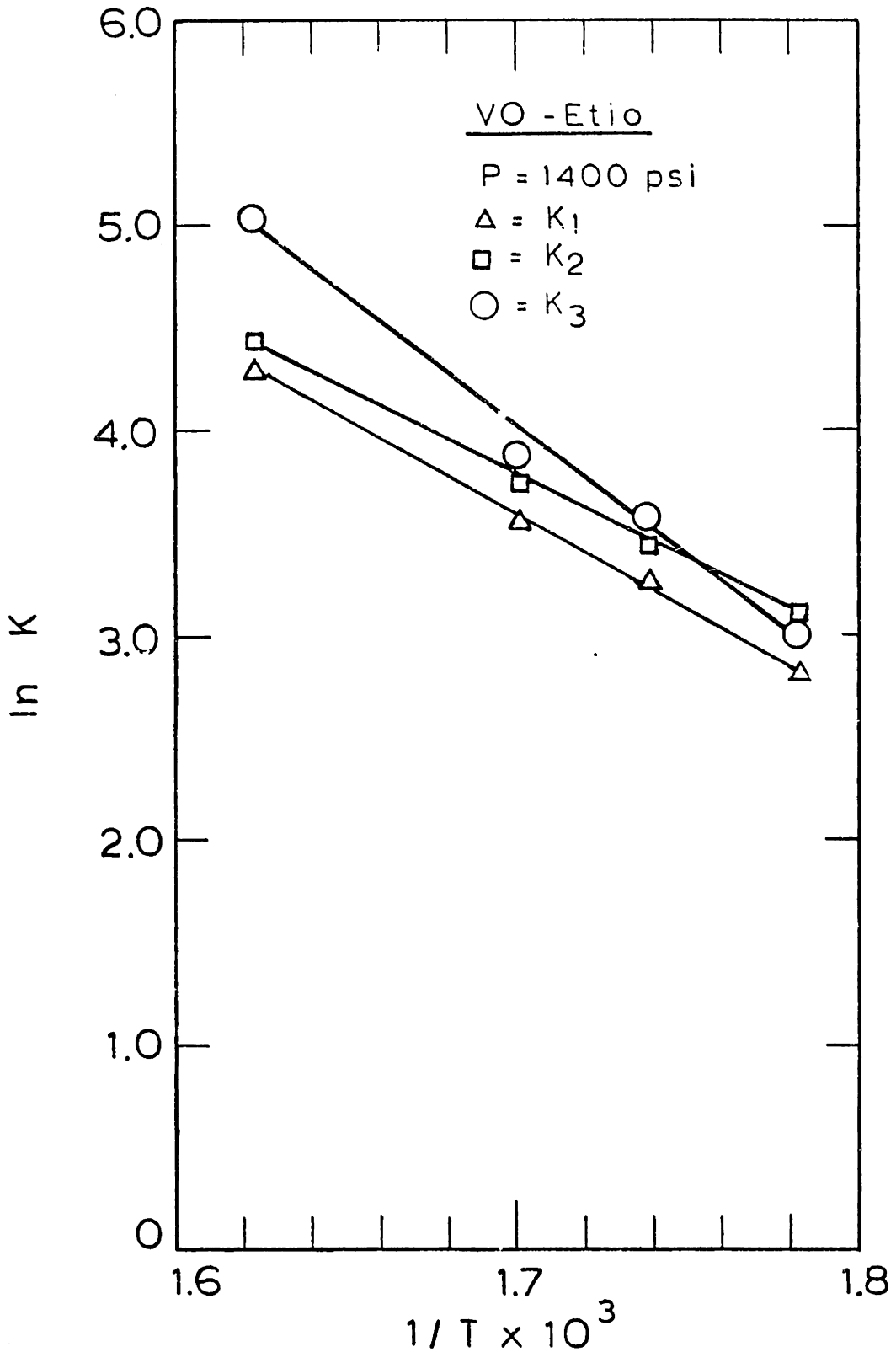

Fig. IV-19: Arrhenius Plot for the Rate Constants k_1, k_2 and k_3 at the Hydrogen Pressure of 9.65 MPa. T is in °K and rate Constants are in ml/g-hr.

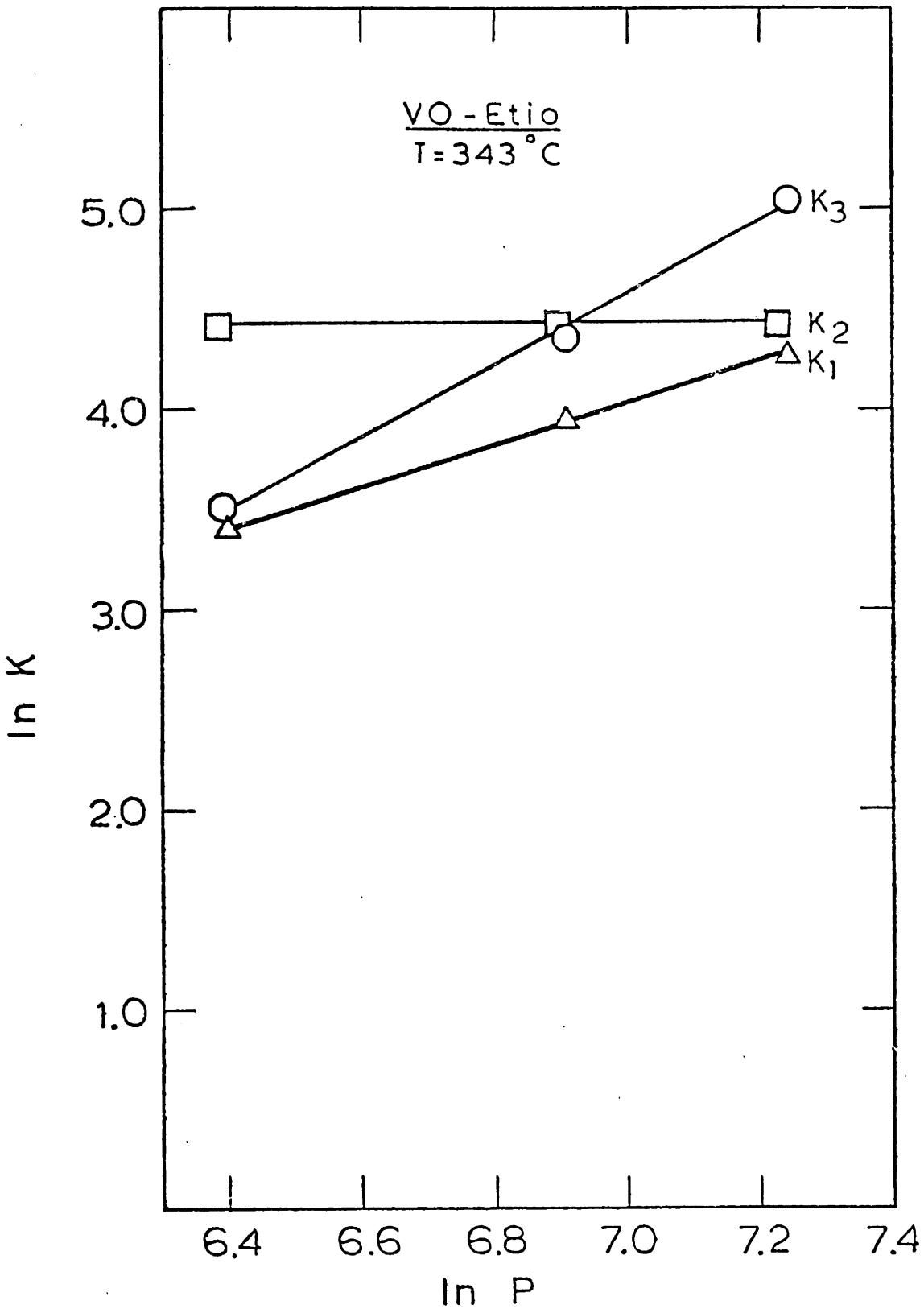

Fig. IV-20: Dependence of the Rate Constants k_1, k_2 and k_3 on the Hydrogen Pressure. P is in psig and rate constants are in ml/g-hr.

for k_1:

$n=1$, $E=18.3$, $\ln k_{10}=11.98\pm0.03$

for k_2:

$n=0$, $E=16.5$, $\ln k_{20}=17.88\pm0.02$

for k_3:

$n=1.82$, $E=24.9$, $\ln k_{30}=12.16\pm0.08$

and for k_3, if the value of n is taken to be 2 then:

$n=2$, $E=24.9$, $\ln k_{30}=10.89\pm0.11$ IV.6

For vandium the various [B/M] ratios are summarized in Table IV-3. As expected, $[B/M]_1$ calculated from the equation A.II.11 agrees reasonably well with the experimental values. Once again, $[B/M]_3$ calculated from the equation A.II.13 does not agree with the experimental values. Therefore, in case of vanadyl Etio-I runs, at high conversions the reaction intermediate and the total metal attain the dynamic and not the thermodynamic equilibrium.

TABLE IV-3

Vanadyl Etio-I

Ratio of the reaction intermediate to the total Metal Concentrations

T(^{o}C)	P(MPa)	$[B/M]_{Exp}$	$[B/M]_1$	$[B/M]_2$	$[B/M]_3$
343	4.14	.236	.216	.205	.265
343	6.89	.270	.270	.243	.385
343	9.65	.305	.283	.242	.465
315	9.65	.313	.314	.276	.451
302	9.65	.312	.317	.277	.461
288	9.65	.323	.349	.309	.459

$[B/M]_{Exp}$: Experimental value

$[B/M]_1$: Calculated from Eq. A.II.11

$[B/M]_2$: Calculated from Eq. A.II.12

$[B/M]_3$: Calculated from Eq. A.II.13

When we compare Tables IV-1 and IV-3 we see two major differences - (i) In case of vanadum the [B/M] ratio is higher than nickel, i.e. for a given metal concentration there is more reaction intermediate formed in the vanadium runs than in the nickel runs. It is due to the fact that in the temperature and pressure range studied, vandium has hydrogenation rate constant two times higher and the dehydrogenation rate constant a little less than the nickel. This leads to $[B/M]_3$ for vandium to be higher than the $[B/M]_3$ for nickel. Furthermore, the values of rate constant k_3 are roughly same in both the cases. Therefore B/M ratio for vanadium are higher than that of nickel. (ii) The second difference between the two tables is that while for nickel $[B/M]_2$ agrees reasonably well with the experimental ratios it does not do so for vanadium. This implies that unlike nickel, for vanadium runs the assumption of $dB/dt = 0$ does not hold. This is easily understood by comparing the figures IV-2 and IV-18. The temperature and pressure of the operation are same for both the figures. It is seen that for nickel in fig. IV-2, the amount of B formed is less and disappears slower than the one for vanadium in fig. IV-18. However, it must be pointed out that for vanadium at lower pressures and temperatures the value of k_3 relative to k_1 and k_2 will become smaller and it is possible to justify the assumption of $dB/dt = 0$; and $[B/M]_2$ would agree reasonably well with the experimental values.

Now the last check of the model is to see the effect on the rate constants of the change in the inlet solution concentrations to the reactor. Two runs at 288^{o}C and 1400 psi and different values of the inlet concentrations were made. For the inlet concentrations of 16 ppm and 28 ppm the values of k_1, k_2, k_3 obtained are 17.0, 20.0, 18.0 and 16.0, 22.0, 20.2 ml of sol./g of cat. hr. respectively. Within the experimental error the agreement between the two runs is fairly good. Therefore it is concluded that for the range of the inlet concentrations studied, the model describes the vanadium kinetics adequately.

The observation that for a given concentration the rate of vanadium removal from the solution is independent of the inlet solution concentration is in agreement with the work of Hung (1979). This behaviour can be again explained in terms of the adhoc model proposed earlier. This time it is not necessary to assume that the final product after the metal removal from the porphyrin ring is adsorbed on the surface. The basic assumption needed is that the total number of the active sites covered by the metallo-porphyrins are the negligible fraction of the total number of active sites available on the catalyst surface. It should be pointed out that there exists a possibility that the vandium porphyrins may adsorb strongly on the nonactive sites and give high physical adsorption coefficient. Of

our interest are the active sites and hence the above assumption leads to eq. A.II.19:

$$[S] = S_o \qquad \text{A.II.19}$$

Use of this equation in equations A.II.20 gives the rate constants:

$$k_1 = k_{1s}\, k_A\, S_o\, P_{H_2}$$

$$k_2 = k_{2s}\, k_B\, S_o \qquad \text{IV.7}$$

$$k_3 = k_{3s}\, k_B\, S_o\, P_{H_2}^{\,2}$$

The rate constants given by equations IV.7 are independent of the inlet solution concentration to the reactor.

Once we have the adequate models for the nickel and vanadium kinetics; the question of why the first order kinetics of the total metal removal works reasonably well for the nickel and not for the vanadium can be addressed. The answer lies in the relative ratios of the eigen values of the $\underline{\underline{K}}$ matrix. It is seen from the equation A.II.9, that depending on the relative values of λ_+ and λ_-, for the values of t greater than some t_1 the second term on the right hand side of the equation can be neglected and the following approximate relation holds:

$$\begin{bmatrix} M \\ \\ B \end{bmatrix} \simeq C_1' \begin{bmatrix} \frac{-k_3}{\lambda_+} \\ \\ 1 \end{bmatrix} e^{\lambda_+ t} \qquad \text{IV.8}$$

For both nickel and vanadium the ratio of the two eigen values λ_-/λ_+, for some of the runs, are listed in Table IV-4. It is seen that for nickel the ratios are more than two times higher than that of vanadium. Therefore in case of nickel equation IV.8 becomes a good approximation at much lower conversions than it does for vanadium. Because of the much higher ratios of λ_-/λ_+ the nickel kinetics for the total metal removal can be explained reasonably well in terms of the first order kinetics. Another implication of this is that the dynamic equilibrium in Table IV-1 for nickel are attained at much lower conversions than for vanadium in Table IV-3.

D. SOME MORE COMMENTS ON THE TRANSIENT BEHAVIOR OF THE CATALYST: In section IV.A. we discussed that there is a rapid deactivation of the catalyst and then the catalyst activity increases again and finally stabilizes to some value for a long period of time. The rapid deactivation is thought to be probably due to rapid coke build up on the catalyst. The spent catalyst from the reactor did show the coke concentration as high as three to four percent.

TABLE IV-4

Ratio of the two eigen values $\frac{\lambda_-}{\lambda_+}$* for some of the nickel and vanadium runs:

T(^{o}C)	P(MPa)	Nickel $\left(\frac{\lambda_-}{\lambda_+}\right)$	Vanadium $\left(\frac{\lambda_-}{\lambda_+}\right)$
343	4.14	60.0	19.5
343	6.89	21.4	9.1
343	9.65	17.8	6.4
315	9.65	16.5	7.2
302	9.65	17.6	6.9
288	9.65	23.7	8.4

* λ_+ and λ_- are calculated from the equation A.II.7

The second phase of the increase in the activity is attributed to the metal deposition in the catalyst. From our model it is seen that the metal Etioporphyrin first goes through hydrogenation and then the demetallation step. This demetallation step may be just the hydrogenolysis step or the combination of hydrogenation and hydrogenolysis steps. In figure IV.2 it is observed that as the catalyst activity is increasing, the concentration of the hydrogenated intermediate in the solution also increases. Thus the net hydrogenation activity of the catalyst is increased during this period. It is also observed from figure IV.2 that the total metal removal from the solution increases by as much as 50 - 75%. If we look at the relative magnitudes of the rate constants in our model, we find that the increase in the concentration of the hydrogenated reaction intermediate cannot explain alone the high increase in the total metal removal activity. Therefore the demetallation activity has also increased.

Bridge and Green (1979) reported that the metal deposit is catalytically active for hydrogenation and demetallation. However in a follow up paper, along with the other workers, Bridge reported that the deposited metals are catalytically active for hydrogenolysis (Tamm et al. - 1979). In this paper there is no comment on the hydrogenation activity. Our work confirms that there is an increase in both the hydrogenation as well as demetallation activities.

E. BATCH AUTOCLAE RESULTS AND THE NEW KINETIC MODEL:

In this section we would re-interpret the results of Hung (1979) in the light of the theory developed here. These runs were made in a batch autoclave. The catalyst and the metal compounds used were the same as in this study. It was observed that the total metal disappearance rate could be explained by a fractional order kinetics. For nickel depending on the temperature and the pressure of the operation the best fit fractional order varied from 0.1 to 0.93. On the average 0.5 order did the job fairly well for both nickel and vanadium.

In this section we will first discuss the general implications of collecting the HDM kinetics data in a batch autoclave and then look at the experimental nickel and vanadium runs.

E.1. General Implications: The basic underlying assumption in the batch runs is that the transient behavior of the catalyst lasts for a time which is negligible with respect to the total reaction time. It is seen from the discussions in the sections A and D that the transients of the catalyst are very important in HDM. For the catalyst to reach steady activity, it takes about 500 ml of solution per gram of the catalyst. Since in batch autoclave, the amount of solution and the catalyst used were in the same amount, the impact of the transients on the observed conversion vs. time data would be significant.

At low conversions the catalyst activity is low but as the conversion increases more metal deposits on the catalyst and its activity increases. Thus if the disappearance of the total metal from the solution was monitored it would appear as if the reaction rate has increased at high conversions. Indeed this is the observed case for both nickel and the vanadium runs. Hung's data for one of the nickel runs is reproduced in the figure IV-21. Even though the total metal disappearance rate for the nickel in the microreactor could be fitted by the first order kinetics the same cannot be done for the data in fig. IV-21. It is seen that at about 75% conversion the demetallation rate starts increasing.

By its very mathematical nature a fractional order gives at large conversions the reaction rates which are higher than the ones given by first order. Therefore even in the case of the new model, it is possible to have the values of k_1, k_2 and k_3 such that the fractional order kinetics will do a reasonable job. It is due to the fact that at low conversions the concentration of the metallo chlorin in the solution is building up and the net rate of metal removal would be a little slower. But beyond some conversion the metallo chlorin concentration in the solution starts dropping and the total metal removal would seem a little faster. This is the cause for the partial success of the 0.5 order in explaining the microreactor data for nickel (see fig. IV-6).

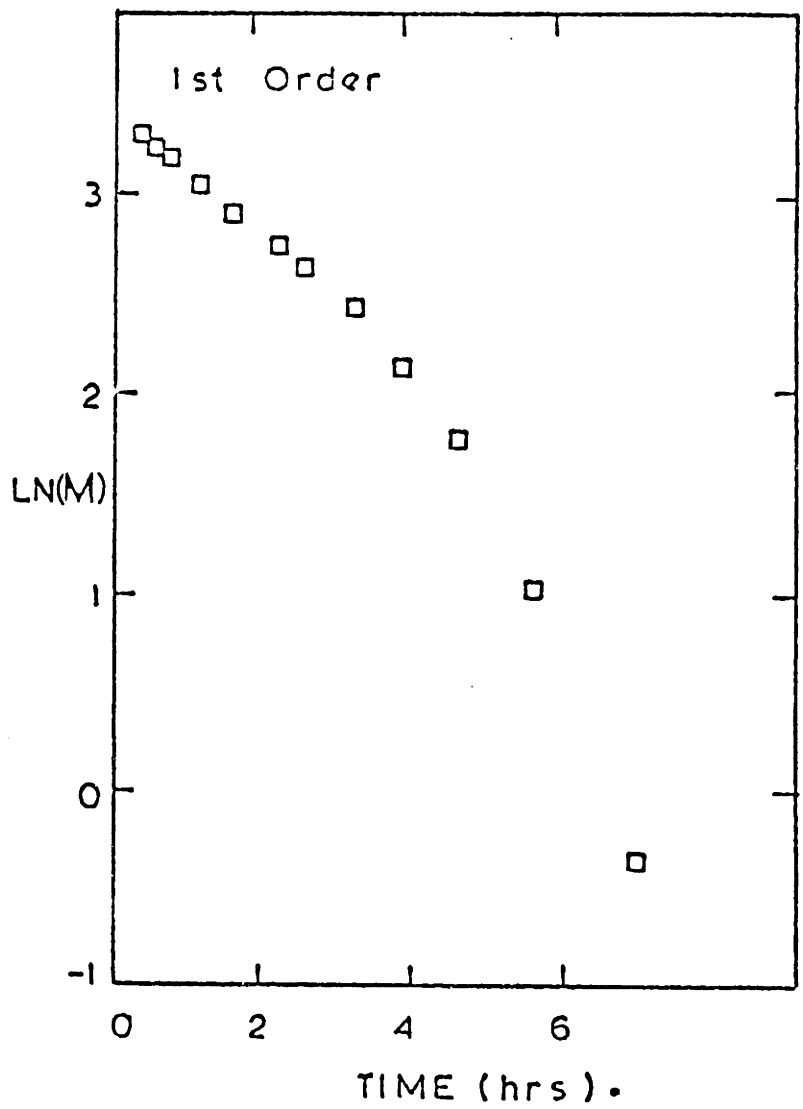

Fig. IV-21: First Order Plot of the Batch Autoclave Run of Ni-Etio-I at 316°C and 6.99 MPa. M is in ppm (Hung - 1979)

It is possible that due to the above two factors the batch data could be explained by the fractional order kinetics. Since the transient behavior of the catalyst depends on the temperature and pressure of the operation, and also the relative values of the rate constants k_1, k_2, k_3 vary with the operating conditions, the best fit fractional kinetic order can also be the function of temperature and pressure.

The third important characteristics of the batch data, which can also be common to the hydrodenitrogenation and hydrodesulfurization are the adsorption effects. All these compounds are known to adsorb strongly on the catalyst surface. When the reaction with a pure compound A is studied, at zero conversion all the catalyst surface is covered by A. As the reaction proceeds some molecules of A on the catalyst surface are converted to reaction intermediate B. But due to the adsorption effects only a fraction of these molecules B appear in the solution. Whereas in the continuous flow microreactor, at each point of the catalyst bed, the catalyst is in steady equilibrium with the bulk solution; and therefore on the catalyst surface there is no net accumulation of any species. An attempt to model the simplest case for the autoclave runs is made in Appendix-II. Instantaneous adsorption equilibrium between the catalyst surface and the solution is assumed. If adsorption is very strong then the values of the rate constants evaluated are strongly influenced by

it. As seen from equation A.II.21, for the strong adsorption effect, if the amount of catalyst per unit volume of the solution is increased then the calculated value of the rate constant would decrease. If this trend is observed experimentally, the proper way would be to make runs at various catalyst to solution ratios and extrapolate the rate constant for the zero ratio.

There are two experimental drawbacks inherent in all the autoclave runs. The first one is that as the catalyst is injected in the solution, due to a rapid adsorption there is a drop in the solution concentration and the zero time point is not exactly defined. The second drawback is that at a constant hydrogen pressure the variation in the operating temperature may change the concentration of hydrogen in the solution and therefore the Arhenius plot might not give the exact activation energy of the reaction.

The above discussion might have given a pessimistic view of the batch autoclave method, but it is a quick and convenient way of gathering information and is a very useful tool.

E.2. Experimental Runs: An attempt to fit the proposed model to the batch results has been made. In the new model the best fit k_1 and k_2 are sensitive to the low conversion data. It is due to the fact that at low conversions there is much more information on the formation of B. At high conversions, B/A reach the dynamic equilibrium and

some information is lost. Unfortunately, in the batch results there is a lot of uncertainity in the low conversion data Specifically in case of vanadium runs, when the catalyst is injected, the concentration of solution drops within the first six minutes from 20 ppm to 10 ppm. Due to this initial uncertainity even though each run can be individually fitted, the calculated rate constants give very poor agreement on the Arhenius plot and would not be discussed here.

Hung made a lot of good runs with nickel Etio-I, but unfortunately during his period of work the importance of the reaction intermediate was not realized. Therefore only a few runs were analyzed for the reaction intermediate. In figure IV-22 the batch data of the fig. IV-21 is replotted with the model results. The calculation results of the best fit fractional order are also plotted

Figure IV-23 is the Arhenius plot for the various rate constants. From the view of the limitations, which have already been discussed the scatter in the figure IV-23 is not a surprise. The calculated values of the activation energies of k_1, k_2 and k_3 are 30, 16.2 and 30.1 Kcal/gmole respectively. The corresponding values from the microreactor are 17.1, 22.9 and 32.6 Kcal/gmole.

Fig. IV-24 is a plot of the dependence of the rate consants on the hydrogen pressure. The order of dependence for the k_1, k_2 and k_3 are 0.73, 0 and 1.4 respectively. The corresponding values for the microreactor are

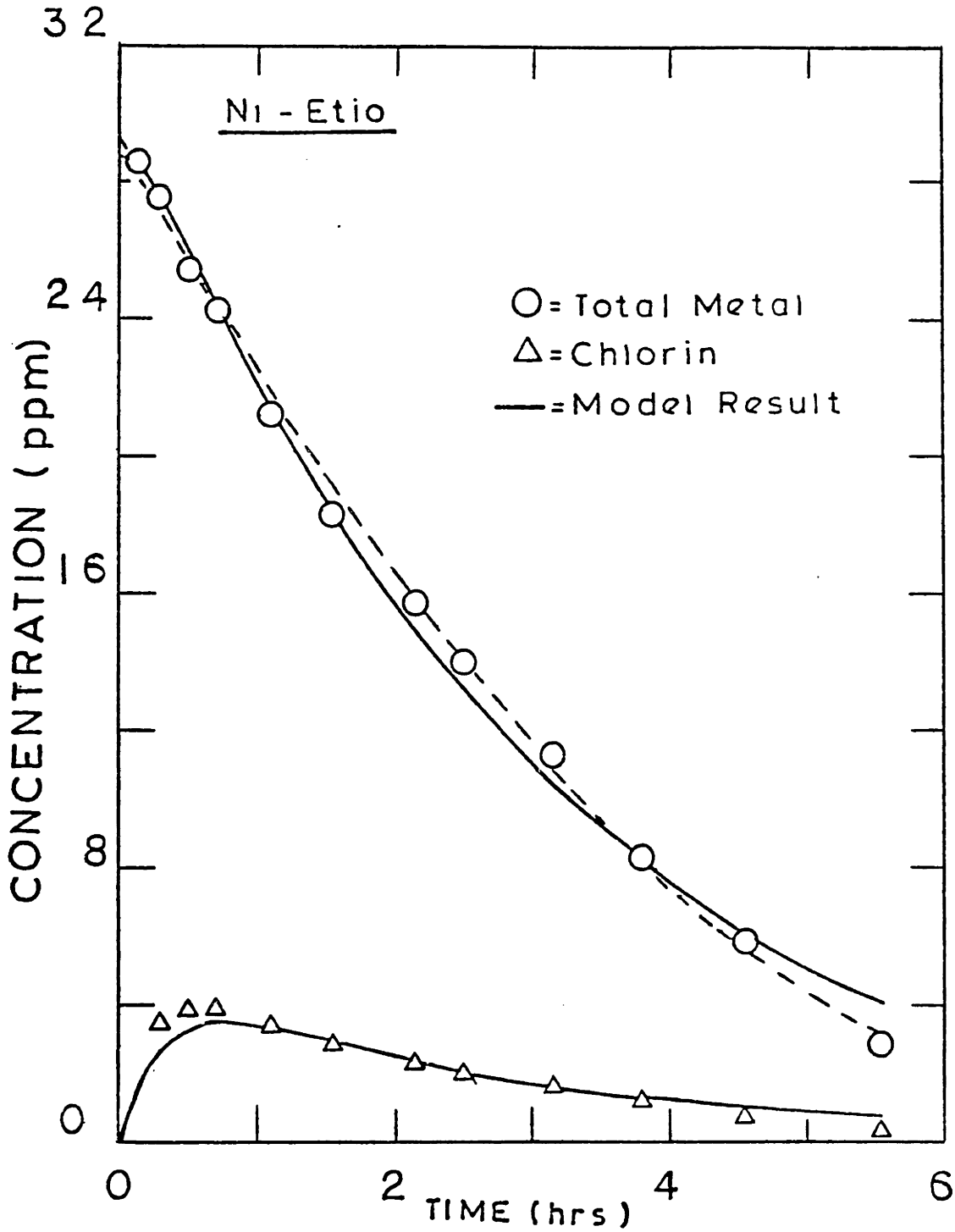

Fig. IV-22: Comparison of the New Model with the Experimental Result of the Batch Autoclave (Hung - 1979). Dotted line is the result of the best fit Fractional Order, which is 0.5. T = 316°C, P = 6.99 MPa.

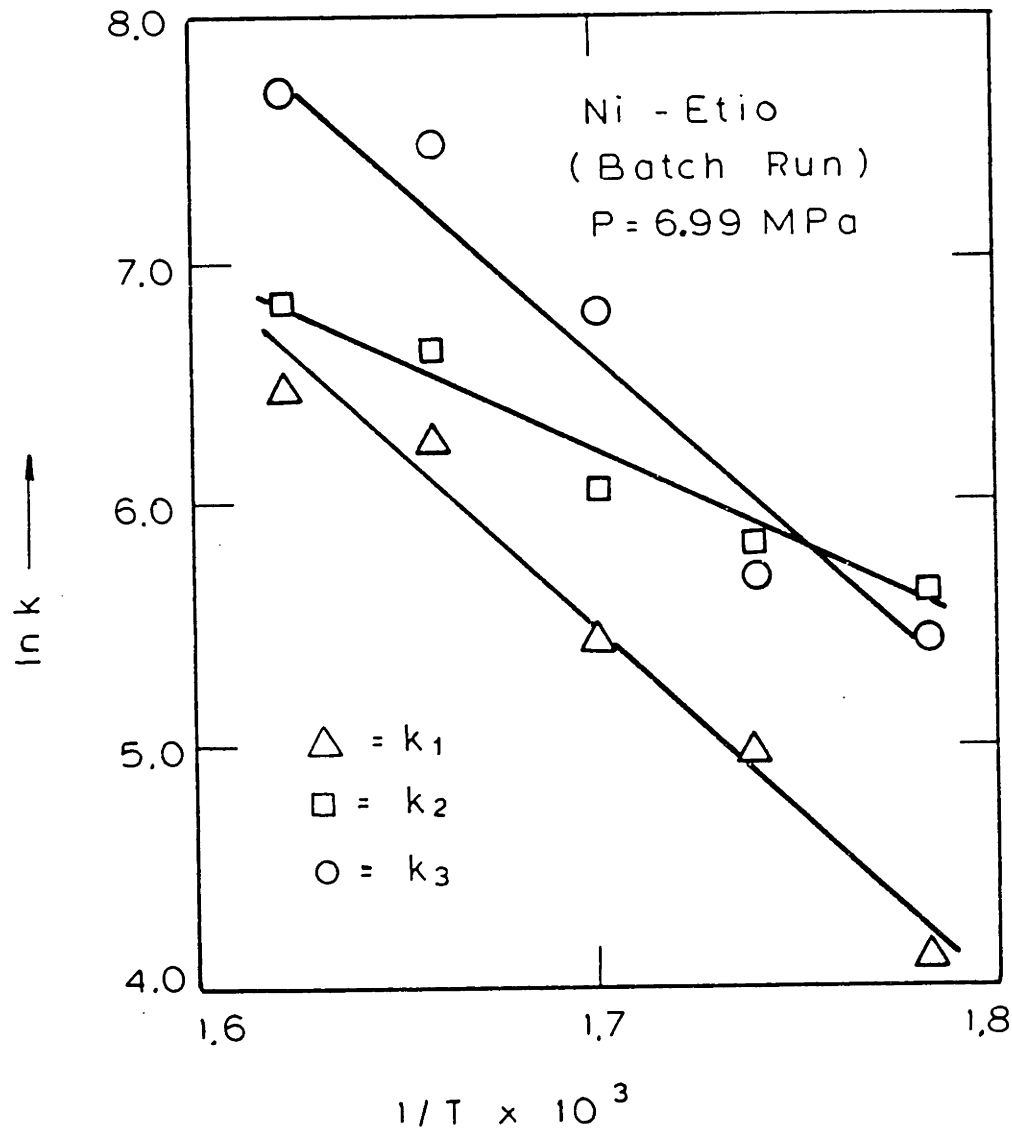

Fig. IV-23: Arhenius Plot for the Batch Data. T is in ^{o}K, and Rate Constants in ml/g-hr.

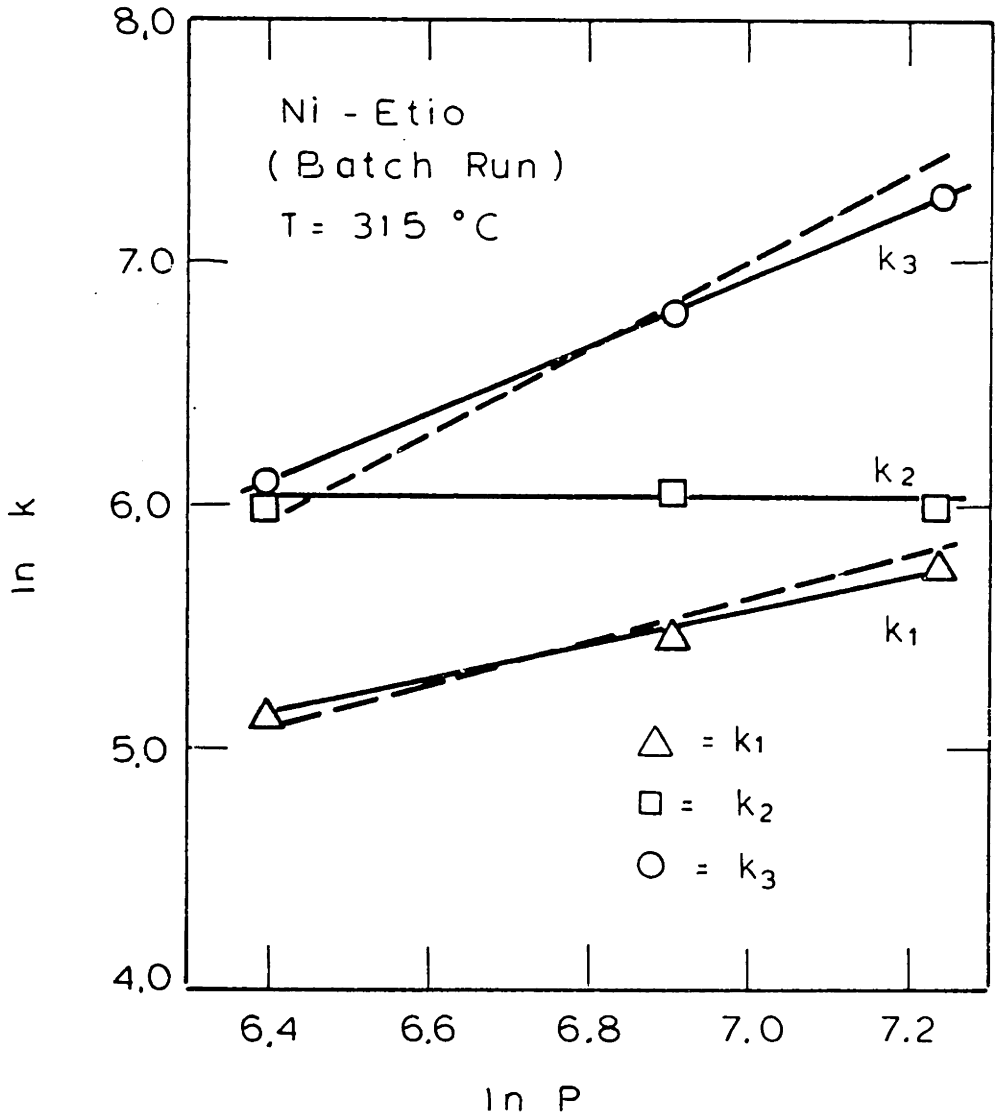

Fig. IV-24: Pressure Dependence of the Rate Constants for the Batch Data. P is in psig and Rate Constants in ml/g-hr.

——— Best fit result
– – – Order of Dependence same as for the Microreactor runs.

1, 0 and 1.83. In fig. IV-24, for comparison purposes, the best fit lines corresponding to the dependence order of the microreactor runs are plotted as the dotted lines.

The final point to be seen in the batch runs is the effect of the ratio of the amount of the catalyst to the volume of the solution. In one of the runs the ratio was doubled and it was observed that the half order rate constant decreased by 21%. The result of these runs are summarized below:

Run #	Initial Conc.	W/V	Half order Rate Constant
NE1	39	0.002	426.5
NE4	35.5	0.002	472.0
NE13	38.7	0.0047	373.8

Run # NE 4 has lower initial concentration than the run NE1. If we use our observation that for nickel the rate constants are directly proportional to the initial concentration, we see that the ratio of the half order rate constants is .90 whereas reciprocal of the ratio of the initial concentrations is 0.91. However, it is not clear that the difference in the rate constants of the runs NE1 and NE13 is due to the statistical experimental error or is the effect of the W/V. This question can only be answered by some additional runs for different W/V ratios.

CHAPTER-V

SIMULTANEOUS REACTION AND DIFFUSION RESULTS AND THEIR DISCUSSION

In this chapter the metal deposition profiles inside the 1/16" catalyst extrudates at various reactor positions are discussed. A model to predict the metal deposition profiles, with the aid of the kinetics of Chapter IV, is developed.

A. EXPERIMENTAL RESULTS: In a typical run the one inch diameter reactor was packed with about five grams of 1/16" catalyst extrudates. To insure that there were no cracks in the catalyst extrudates and their ends were not badly broken, each of the catalyst extrudates were carefully handpicked. Also the length of catalyst used was controlled with in the range of 5 mm to 7 mm. As discussed in Chapter III, the catalyst bed was diluted with the inert, to a ratio of 1:2.5 by volume of catalyst to volume of inert.

Through the reactor the metal solution was passed at the flow rates of 10 ml/hr to 40 ml/hr (0.5-2.0 hr^{-1} L.H.S.V.). In any single run the total amount of the solution pumped was about 1500 ml and the total number of hours on stream were 35-100 hrs. During the run, the liquid samples were collected at various time intervals. At the end of the run, the catalyst from various reactor positions were collected and analyzed for the metal deposition profiles.

Similar to the microreactor, the transport limitation calculations for this reactor are done in Appendix-I. It is seen that there are no radial temperature gradients, the catalyst extrudates are isothermal and the interphase heat and the mass transfer resistances are negligible. The axial and the radial dispersion effects are also negligible and therefore reactor operates as a plug flow reactor.

The variation of the reactor outlet solution concentration with time on stream are plotted in figures IV-1 and IV-3. Similar bahaviour is observed for both the vanadium and the nickel runs, and has already been discussed in sections IV.A. and IV.D.. It may be thought that the results in these figures are the outcome of the catalyst pretreatment, so two Ni runs were made with the catalyst reduced with hydrogen for 30 minutes at the temperature of 370^{o}C. The results were identical to the one shown in figure IV-1.

Metal deposition profiles for some of the vanadium runs are plotted in figures V-1 to V-6. Operating conditions for the runs in these figures are tabulated in Table V-1. For the time being the continuous and the dashed curves in these figures should be overlooked; they are the results of the theoretical calculations and are discussed in the next section. These figures show that at the entrance of the bed, the maximum in the metal deposition occurs inside the catalyst and not at the external surface. In the middle and the top sections of the bed, the maxima moved to the external surface, and the metal deposition profiles look like the classical U shape profiles.

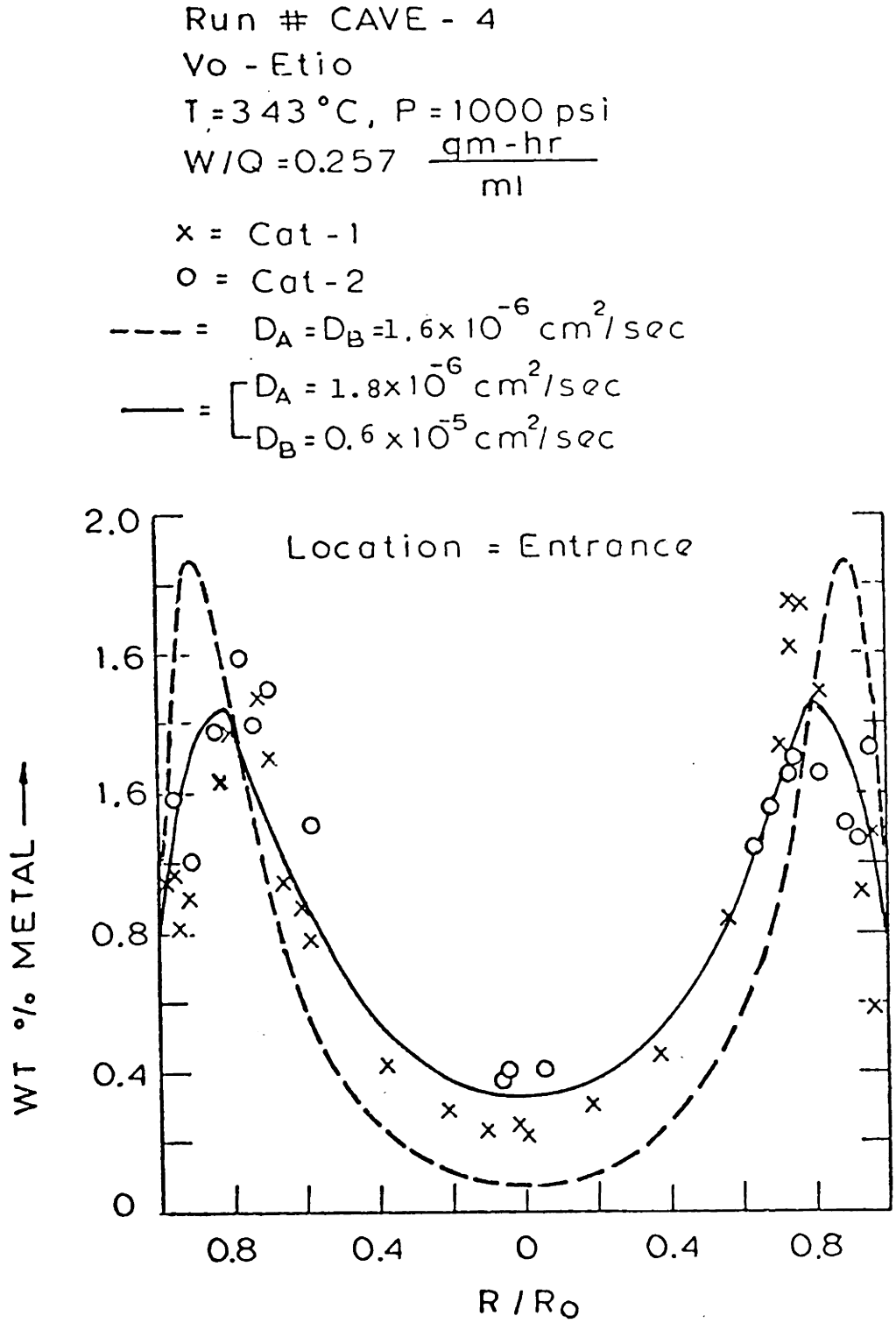

FIGURE V-1a: Vanadium Deposition Profile in the Catalyst

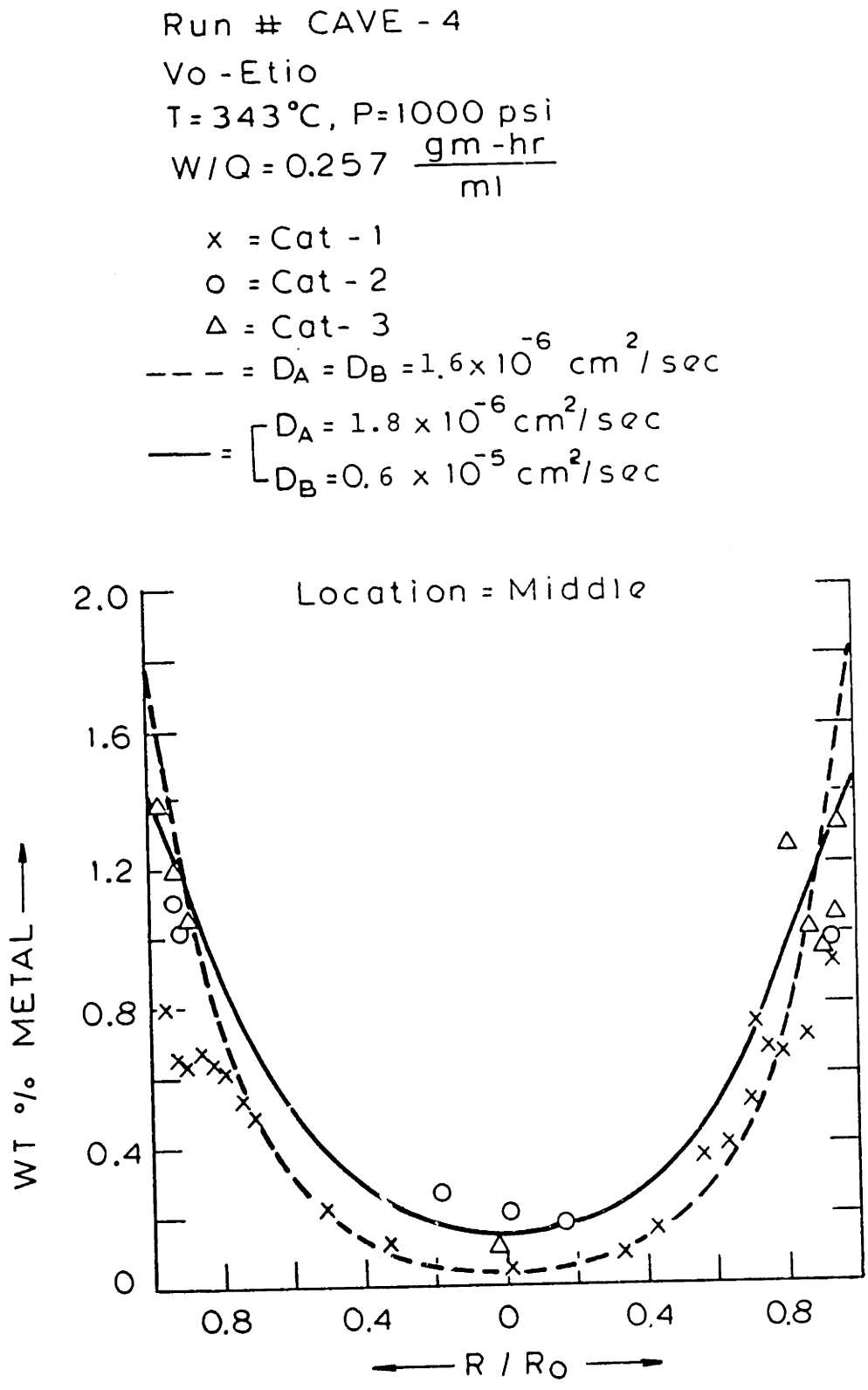

FIGURE V-1b: Vanadium Deposition Profile in the Catalyst

Run # CAVE - 4
Vo - Etio
T = 343 °C, P = 1000 psi
W/Q = 0.257 $\frac{gm-hr}{ml}$

x = Exp Value
--- = $D_A = D_B = 1.6 \times 10^{-6}$ cm²/sec
——— = $D_A = 1.8 \times 10^{-6}$ cm²/sec, $D_B = 0.6 \times 10^{-5}$ cm²/sec

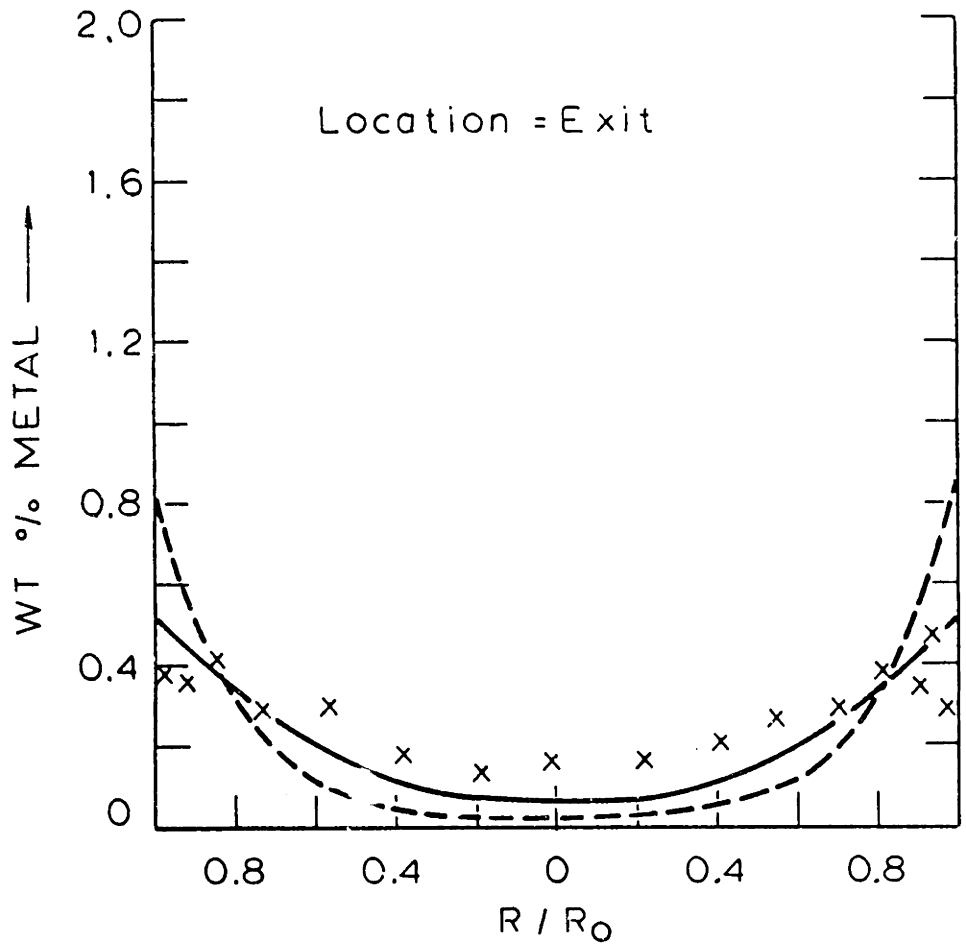

FIGURE V-1c: Vanadium Deposition Profile in the Catalyst

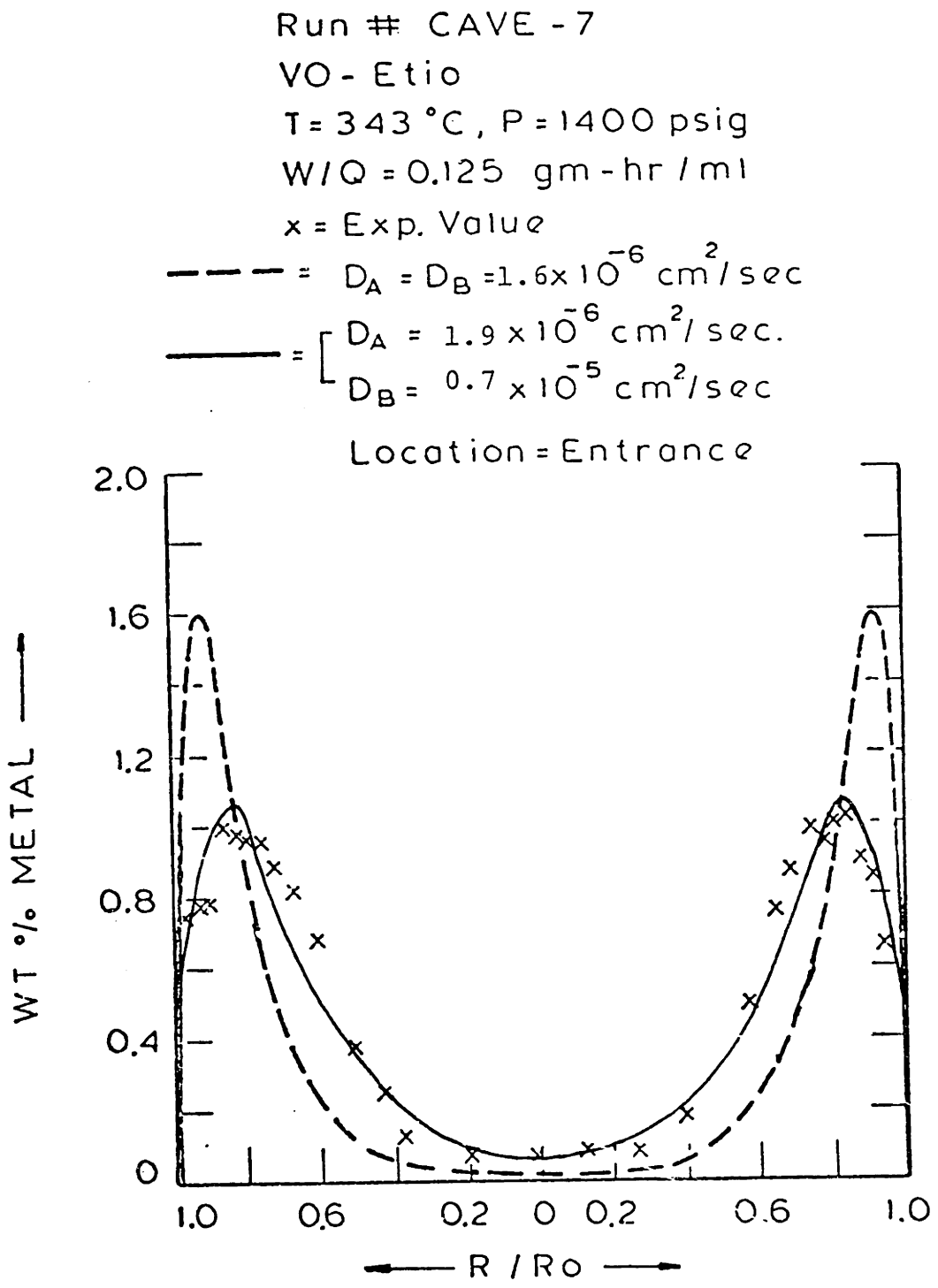

FIGURE V-2a: Vanadium Deposition Profile in the Catalyst

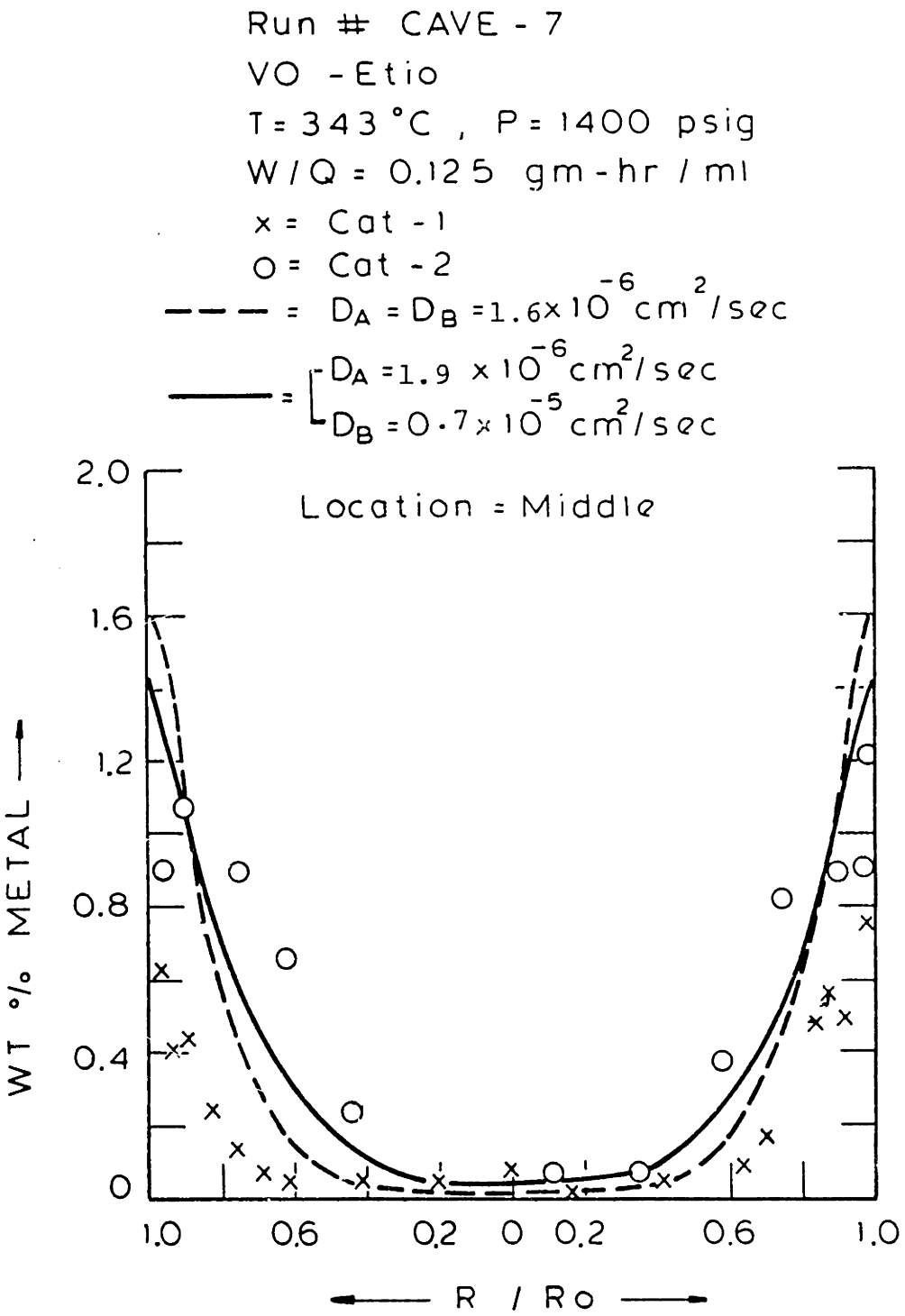

FIGURE V-2b: Vanadium Deposition Profile in the Catalyst

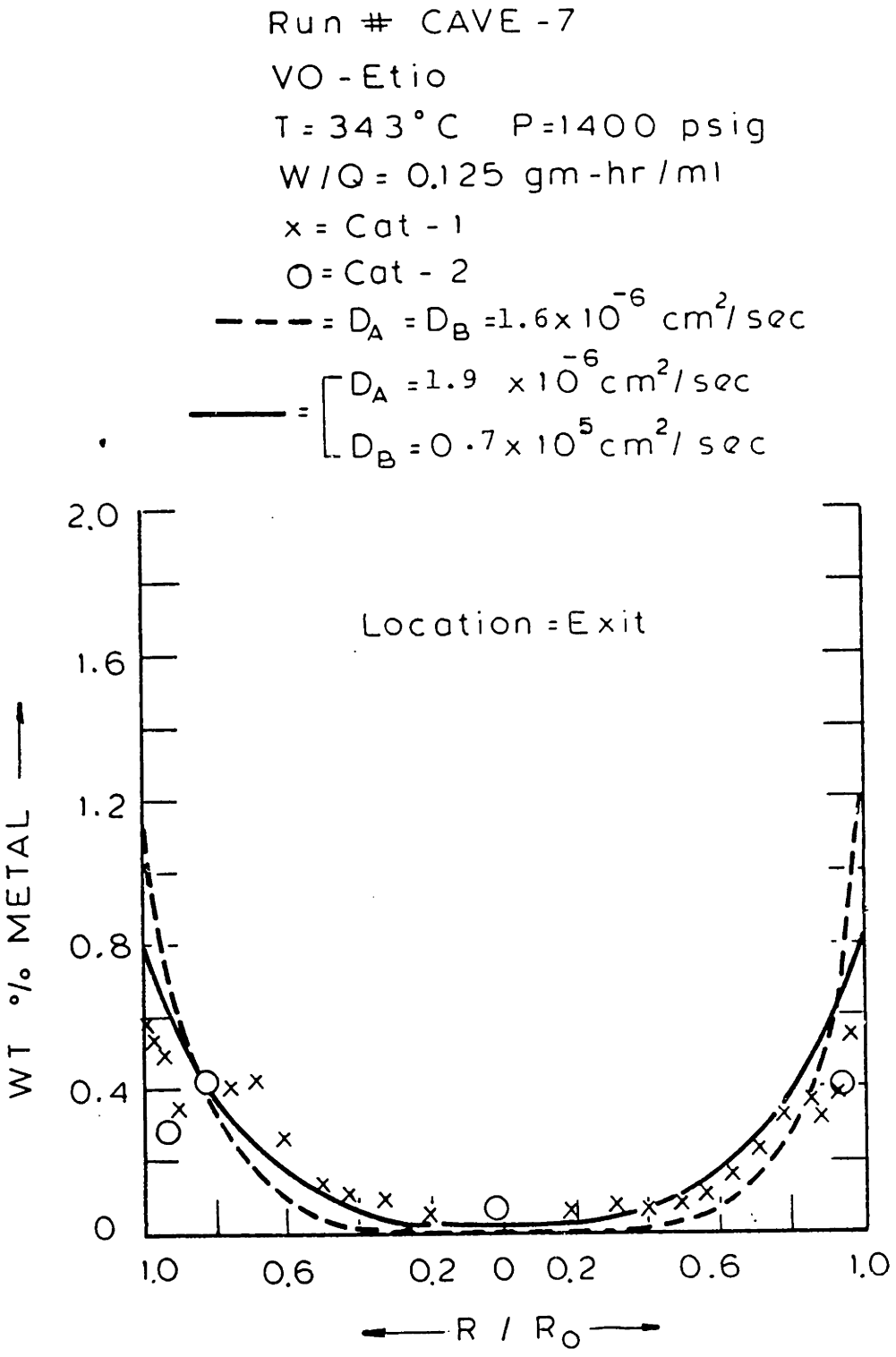

FIGURE V-2c: Vanadium Deposition Profile in the Catalyst

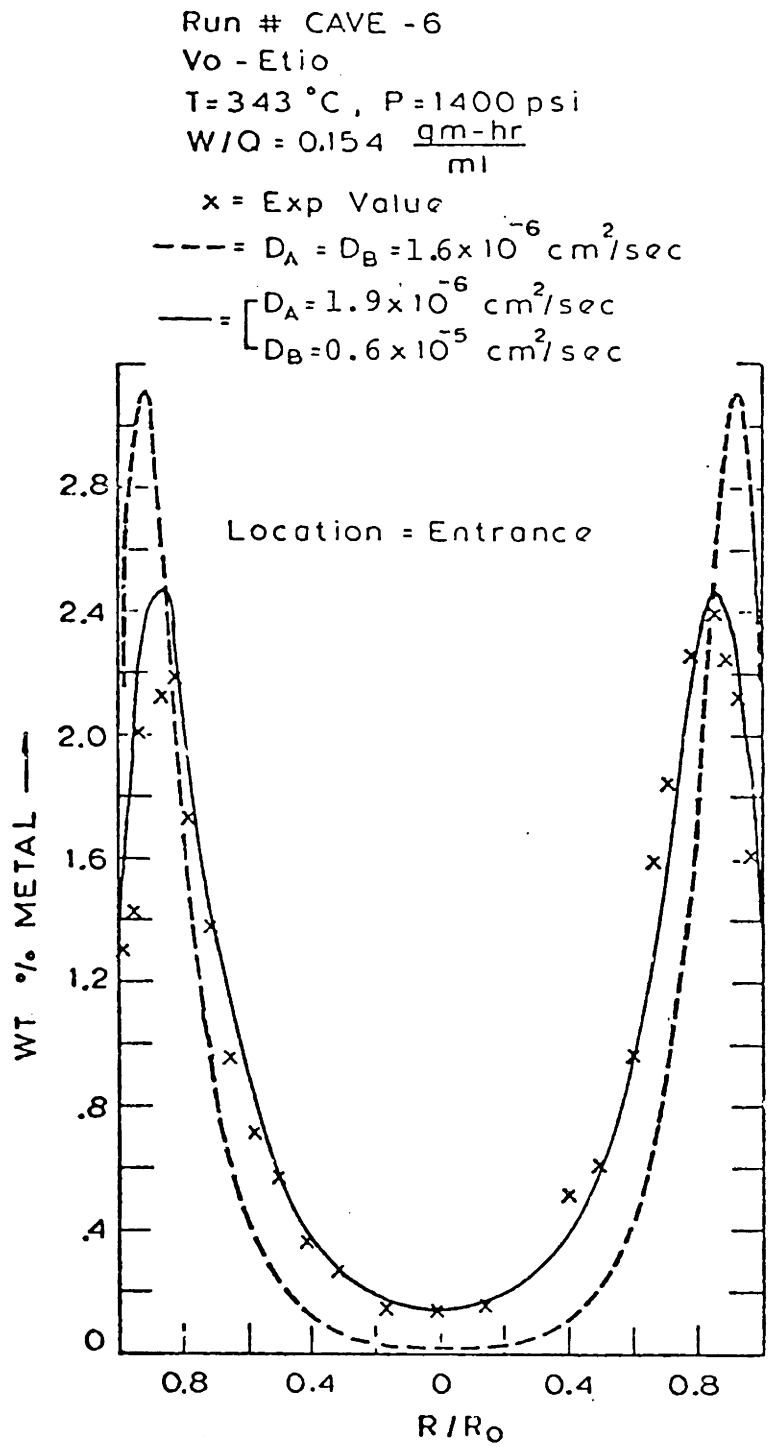

FIGURE V-3a: Vanadium Deposition Profile in the Catalyst

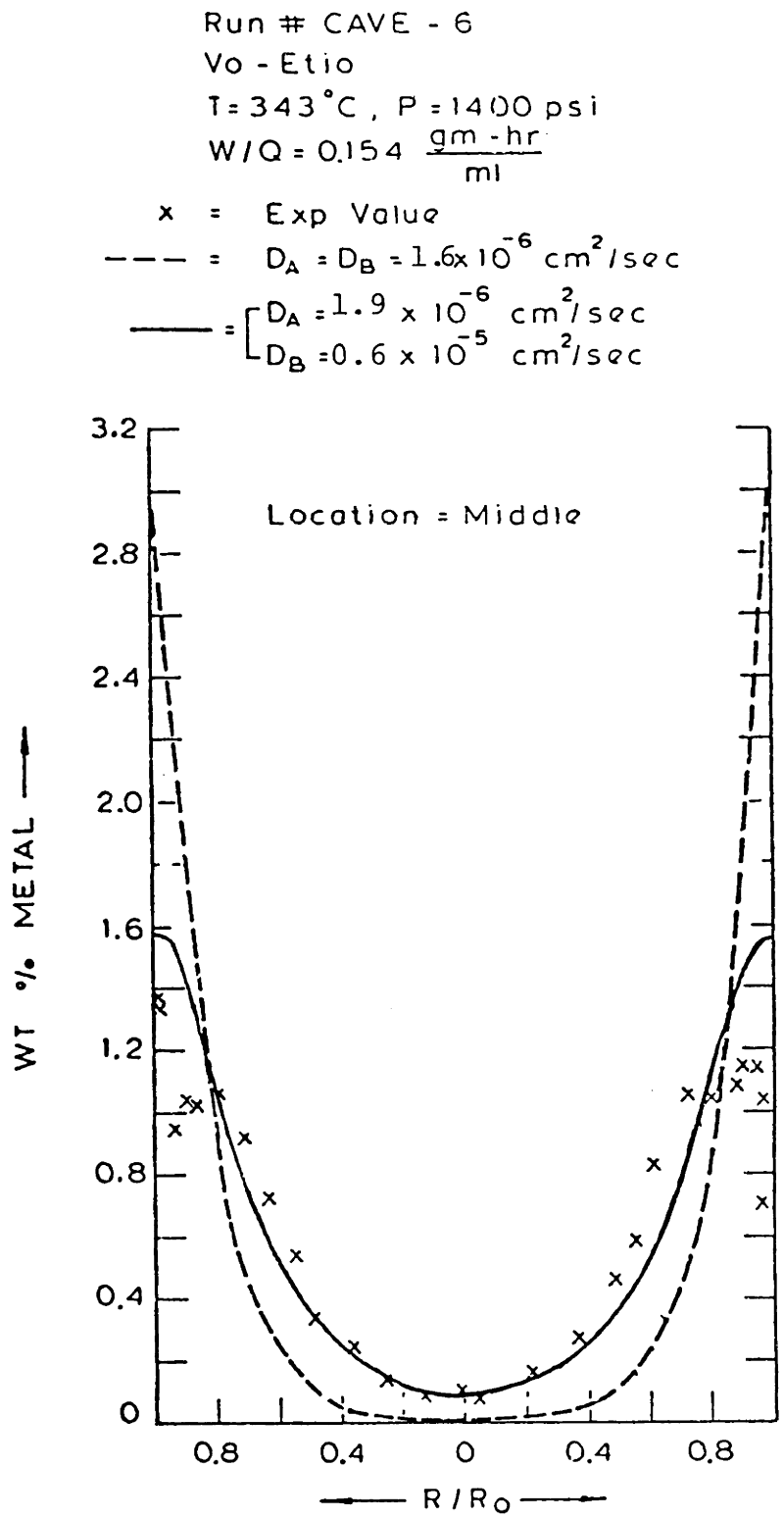

FIGURE V-3b: Vanadium Deposition Profile in the Catalyst

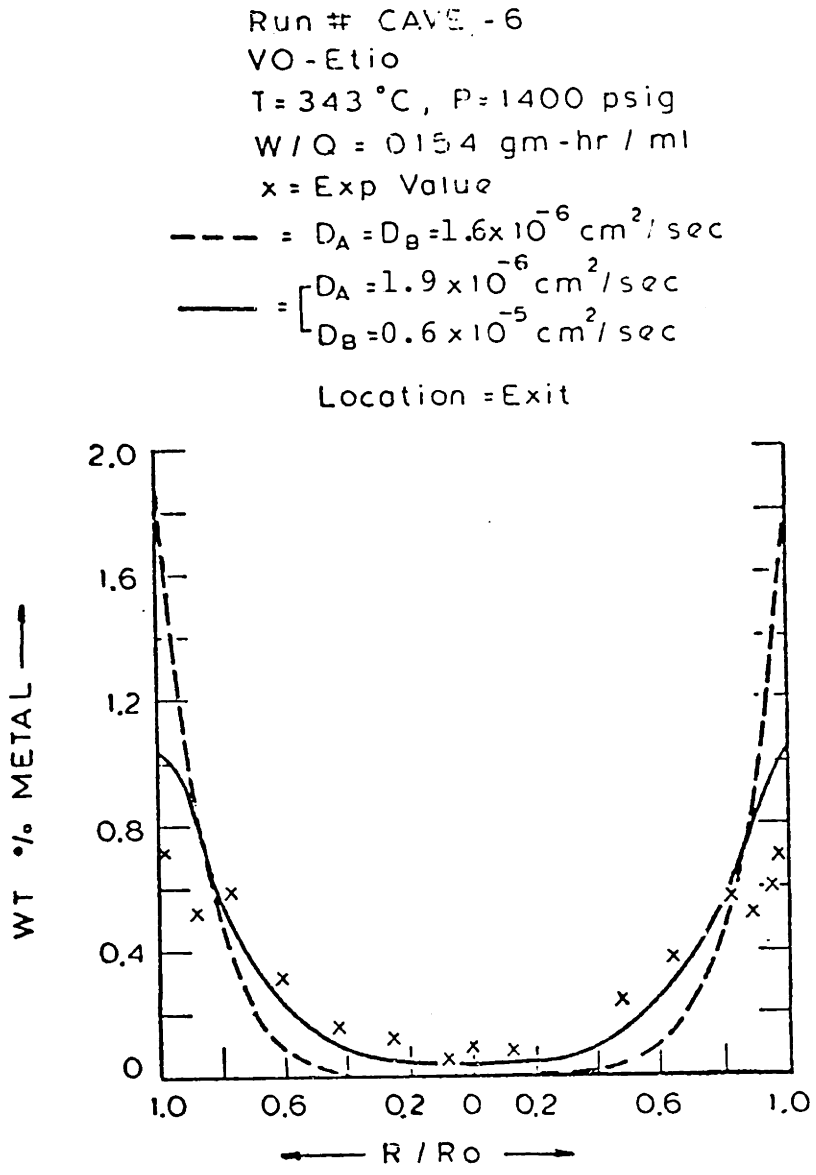

FIGURE V-3c: Vanadium Deposition Profile in the Catalyst

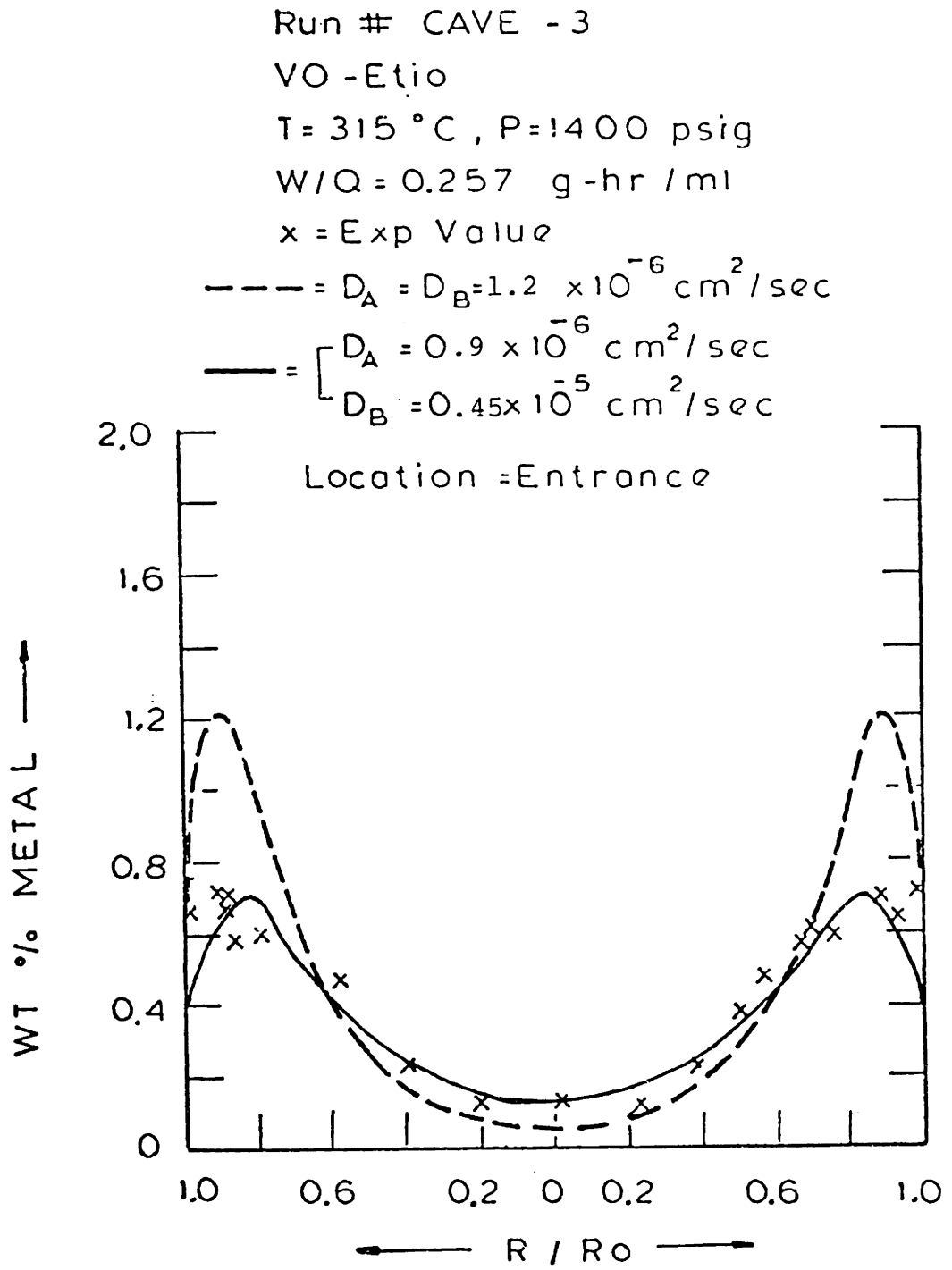

FIGURE V-4a: Vanadium Deposition Profile in the Catalyst

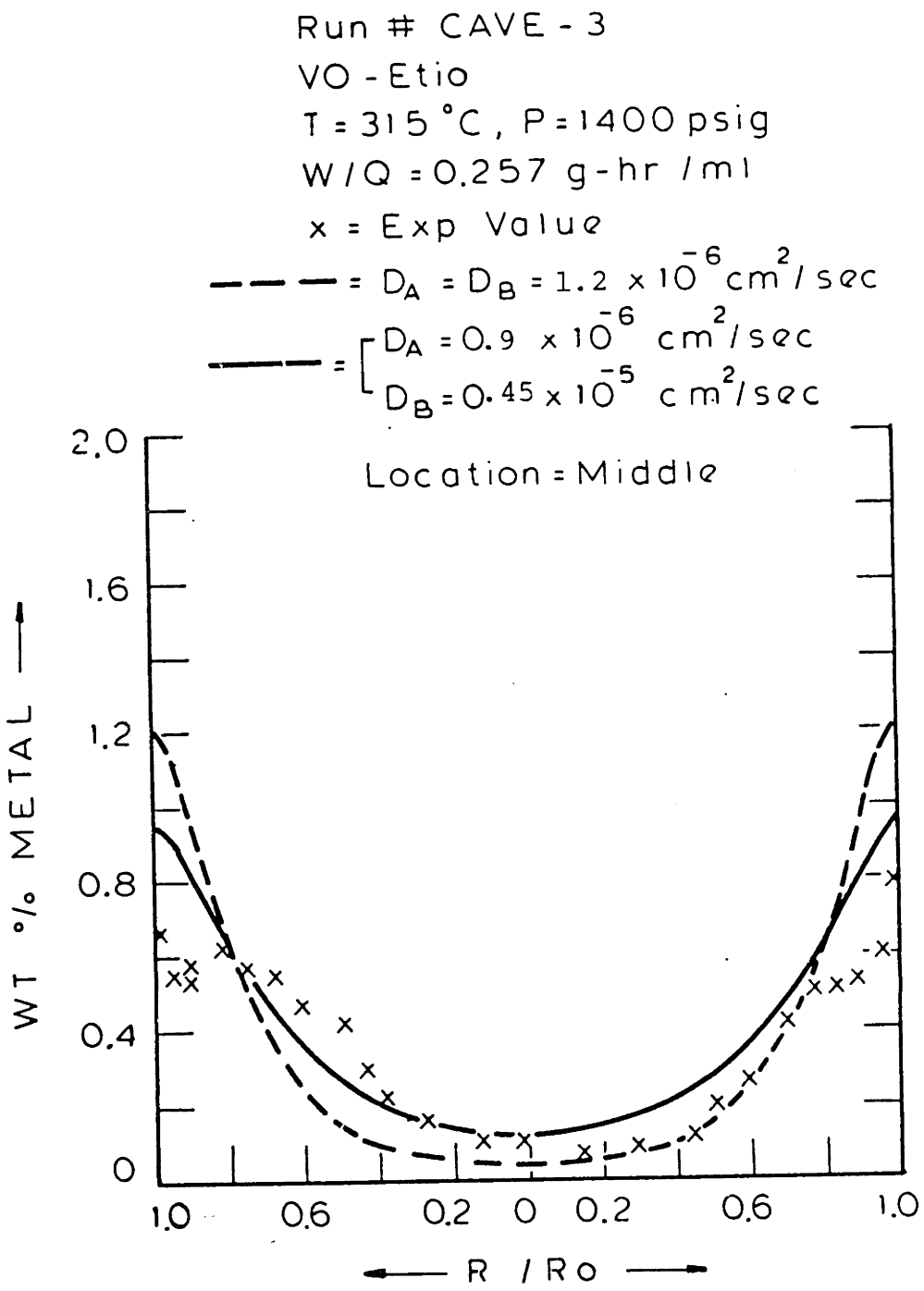

FIGURE V-4b: Vanadium Deposition Profile in the Catalyst

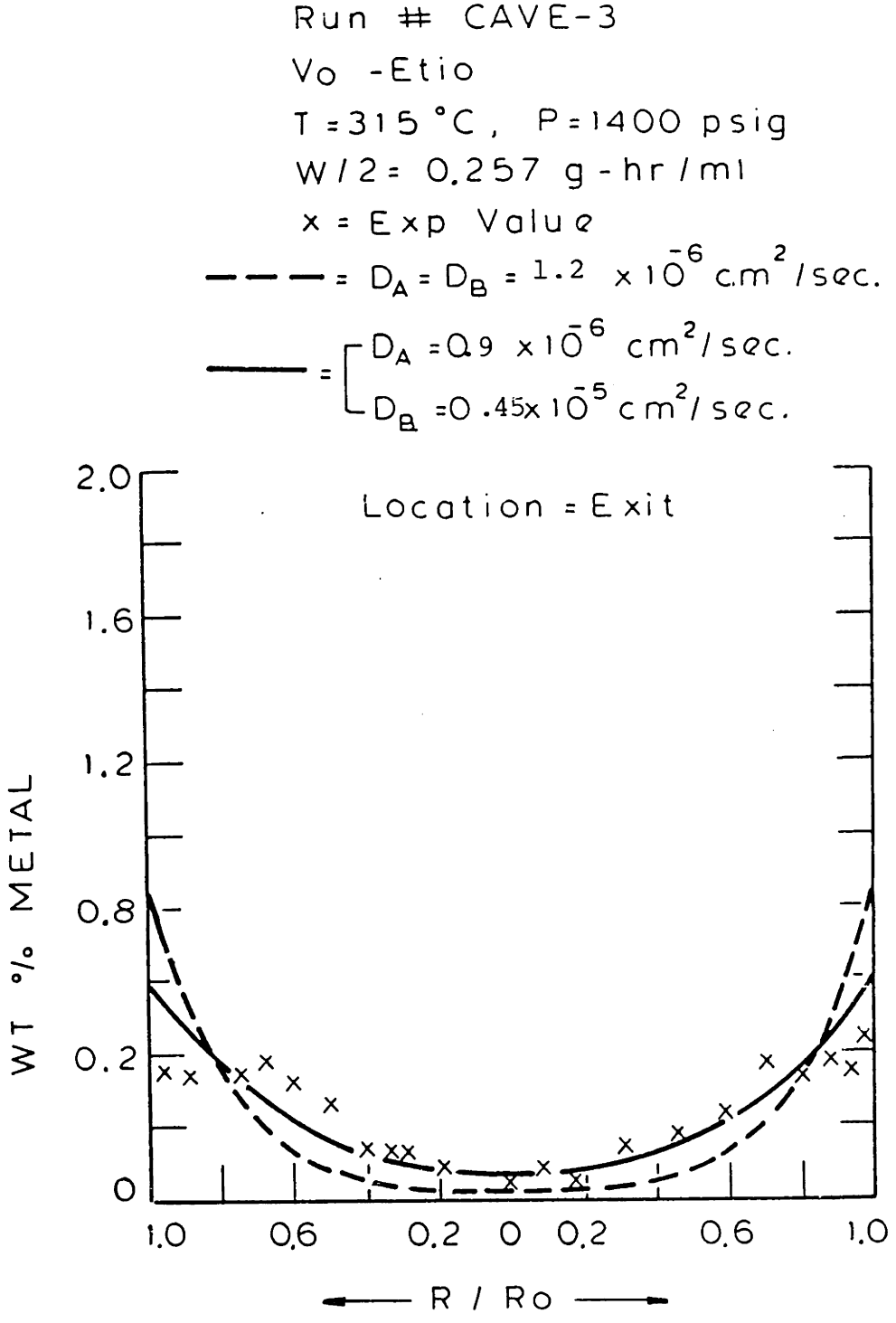

FIGURE V-4c: Vanadium Deposition Profile in the Catalyst

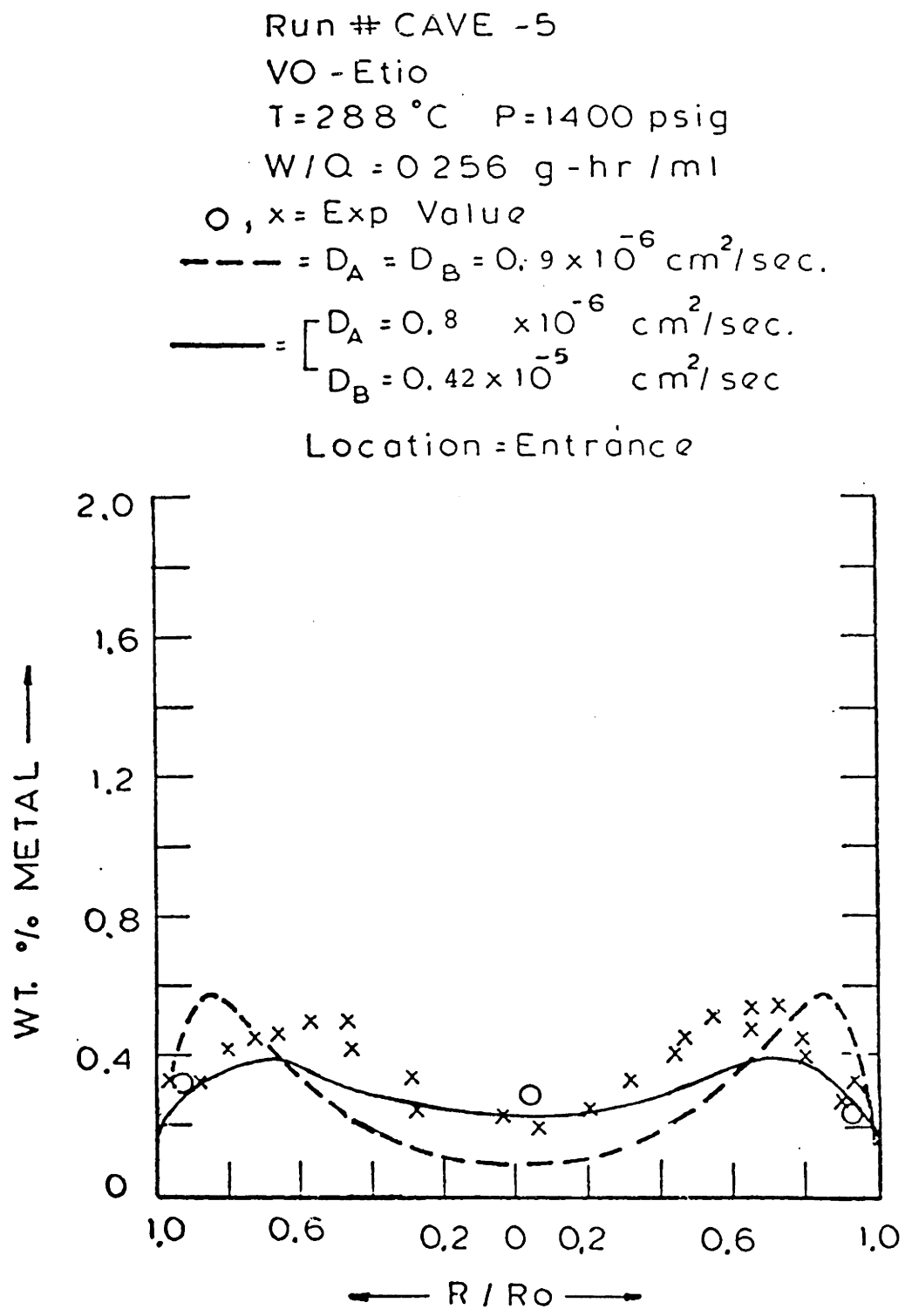

FIGURE V-5a: Vanadium Deposition Profile in the Catalyst

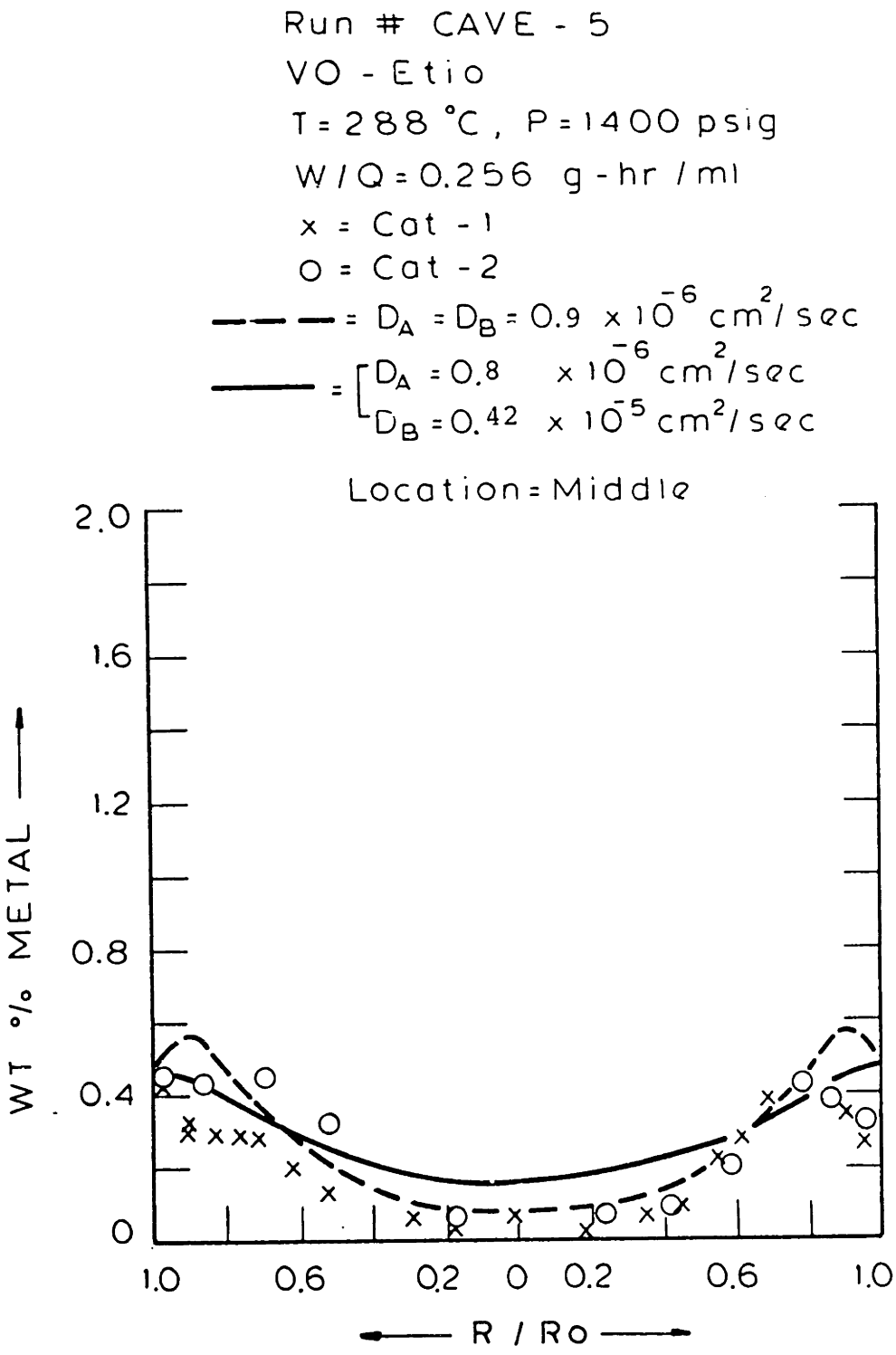

FIGURE V-5b: Vanadium Deposition Profile in the Catalyst

Run # CAVE - 5
VO - Etio
T = 288 °C , P = 1400 psig
W/Q = 0.256 g - hr / ml
x = Exp Value
--- = $D_A = D_B = 0.9 \times 10^{-6}$ cm²/sec.
——— = $D_A = 0.8 \times 10^{-6}$ cm²/sec.
$D_B = 0.42 \times 10^{-5}$ cm²/sec.

Location = Exit

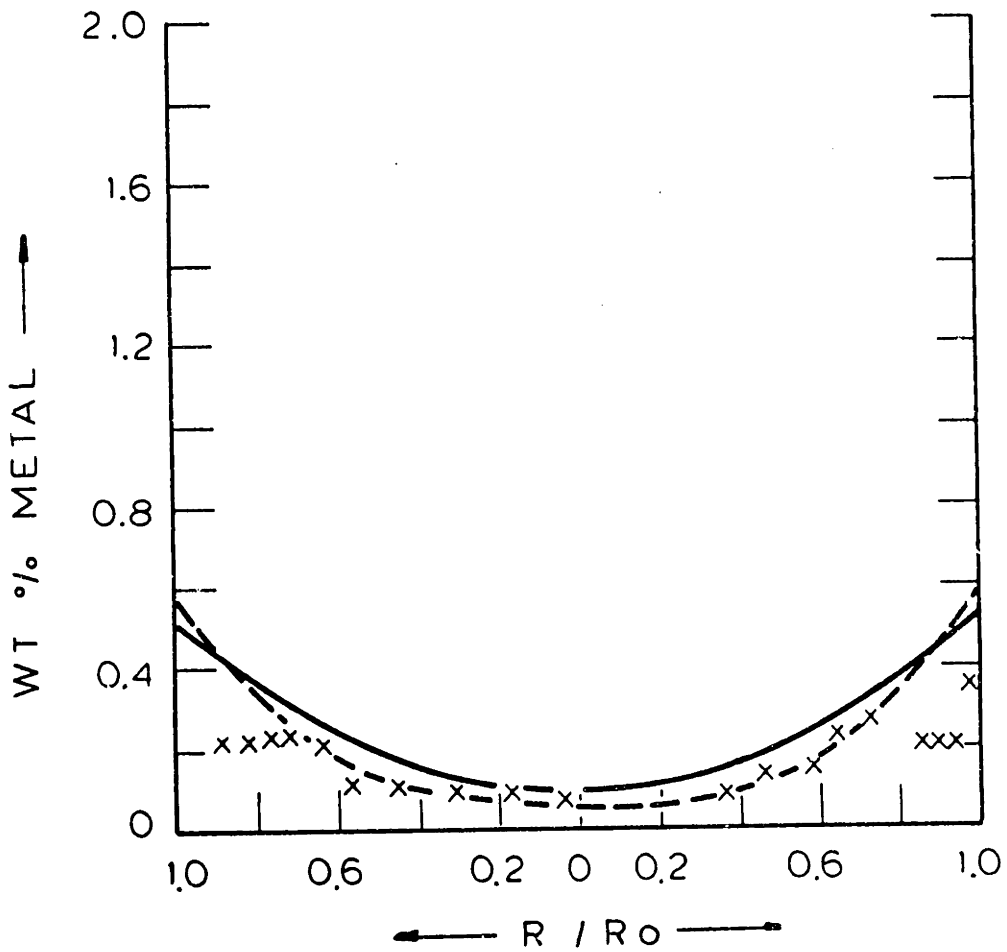

FIGURE V-5c: Vanadium Deposition Profile in the Catalyst

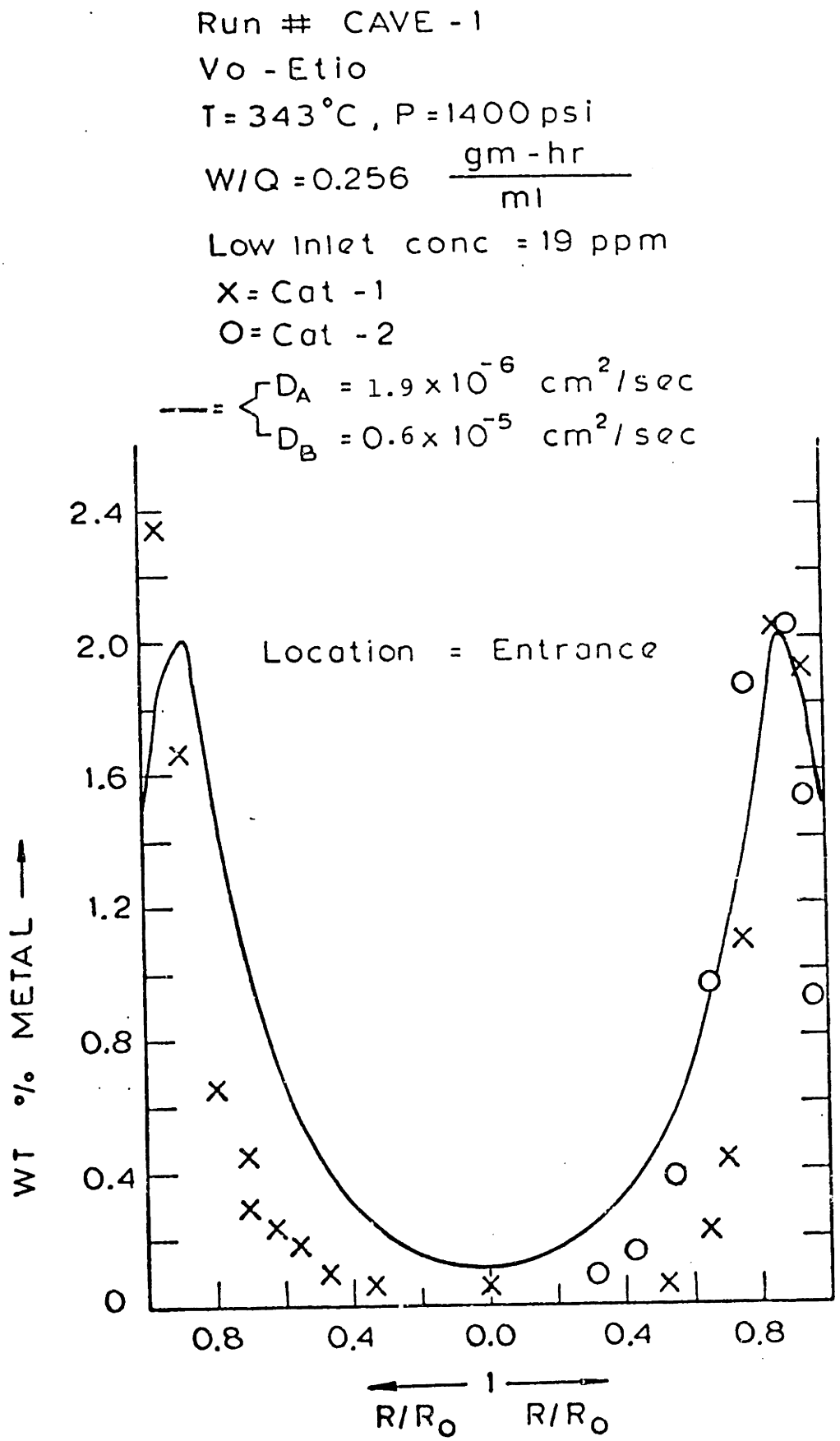

FIGURE V-6a: Vanadium Deposition Profile in the Catalyst

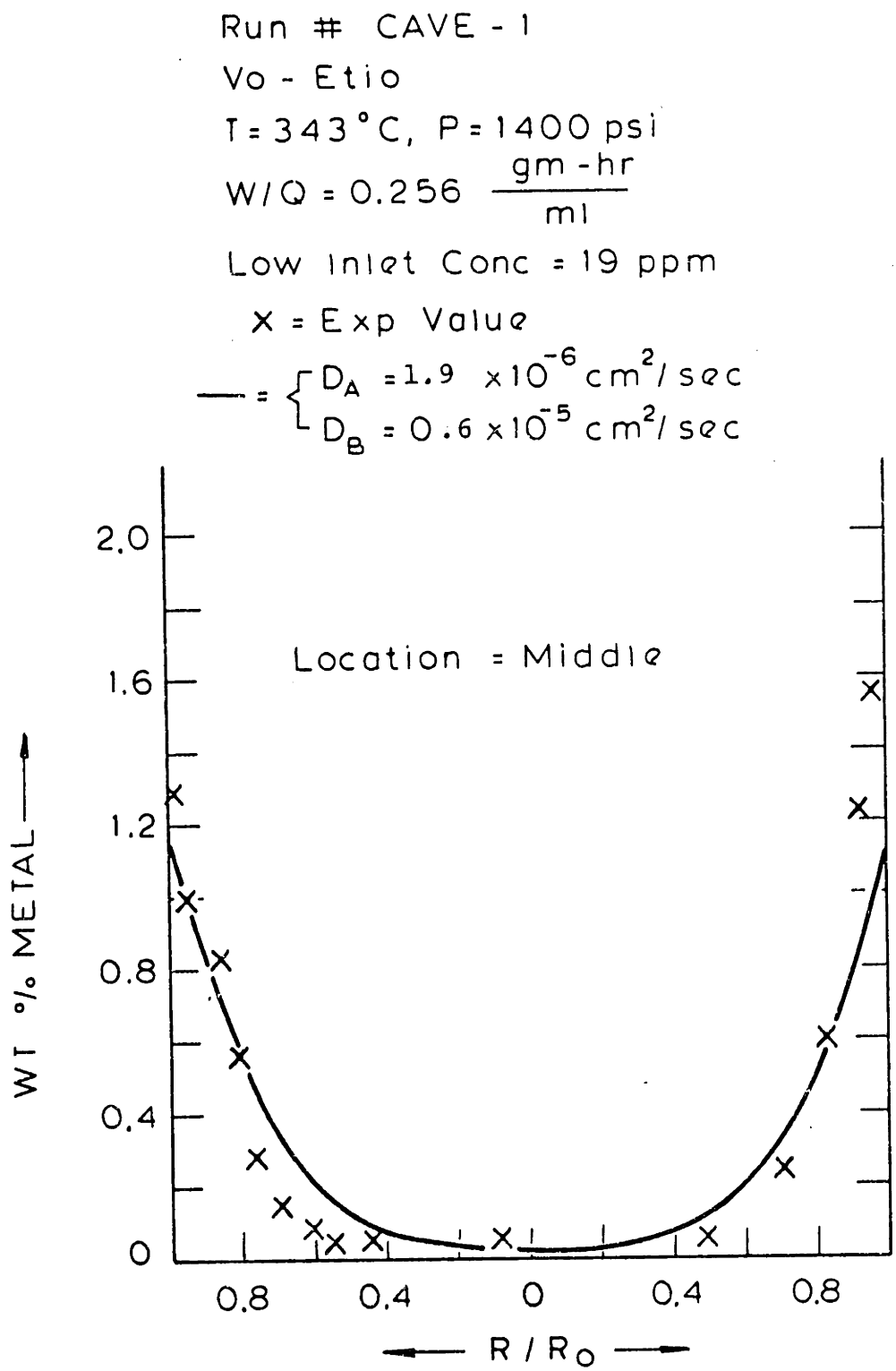

FIGURE V-6b: Vanadium Deposition Profile in the Catalyst

Run # CAVE -1
Vo - Etio
T=343°C, P=1400 psi
$W/Q = 0.256 \frac{gm-hr}{ml}$

Low Inlet Conc = 19 ppm
X = Exp. Value

$$\text{——} = \begin{cases} D_A = 1.9 \times 10^{-6} \text{ cm}^2/\text{sec} \\ D_B = 0.6 \times 10^{-5} \text{ cm}^2/\text{sec} \end{cases}$$

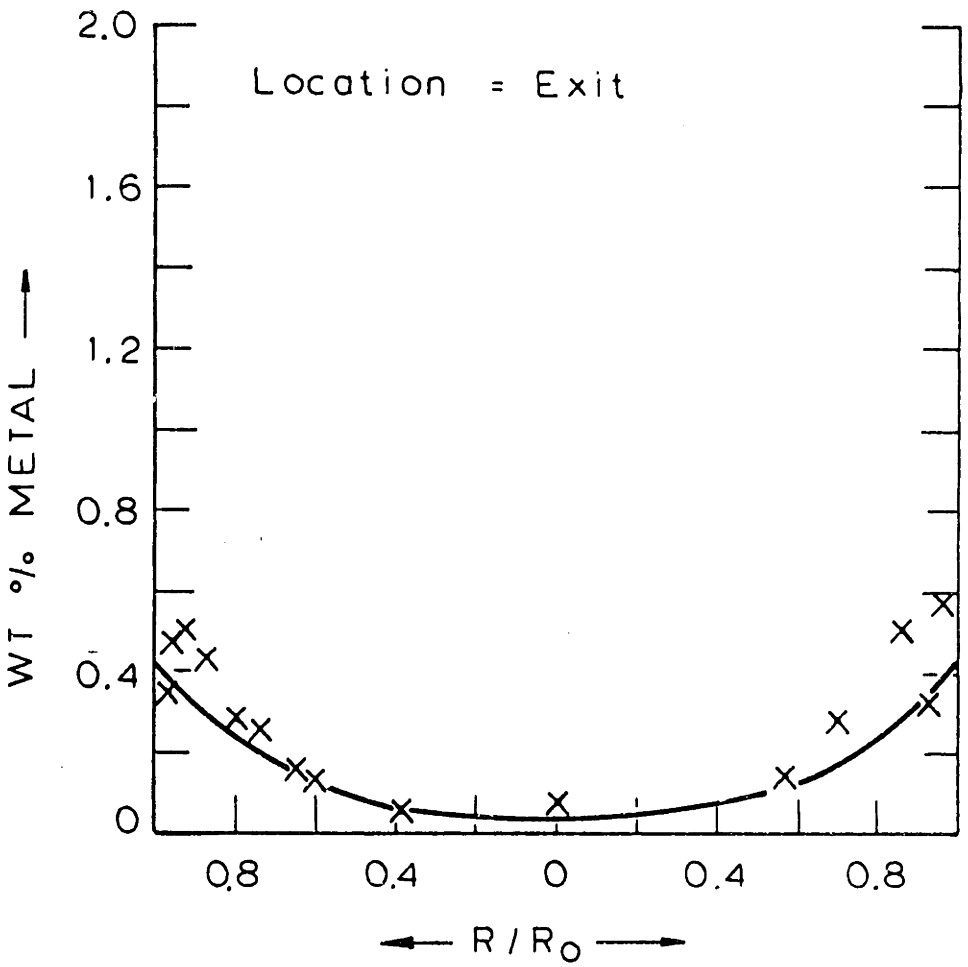

FIGURE V-6c: Vanadium Deposition Profile in the Catalyst

TABLE V-1

OPERATING CONDITIONS FOR THE FIGURES V-1 to V-8

Fig.#	T(^{o}C)	P(Psig)	Q (ml/hr)	W(g)	A_o	Compound	H*
V-1	343	1000	19.5	5.005	28.4	VO	0.40
V-2	343	1400	40.0	4.999	27.5	VO	0.40
V-3	343	1400	19.5	2.999	26.6	VO	0.50
V-4	315	1400	19.5	5.003	27.1	VO	0.46
V-5	288	1400	19.5	4.991	29.3	VO	0.40
V-6	343	1400	19.5	4.998	19.1	VO	0.49
V-7	343	1400	19.5	4.999	26.4	Ni	0.52
V-8	315	1400	19.5	4.998	27.2	Ni	0.57

W = Amount of catalyst in the reactor

A_o = Reactor inlet concentration of the model metal etioporphyrin in ppm.

* H = Fractional bed height from the entrance for the location of the middle catalyst.

In figures:

a = Entrance of bed.

b = middle of bed.

c = exit of bed.

At the entrance of the bed, the location of the internal maxima inside the catalyst depends on the temperature and the pressure of the operation. Low temperature and low hydrogen pressure lead to inward movement of the maxima. The decrease in the hydrogen pressure moves the internal maxima more to the inside of the catalyst. This is observed by comparing the fig. V-1a which is for 1000 psig with the figures V-2a and V-3a which are for 1400 psig. Figures V-2a, V-4a and V-5a are at the temperature of 343^{o}C, 315^{o}C and 288^{o}C respectively and it is observed that the decrease in the operating temperature also moves the location of the internal maxima further inside the catalyst.

For the run in figures V-3a, b and c the bed height was kept same as in the other runs but the ratio of the volume of the inert to that of the catalyst was 4.8 instead of 2.5 used in all other runs. This run was made to study the effect of the inert volume on the reactor performance. In the run of figures V-6a, b, and c the inlet solution concentration was 19 ppm instead of about 28 ppm used in all other runs. This run was done to study the effect of the inlet concentration on the metal deposition profiles inside the catalyst. In the next section the effect of these variables are discussed with respect to the theoretical calculations.

Results similar to the vanadium are also observed for nickel. The results for the two operating temperatures of 343^{o}C and 315^{o}C and the same pressure of 1400 psig are plotted in figures V-7 and V-8.

Run # CANE -4
NI-Etio
T=343°C, P=1400 psi
$W/Q = 0.256 \frac{gm-hr}{ml}$

O, Δ = Exp Value on two Catalyst
—— = $D_A = D_B = 1.1 \times 10^{-6} cm^2/sec$

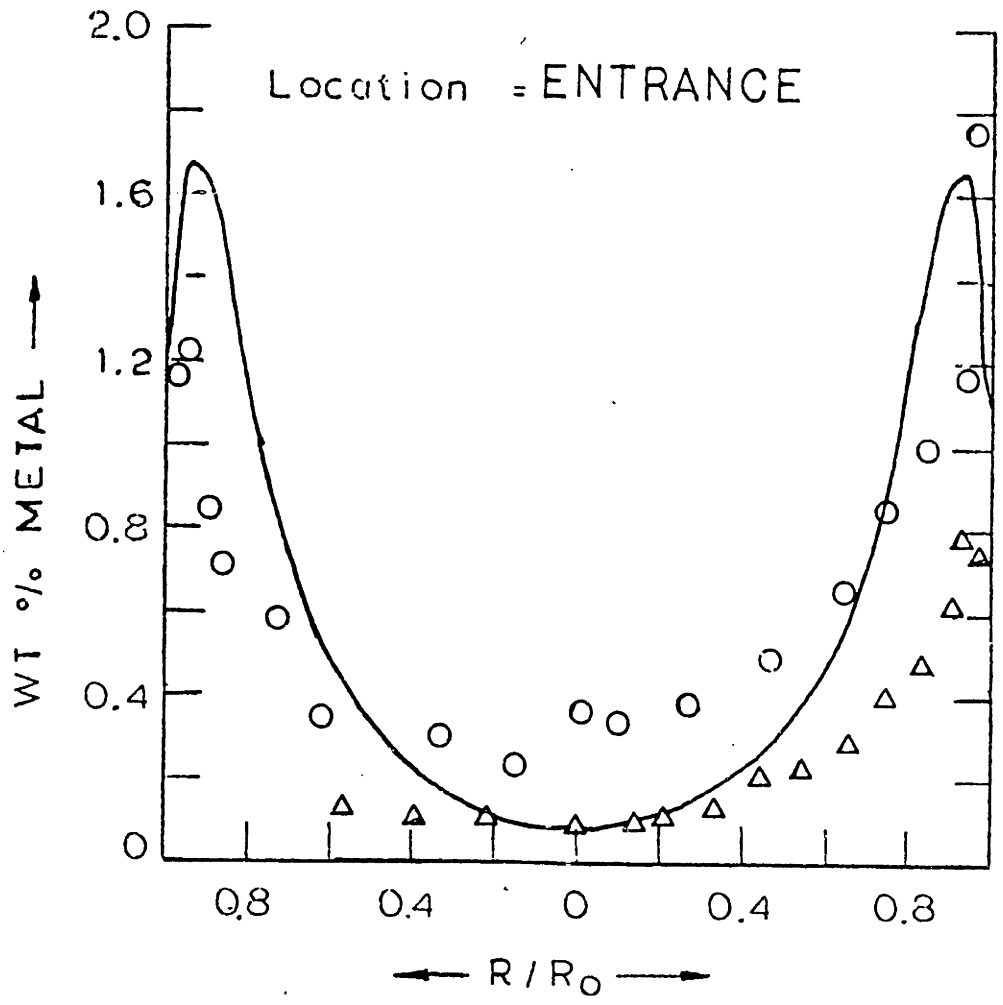

FIGURE V-7a: Nickel Deposition Profile in the Catalyst

Run # CANE -4
Ni-Etio
T=343°C, P=1400 psi
$W/Q = 0.256 \frac{gm-hr}{ml}$

O = Exp Value
—— = $D_A = D_B = 1.1 \times 10^{-6} cm^2/sec$

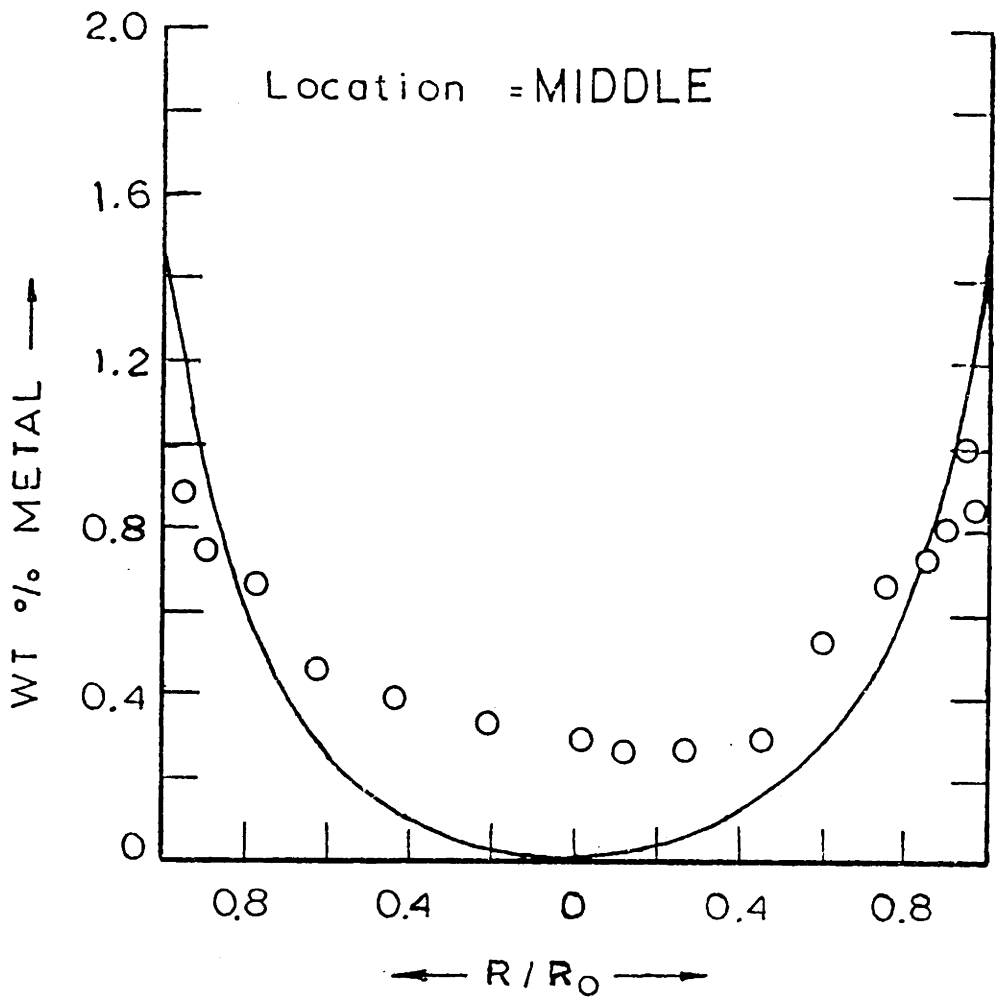

FIGURE V-7b: Nickel Deposition Profile in the Catalyst

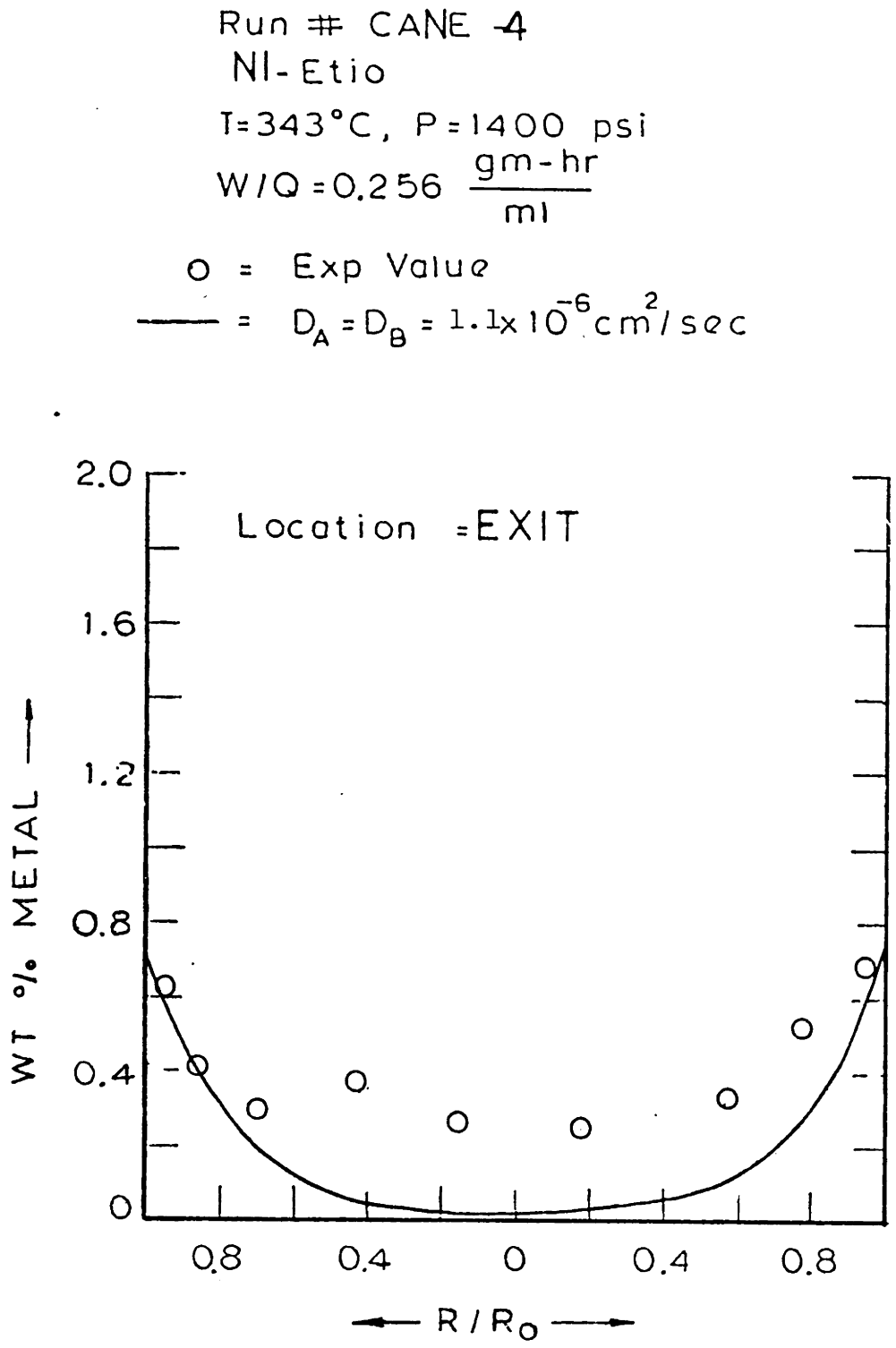

FIGURE V-7c: Nickel Deposition Profile in the Catalyst

Run # CANE - 8
NI - Etio
T=315 °C, P=1400 psi
W/Q = 0.256 $\frac{gm-hr}{ml}$

o = Exp Value
—— = $D_A = D_B = 2.5 \times 10^{-6} cm^2/sec$

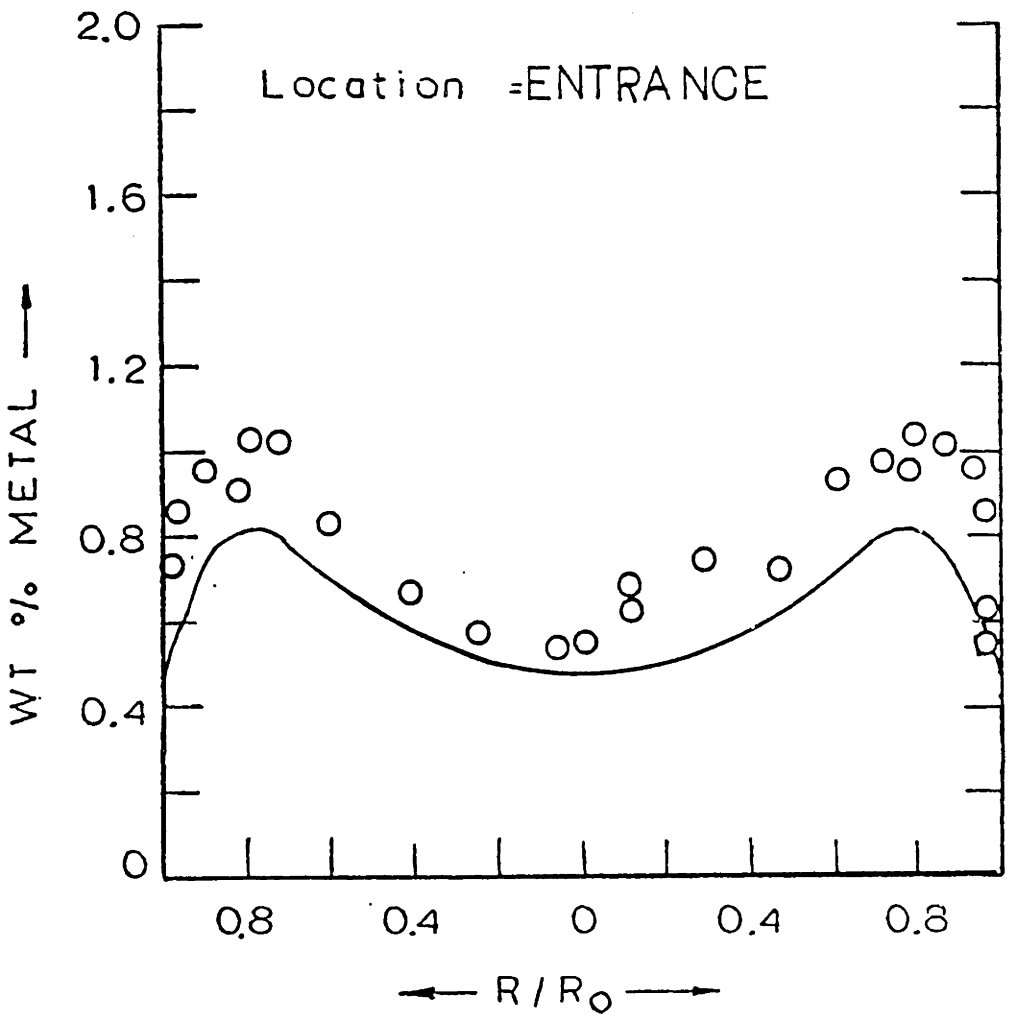

FIGURE V-8a: Nickel Deposition Profile in the Catalyst

Run # CANE - 8
NI - Etio
T = 315°C, P = 1400 psi
$W/Q = 0.256 \frac{gm-hr}{ml}$

O = Exp Value
—— = $D_A = D_B = 2.5 \times 10^{-6} cm^2/sec$

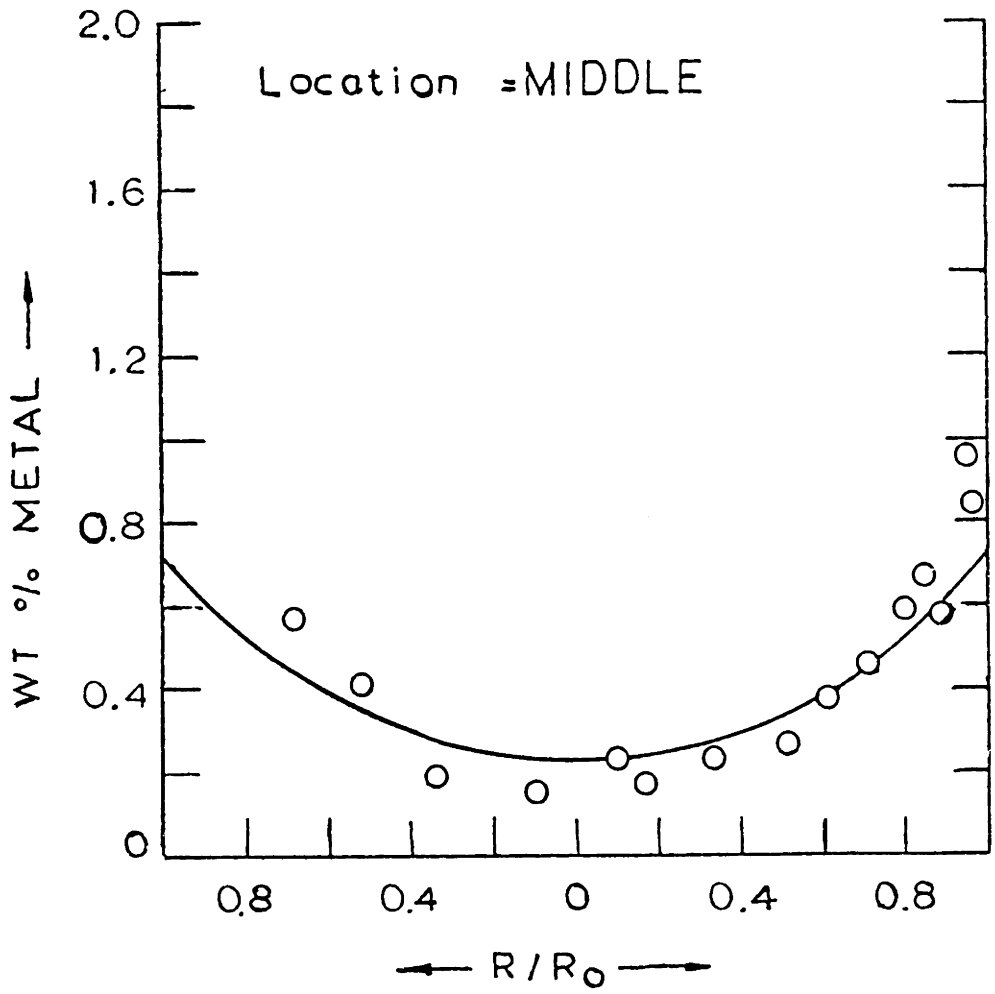

FIGURE V-8b: Nickel Deposition Profile in the Catalyst

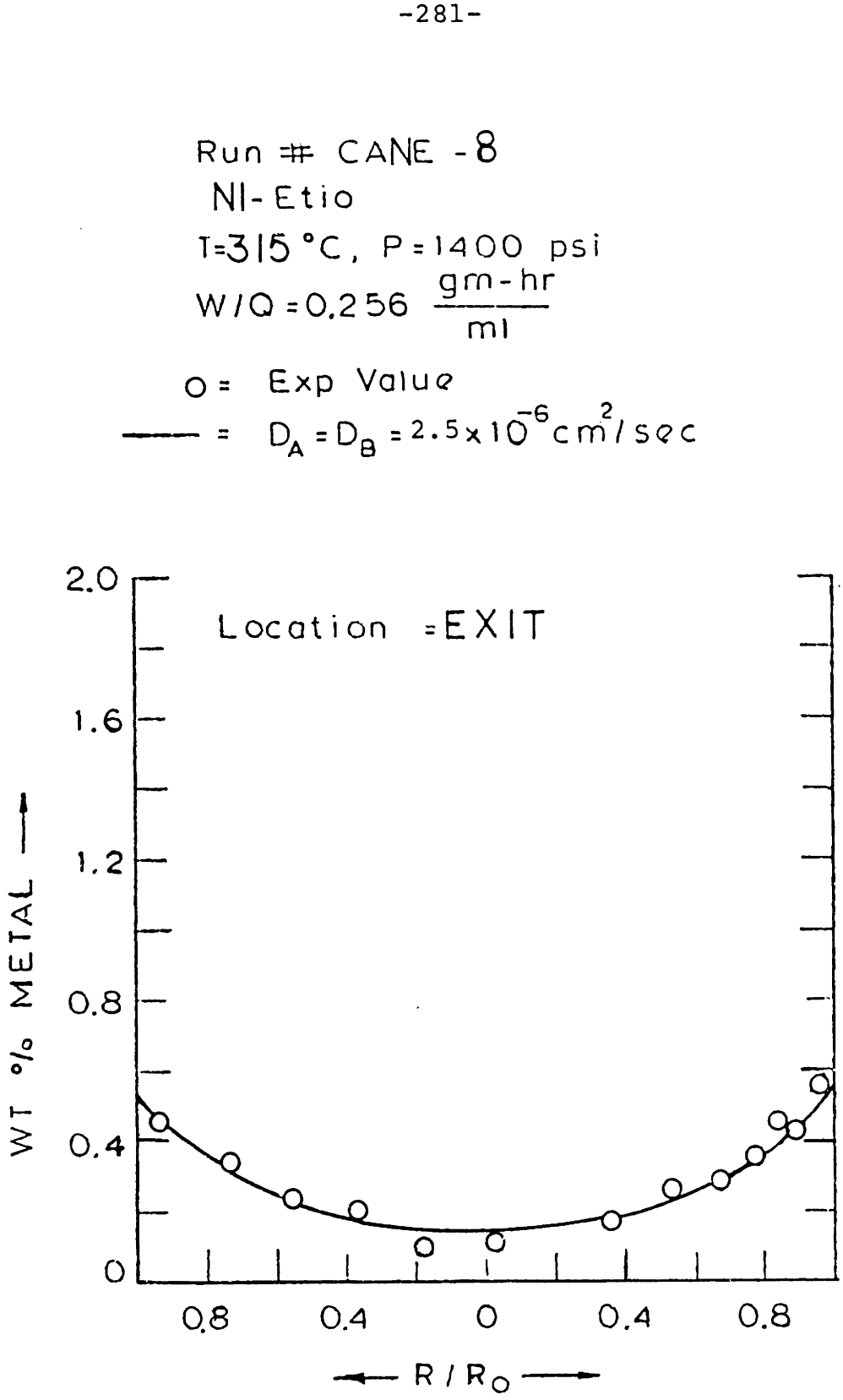

FIGURE V-8c: Nickel Deposition Profile in the Catalyst

One basic draw back in all the runs is the low metal loading on the catalyst. Because of the low metal content the error in the curves shown in figures V-1 to V-8 are fairly large. The magnitude of the error for vanadium can be seen from the curves in figures V-1a and V-2b and for the nickel from figure V-7a. The larger error for the nickel is due to the scanning electron x-ray microanalyzer. The machine is much more sensitive to the vanadium than to the nickel. Even when the same spot on the catalyst surface is analysed in succession for a couple of times, the variation in the vanadium readings is $\pm$ 0.07 wt % whereas for the nickel it is as high as $\pm$ 0.13 wt %. Therefore the magnitude of the error involved near the center of the catalyst, due to the low metal loadings, is fairly high.

The second kind of the error involved in our results is due to the sampling procedures of the catalyst from the reactor bed. Since the metal porphyrins are expensive, we were forced to use low flow rates and the smaller catalyst bed heights. The catalyst bed height depends on the fact that at reasonable flow rates we do not want 100% conversion but some reasonable value so that the reactor outlet solution concentration may be monitored reasonably. Low flow rates are desirable because for the same amount of solution the reactor is on stream for a longer time and hence more metal deposition on each catalyst. Thus the height of the catalyst bed used in our study was about 10 cm. Since the average length of the catalyst extrudate used is about 6 mm, the

problem of the exact location of the catalyst sample in the bed is clear. From each location in the bed about seven to eight catalyst extrudates were collected for the analysis. This will also explain for some of the scatter in the figures V-1a, V-2b and V-7a.

The best way to analyze the samples would be to analyze for the metal deposition at more than one axial position in the same catalyst extrudate and also on more than one catalyst at the same location of the bed and then take the statistical mean of all the readings. However, the cost and the time involved in the analysis prohibit such an elaborate procedure. Therefore, in most cases only one catalyst extrudate at the center of its axial position was scanned. But to get the feel of the error involved in such an analytical produre, sometimes more than one catalyst and at the various axial positions were scanned. The general magnitude of the error involved is shown in figures V-1a and V-2b.

For the analysis of the carbon, hydrogen, nitrogen and nickel on the used catalyst, some of the used samples from the nickel runs were sent to Galbraith Laboratories (Knoxvill, Tennessee). The size of the samples required for this analysis are fairly large, and therefore the exact location of the samples in the bed is not known. Within each sample collected, from one catalyst particle to the other, there is a variation in the concentration of the above species. As a result, no conclusion regarding the variation of the concentrations of the above elements with respect to

the bed location could be made. This difficulty is further compounded with the low magnitudes involved. On the average the nitrogen and carbon content of the catalyst seem to be functions of temperature, whereas hydrogen content is not. At 1400 psig, the % C and % N at 343°C are 1.56±0.39 and 0.33±0.05 and at 315°C are 2.49±0.54 and 0.41±0.04 respectively. Whereas % hydrogen at both the temperatures is 0.78±0.09. The metal deposition values agree with those found by the scanning electron X-ray microanalyzer.

B. THEORETICAL MODELLING: In order to develop the mathematical equations, which would predict the performance of the reactor, the following main assumptions are invoked:

a) There are no axial and radial dispersion effects.

b) The interphase resistance between the catalyst particle and the solution is negligible.

c) The end effects in the catalyst particle can be neglected. This assumption would allow the treatment of the catalyst particle as an infinitely long cylinder.

d) The diffusivities of A and B inside the catalyst do not change with time. For our runs the metal loadings on the catalyst particles are not large and the assumption is justified. If the metal loadings were large, then the use of configurational diffusivities as function of loading have to be made.

Assumptions a) and b) are justified in appendix-I and simplify the equations a great deal.

First we will develop the equations for the flux and the concentration profiles inside a catalyst particle for an arbitrary surface concentrations. Then these equations will be integrated over the total bed height to give the exit stream concentrations as a function of the inlet concentrations. The method used for solving the equations has been described in the classical treatment by Wei (1962 - a,b).

From the Fick's law, the steady state diffusion with the hydrodemetallation reactions inside an infinite cylinder can be described by the following equations:

$$-\frac{D_A}{\rho_c} \nabla^2 a = -k_1 a + k_2 b \qquad \text{V.1}$$

$$-\frac{D_B}{\rho_c} \nabla^2 b = k_1 a - k_2 b - k_3 b \qquad \text{V.2}$$

where ∇^2 is the Laplace operator for the cylinderical coordinates. a and b are the concentrations of A and B inside the catalyst particle respectively. The concentration is in parts per million of metal by weight in the solution. In the above equations the units of the rate constants are ml of solution/gm of cat.-hr, whereas on the right hand sides of the equations we need the rate constants as gm of solution/volume of cat.-hr. Therefore the actual rate constants used should be $\rho\rho_c k$; where ρ is the density of the solution, ρ_c is the density of the catalyst and k is in ml of solution/gm of cat.-hr. Since the density of the solution also appears on the left hand side of the equation, it cancels away. But

catalyst density term remains and appears in the denominator of the left hand side of the above equation. The diffusion coefficients are in cm^2/sec. The value of the catalyst density used is 1.49 g/ml.

The boundary conditions for the equations V.1 and V.2 are:

$$\text{at } r = 0, \quad \frac{\partial a}{\partial r} = \frac{\partial b}{\partial r} = 0 \qquad \text{V.3}$$

$$\text{at } r = R_c, \; a = A_s \; , \; b = B_s \qquad \text{V.4}$$

where A_s and B_s are the concentrations in the solution at the outersurface of the catalyst. The solutions of the above set of equations are given by:

$$a = d_1 I_1 - \frac{e_6}{e_3} d_2 I_2 \qquad \text{V.5}$$

$$b = \frac{e_6}{e_2} d_1 I_1 + d_2 I_2 \qquad \text{V.6}$$

where:

$$e_1 = \frac{k_1 \rho_c}{D_A}$$

$$e_2 = \frac{k_2 \rho_c}{D_A} \qquad \text{V.7}$$

$$e_3 = \frac{k_1 \rho_c}{D_B}$$

$$e_4 = \frac{(k_2 + k_3)\rho_c}{D_B}$$

$$\lambda_1, \lambda_2 = 0.5 \left(e_5 \pm \sqrt{e_5^2 - 4 (e_1 e_4 - e_2 e_3)}\right) \qquad V.8$$

$$e_5 = e_1 + e_4$$

$$e_6 = e_1 - \lambda_1$$

$$d_1 = d_i (e_2 e_3 A_s + e_2 e_6 B_s) \qquad V.9$$

$$d_2 = d_i (e_2 e_3 B_s - e_3 e_6 A_s) \qquad V.10$$

$$d_i = 1/(e_2 e_3 + e_6^2)$$

$$I_1 = I (r\sqrt{\lambda_1}) \qquad V.11$$

$$I_2 = I (r\sqrt{\lambda_2}) \qquad V.12$$

I(x) is the modified Bessel function of the first kind of order zero and is given by:

$$I(x) = \sum_{j=0}^{\infty} \frac{x^{2j}}{2^{2j}\, j!\, j!} \qquad V.13$$

Once the concentration profiles inside the catalyst are known, the flux per unit mass of the catalyst can be easily calculated from the following equations:

$$f_A = \rho d_A \left.\frac{\partial a}{\partial r}\right|_{r=R_c} \qquad V.14$$

$$f_B = \rho d_B \left.\frac{\partial b}{\partial r}\right|_{r=R_c} \qquad V.15$$

where

$$d_A = \frac{2D_A}{R_c \rho_c}$$

$$d_B = \frac{2D_B}{R_c \rho_c} \qquad V.16$$

The derivatives of the concentration are calculated from the equations V.5 and V.6 and are substituted into equations V.14 and V.15 to give:

$$f_A = \rho \left[(k_1^+ + k_4^+)\ A_s + k_2^+\ B_s \right] \qquad V.17$$

$$f_B = \rho \left[k_1^+\ A_s + (k_2^+ + k_3^+)\ B_s \right] \qquad V.18$$

where:

$$k_1^+ + k_4^+ = d_A d_i e_3 (e_2 d_7 - e_6\ d_{10})$$

$$k_2^+ = d_A d_i e_2 \ (e_3 d_{10} + e_6 d_7)$$

$$k_1^+ = d_B d_i e_3 \ (e_2 \ d_9 - e_6 \ d_8)$$

$$k_2^+ + k_3^+ = d_B d_i e_2 \ (e_3 d_8 + e_6 \ d_9)$$

$$d_7 = \frac{1}{I(R_c\sqrt{\lambda_1})} \cdot \left.\frac{\partial I_1}{\partial r}\right|_{r=R_c}$$

$$d_8 = \frac{1}{I(R_c\sqrt{\lambda_2})} \cdot \left.\frac{\partial I_2}{\partial r}\right|_{r=R_c}$$

$$d_9 = (e_6 d_7)/e_2$$

$$d_{10} = - \ (e_6 d_8)/e_3$$

and I_1 and I_2 are given by equations V.11 and V.12 . In equations V.17 and V.18, the parameters k_1^+, k_2^+, k_3^+ and k_4^+ are just the functions of the kinetic rate constants, radius and the density of the catalyst and the diffusivities; and are called diffusion disguised rate parameters. Therefore, if the diffusivities are known, then for the given solution concentrations the flux per unit mass of the catalyst can be easily calculated. Now with the help of equations V.17 and V.18, the mass conservation equations along the length of the reactor can be written. The mass balance over the differential section of the bed gives:

$$-Q \frac{dA_s}{dW} = (k_1^+ + k_4^+)A_s + k_2^+ B_s \qquad V.19$$

$$-Q \frac{dB_s}{dW} = k_1^+ A_s + (k_2^+ + k_3^+) B_s \qquad V.20$$

where dW is the weight of the catalyst in the differential length of the bed. Since in our runs only pure A enters the reactor, the initial conditions for the above two equations are:

$$\text{at } W=0,\ A_s = A_0\ ,\ B_s = 0 \qquad V.21$$

The above set of equations are similar to the equations used in the kinetics calculations and are solved by the method outlined in Appendix-II.

Thus now we have the set of governing equations for the reactor. The kinetic rate constants have already been determined in the chapter IV and the only unknowns are the diffusivities.

In the early phase of the research an attempt to measure the diffusivities of VO and Ni Etioporphyrins was made. It was thought that at sufficient low temperatures of about 60 - 200^{o}C and in the absence of hydrogen the diffusivity could be measured. If the diffusivities at various low temperatures were known, the one at the reactor temperature could be calculated by some extrapolation correlations. Various techniques with the required modifications were used (Komiyama and Smith - 1974, Satterfield et

al. - 1973 and Weisz - 1966). In all these techniques it is necessary to know the equilibrium adsorption isotherm. Unfortunately it was found that even at the low temperature of 60°C, the catalyst when left in the metal solution, kept adsorbing and did not attain the equilibrium. It was found that the chloroform extract of the used catalyst showed new peaks in the visible spectrum range. Thus there is a chemical reaction going on the catalyst surface and what one has is the chemisorption on the surface. In order to uncouple the diffusion effect it is necessary to know the rate of the reaction on the surface. Finding the rate and then the diffusivity reduces the nature of the problem to the same as our HDM reactor problem. Moreover, we do not have pure reaction intermediate with us, and in order to predict the reactor performance it is necessary to know its diffusivity. Due to all these problems and the uncertainities involved this project was abandoned.

In fact we can get the values of the diffusivities from the equations V.19 - V.21 and the experimental values of solution concentrations at the inlet and the outlet of the reactor. The amount of the catalyst in the reactor is known, therefore for a given inlet solution concentration the values of D_A and D_B are adjusted so that the outlet concentrations calculated from equations V.19 - V.21 match with the experimental values. If the model derived above is taken to be true, then the values of the diffusivities calculated would be very reliable. It is so because we

have used the bulk solution concentrations which are analytically very reliable.

However, it would be good to have at least the order of magnitude of the diffusivities from an independent source. The diameter of the metallo-porphyrins are about 14.2 Å. In appendix-I, from Stokes-Einstein equation it is estimated that the bulk diffusivity of a molecule of diameter 14.2 Å in Nujol at 315°C is 10^{-4} cm^2/sec. To estimate the effective diffusivity in the catalyst, the configurational correction of Spry and Sawyer (1975) along with the tortuosity factor of 8 suggested by Shah and Paraskos (1975) is used. Catalyst porosity and void fraction are used from Table III-1. The effective diffusivity thus calculated is $2.5X10^{-6}$ cm^2/sec.

The critical test of the above set of the equations depend on the prediction of the metal deposition profiles inside the catalyst at various bed locations. Once the diffusion coefficients are known, then from equations V.19 - V.21 the concentration of B in the solution phase at any point in the reactor can be calculated. This value of B along with the equation V.6 would give the concentration profile of B in the catalyst and therefore in time T the metal deposition profile is given by

$$m_d = (k_3 b T \rho) 10^{-4} \qquad V.22$$

The calculated metal deposition profiles can be compared with the experimental profiles. The net weight average metal deposited in the catalyst can be calculated from the equation:

$$\bar{m}_d = \frac{2 \int_0^{R_c} m_d \, r \, dr}{R_c^2} \qquad V.23$$

A computer program to do all the pertinent calculations is given in Appendix IV. Now we will compare the theoretical calculation results with the experimental ones.

B.1. VANADYL ETIOPORPHYRIN-I: As a first step to calculate diffusivities D_A and D_B, it was assumed that at the reaction temperatures the diffusivities of the vanadyl Etioporphyrin-I and the reaction intermediate are equal. A value of the diffusivity was guessed, and the corresponding diffusion disguised rate parameters were calculated. With these values of the parameters, the reactor exit solution concentration were calculated by the use of equations V.19 - V.21. If the calculated concentrations matched with the experimental values, the guessed value was accepted as the desired values of the diffusivities. If the two did not agree, then the calculation cycle was repeated with a new guessed value. It is found that with the assumption of equal diffusivities, there is no single value of the diffusion coefficient which would simultaneously match both the total metal concentration and the

reaction intermediate concentration in the outlet solution of the reactor. When the total metal concentrations are matched, it is found that for all the vanadium runs the calculated concentrations of the reaction intermediate are higher than the experimental values. The experimental and the calculated values of the outlet solution concentrations are summarized for some of the runs in Table V-2. It is seen that with the assumption of equal diffusivities, calculated concentrations of the B are on the average 50% higher than the experimental values.

As a next step, the assumption of the equal diffusivities is relaxed. A remarkable agreement for both the total vanadium and the reaction intermediate concentrations were obtained. However, the values of the diffusion coefficients so obtained were not accepted as the real values of the diffusion coefficient. Instead a range of the diffusion coefficients which would give the outlet total metal concentrations within ± 2 ppm were accepted. In this range, the maximum variation in the values of the diffusivities is 40%. It should be pointed out that the error in the analysis of the vanadium in the solution by atomic absorption can be easily as large as 1.5 ppm. As a next step, from this range of the diffusivities, some were tried to match the location and the magnitude of the internal maxima in the metal deposition profile of the catalyst at the entrance of the reactor bed, and the ones which gave the best agreement were accepted as the desired values of the

TABLE V-2

COMPARISON OF THE EXPERIMENTAL AND THE CALCULATED REACTOR OUTLET SOLUTION CONCENTRATIONS FOR VANADIUM RUNS

Run #	Experimental		Calculated			
			Equal Diffusivity		Unequal Diffusivity	
	M	B	M	B	M	B
CAVE-3	10.8	1.62	9.2	2.63	10.5	1.75
CAVE-4	6.5	1.05	5.9	1.55	5.0	1.04
CAVE-5	16.8	2.82	16.8	4.04	16.5	3.45
CAVE-6	8.4	1.16	7.1	1.76	5.7	1.11
CAVE-7	9.6	1.5	9.6	2.26	8.0	1.45

M = Total metal concentration. It is the sum of the vanadyl etio and the reaction intermediate concentrations (in ppm).

B = Reaction intermediate concentration (in ppm).

diffusivities. Looking at the magnitude of the error involved in the analysis of the total vanadium concentration in the reactor outlet solution, this method of the search of the diffusion coefficients is justified.

It turns out that the diffusion coefficients for the reaction intermediate B are higher than that of VO-Etio porphyrin. Once again the calculated values of the reactor outlet solution concentrations are listed in Table V-2. A good agreement for both the total vanadium and the intermediate concentrations is obtained.

The calculated values of the diffusion coefficients for the various vanadium runs are tabulatd in Table V-3. From this table we can quickly draw the following observations:

(a) We have earlier estimated theoretically that the diffusion coefficient for the metal etioporphyrin in Nujol at 315^{o}C is 2.5X10^{-6} cm^{2}/sec. The calculated values are of the same order of magnitude as the estimated values. This is an encouraging result.

(b) The values of the diffusivities do increase with the increase of temperature and are independent of the operating pressure. This is again in agreement with the expected trend for the diffusions in the liquid phase.

(c) For a given temperature the variation in the other operating parameters does not change the value of the diffusion coefficient. (i) As compared to runs CAVE-2, CAVE-4, CAVE-6 and CAVE-7 the reactor inlet concentration for the run CAVE-1 is lower, (ii) The LHSV for run

TABLE V-3

CALCULATED DIFFUSIVITIES FOR THE VARIOUS VANADIUM RUNS

Run #	T	P	Q	W	A_o	$D_A = D_B$ $D_A X 10^6$	$D_A \neq D_B$ $D_A X 10^6$	$D_B X 10^6$
CAVE-1	343	1400	19.5	4.998	19.1	1.6	1.9	6.0
CAVE-2	343	1400	19.5	4.997	25.7	1.6	1.9	6.0
CAVE-3	315	1400	19.5	5.003	27.1	1.2	0.9	4.5
CAVE-4	343	1000	19.5	5.005	28.4	1.6	1.8	6.0
CAVE-5	288	1400	19.5	4.991	29.3	0.9	0.8	4.2
CAVE-6	343	1400	19.5	2.999	26.6	1.6	1.9	6.0
CAVE-7	343	1400	40	4.999	27.5	1.6	1.9	7.0

Units of diffusion coefficient are cm^2/sec.

T = Temperature in ^oC

P = Pressure in psig

Q = Flow rate of solution in ml/hr.

W = Amount of catalyst in reactor (gms)

A_o = Inlet concentration of vanadyl etioporphyrin (ppm)

Inlet concentration of B is zero

CAVE-7 is higher than runs CAVE-1, CAVE-2, CAVE-4 and CAVE-6, (iii) Even though by the help of inerts the total volume of the reactor is kept constant, run CAVE-6 has only 3/5 catalyst of the runs CAVE-1, CAVE-2, CAVE-4 and CAVE-7, (IV) The operating pressure for the run CAVE-4 is lower than the runs CAVE-1, CAVE-2, CAVE-6 and CAVE-7. The same value of the diffusivities from the various runs is very encouraging.

(d) For unequal diffusivities of A and B, the relative ratio of D_B to D_A is about 3 to 5. It is not exactly clear why the diffusion coefficient for the reactor intermediate should be so much higher than the VO-Etioporphyrin. We know that the VO-Etioporphyrin is strongly adsorbed on the catalyst surface, but it may be that chlorins are not strongly adsorbed on the surface and instead diffuse on the surface. In the separation technique of section III.I., it was found that while the VO-Etioporphyrin adsorbs as a thin ring at the entrance of the alumina bed, the reaction intermediate travelled far down in the column. Therefore it is possible that even under reaction conditions the adsorption of the reaction intermediate is less than that of the VO-Etioporphyrin. For the surface diffusion to be significant, the adsorption on the surface should be strong but not too strong so as to immobilize the molecules on the surface. Since Nujol is not a very good solvent for the VO-Etioporphyrin, it is adsorbed

strongly on the surface and it may be that the hydrogenated product of the VO-Etio has just the right range of adsorptivity.

It is possible to have surface diffusion contribution in the liquid filled pores to be 3 to 5 times higher than the pore volume diffusion contribution. Komiyama and Smith (1974) studied the diffusion of benzaldehyde in hydrophobic polymeric porous amberlite particles and found that for water as the solvent, the surface diffusion flux was about 5 to 14 times the pore volume diffusion flux.

Once the values of the diffusion coefficients have been calculated, the next test of the model is to predict the metal deposition profiles inside the catalyst extrudates of various catalyst bed locations. It should be pointed out that most of the runs were made for 70 - 100 hours and as is seen from the figures IV-1 and IV-3 the transient activity of the catalyst lasts for about 25 - 40 hours. Since we are using the steady state kinetics, therefore even though the values of the diffusion coefficients calculated might be accurate, one might not get a good agreement between the calculated and the experimental metal deposition profiles. At the entrance of the bed the concentration of the metal in the solution is the highest and the effect of the initial transient period on the metal profiles would be most pronounced. Due to the slow kinetics in the transient period, a significant portion of the VO-Etio would be adsorbed at the entrance of the bed and metal would deposit more inside the

catalyst than it would under the steady state activity, and also the location of the internal maxima will be more towards the center of the catalyst. However, it should be pointed out that during the total transient period of the catalyst, at 315 and 343^{o}C, the net vanadium deposited is not much different from what it would have been under steady state.

Inspite of all the uncertainities involved due to the sampling and analytical techniques and also due to the short time durations of the runs, the agreement between the calculated and experimental profiles are fairly good. The calculated profiles are also plotted in figures V-1 to V-6. These profiles are calculated by the use of equations V.19 - V.21, V.6 and then V.22. The dotted curves are the result of the assumption of equal diffusion coefficients while the continuous curves are obtained by the relaxation of this assumption. Just like the concentrations of the metal in the exit stream, the unequal diffusivities calculations give better agreement with the experimental metal deposition profiles.

As seen from the figures V-1a, V-2a, V-3a, V-4a and V-5a, at the entrance of the reactor, the assumption of the equal diffusivities gives much higher internal peak which is more nearer to the edge of the catalyst and also the lower metal deposition at the center of the catalyst. This trend of higher metal deposition at the edge and the lower depositions near the center of the catalyst continues over the whole reactor bed. This later statement is readily observed in any of the figures V-1 to V-5.

At the entrance of the bed, the assumption of the unequal diffusivities improves the agreement between the calculated and the experimental values. This can be observed from the 'a' series of the figures V-1 to V-6. However, the effect is more dramatic at the other catalyst bed locations. As seen from the 'b' and 'c' series of the figures V-1 to V-6, with in the error limits, the agreement between the calculated and the experimental metal deposition profiles is remarkably good.

In conjunction with the value of diffusivities of the Table V-2, it was discussed that the model withstood the test of the change in the various operating parameters. Similiarly we again find that for the changes in the (i) inlet solution concentration, (ii) LHSV, (iii) catalyst to inert ratio and (IV) the operating pressure, the calculated and the experimental profiles agree well.

Good agreements have been obtained for the temperatures of 343^{o}C and 315^{o}C. However it is seen from the figures V-5 that the agreement between the calculated and the experimental values of 288^{o}C is not very good. A similar observation with respect to the concentration of B in the exit stream, for the run CAVE-5 in Table V-2, is made. The outlet solution concentration with respect to the time on stream, for the temperatures of 343, 315 and 288^{o}C are plotted in figure V-9. These curves are similar to those in figures IV-1 and IV-3. It is observed that at 288^{o}C the reactor performance shows some scatter and it is not clear that the catalysts have achieved the steady state activity or

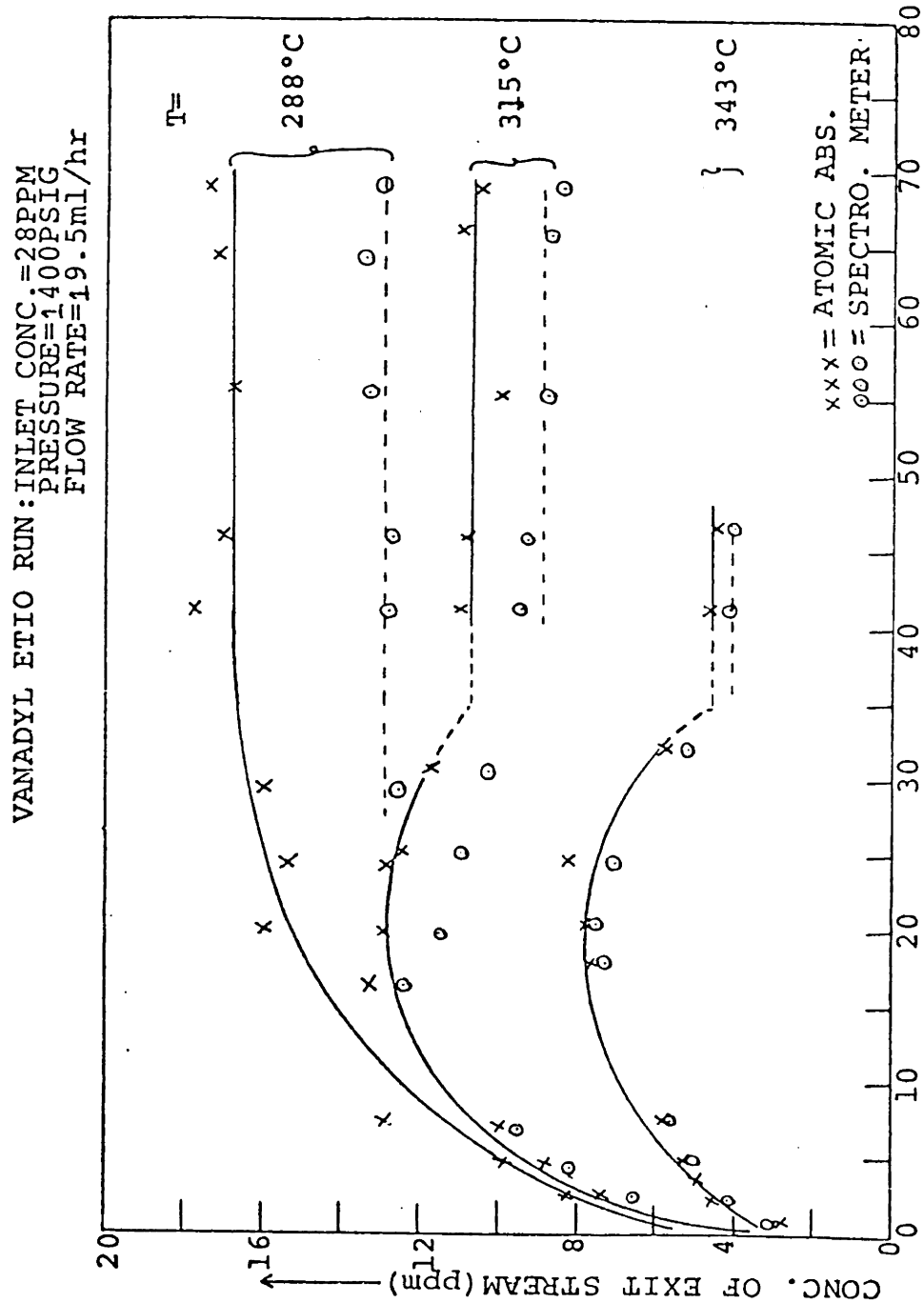

FIGURE V-9: Plot of the Reactor Outlet Solution Concentration vs. time on Stream at 343, 315 and 288°C.

not. This uncertainity is reflected in the results of the run CAVE-5 in Table V-2 and in figures V-5. Moreover, it is observed in fig. V-9, that during transient period there is much more metal deposition than would be predicted by steady state kinetics. It is because of this excess metal deposition that the calculated metal deposition profile in fig. V-5a is lower than the experimental one.

Therefore, it is necessary to make some long time duration runs. The major advantage would be that with respect to the total period of operation the initial transient period would be negligible. The second advantage is that by monitoring the exit solution concentrations over a long period of time, the useful information about the configurational diffusional resistance in the catalyst pores can be obtained. This later point would become more clear with respect to the discussion of the poisoning models in the next chapter.

Now we have a model which predicts the metal deposition profiles inside the catalyst particles at various bed locations. It would be interesting to see the net weight averaged metal deposition profile, given by equation V.23, along the length of the bed. If a catalyst particle was dissolved in a suitable acid and the concentration of the metal analyzed, the wt. % metal obtained would be same as given by equation V.23. For the unequal diffusivities calculations, the results for three different temperatures and two pressures are plotted in figure V-10. It is seen that along the reactor bed length the total metal deposition

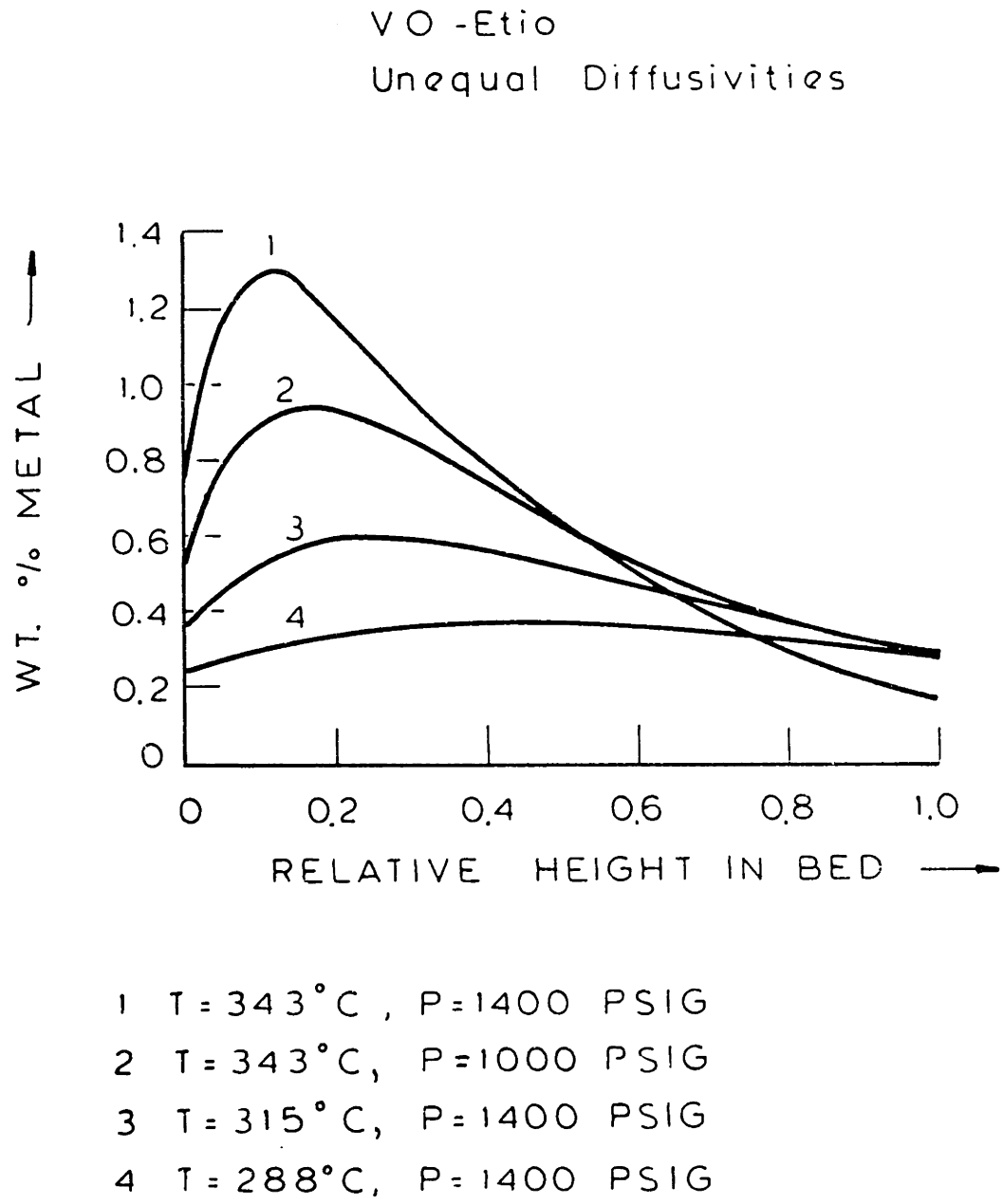

FIGURE V-10: Net Weight Averaged Vanadium Deposition (in the Catalyst) Profile Along the Length of the Reactor. The Approximate Values of the Parameters are:
Q = 19.5 ml/hr, W = 5 gms, M_o = 28 ppm and total time on stream = 68 hrs.

profile has a maxima, which is not at the entrance. As the temperature is lowered the maxima becomes more flat and moves more towards the exit of the reactor. At high temperatures, near the entrance of the reactor the profile is very steep. Therefore while matching the theoretical curves with the experimental ones in the 'a' series of the figures V-1 to V-6, a little variation in the location of the catalyst was allowed. The metal deposition profiles at the intervals of 0.1 grams and upto total of 0.5 grams from the entrance of the bed were calculated and the experimental profile was compared with them. By visual inspection the curve with the best agreement was picked up and is plotted for each run in the 'a' series of the figures V-1 to V-6. Even a small error in the catalyst location, at the entrance of the bed, produces a large error in the calculated metal deposition profile inside the catalyst, and this minor adjustment in the location of the catalyst is necessary. Moreover, it is found that at the entrance of the bed, within 1 cm of the bed height, the concentration of B rises rapidly from zero to as high as 2.5 ppm. Since the length of the catalyst extrudates are about 7 mm, the value of the concentration of B to be used at the catalyst surface is not clear. We chose the value of the B so as to approximately match the surface concentration of the deposited metal on the catalyst. However for the middle and the top sections of the bed no such adjustments are needed, and were therefore not made.

Under the asumption of equal diffusivities, figure V-11 has the plots similar to those of figure V-10. We observe that at the entrance of the bed the net metal deposition profiles are not as steep as they were for figure V-10. In the middle and the exit sections of the reactor bed the profiles in the figures V-10 and V-11 are very close to being identical.

Near the entrance of the bed the steep nature of the curve in figure V-10 is easily understood by the fact that the diffusivity of B is nearly five times higner than that of A. Therefore, near the entrance where the concentration of B in the solution is low, a lot of B diffuses out of the catalyst. This continues till the concentration of B in the solution phase has built to some significant value. Whereas in figure V-11, the B molecules spend more time inside the catalyst and the steep peaks of figure V-10 are damped out. The nature of the curves in figure V-10 can be easily verified by making runs at very high flow rates and then by analyzing their catalyst samples.

B.2. NICKEL ETIOPORPHYRIN-I: Calculations similar to vanadium have also been done for the nickel. The calculated profiles along with the experimental ones are shown in figures V-7 and V-8. Figures V-7 are the plots for the 343^{o}C and figures V-8 are the plots for 315^{o}C. For both the temperatures there is a good qualitative agreement between the calculated and the experimental profiles. However, the quantitative agreement is not as good as was for the vanadium runs.

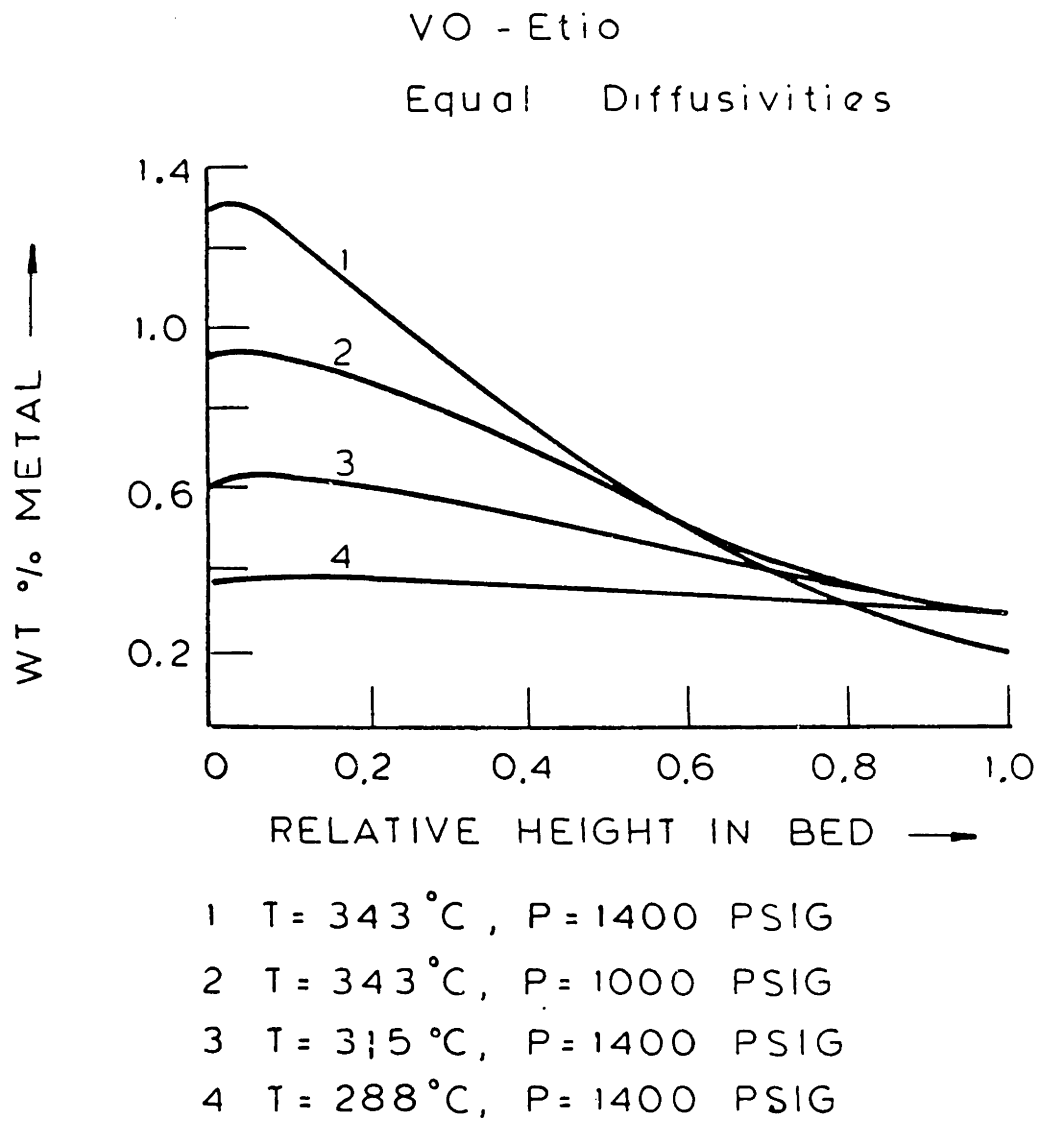

FIGURE V-11: Net Weight Averaged Vanadium Deposition (in the Catalyst) Profile along the Length of the Reactor. Parameters same as in figure V-10.

The not so good agreement may be due to one or more errors involved. It has already been pointed out that at low metal loadings the error in the analysis of the nickel from the scanning X-ray microanalyzer is about twice of the vanadium. Then there are usual errors of the sampling and the initial transient period of the catalyst. One more error, which may be important for the nickel runs is due to the equations V.1 and V.2 . It is found out that the rate constants k_1, k_2 and k_3 are the functions of the inlet concentration. It was speculated in chapter IV, that it may be due to the surface coverage by the final reaction product. If it is indeed true then the third transport equation for this third species should also be written. If the net surface coverage by the adsorbed species varies along the diameter of the catalyst, the rate constants in equations V.1 and V.2 may be functions of the radial position in the catalyst. On the other hand it may be assumed that inside the catalyst, the concentration profile of the metal free product is such that the total surface coverage by the adsorbed species does not vary much along the radius of the catalyst, and as an approximation the rate constants can be treated constant along the diameter of the catalyst. It is with this assumption that all the theoretical calculations for the nickel are done.

Unlike the vanadium the number of runs for the nickel are not very extensive. The results are tabulated in Table V-4. With reference to this table, the following observations are made:

TABLE V-4

SUMMARY OF THE CALCULATED AND THE EXPERIMENTAL RESULTS FOR NICKEL

Run #	T	Q	A_o	OUTLET SOLUTION CONC.				$D_A = D_B$
				EXPERIMENTAL		CALCULATED		$D_A X 10^6$
				M	B	M	B	$Cm^2/sec.$
CANE-7	343	30	28.6	11.1	1.33	11.0	1.33	1.6
CANE-6	343	19.5	28.1	7.6	0.93	7.7	0.94	1.2
CANE-9	343	14.7	27.5	5.5	0.97	5.7	0.7	1.0
CANE-10	343	30	16.8	5.1	0.62	5.0 5.1	0.62 0.62	1.5 2.7*
CANE-4	343	19.5	26.4	7.5	--	7.5	0.92	1.1
CANE-5	343	19.5	25.8	6.9	--	6.8	0.84	1.3
CANE-8	315	19.5	27.2	10.6	1.64	10.6	2.04	2.5

T = Temperature in ^oC

Q = Flow rate of solution in ml./hr.

A_o = Inlet concentration of nickel etioporphyrin (ppm)

M = A+B = sum of the concentrations of the nickel etio and the nickel chlorin.

* These calculations are done with the rate constants which are not corrected for the lower inlet concentration. For all the runs the pressure is 1400 psig and the amount of catalyst in the reactor is about 5 gms.

a) Unlike the vanadium runs, the assumption of equal diffusivity gives excellent agreement between the calculated and the experimental outlet concentrations. This does not precludes the possibility of the surface diffusion for the nickel runs. Since Ni-Etio is adsorbed less strongly than VO-Etio, it is possible that both the Ni-Etio and Ni-Chlorin diffuse on the surface to the same extent.

b) Runs CANE-4, CANE-5 and CANE-6 are at the identical temperature, pressure and flow rate and also about the same inlet concentration. The only difference between them is that for the runs CANE-5 and CANE-6, prior to the solution flow rate through the reactor the catalyst was purged with hydrogen for about half hours at the temperature of around $370^{o}C$. For the run CANE-4 the catalyst pretreatment was similar to all other runs. The values of the diffusivities calculated for runs CANE-4, CANE-5 and CANE-6 are $1.1X10^{-6}$, $1.3X10^{-6}$ and $1.2X10^{-6}$ $cm^2/sec.$ respectively. This is a remarkable agreement, and proves our earlier claim that the pretreatment of the catalyst with hydrogen does not influence the catalyst performance. Moreover, it gives us the confidence in the reproducibility of our runs.

c) Except the flow rate Q, all other operating conditions are same for the runs CANE-7, CANE-6 and CANE-9. One would expect the value of the diffusivity to be the same for all the three runs. However, the space velocity is in the decreasing order from run CANE-7, CANE-6 to CANE-9

and so is the diffusivity. Since the calculated value of B in run CANE-9 does not agree well with the experimental value, the chances are high that the observed pattern of the diffusivity with the space velocity is just a mere statistical coincidence. In order to make sure that this is just a random statistical pattern and not an artifact of our model calculations, some more runs at different flow rates should be made. It should be pointed out that if the mean of all the three runs are taken and the value of the diffusivity at 343°C is written as $1.3 \pm 0.3 \times 10^{-6}$, the magnitude of the error is not significant at all. In the literature, even under nonreacting conditions, the normal errors in the diffusivities measured for the liquid in the porous solids have been reported to be 50 - 100% and often they are even as high as 300 - 400% (Copeland - 1978, Pitcher - 1972).

d) One of the most critical test for our model would be the impact on the diffusivity of the change in the inlet solution concentration. It would check the assumption that inside the catalyst, the rate constants are not the function of the radial position. For run CANE-10, the inlet concentration is lower than CANE-7, otherwise all the conditions are identical for both the runs. At 343°C, 1400 psig and for the inlet concentration of 27 ppm the rate constants k_1, k_2 and k_3 measured are 39.75, 153.5 and 146.2 ml/g-hr respectively. When the direct proportionality of the rate constant to the inlet concentration is taken, the estimated rate constants k_1, k_2 and k_3 for the run

CANE-10 are 63.9, 246.7 and 235.7 ml/g-hr respectively. With these estimated values of the rate constant, the value of the diffusion coefficient is calculated to be $1.5X10^{-6}$ cm^2/sec. This is in excellent agreement with the values found for the other runs at 343°C. This indeed proves the validity of our diffusion as well as kinetic models.

If in the run CANE-10, the rate constants are not corrected for the inlet concentration, the calculated value of the diffusion coefficient is $2.7X10^{-6}$ which is much higher than the expected value of $1.3\pm0.3X10^{-6}$ cm^2/sec.

e) The most difficult result to explain in Table V-4 is the high value of the diffusivity for the run CANE-8. For this run, the temperature is 315°C and the value of the diffusion coefficient calculated is higher than the one at 343°C. Since for this run the calculated value of B is about 25% off from the experimental value, it may be that the results of this run are not very reliable and some more runs at 315°C and the lower temperatures are needed. If the value of diffusivity used is $1.5X10^{-6}$, the calculated exit stream concentrations for M and B are 12.6 and 2.36 ppm respectively, and are within 18% of the values calculated with the diffusivity of $2.5X10^{-6}$. Therefore just with this one run at the lower temperature we are unable to draw any definite conclusion. However, if it is thought that the above observation is a truth and not just a random statistical fluctuation then one might invoke the assumption of the surface diffusion to explain the phenomenon. It has

already been discussed that for surface diffusion a right amount of adsorptivity is needed. Since the adsorptivity is a function of temperature, it is possible that in some range of temperature the surface diffusion would increase with the decrease of temperature. Bienert and Gelbin (1967) did observe that the surface diffusion of isopropanol on the γ-alumina shows a maximum in the temperature range of 200 - 250^{o}C. But in our case it is just a mere speculation and needs further investigation.

The encouraging aspect of the diffusion coefficients listed in Table V-4 is that the order of magnitudes are in agreement with the theoretical estimated value of $2.5X10^{-6}$ cm^2/sec.

In figure V-12, the calculated net weight averaged nickel deposition along the length of the reactor are plotted. This figure is similar to figures V-10 and V-11 for vanadium. By comparing the figures V-10 and V-12, it is clear that the nickel deposition along the reactor is not as steep as the vanadium.

This chapter is concluded with the final observation that the order of the magnitude of the diffusion coefficients for the VO-Etioporphyrin and Ni-Etioporphyrin is same. The calculated values of the metal deposition profiles in the catalysts, at various bed positions, are in fairly good agreement with the experimental values.

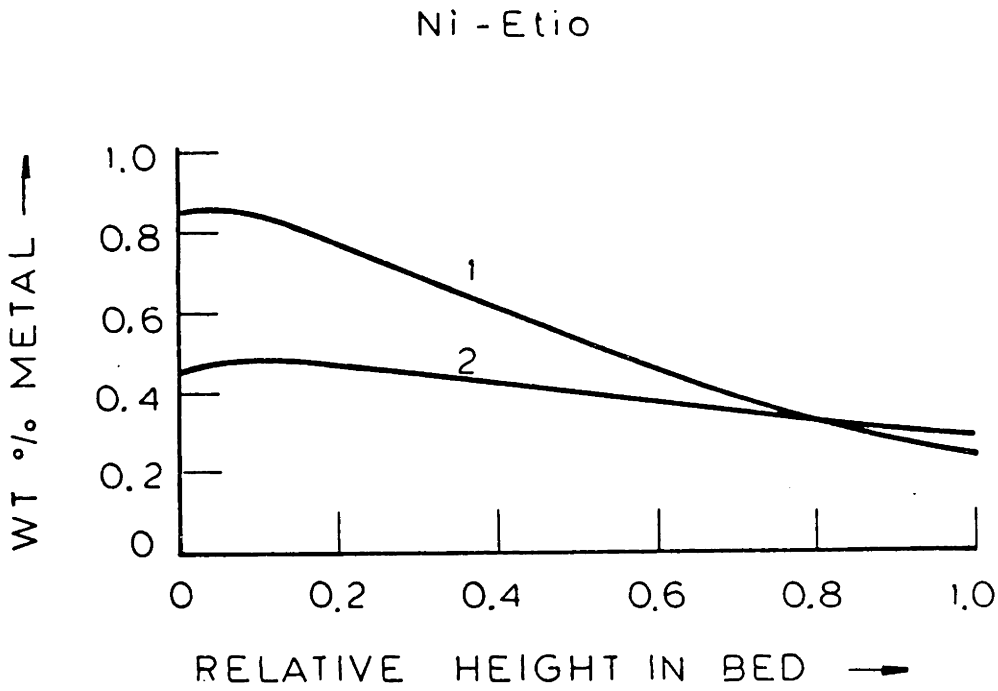

FIGURE V-12: Net Weight Averaged Nickel Deposition (in the Catalyst) Profile along the Length of the Reactor.

CHAPTER-VI

THEORETICAL POISONING STUDIES

In the last chapter it is found that the initial HDM activity of a given catalyst can be adequately explained by a constant diffusivity model. In the runs of long time periods, the metal deposits inside the catalyst and the intraparticle diffusivity changes. When the performance of the reactor is to be predicted over long time periods, this change of the diffusivity has to be taken into account. One of the objectives of this chapter is to develop a theoretical model to predict the catalyst activity for long reaction periods. The second objective is to find the optimum pore size distribution in the catalyst, so that the initial rate of the catalyst and also its life span are optimized. The discussions with Raymond R. Cwiklinski of the Massachusetts Institute of Technology have been of immense help to the development of the model.

The effect of the pore size distribution on the catalyst activity has been discussed in section II.B.5 and following are the pertinent observations:

(a) It is seen that for a fixed porosity, the decrease in the pore radius increases the surface area of the catalyst but also increases the configurational diffusion resistance. Therefore, for a given molecular size, the maximum in the initial catalyst activity is

achieved for a certain intermediate pore size. Hardin et al. (1978) observed this phenomenon experimentally and their results were plotted in figure II-10.

(b) Bridge and Green (1979) observed that for a given size of the molecule, when the particle size is reduced, the rate could be further increased by the reduction of the pore diameter. This is due to the fact that when particle size is decreased, a higher intraparticle diffusional resistance can be tolerated.

(c) Since the petroleum residuum has a distribution of the molecular sizes, it is suggested that the bimodal catalyst should be used (Bridge and Green - 1979, Richardson and Alley - 1975). The big pores would facilitate the diffusion of the big molecules.

(d) Inoguchi et al. (1971-b) studied the long run tests of 1,000 to 3,000 hours on catalysts with different physical properties. They found that the catalysts with comparetively small pores had a high initial activity, but the activity fell rapidly with time. On the other hand, in catalysts with comparatively large pore diameters, vanadium deposited in large quantities and maintained its activity for a longer time. Therfore, there is a need for a pore size distribution which would be a good compromise for both the initial activity and also the long range activity.

All these four criteria (a) - (d) are easily met by a bimodal catalyst. They have large pores called macropores,

and small pores called micropores. In most of the bimodal catalysts, the micropore diameters range from 20 - 200 Å, whereas the macropore diameters are in the range of 1000 - 50,000 Å. The macropores provide a low diffusional resistance for the molecules to reach the micropores, which provide the large surface area for the reaction. When the micropores near the external surface of the catalyst are plugged with the deposited metal, the macropores provide access to the inner micropores. As a result the catalyst maintains its high activity over a longer period of reaction time.

A. EXISTING POISONING MODELS: A few attempts have been made to model the initial and long run activity of the catalyst. Newson (1972 and 1975) modelled the pore plugging due to deposition of metal sulfides and coke. He assumed the uniform pore plugging. Dautzenberg et al. (1978) developed a two parameter model describing the deactivation behaviour due to the metals deposition. However, the above investigators neglected the change in the restricted diffusion with the decreasing pore size. Rajagopalan and Luss (1979) considered the restricted diffusion effect with the increase in the metal loading on the catalyst; and developed a model to predict the optimal initial activity and the optimal pore size.

All these authors assumed that the catalyst pore structure could be represented by a set of idealised parallel nonintersecting pores of variable radius, but each of a

certain length L. This model is also refered as 'parallel bundel' model. This model has been used to predict the activity for the various pore size distributions. As we have already discussed, the basic advantage of the bimodal catalyst is its connectivity of micropores with the macropores. Therefore, in order to get the correct prediction for a bimodal catalyst, the model must allow for this connectivity of the pores.

All the above authors used the pseudo first order kinetics, and therefore did not have any internal maxima in the metal deposition on the catalyst. There is a need for a poisoning model which can take this internal maxima in to account.

In this chapter we will develop the poisoning models for the new proposed HDM kinetics. A model for the unimodal catalyst is developed. The parallel pore bundle model with the restricted diffusivity as a function of the metal loading has been used. Since the HDS 16-A catalyst used in our studies is very close to the unimodal catalyst (figure III-1), it is hoped that this model would be useful in the long period activity tests of the catalyst. A second model for the bimodal catalysts has been developed. This model allows the connectivity between the micro and the macro pores. It is shown that both in terms of the initial activity and the long term activity, bimodal catalyst gives much better performance than the unimodal catalyst.

B. DEVELOPMENT OF THE POISONING MODELS FOR THE BIMODAL AND THE UNIMODAL CATALYSTS: Since some of the expressions derived for the bimodal catalyst are directly applicable to the unimodal catalyst, the poisoning model for the bimodal catalyst is developed first.

Diffusion without any chemical reaction in the bimodal catalysts have been studied extensively (Hashimoto and Smith - 1974, Hashimoto et al. - 1976, Ma and Ho - 1974, Ma and Lee - 1976 and 1977, Ruckenstein et al. - 1971). All these authors have modelled the spherical catalyst as a spherical macroporous particle consisting of small spherical microporous particles of uniform size. The schematic sketch of such a catalyst is given in figure VI-1. The radius of the microspheres is much less than the macrosphere. Macropore is the interstitial space between the microspheres, which contain all the micropores. In order to reach to the micropores, a diffusing substance has to diffuse through the macropores. Some of the authors have also allowed for the adsorption on the microsphere surfaces. It has been found that such a model gives good agreement with the experimental diffusion data (Hashimoto and Smith - 1974, Ma and Ho - 1974, Ma and Lee - 1976, and Ruckenstein et al. - 1971).

For the catalyst in figure V-1, Sohn and Szekely (1972 and 1974) have developed the model for the non-catalytic gas-solid reactions. Szekely et al. (1973) applied the model to the analysis of experimental results on the reduction of porous nickel-Oxide pellets. For this catalyst, Pigford and

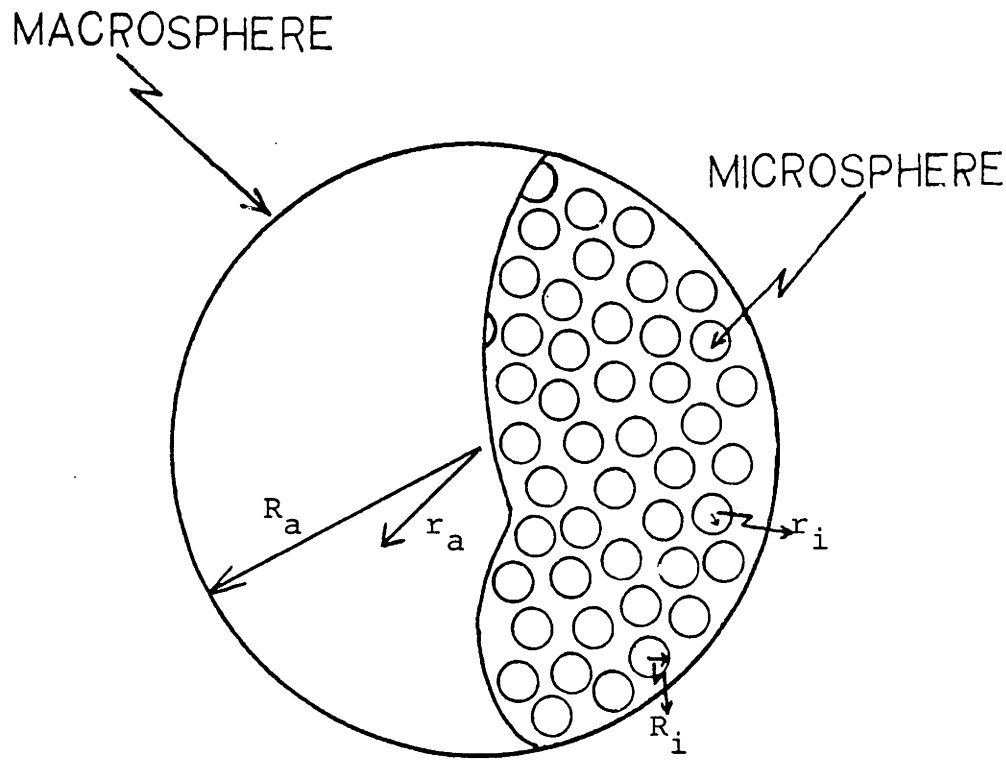

FIGURE VI-1: Schematic Sketch of the Grain Model Catalyst.

Sliger (1973) developed a similar model and applied it to the removal of sulfur dioxide by limestones. These authors call the microspheres as grains and the model as grain model. To be consistent with the literature, we would call our model as grain poisoning model.

When the catalyst is a pellet and its building blocks are small particles, the grain model is a good approximation to the real situation. In our model, the metallo porphyrins would diffuse in macropores and from macropores to the micropores in the grains. The pertinent assumptions of the model are:

(a) A spherical macroporous catalyst particle is an assembly of small microporous particles called grains.

(b) The grains are spheres with a uniform size.

(c) As seen in Chapter V, the diffusion in both the micropores and the macropores can be described by Fick's equation.

(d) Beuther and Schmid (1963), Dautzenberg et al. (1978) and Sato et al. (1971) observed that the coke deposit builds up very rapidly to an equilibrium level. The model developed would be applicable to the time after this initial period. Therefore, coke deposition would not be considered in our model.

(e) It would be assumed that the metal deposit does not affect the intrinsic demetallation activity per unit surface area, but it reduces the surface area and may affect the restricted diffusion in the pores. This

assumption is consistent with our experimental observation that upto 10 wt % metal loading no significant change in the catalyst activity is observed. This observation is consistent with the experimental observations of the other investigators also.

(f) When the metal deposites in the pores, the diameter gets reduced and therefore it is necessary to take the restricted diffusivity into account. The concept of a steric limitation of large molecules in pores was first introduced by Ferry (1936). Later, Renkin (1954) derived an expression for the enhanced drag. It has been found that the restricted diffusivity in the pore can be written as:

$$D = D_o \, G \, (\alpha) \qquad \text{VI.1}$$

where D_o is the bulk diffusivity and α is given by:

$$\alpha = R_m/R \qquad \text{VI.2}$$

where R is the pore radius and R_m is the radius of diffusing molecule . For $\alpha < 0.1$, $G(\alpha)$ is nearly unity. Spry and Sawyer (1975) have suggested that $G(\alpha)$ may be approximated by:

$$G(\alpha) = (1 - \alpha)^4 \qquad \text{V.3}$$

Spry and Sawyer found the approximation to be useful for the interpretation of the hydrotreatment of the heavy Venezuelan crude. This approximation will be used in our analysis also.

(g) To describe the demetallation and the diffusion in the catalyst pores, pseudo steady state approximation would be invoked. Since the time associated with the changes in the shape of pores is much larger than the characteristic times for the rate process involved, the approximation is a justified one.

(h) The surface area available for the chemical reaction in the macropores is much smaller than the one in microspheres. Therefore the reaction in macropores would be neglected. In a detailed model, it is not necessary to invoke this assumption. Due to this assumption, there would be no metal deposition in the macropores, and therefore macropore diffusivity would not be a function of time. However, it must be pointed out that even if the metals were depositing in the macropores, the diffusivity in the macropores could be treated as independent of time. It is due to the fact that macropores are very large and α in equation VI.1 will always be much less than 0.1.

(i) For the purpose of quick analysis, we would assume that the diffusivities of A and B are equal. It must be pointed out that this assumption is not necessary. We have already seen in chapter V that the calculations for

unequal diffusivities can also be readily made (equations V.7). However, this assumption would reduce the number of dimensionless parameters by one.

The conservation equations for the macropores are:

$$\frac{D_a}{r_a^2} \cdot \frac{\partial}{\partial r_a}\left[r_a^2 \frac{\partial A_a}{\partial r_a}\right] = n4\P R_i^2 D_i \left(\frac{\partial A_i}{\partial r_i}\right)_{r_i=R_i} \qquad \text{VI.4}$$

$$\frac{D_a}{r_a^2} \frac{\partial}{\partial r_a}\left[r_a^2 \frac{\partial B_a}{\partial r_a}\right] = n4\P R_i^2 D_i \left(\frac{\partial B_i}{\partial r_i}\right)_{r_i=R_i} \qquad \text{VI.5}$$

In the above equations and throughout this chapter, subscripts a and i refer to macrosphere and microspheres respectively. R_i is the radius of the microsphere and n is the number of microspheres per unit volume of macrosphere. D_a and D_i are effective diffusivities and are related to the D of equation VI.1 by the expression:

$$D_a = \frac{\varepsilon_a D_o G(\alpha_a)}{\tau_a} \qquad \text{VI.6}$$

$$D_i = \frac{\varepsilon_i D_o G(\alpha_i)}{\tau_i} \qquad \text{VI.7}$$

where ε_a and ε_i are the porosites and τ_a and τ_i are tortuosities. For macrospheres $G(\alpha_a)$ is very close to unity. The value of n is given by:

$$n = \frac{3(1-\varepsilon_a)}{4\P R_i^3} \qquad \text{VI.8}$$

From equations VI.4 and VI.5, it is seen that the dimensionless variable of interest is:

$$\alpha_1 \equiv 3(1-\varepsilon_a)\frac{D_i}{D_a}\frac{R_a^2}{R_i^2} \qquad \text{VI.9}$$

α_1 is the measure of the relative importance of the macropore diffusional resistance to that of micropore diffusional resistance. Large values of α_1 mean that the macropore diffusion process is rate limiting and very small values ($\alpha_1 << 1$) indicate that micropore diffusion is rate controlling. If it is thought that the restricted diffusion in the macropore can be also important, then in order to evaluate $G(\alpha_a)$ one would need equivalent macropore size. Following Wheeler (1951) it can be written:

$$\text{Equivalent Macropore Radius} = \frac{2}{3}\left(\frac{\varepsilon_a}{1-\varepsilon_a}\right)R_i \qquad \text{VI.10}$$

The pores in the microspheres would be idealized as parallel pores. Each of these pores are of same length L and radius R_p. From Wheeler (1951):

$$L = \frac{R_i \sqrt{\tau_i}}{3} \qquad \text{VI.11}$$

$$N_p = \frac{4\varepsilon_i R_i^2}{R_p^2 \sqrt{\tau_i}} \qquad \text{VI.12}$$

where N_p is number of idealized micropores in a microsphere. Now in order to solve the mass conservation equations in the microsphere, they will be solved for an idealized cylinderical pore and the result would be multiplied by N_p. The resulting conservation equations are:

$$\frac{\partial}{\partial x}\left(R^2 D \frac{\partial A_i}{\partial x}\right) = 2 R (K_1 A_i - K_2 B_i) \qquad \text{VI.13}$$

$$\frac{\partial}{\partial x}\left(R^2 D \frac{\partial B_i}{\partial x}\right) = 2R (K_3 B_i + K_2 B_i - K_1 A_i) \qquad \text{VI.14}$$

where R is the radius of the pore at any time, D is the diffusivity given by equation VI.1, A_i and B_i are concentrations of A and B inside the pore, K_1, K_2 and K_3 are rate constants per unit surface area and x is the axial length coordinate. The boundary conditions are

$$\text{at } x=L \quad , \quad A_i = A_a, \; B_i = B_a$$

$$x=o \quad , \quad \frac{\partial A_i}{\partial x} = \frac{\partial B_i}{\partial x} = 0 \qquad \text{VI.15}$$

It is found that the pertinent dimensionless variables for equations VI.13 and VI.14 are:

$$\phi_1^2 = \frac{2\lambda_1 R_i^2 \varepsilon_i}{9 R_p D_i} \qquad \text{VI.16}$$

$$\phi_2^2 = \frac{2\lambda_2 R_i^2 \varepsilon_i}{9 R_p D_i} \qquad \text{VI.17}$$

$$h(x,r_a,t) = R(x,r_a,t)/R_p \qquad \text{VI.18}$$

$$g(x,r_a,t) = D(x,r_a,t)/D(x,r_a,o) \qquad \text{VI.19}$$

where λ_1 and λ_2 are the eigen values of the rate constant matrix and are given by equations V.8. Due to the metal deposition in the pores, R and D are the functions of the position in the pore and also the time. In equations VI.4 and VI.5, the flux per unit macrosphere is given by:

$$4\P R_i^2 D_i \left(\frac{\partial A_i}{\partial r_i}\right)_{r_i=R_i} = 2\P N_p \int_o^L R(K_1 A_i - K_2 B_i)\,dx \qquad \text{VI.20}$$

$$4\P R_i^2 D_i \left(\frac{\partial B_i}{\partial r_i}\right)_{r_i=R_i} = 2\P N_p \int_o^L R(K_2 B_i + K_3 B_i - K_1 A_i)\,dx \qquad \text{VI.21}$$

The boundary conditions for the macrosphere and the equations VI.4 and VI.5 are:

$$\text{at } r_a = R_a \quad , \quad A_a = A \quad , \quad B_a = B \qquad \text{VI.22}$$

$$r_a = o \quad , \quad \frac{\partial A_a}{\partial r_a} = \frac{\partial B_a}{\partial r_a} = 0 \qquad \text{VI.23}$$

Under pseudosteady state, once the metal deposition profiles inside the pores are known the concentration profiles in the solution phase of the pores can be found numerically from the equations VI.4, VI.5, VI.13, VI.14, VI.20 and VI.21 with the boundary conditions given by equations VI.15, VI.22 and VI.23.

In the above calculations we presumed that $h(x,r_a,t)$ at various points in the microspheres was known. Now we proceed to set up equations for it. That is done by considering the time dimension of the problem. It can be readily shown that

$$\frac{dh}{dt} = \frac{-10^{-6} K_3 \rho B_i}{\rho_m R_p} \qquad \text{VI.24}$$

where ρ_m is the density of the metal deposited on the surface. In the above expression the factor of 10^{-6} is due to the fact that B_i is in ppm. For a value of h, D can be calculated through equations VI.18, VI.2 and VI.1.

At time t=o, in every microsphere of the macrosphere, the values of h and g in equations VI.18 and VI.19 are unity. Therefore, the differential equations VI.4, VI.5, VI.13 and VI.14 are numerically solved. Once the concentration profiles for A and B in each microsphere of the macrosphere are known, equation VI.24 is used to calculate new values of h. A suitable time increament to allow for a small change in the micropore geometry is chosen. Once h is known at time t, the differential equations are resolved for

the concentration profiles of A and B. This procedure is continued till the significant plugging of the catalyst pellet is observed. A computer program to do this job has been written and is given in appendix IV.

Petersen (1965) pointed out that the prediction of the effectiveness factor of a bimodal catalyst from a single parameter, namely, the Thiele modulus, may give erroneous results. If we follow Örs and Dogu (1979), the dimensionless parameters which characterize the effectiveness factor for our system are α_1, ϕ_1, and ϕ_2; and are given by equations VI.9, VI.16 and VI.17.

Once we have the expression for the bimodal catalyst pellet, it is easy to derive the govering equations for a unimodal catalyst. If we imagine a microsphere as a big unimodal catalyst then equations VI.11 to VI.21 can be used to simulate a unimodal catalyst. Now the boundary conditions at x=L in equation VI.15 would refer to the bulk solution concentrations A and B. R_i would be the radius of the unimodal catalyst sphere. A computer program to simulate the unimodal catalyst sphere has also been written and is given in appendix IV.

C. MODEL RESULTS: In this section, we will first discuss the grain model results, and then a comparison with the unimodal catalyst.

When a catalyst pellet is made of crushed powder, there is no reason to believe that the tortuosity for the macropores would be the same as that of the micropores. It is due to the fact that micropore structure in the powder may not be same as the macropore structure formed from the interstitial spaces in the packed powder. The ratio of the effective macropore to micropore diffusivities may be anywhere between 10 to 10^5. Shah and Paraskos (1975) have suggested a tortuosity of 8 for the nickel and vanadium compounds. So it is possible that the microspheres may have tortuosity of 8 while the macropores in macrospheres may be around two.

Figures VI-2 to VI-8 are the plots for some of the computer simulations of the grain poisoning model and show the typical characteristics of this model. The pertinent parameters used for these figures are: $K_1 = 0.407$, $K_2 = 0.467$, $K_3 = 0.883$ ml/hr-meter^2; radius of the metal porphyrin molecule = 7.1 Å, density of the deposited metal = 6.1 g/cm^3, $D_a \simeq 1.1 \times 10^{-6}$ cm^2/sec, $\varepsilon_a = 0.26$, $\varepsilon_i = 0.5$, $\rho = 1.0$ g/cm^3, $\varepsilon_i D_o / \tau_i = 0.28 \times 10^{-6}$ cm^2/sec., the radius of the macrosphere = 0.079 cm and the concentrations of A and B at the surface of the macrosphere are 50 ppm and 0 ppm respectively. In the computer simulations of the figures VI-2 to VI-8, all these parameters are held constant and the effect of the change in micropore radius and the grain size is observed. The macroporosity of 0.26 is chosen for the close hexagonal spherical packing. The units of the reaction rate

are 10^{-6} gm of metal/hr. pellet. From the values of the physical parameters given, the pertinent dimensionless parameters for each simulation can be easily calculated from VI.9, VI.16 and VI.17. It must be pointed out that we have chosen the value of macro and micropore diffusivities such that $D_a\tau_i/\varepsilon_i D_o \simeq 4$ and is consistent with the values in the literature. In terms of the quantitative numbers, this ratio of the diffusivities will definitely have an impact on the calculated results. However, the salient qualitative observations would be still valid and are listed below:

(a) For different grain sizes, figure VI-2 is the plot of the initial reaction rate per pellet versus pore radius. The microporosity is fixed at a value of 0.5. It is seen that for a given grain radius, there is a maximum in the initial reaction rate. For a given grain size, when the pore size is reduced beyond some value, the intragrain diffusion becomes controlling factor. Thus, there is an optimum between decrease in the intragrain diffusion and increase in the surface area available. A plot given by Spry and Sawyer (1975), looks very similar to fig. VI.2. However, these authors varied the molecular diameter, and for each molecular diameter observed the effect of the pore diameters on the reaction rate, whereas in fig. VI.2, molecular diameter is held at a constant value, and the effect of various grain sizes has been studied.

(b) Another important observation from figure VI-2 is that with the decrease of the grain radius the micropore

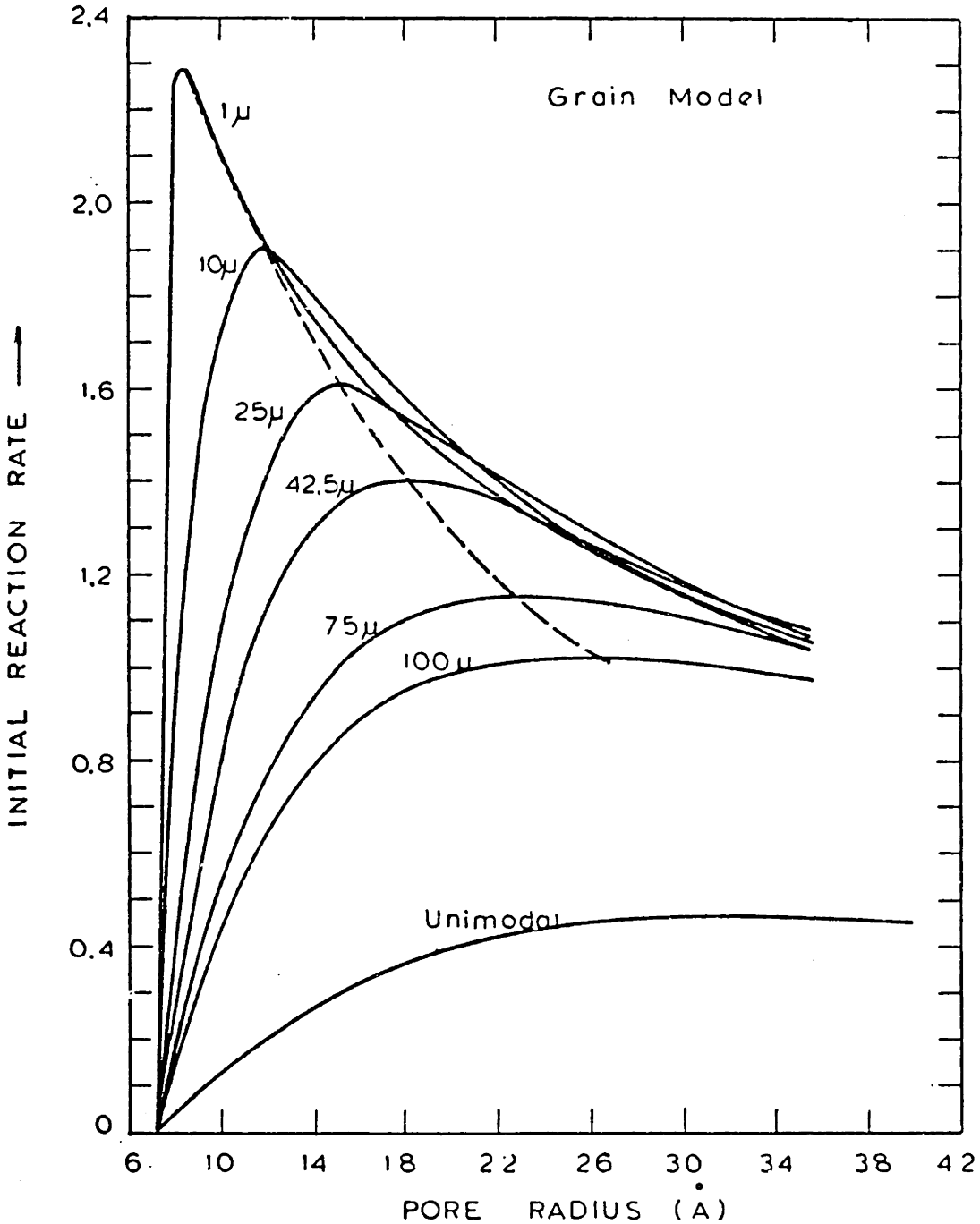

FIGURE VI-2: Initial Reaction Rate vs. Micropore Radius for Different Grain Sizes and at a Fixed Porosity. The Numbers Given on the Figure are the Radius of the Microspheres. Units of Reaction Rate are 10^{-6} gm of metal/hr.-pellet

radius for which initial rate is maximum also decreases. This observation can be easily understood from the dimensionless parameters ϕ_1 and ϕ_2 of equations VI.16 and VI.17. As the radius R_i is decreased, the Thiele's modulus for the microspheres decrease and one can tolerate a decrease in the micropore diffusivity. Therefore, it is possible to decrease the pore radius more.

As the pore radius is decreased at the fixed porosity, the available surface area for the reaction increases and an increase in the initial rate is observed. Therefore, as the grain radius is reduced, the maximum initial rate per pellet also increases. Because of this property, it is possible to have very high initial rates with the bimodal catalysts. Fig. VI-3 gives two curves; curve 1 is the locus of maximum possible initial rate for a given grain size vs. the grain size; and curve 2 is the locus of pore radius which gives the maximum initial rate vs. the grain size.

(c) Fig. VI-4 shows the drop in the reaction rate of the catalyst pellet with time on stream. It is observed that for any grain size, when the micropore radius is reduced, the catalyst deactivates at a faster rate. For a given micro porosity, the decrease in micropore radius reduces the physical capacity of the pellet for metal. It can be seen from the following equation:

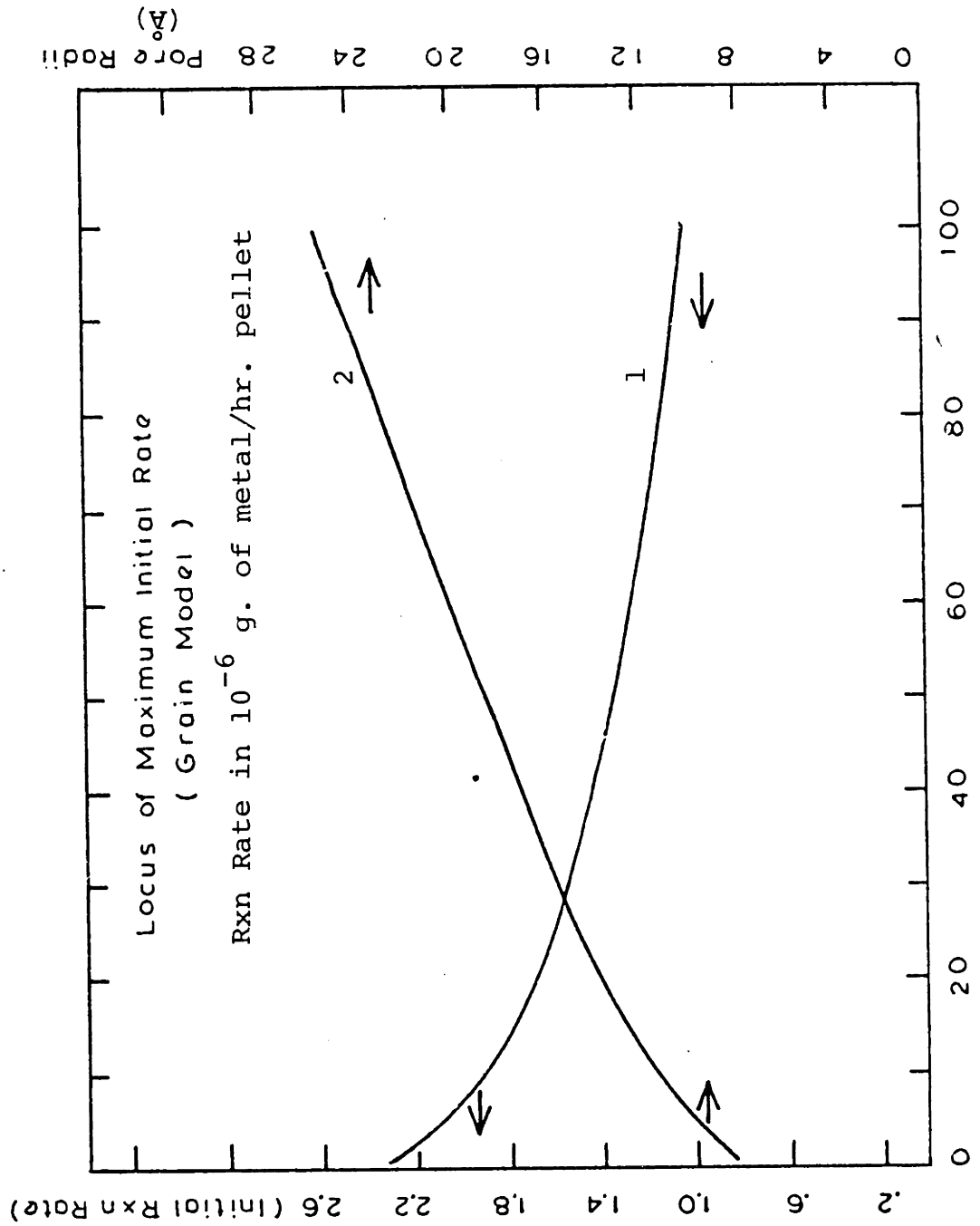

FIGURE VI-3: Maximum Initial Rate vs. Grain Size and the Corresponding Micropore Radius vs. Grain Size at the Constant Porosity.

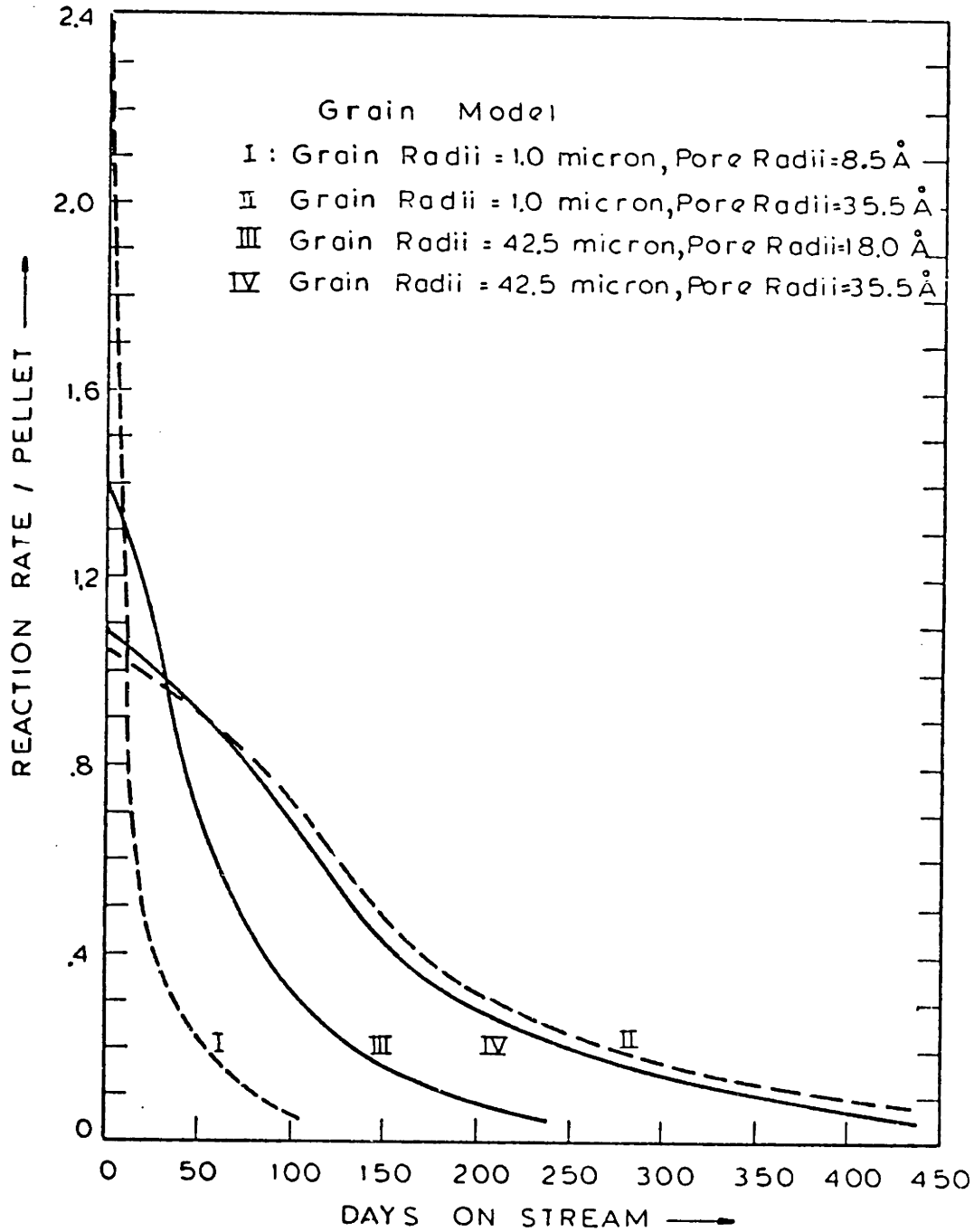

FIGURE VI-4: Drop in the Rate of the Catalyst Pellet with Time on Stream. Porosity of all the Pellets is Same. Units of Rxn Rate are 10^{-6} g.of metal/hr.

$$\text{Maximum possible volume of metal deposition in a grain} = \frac{4}{3}\pi\varepsilon_i R_i^3\left[1-\left(\frac{R_m}{R_p}\right)^2\right] \qquad \text{VI.25}$$

In fig. VI-4, curves I and III correspond to maximum initial rate for the respective grains of 1.0 and 42.5 micron.

(d) Figures VI-5 and VI-6 show the changes in the concentration profiles of A and B in the macropores with days on stream. In figures VI-5, it is seen that with the elapse of reaction time, the microspheres near the edge of the macrosphere get plugged and therefore concentration profile of A moves more towards the center of the macrosphere. A similar trend is observed for the concentration profile of B in fig. VI-6.

(e) Fig. VI-7 shows the progression of the metal deposition profile in the pellet with days on stream. Initially more metal deposites near the outer edge of the pellet but once these microspheres are plugged, the rate of the metal deposition in the inner microspheres increases. The maximum in the curves V to VIII near the edge of the pellet can be easily understood with reference to fig. VI-8. At the surface of the pellet the solution concentrations of A and B are 50 and 0 ppm respectively. Therefore in the micropores at the surface metal deposition is zero. Just below the surface of the pellet, A diffuses inside the micropore and a maximum in the concentration of the B inside the pore occurs. As a result the maximum

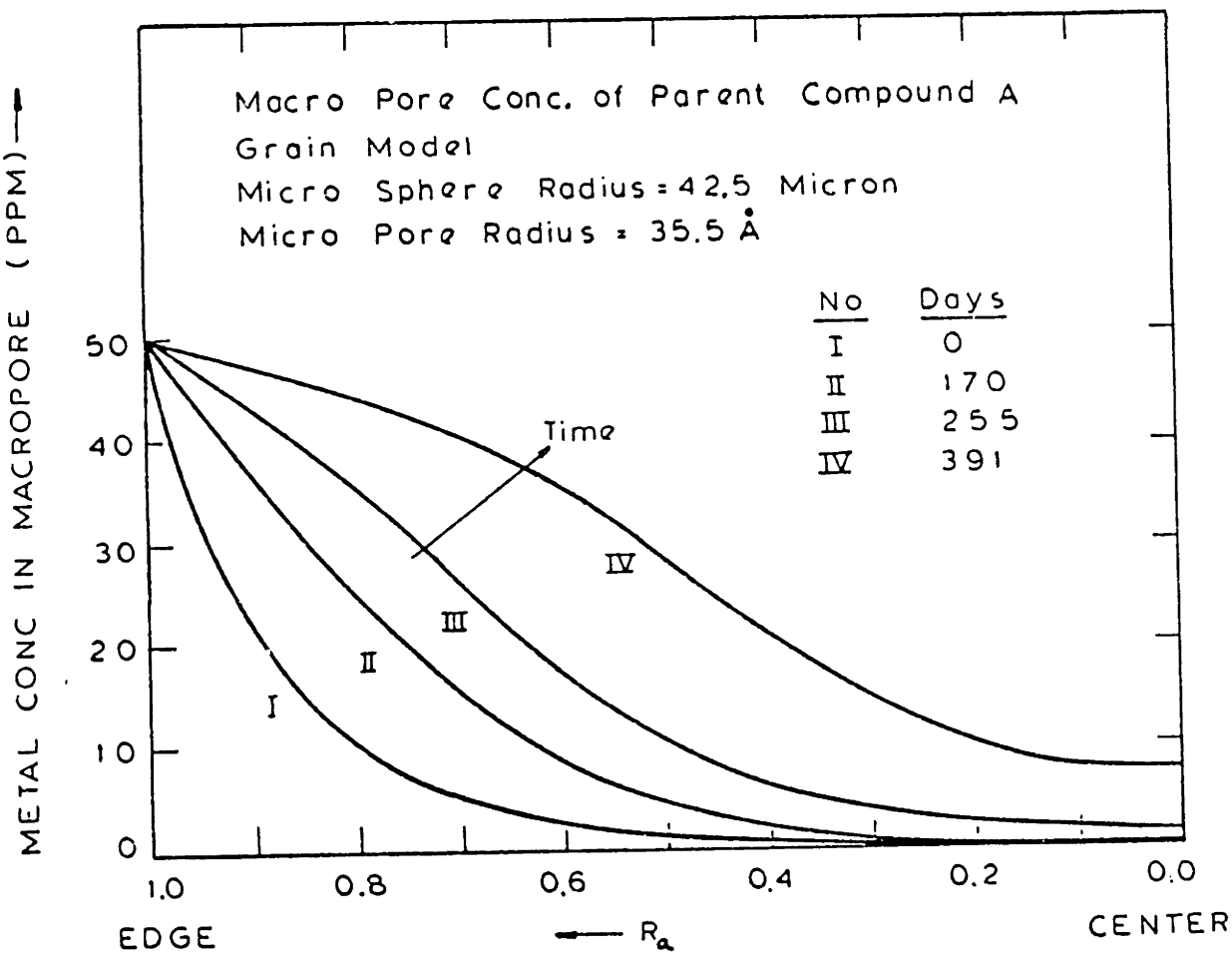

FIGURE VI-5: Concentration Profile of A in Macropores of a Bimodal Catalyst Pellet at Various Reaction Times.

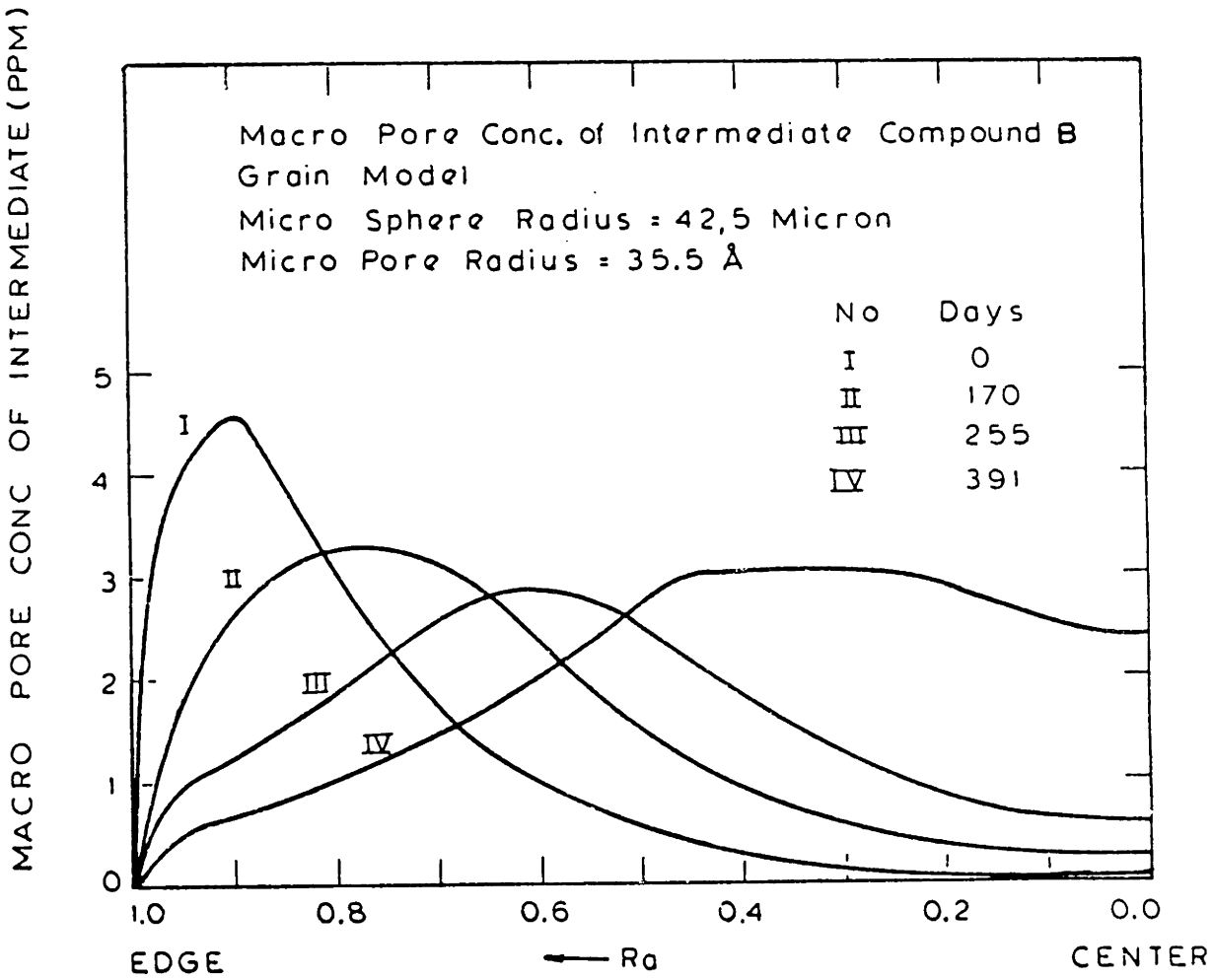

FIGURE VI-6: Concentration Profile of B in Macropores of a Bimodal Catalyst Pellet at Various Reaction Times.

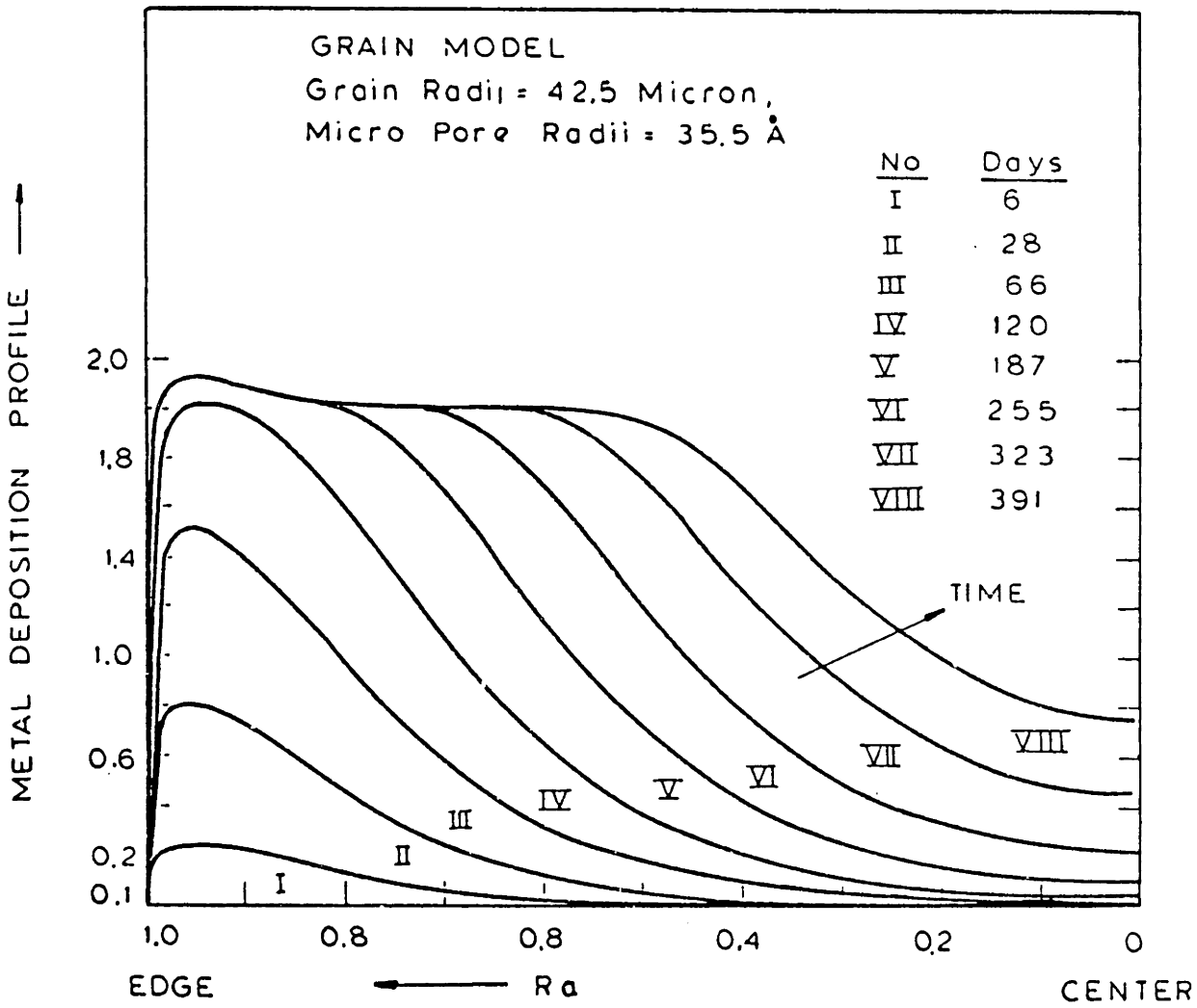

FIGURE VI-7: Progression of the Metal Deposition Profile (g. of metal/cm^3 of Macrosphere Volume) in the Macrosphere with Days on Stream.

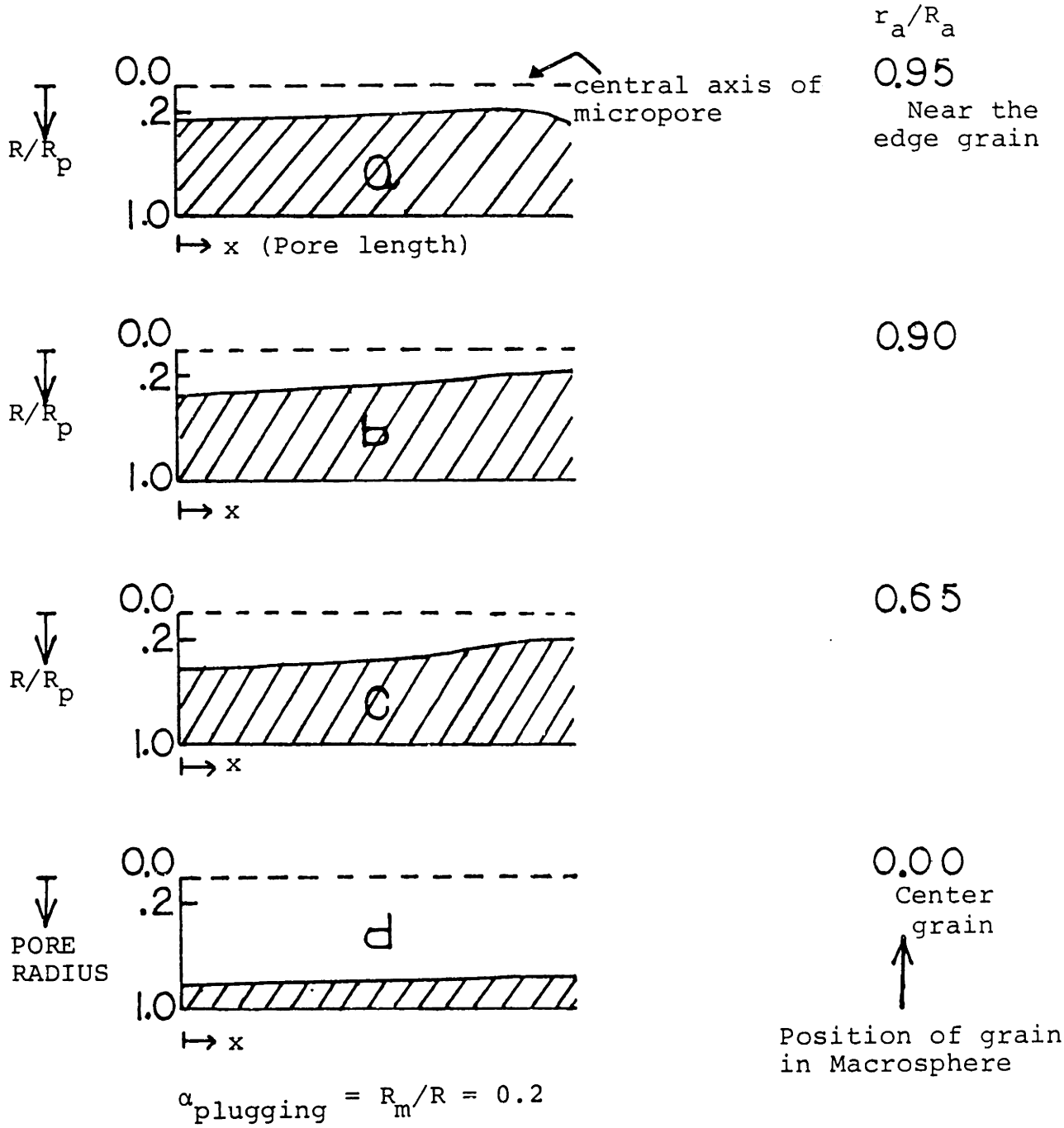

FIGURE VI-8: Metal Deposition in Micropores Plotted at Various Radial Locations in Macrosphere. The Days on Stream have been 391 Days. The Shaded region is the Metal Deposited in a Pore. The Simulation is same as in Fig. VI-7.

in the metal deposition occurs inside the pore. However in the micropores, which are much inside the pellet the maximum in metal deposition occurs at the micropore mouth, and the volume at the end of the micropores are not used as effectively as for the micropores near the surface. This can be easily understood from the metal deposition profiles in micropores a, b and c of fig. VI-8. None of the molecules of A and B can diffuse in the pores b and c but the pore mouth of a is still not completely blocked to the diffusion of these molecules. If the grain size is reduced, the maximum in the corresponding metal deposition profile of fig. VI-7 would become less pronounced.

Now it would be interesting to look at some of the pertinent results of the unimodal model. The results of one of the computer simulation runs are shown in figures VI-9 to VI-11. In these figures the values of the rate constants, diffusivities and all the other pertinent parameters are the same as for the microspheres in the grain model of figures VI-2 to VI-8. The values of these parameters have already been given. The radius of the unimodal catalyst has been chosen to be same as that of the macrosphere in the grain model.

From figures VI-9 and VI-10 it is observed, that unlike the bimodal catalyst, the concentration profiles of A and B move outward with reaction time. The explanation for it can be seen in figure VI-11. The maximum in the metal deposition

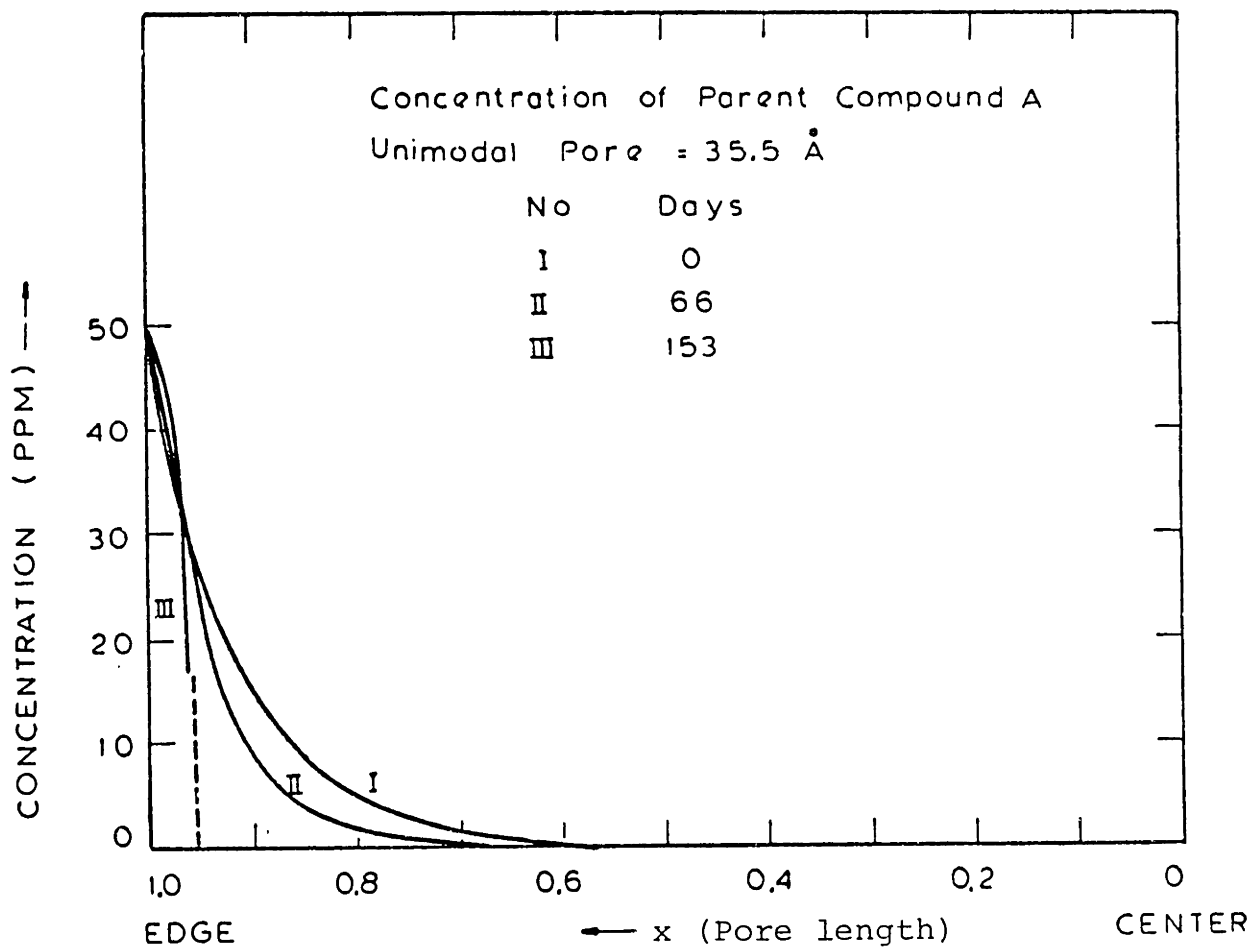

FIGURE VI-9: Concentration Profile of A in the Unimodal Catalyst at Various Reaction Times.

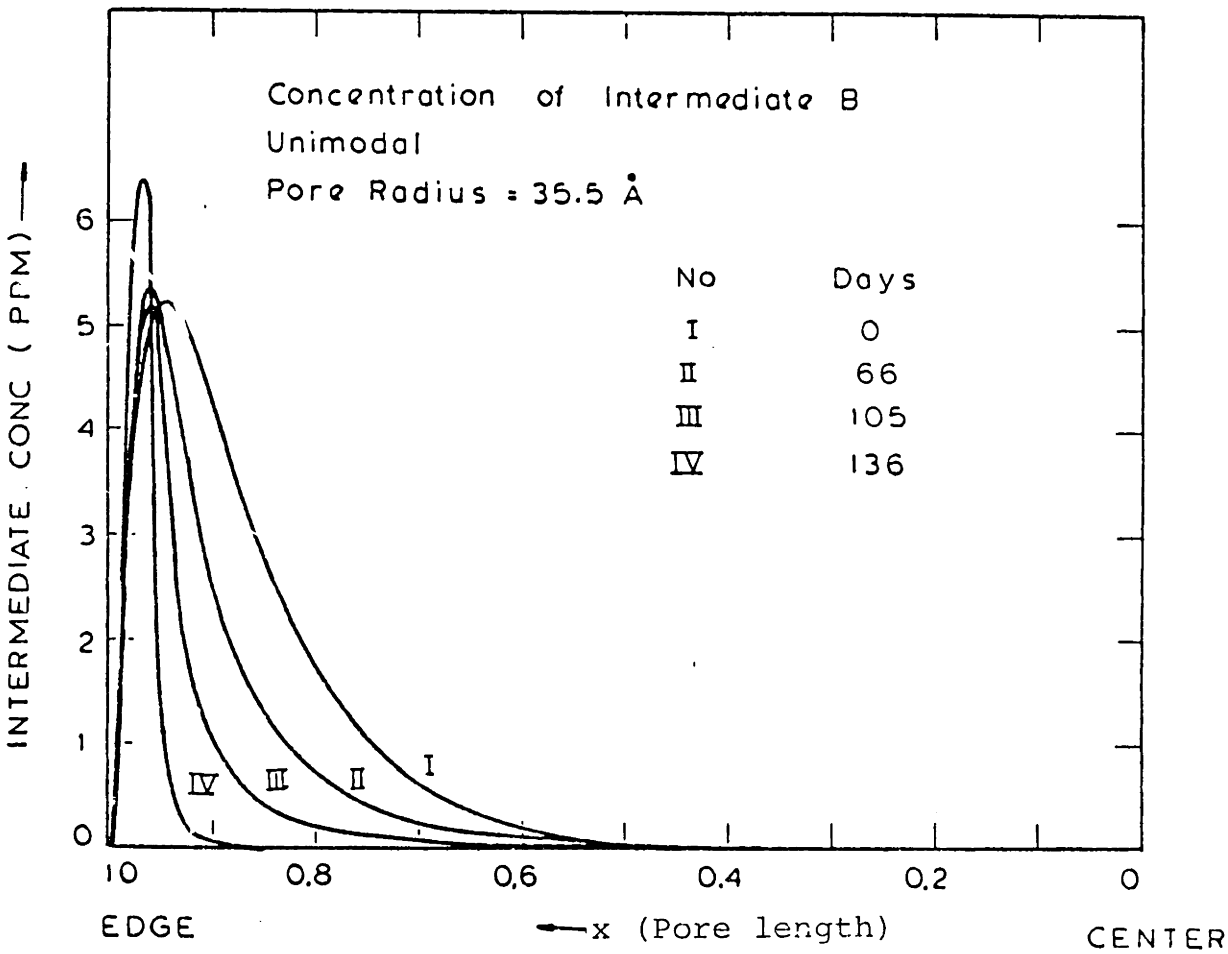

FIGURE VI-10: Concentration Profile of B in the Unimodal Catalyst at Various Reaction Times.

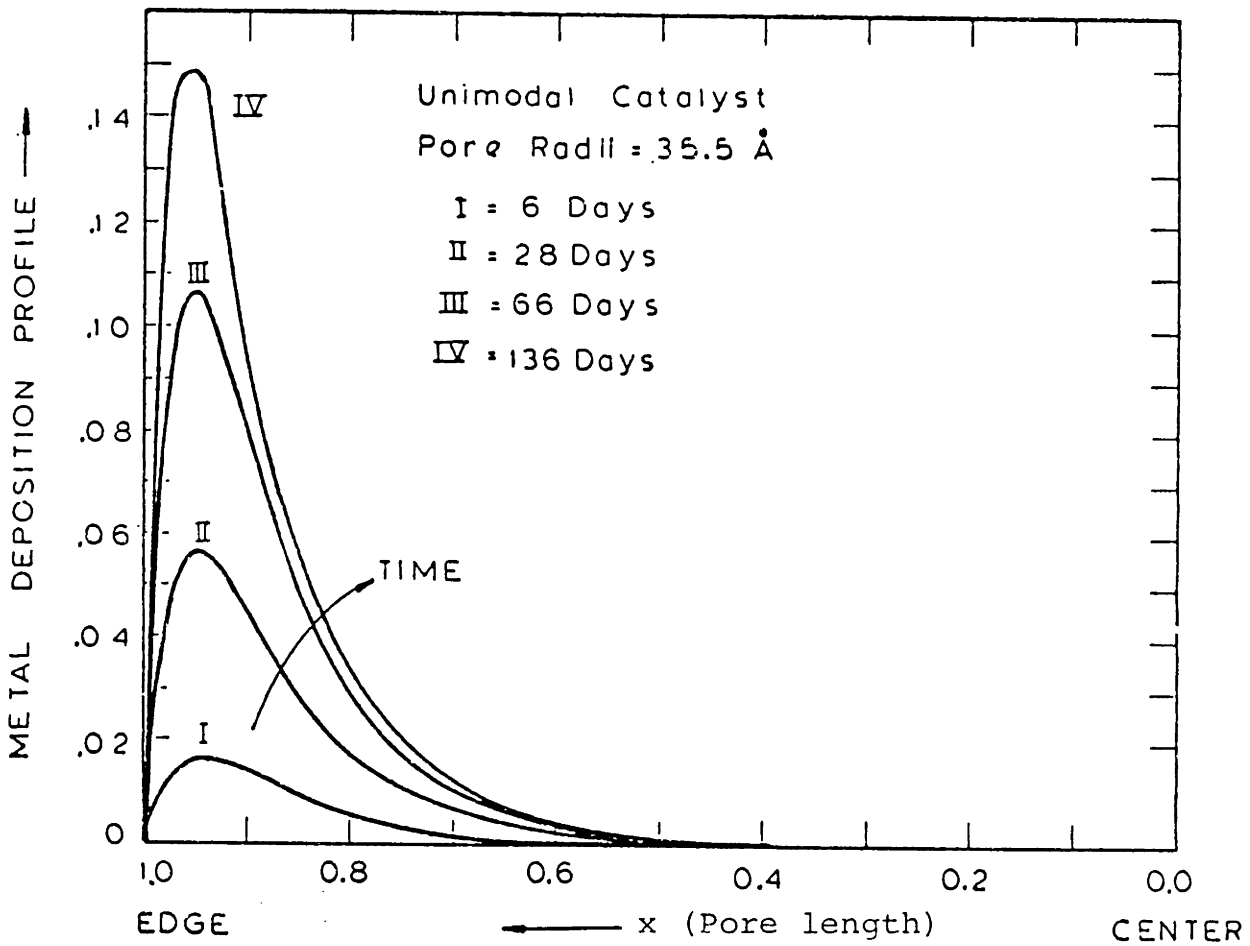

FIGURE VI-11: Progression of the Metal Deposition Profile in the Unimodal Catalyst with Days on Stream.

occurs near the edge of the catalyst and therefore after some reaction time a major central portion of the catalyst is unavailable for the reaction. Because of the boundary conditions of the problem, with elapse of reaction time, the pore plugging moves from inside to the outside of the catalyst and therefore the concentration profiles of A and B also move outward.

Another point to be noted is that for a given porosity, the variation in the pore sizes brings about the change in the initial reaction rate of the catalyst. The behaviour is similar to that of micropore size variation in the grain model. The result of the pore size on the initial rate is shown in fig. VI-2. It is seen that for our values of the physical parameters, the maximum in the rate is observed at the pore radius of 35.5 Å. It was this value of the pore size which was used in figures VI-9 to VI-11. Rajagopalan and Luss (1979) have pointed out that for a large value of Thiele modulus and the first order reaction, the maximum in the reaction rate is obtained when the pore radius is about five times of the molecular radius. It turns out that in our case molecular radius is 7.1 Å and the pore radius is 35.5 Å, which is also five times of the molecular radius. Since our kinetic system is also first order linearly coupled system, this agreement is not a surprise.

Now a comparison between the unimodal and the granular catalyst would be made. This would be done with reference to figure VI-12 and Table VI-1. With respect to the initial

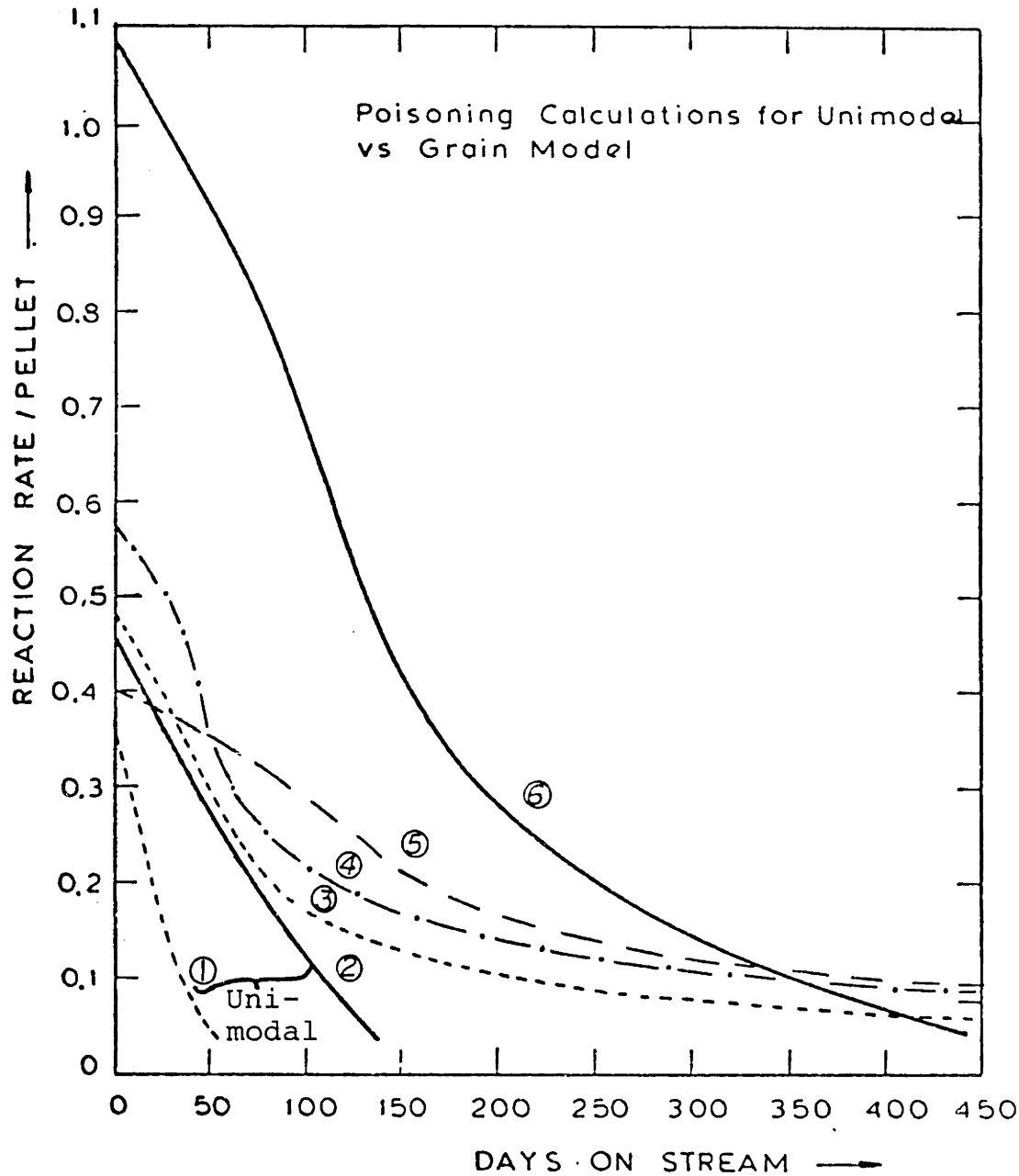

FIGURE V-12: Comparison of the Poisoning Behaviour of the Unimodal Model with the Grain model. The Curves are explained in Table VI-1.

TABLE VI-1

Poisoning Calculations for Unimodal and Bimodal catalysts

Curve #	MODEL	R_i	R_p	r_p	r_v	$m_p X 10^3$	m_v	T_S
1	U	--	18.0	0.37	179	0.23	0.11	36
2	U	--	35.5	0.46	223	0.80	0.39	110
3	G	42.5	18.0	0.49	321	1.19	0.78	204
4	G	1.0	15.9	0.58	380	1.83	1.20	340
5	G	42.5	35.5	0.40	264	2.00	1.31	391
6	G	42.5	35.5	1.08	707	3.99	2.61	357

where:

U = Unimodal catalyst model

G = Grain model

R_i = microsphere radius in micron

R_p = micropore radius in Å.

r_p = Initial rate/pellet

r_v = Initial rate/volume of catalyst material

[when r_p is corrected for the macropore volume, r_v is obtained].

m_p = gm of metal deposited/catalyst pellet

m_v = gm of metal deposited/volume of catalyst meterial

T_S = Days elapsed before the cutoff rate of r_p = 0.1 is achieved.

The value of $D_a \tau_i / \varepsilon_i D_o$ is 3.93 for curve ⑥, and for all others it is 0.52.

activity and overall life of the catalyst, a series of the questions can be asked and will be discussed one by one.

For a given porosity, a unimodal catalyst with the maximum initial activity is designed. This catalyst is then crushed and a pellet is made out of it. We will compare the performance of this pellet with respect to the original unimodal catalyst. In figure VI-12, curves ②, ⑤ and ⑥ provide such a comparison. Curve ② shows the activity of the unimodal catalyst. The parameters for this catalyst are same as in figures VI-9 to VI-11. For the catalyst porosity of 0.5, and the given values of other rate constants and physical parameters, the initial rate for this catalyst is maximum. When this catalyst is crushed and the pellet is made out of it, then the performance of the pellet would depend on the macropore diffusivities. Curves ⑤ and ⑥ are the results of the two values of the macropore diffusivities. For curve ⑥, $D_a\tau_i/\varepsilon_i D_o$ is about 4 and the simulation is the same as in figures VI-5 to VI-8. It is observed that as compared to the original unimodal catalyst the performance of this catalyst is phenomenal. The initial rate is 2.3 times more and the time on stream is about 3.2 times more (Table VI-1). However, more impressive fact is that per unit volume of the catalyst material, this catalyst can take 6.7 times more metal loading than the unimodal catalyst.

The phenomenal increase in the performance of the catalyst of curve ⑥ is attributed to high macropore diffusivity.

For the curve ⑤, the tortuosity in the macropore and the micropore are taken to be same, and therefore $D_a \tau_i / \varepsilon_i D_o = 0.52$. This time it is observed that the initial rate of the catalyst is about 87% of the unimodal catalyst. But in terms of the long range activity and the metal loading capacity, this catalyst is still much superior to the unimodal catalyst. Within 20 days of operation the activity of the bimodal pellet catches up with the original unimodal catalyst, and from then onwards it is always higher. As a comparison it can be seen from the figure VI-12 that at the time when unimodal catalyst has reached to the cutoff rate of 0.1 per pellet, the rate of the bimodal pellet is still 0.275 per pellet. From Table VI-1 it is observed that bimodal pellet can last on stream for 3.6 times more days and the metal loading per unit volume of the catalyst material is 3.4 times more than the unimodal catalyst.

The next question to consider is that whether it is possible with the assumption of tortuosity in macro and micropore same, to get the initial rate of bimodal pellet higher than the most optimum unimodal catalyst pellet. Curve ③ in figure VI-12 answers this question. For this curve the grain size is same as that of curves ⑤ and ⑥, but the micropore size has been chosen to be 18.0 Å. For this pore size the bimodal catalyst gives the maximum initial rate. It is seen that the curve ③ gives the rate always higher than curve ②. However, in terms of long

range activity and the metal loading, the performance of catalyst ⑤ was better than this one. It is interesting to compare the performance of the catalyst ③ with a unimodal catalyst of the same pore size. Curve ① shows the rate of the unimodal catalyst with pore size of 18.0 Å. It is seen that the performance of the unimodal catalyst ① is much worse than the unimodal catalyst ② , but the bimodal pellet ③ made out of catalyst ① shows performance better than the catalyst ② . It is easily understood from the fact that macropores provide channels to the microspheres made of catalyst ① , and the large surface area of the material of catalyst ① is utilized more efficiently.

It has already been seen in figure VI-2, that the value of the maximum initial rate increases with the decrease of the grain size. Therefore, even with the assumption of equal tortuosity of micro and macro pores it is possible to design a bimodal catalyst pellet which would give the initial rate much higher than the initial rate of the most optimum unimodal catalyst. Curve ④ in fig. VI-12 is such a catalyt. The pore and the grain sizes are 15.9 Å and 1.0 μ respectively. For the grain radius of 1.0 μ the maximum initial rate is obtained for the pore radius of 8.5 Å and the corresponding initial rate is 0.73/pellet. However, the reaction rate curve for this optimum pore size has not been plotted in figure VI-12.

Uptill now we have compared the catalysts such that the microporosity of the microspheres in the grain model is same as of the unimodal catalyst. Since macroporosity also contributes to the total porosity of the pellet, its total porosity would be higher than the unimodal catalyst and is given by:

$$\varepsilon_p = \varepsilon_i (1-\varepsilon_a) + \varepsilon_a \qquad \text{VI.26}$$

For all the simulation runs discussed uptill now the values of the microsphere and macropore porosities are 0.5 and 0.26 respectively. Therefore the net porosity of the catalyst pellets is 0.63.

Now we will compare the bimodal catalyst with a unimodal catalyst of the same porosity as the net porosity of bimodal catalyst pellet. The results are plotted in figure VI-13. For the porosity of 0.63, it is found that the maximum initial rate of the unimodal catalyst is given for a pore size of 35.5 Å; and its activity with days on stream is plotted as curve ① in fig. VI-13. We find that the initial activity of this unimodal catalyst is higher than the curve ② in figure VI-12. But by decreasing the grain size, we can always find a bimodal catalyst pellet which would give the initial rate higher than the unimodal catalyst. For the calculations of bimodal pellet, the tortuosity of the micro and macropores have taken to be same. For example when the grain radius is chosen to be 1 micron, then for the pore

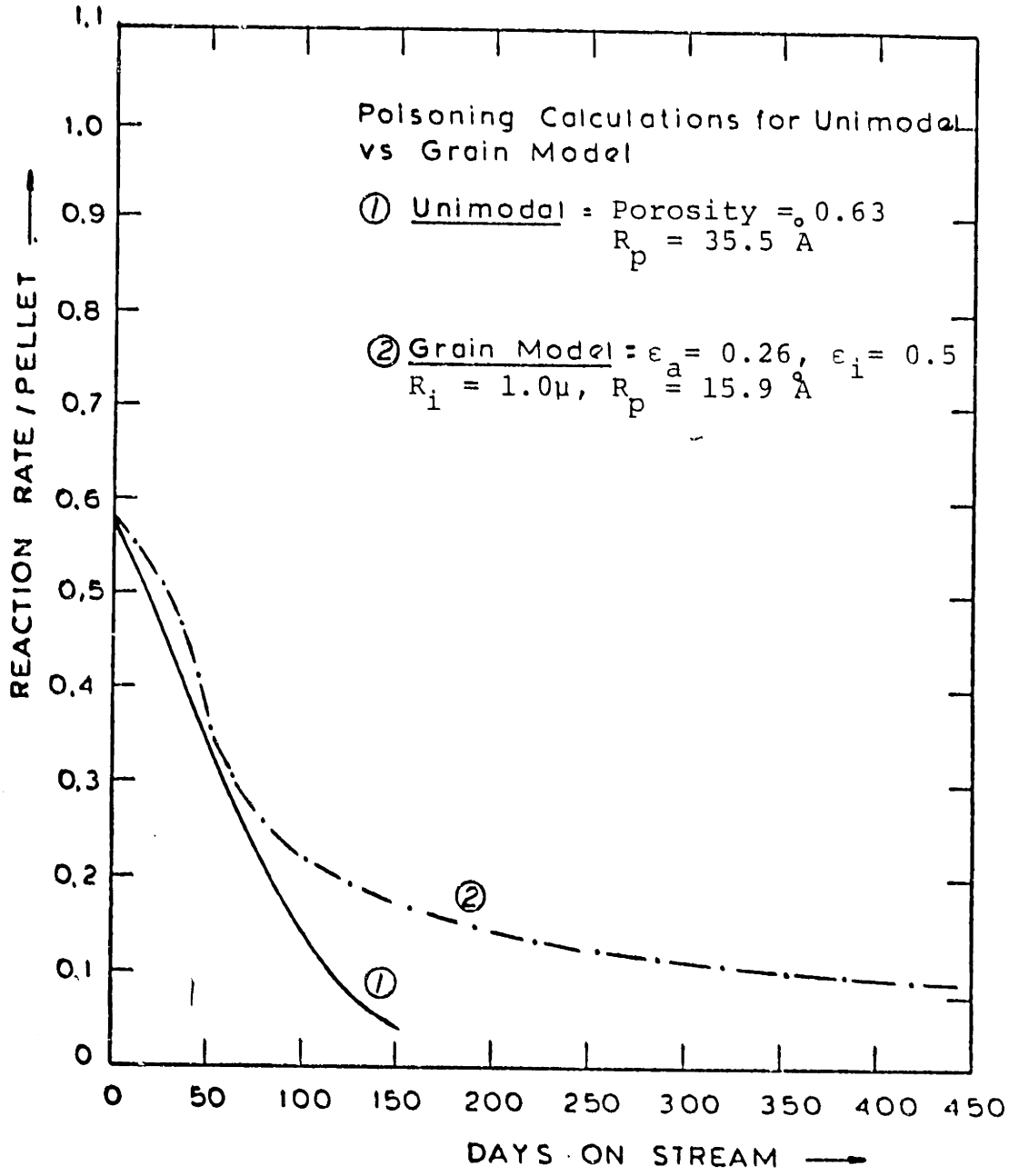

FIGURE VI-13: Comparison of the Unimodal Catalyst with the Bimodal Catalyst Pellet. The Net Porosity of both the Catalyst is same. For the Unimodal Catalyst: T_s=115 Days, m_v=0.48; and for Bimodal Catalyst See Curve ④ in Table VI-1.

radius of 8.5 Å the initial rate is 0.73/pellet and this rate is higher than 0.58 for the unimodal catalyst particle. For 1 micron grain radius the micropore size of 15.9 Å gives initial rate equal to the maximum of the unimodal catalyst. The catalyst pellet activity for this bimodal pellet is plotted as curve ② in figure VI-13. Even though both the catalyst ① and ② start with the same initial rate, the activity of the unimodal catalyst ① drops much faster. As compared to the catalyst ①, catalyst ② lasts 3 times more days on stream and the metal loading per unit of catalyst material volume is 2.5 times more. Therefore even on the basis of the net porosities of the catalyst particle, it is possible to design a bimodal catalyst particle which would give the performance better than the best unimodal catalyst.

One of the important conclusion of the Rajagopalan and Luss (1979) is that among all catalysts with the same surface area and porosity, the largest initial activity is attained for pellets with a uniform pore size. For a constant porosity, the variation in the uniform pore size would also bring about the changes in the surface area. In our search for the optimum unimodal catalyst, we vary the pore size to get the maximum in the initial rate. If the conclusion of these authors is valid to our reaction system, then the optimum unimodal catalyst will give the maximum possible initial reaction rate and any other pore size distribution would give lower values. We have already seen that for a bimodal catalyst with grain radius of 1 micron

and micropore radius of 8.5 Å the initial reaction rate is 1.26 times more than the unimodal catalyst ① of figure VI-13. for the grain model, tortuosity of the macro and micropore have been taken to be same. The values of the net porosities of the unimodal and bimodal catalyst particles are 0.63. Therefore, it is clear that the conclusion of the authors is not valid to our case.

Rajagopalan and Luss (1979) made the conclusion for the simple one step first order hydrodemetallation reation. Therefore at the first sight the nonapplicability of their conclusion to our case may be attributed to the difference in the reaction network. To check this assumption, simulation runs with the new values of the parameters are made. The new values are: $K_1 = 1.0X10^{-8}$, $K_2 = 1.0X10^{-10}$, $K_3 = 0.1$ ml/hr-meter^2; bulk solution concentration at the surface of the pellet are A = 0, B = 50 ppm; catalyst porosity of the unimodal catalyst = 0.63, for the grain model the porosities of the microsphere and macropores in the macrosphere are 0.5 and 0.26 respectively; and in grain model tortuosities of the micro and macropores are taken to be of same value. The values of the other parameters are same as in earlier simulations. The values of the rate constants and the boundary conditions are such that the one step first order reaction kinetics is simulated. With the grain radius of 1 micron and the micropore radius of 8.5 Å the initial rate for this bimodal catalyst pellet is 0.599/pellet. The size of the macropore radius can be

approximated by equation VI.10 and is 2342 Å and therefore according to the authors the harmonic pore radius can be calculated to be about 14.4 Å. If the conclusion of the authors is valid then the unimodal model with the pore size of 14.4 Å should give the reaction rate larger than 0.599/pellet. By varying the pore size of the unimodal catalyst the maximum possible initial reaction rate has been found out. For 35.5 Å pore radius, the unimodal model gives the rate of 0.528/pellet. For any other pore size (including 14.4 Å) the unimodal catalyst would have reaction rate lower than 0.528/pellet. We see that even the maximum possible initial rate for the unimodal catalyst is less than the bimodal catalyst rate of 0.599/pellet. It should be pointed out that by reducing the grain size and the pore size the initial rate obtained from the grain model can still be increased, eg. for a grain size of 0.25 micron and pore radius of 8.1 the initial reaction rate is 0.606/pellet. Therefore it is clear that the conclusion of the Rajagopalan and Luss (1979), that among all catalysts with the same surface area and porosity, the largest initial activity is attained for pellets with a uniform pore size is not universally valid. The authors used the parallel bundle model which does not allow for any connectivity of the pores. It may be that their conclusion is due to this inherent draw back of the parallel bundle model. Real catalysts have the pores interconnected and for the bimodal catalyst the suggested model is a better approximation.

Finally we conclude this chapter with the theoretical observation that for hydrodemetallation bimodal catalyst should be designed and used. In terms of the initial activity and also the long range activity, its performance is much better than the unimodal catalyst.

CHAPTER - VII

CONCLUSIONS

1. In the initial transient phase of the reactor, the activity of the catalyst first decreases, then increases and finally levels off. The increse in the activity can be attributed to the nickel and vanadium deposition on the catalyst, which leads to an increase in both the hydrogenation and demetallation activities.
2. In this study the maximum metal deposited on the catalyst in any single run was about 10 wt %. Once the catalyst has achieved its steady state activity, it is maintained for the rest of the run time. Therefore upto 10 wt % metal loading, there is no significant pore blockage.
3. Prior to the metal removal from the etioporphyrin ring, one major hydrogenated reaction intermediate is formed. For both the nickel and vanadium runs, the intermediates have been isolated and the corresponding peaks in the visible spectrum have been identified. The reaction intermediate for the nickel etio runs has been identified on mass spectrometer, and is found to be nickel etio chlorin.
4. In both nickel and the vanadium hydrodemetallation, three major kinetic steps are involved. The first step is hydrogenation to the reaction intermediate (rate constant k_1). The other two steps are dehydrogenation (rate

constant k_2) and the demetallation (rate constant k_3) of the reaction intermediate.

5. For both the metals, hydrogenation steps is first order with respect to the metal etioporphyrin concentration in the solution; and dehydrogenation and the demetallation rates have first order dependence on the reaction intermediate concentration in the solution. The order of dependence of hydrogenation, dehydrogenation and demetallation rates on the hydrogen pressure are first, zero and second respectively.
6. For the hydrodemetallation of nickel Etioporphyrin-I, the activation energies of k_1, k_2 and k_3 have been found to be 17.1, 22.9, and 32.6 kcal/g mole respectively. In case of vanadyl Etioporphyrin-I, the activation energies of k_1, k_2 and k_3 are 18.3, 16.5 and 24.9 kcal/g mole respectively.
7. In the concentration range of metal in solution studied, it is found that in case of vanadium the rate constants k_1, k_2 and k_3 are independent of the inlet solution concentrations to the reactor. However in case of nickel, all the three rate constants are found to be inversely proportional to the inlet solution concentration to the reactor. An attempt to explain this behavior by a Langmuir-Hinshelwood type kinetic expression has been made. This model assumes the adsorption of the final metal free product molecule. Since the final product has not been identified, the validity of the proposed model could not be checked.

8. For nickel, the total metal disappearance rate from the solution can also be adequately expressed as the single step, irreversible, first order kinetics. However, the same cannot be done for the vanadium.
9. Metal deposition profiles in 1/16 inch catalyst extrudates, at various reactor bed positions, have been studied. At the entrance of the bed, the maximum in the metal deposition occurs inside the catalyst and not at its external surface. In the middle and the top sections of the bed, the maxima moved to the external surface, and the metal deposition profiles look like the classical U shape profiles.
10. At the entrance of the bed, the location of the internal maxima inside the catalyst depends on the temperature and the pressure of the operation. Low temperature and low hydrogen pressure lead to inward movement of the maxima. Under identical conditions of operation, for vanadium the internal maxima is much better defined and is more inside the catalyst than the nickel.
11. Theoretical calculations to simulate the continuous reactor data with intraparticle mass transport limitations have been made. Both nickel and the vandyl etio porphyrins have diffusivities of the order of 10^{-6} cm^2/sec. This order of magnitude agrees with theoretically estimated value of the diffusion coefficient. For vanadium, depending on the temperature of the operation, the reaction intermediate has 3 to 5 times

higher diffusivity than the vanadyl etioporphyrin. For nickel, both the etio and the chlorin have the same diffusivities.

12. Theoretical calculations are not only successful in giving the proper values of the concentrations of the reactor outlet solutions but are also successful in adequately describing the metal deposition profiles in the catalyst particles at various bed locations.
13. Theoretical poisoning models to predict the initial and the long range activity of the unimodal and bimodal catalysts have been proposed. The calculation results show that for hydrodemetallation, bimodal catalyst pellets have much better performance. They not only have a higher initial rate, but also much higher catalyst life time. The bimodal catalyst can take many times more metal loading than the unimodal catalysts.
14. One important result of the new theoretical poisoning model is that it challenges a claim of the model developed by Rajagopalan and Luss (1979). Their conclusion that among all catalysts with the same surface area and porosity, the largest initial activity is attained for pellets with a uniform pore size, is not universally valid. The authors did not allow for the connectivity of the pores at all, whereas the new model allows for some connectivity.

CHAPTER-VIII

RECOMMENDATIONS

1. The catalysts were not aged for long enough reaction times. Therefore runs of 10-30 days long should be made. It will give useful information on the configurational diffusion resistance. Also a higher metal loading on the catalyst would be obtained and therefore the analytical errors would be minimized.
2. Surface area and the pore size distribution of the used catalyst should be measured.
3. Nuclear magnetic resonance and the electronic spin resonance studies of the used catalyst surface should be done. It would give information on the chemical state of the metal deposited on the catalyst surface.
4. Diffusional studies with some substance whose molecular diameter is close to the porphyrin molecule diameter should be done on the used and fresh catalysts. This would give information on the change in the tortuosity of the catalyst with metal loading.
5. Carbon deposition profile in the reactor should be studied.
6. The mixture of nickel and vanadium compounds should be run. Due to the great difference in the adsorptivity of each compound, some interference results are anticipated.

7. Further careful separation of the reaction intermediate should be done. From the chemistry point of view, it would lead to a better understanding of the reaction mechanism.
8. The increase in the catalyst activity should be further studied. Instead of Cobalt-molybdenum catalyst, some nickel loaded catalysts on alumina support should be used for nickel runs and vanadium loaded catalysts for vanadium runs.
9. Synthesize the reaction intermediates and runs with different relative inlet metal compound concentrations of A and B should be made. This would verify the model more strongly.
10. The poisoning model has been developed for one catalyst particle. It can be extended to simulate the whole reactor bed. This would enable one to predict the performance of the whole reactor with days on stream. Moreover, this model should be checked with the experimental results.
11. The grain model developed shows that the bimodal catalyst performance is much better than the unimodal catalyst. Catalyst pellets from the crushed powder of the presently used catalyst should be made and long runs to test the theoretical results should be made.
12. Studies with the controlled pore size catalysts should be made. This would give a good information on the mechanism of the pore blockage and therefore also on the

configurational diffusion resistance. This would also give information on whether with metal deposition, the activity per unit surface area of the pore remains constant or not.

13. For all this information to be of industrial significance, studies with pretreatment of the catalyst with hydrogen sulfide should be made. Some carbon disulfide should be added to the solution feed of the reactor.
14. Papers in the literature show that there is some relation between the hydrodemetallation and the hydrodesulfurization. It would be interesting to run the hydrodesulfurization of some of the sulfur compounds like thiophene, dibenzothiophene, etc. on pure Co-Mo catayst and then on the catalysts which already have some nickel or vanadium loading. This can be easily achieved by the proper use of the two autoclaves in the present apparatus set up. These results would be of industrial relevance.

NOMENCLATURE

The following is a list of generalized nomenclature used in this thesis. In some cases temporary alternate definitions may be specified within the text.

A = concentration of model metal etioporphyrin in solution (parts per million by weight, ppm)

A_a = concentration of model metal etioporphyrin inside the macrosphere pores

A_i = concentration of model metal etioporphyrin inside the idealized cylindrical micropore

a = concentration of model metal etioporphyrin inside the catalyst extrudate pores

B = concentration of the reaction intermediate in the solution (ppm)

B_a = concentration of the reaction intermediate inside the macrosphere pores

B_i = concentration of the reaction intermediate inside the idealized cylindrical micropore

b = concentration of the reaction intermediate inside the catalyst extrudate pores

C = The final metal free reaction product from the metal etioporphyrin

C_b = concentration of the reactant in the bulk fluid

C_f = effluent concentration of the reactant

C_o = initial concentration of the reactant

C_p = solution heat capacity

D = restricted diffusivity in the pore

D_A = effective diffusivity of A in the catalyst extrudate

D_B = effective diffusivity of B in the catalyst extrudate

D_{eff} = effective diffusivity of the species in the catalyst

D_o = bulk solution diffusivity

D_a = effective diffusivity in the macrosphere

D_i = effective diffusivity in the microsphere

d_c = diameter of the extrudate catalyst

d_p = diameter of the catalyst in the micro reactor

d_s = equivalent spherical diameter of a cylindrical catalyst

E = activation energy

h = heat transfer coefficient between fluid and particle

K_1, K_2, K_3 = rate constants per unit surface area of the catalyst

k = rate constant $\left(\frac{\text{ml of solution}}{\text{g of cat. hr.}}\right)$

k_1 = first order rate constant for hydrogenation step

k_2 = first order rate constant for dehydrogenation step

k_3 = first order rate constant for the metal removal step

k_{1s}, k_{2s}, k_{3s} first order rate constants defined in terms of surface concentrations on the catalyst surface

k_A, k_B, k_p = adsorption constants for A, B and the final metal free reaction product C respectively

k_c = mass transfer coefficient between fluid and the solid catalyst

k_T = solution thermal conductivity

L = length of the idealized micropores

L_b = catalyst bed length including diluent

l_c = length of the catalyst extrudate

M = total metal concentration in solution

m_d = wt. % metal deposition on the catalyst

$\bar{m}_d$ = net weight averaged metal deposition on the catalyst

m_p = g. of metal deposited/catalyst pellet

m_v = g. of metal deposited/volume of catalyst material

N_p = number of micropores in a microsphere

n = number of microspheres per unit volume of macrosphere

Q = solution flow rate (ml/hr)

R = radius of the pore at any time

R_a = radius of the macrosphere

R_c = radius of the catalyst particle

R_g = universal gas constant

R_i = radius of the microspheres

R_m = radius of the metallo molecules diffusing

R_p = initial radius of the micropore

r_A = kinetic rate for A

r_B = kinetic rate for B

r_a = radial distance in macrosphere

r_i = radial distance in microspheres

r_p = initial rate of metal deposition/pellet

r_v = initial rate of metal deposition/volume of the catalyst material

$[S]$ = number of active sites on the catalyst surface

T = real time (hours)

T_s = reaction time elapsed before the cut off rate for the pellet is approached

t = W/Q, contact time $\left(\frac{\text{g. cat. hr.}}{\text{cm}^3}\right)$

V = volume of the solution in batch autoclave

v = superficial solution velocity

W = weight of the catalyst (g.)

x = length coordinate for an idealised micropore

α = ratio of molecular radius to pore radius (eq. VI.2)

δ = relative percent error in the conversion

ε_a = macropore porosity of the macrosphere

ε_b = bed void fraction

ε_i = micropore porosity of the microsphere

ε_p = net porosity of the bimodal catalyst pellet

μ = solution viscosity

ρ = solution density

ρ_c = bulk density of the catalyst

ρ_m = density of the metal deposited on the surface

τ_a = macropore tortuosity

τ_i = micropore tortuosity

BIBLIOGRAPHY

Adams, C.R., Sartor, A.F. and Welch, J.G., AIChE Symposium Series-143, 70, 49 (1974).

Anderson, R.B., "Experimental Methods in Catalytic Research", Chapter 1, Academic Press, New York, N.Y., (1968).

Arey, W.F., Jr., Blackwell, N.E. III and Reichle, A.D., Seventh world Petroleum Congress, P. 167, (1967).

Audibert, F., and Duhaut, P., Paper at the 35th mid year meet of the American Pet. Inst., Div. of Refining, Houston, Texas, May 13-15 (1970).

Baker, E.W., J. of Am. Chem. Soc., 88 (10), 2311 (1966).

Baker, E.W., and Palmer, S.E., "The Porphyrins", Vol I, Chap. II, edited by Dolphin D., Academic Press (1978).

Baker, E.W., Yen, T.F., Dickie, J.P., Rhodes, R.E., and Clark, L.F., J. of Am. Chem. Soc., 89 (14), 3631 (1967).

Berti, V. et al., Riv. Combust, 29 (4), 121 (1975).

Beuther, H., Schmid, B.K., Proc. 6th world Petrol. Cong., Sec. III, Paper 20, pp. 1-11 (1963).

Bhinde, M.V., "Quinoline Hydrodenitrogenation Kinetics & Reaction - Inhibition", Ph.D. Thesis, University of Delaware, U.S.A. (1979).

Bienert, R., and Gelbin, D., Chem. Tech. (Berlin), 19, 207 (1967).

Blumer, M., and Rudrum, M., J. of the Inst. of Pet., 57 (548), 99 (1970).

Bridge, A.G., and Green, D.C., Div. of Pet. Chem., ACS Preprint, 24 (3), 791 (1979).

Broderick, D.H., "Catalytic Hydrodesulfurization of Organic Sulfur Compounds", Doctoral dissertation, University of Delaware, 1979.

Brunn, L.W., Montagna, A.A., and Paraskos, J.A., Div. of Pet. Chem., ACS Preprint, 20 (4), 762 (1975).

Cecil, R.R., Mayer, F.X., Cart, E.N., Paper presented at Am. Inst. Chem. Engr. Meeting, Los Angeles, 1968.

Chang, C.D., and Silvestri, A.J., Ind. Eng. Chem., Process Des. Dev., 13 (3), 315 (1974).

Chang, C.D., and Silvestri, A.J., Ind. Eng. Chem., Process Des. Dev., 15 (1), 161 (1976).

Chao, K.C., and Seader, J.D., AIChE J., 7, 598 (1961).

Chervenak, M.C., Maruhnic, P., and Nongbri, G., U.S. Environmental Protection agency, report no. EPA-650/2-73-041-a (1975).

Chervenak, M.C., Maruhnic, P., and Nongbri, G., U.S. Enviromental Protection agency, report no. EPA-600/2-76-165 (1976).

Copeland, T.M., "Equilibrium Partitioning and Counterdiffusion of Polystyrenes in Fine Pores", Ph.D. Thesis, Mass. Inst. of Technology, Cambridge (1978).

Costantinides, G., and Guido, A., Sixth World Petroleum Congress, Section 5, Paper 11, (1963).

Cukor, P.M., and Prausnitz, J.M., The J. of Phys. Chem., 76 (4), 598 (1972).

Dautzenberg, F.M., Van Klinken, J., Pronk, K.M.A., Sie, S.T., and Wijffels, J.B., ACS Symposium Series, 65, 254 (1978).

Dean, R.A., and Whitehead, E.V., Proceedings Sixth World Petroleum Congress, Section V, Paper 9, June 1963.

Dickie, J.P., Hallers, M.N., and Yen, T.F., J. of Colloid and interface Science, 29 (3), 475 (1969).

Difford, A.M.R. and Spencer, M.S., A.I.ChE. Symposium Series-143, 70, 42 (1974).

Dolphin, D., Editor of "The Porphyrins", Vol. 1-VII, Academic Press (1978).

Doraiswamy, L.K., Tajbl, D.G., Catal. Rev. Sci. Eng., 10, 177 (1974).

Doyle, G., Div. of Pet. Chemistry Inc., ACS, 21 (1), 165 (1976).

Dudukovic, M.P., and Mills, P.L., ACS Symposium Series, 65, 387 (1978).

Edison, R.R., Siemssen, J.O., and Masologites, G.P., The Oil and Gas Journal, pp. 54, Dec. 20 (1976).

Eliezer, K.F., Bhinde, M., Houalla, M., Broderick, D., Gates, B.C., Katzer, J.R. and Olson, J.H., Ind. Eng. Chem., Fundam., 16 (3), 380 (1977).

Evans, R.M., "An Introduction to Color", pp. 107-108, John Wiley & Sons (1948).

Ferry, J.D., J. of General Physiology, 20, 95 (1936).

Fiero, G.W., Annals of Allergy, 23, 226 (1965).

Filby, R.H., Div. of Pet. Chem., ACS Preprint, 18 (4), 630 (1973).

Fischer, R.H., Garwood, W.E., and Heinemann, H., Ind. Eng. Chem., Proc. Des. & Dev., 15 (4), 570 (1970).

Fischer, R.H. and Milstein, D., U.S. Patent No. 4,016,067, (1977).

Fleischer, E.B., J. Amer. Chem. Soc., 85 (2), 146 (1963).

Franks, A.J., Soap, Perfumery and Cos., pp. 221, March, (1964-a).

Franks, A.J., Soap, Perfumery and Cos., pp. 319, April, (1964-b).

Fuhrhop, J.H., Z. Naturforsch, 25b, 255 (1970).

Goto, S., and Smith, J.M., AIChE J., 21 (4), 706 (1975).

Grayson, H.G., and Streed, C.W., Proc. of Sixth world Pet. Congress in Frankfurt/Main, Section VII, paper 20, 169 (June 1963).

Greensfelder, B.S., Voge, H.H., and Good, G.M., Ind. Eng. Chem., 37, 1168 (1945).

Gültekin, S., "Effect of Hydrogen Sulfide on the Kinetics of Hydrodenitrogenation of Quinoline and Its Reaction Intermediates in Vapor Phase", Ph.D. Thesis, M.I.T., Cambridge, U.S.A. (1980).

Habib, E.T., Owen, H., Snyder, P.W., Streed, C.W. and Venuto, P.B., Presented at AIChE 83rd National Meeting, Houston (1977).

Haensel, V., Adv. in Catalysis, 3, 179 (1951).

Prof. P. Hambright, Howard University, Washington, D.C.-Private Communications.

Hardin, A.H., Packwood, R.H., and Ternan, M., Div. of Pet. Chem., ACS Preprint, 23 (4), 1450 (1978).

Hashimoto, N., and Smith, J.M., Ind. Eng. Chem., Fundam., 13 (2), 115 (1974).

Hashimoto, N., Moffat, A.J., and Smith, J.M., AIChE J , 22 (5), 944 (1976).

Hastings, K.E., James, L.C. and Mounce, W.R., The Oil and Gas Journal, pp. 122-130, June 30, (1975).

Herskowitz, M., and Smith, J.M., Part I and II, AIChE J., 24 (3), 439 (1978).

Himmelblau, D.M., Jones, C.R., and Bischoff, K.B., I&EC Fundamentals, 6 (4), 539 (1967).

Hodgson, G.W., and Baker, B.L., Bull. of the Am. Ass. of Pet. Geologists, 41 (11), 2413 (1957).

Hodgson, G.W., Baker, B.L., and Peake, E., Seventh world petroleum Congress, 9, 117 (1967).

Hofstader, R.A., Milner, O.I., and Runnels, J.H., "Analysis of Petroleum for Trace Metals", Advances in Chemistry Series, 156 (1976).

Hung, C.W., "The Kinetics of Hydrodemetallation of Metalloporphyrins", Ph.D. Thesis, M.I.T., Cambridge, U.S.A. (1979).

Inoguchi, M., Nishiyama, R., Satomi, Y., Mizutori, T., Inaba, K., Kagaya, H., Tate, K., Hosaka, K., Niume, K., and Ota, T., Bull. Japan Pet. Inst., 13 (1), 3 (1971-a)

Inoguchi, M., Inaba, K., Satomi, Y., Mizutori, T., Sakurada, S., Kagaya, H., Nishiyama, R., Tate, K., Onishi, S., and Nagai, T., Bull. Japan Pet. Inst., 13 (1), 11 (1971-b)

Inoguchi, M., Kagaya, H., Daigo, K., Sakurada, S., Satomi, Y., Inaba, K., Tate, K., Nishiyama, R., Onishi, S., and Nagai, T., Bull. Japan Pet. Inst., 13 (2), 153 (1971-c)

Kerber, J.D., Applied Spectroscopy, 20 (4), 212 (1966).

Komiyama H., and Smith, J.M., AICHE J., 20 (4), 728 (1974).

Kubo, J., Oil and Gas J., 73, 105 (Aug. 18, 1975).

Kurito, S., Watanabe, T., Satori, H., Nishizaki, S., Takayami, N., Tabuchi, K., Sakuma, J., Bull. Japan Petr. Inst., 13, 169 (1971).

Kwan, T., and Sato, M., Nippon Kagaku Zasshi, 91 (12), 1103 (1970).

Lang, S.I., Vavrecka, P., Sychra, V. and Weisser, O., Analytica Chimica Acta, 78, 99 (1975).

Larson, O.A., and Beuther, H., Div. of Pet. Chem., ACS Preprint, 11 (2), B95 (1966).

Loev. B., and Goodmand, M.M., "Progress in Separation and Purification", vol. 3, pp. 73-95, Editors: Perry, E.S. and Van Oss, C.J., John Wiley & Sons (1970).

Ma, Y.H., and Ho, S.Y., AIChE J., 20 (2), 279 (1974).

Ma, Y.H., and Lee, T.Y., AIChE J., 22 (1), 147 (1976).

Ma, Y.H., and Lee, T.Y., I&EC Fundamentals, 16 (1), 44 (1977).

Manning, D.C., Perkin-Elmer Atomic Absorption Newsletter, 4 (4), 267 (1975).

Massagutov, R.M., Berg, G.A., Kulinich, G.M., and Kirillov, T.S., Proceedings of Seventh World Petroleum Congress, pp. 177, Elsevier Publishing Co. LTD (1967).

Mears, D.E., Chem. Eng. Sci., 26, 1361 (1971).

Mears, D.E., Ind. Eng. Chem., Process Des. Dev., 10 (4), 541 (1971).

Meyer, E., "White Mineral Oil and Petrolatum and Related Products", Chemical Publishing Company (1968).

Millensifer, T.A., The Oil and Gas Journal, pp. 82 (MAR.28, 1977).

Moore, E.J., Milner, O.I., and Glass, J.R., Microchemical Journal, 10, 148 (1966).

Mosby, J.F., Hochatro, C.B., Kleinheinz, T.A., Stroke, J.M., Hydrocarbon Process, 94 (May 1973).

Nelson, W.L., "Petroleum Refinery Engineering", 4th Edition, McGraw Hill (1974).

Nelson, W.L., The Oil and Gas Journal, pp. 191 (NOV. 8, 1976).

Nelson, W.L., The Oil and Gas Journal, pp. 247 (May 2, 1977).

Newson, E.J., Preprints, 17 (2), pp. 49-63, Div. of Fuel Chem., 164th National Meeting of the Am. Chem. Soc., New York, N.Y., Aug. 27-Sept. 1, 1972.

Newson, E., Ind. Eng. Chem., Proces. Des. Dev., 14 (1), 27 (1975).

Oleck, S.M., and Sherry, H.S., Ind. Eng. Chem., Process Des. Dev., 16 (4), 525 (1977).

Örs, N., and Dogu, T., AIChE J., 25 (4), 723 (1979).

Oxenreiter, M.F., Frye, C.G., Hoekstra, G.B., and Sroka, J.M., Paper presented at the Japanese Pet. Inst., Nov. 1972.

Perry, R.H. and Chilton, C.H., "Chemical Engineers Handbook", Fifth Edition, McGraw Hill (1973).

Petersen, E.E., Chemical Reaction Analysis, Prentice Hall, Englewood Cliffs, N.J. (1965).

Pigford, R.L., and Sliger, G., Ind. Eng. Chem., Process Des. Develop., 12 (1), 85 (1973).

Pitcher, W.H., Jr., "Restricted Diffusion in Liquids within Fine Pores", Sc.D. Thesis, Mass. Inst. of Technology, Cambridge (1972).

Prather, J.W., Ahangar, A.M., Pitts, W.S., Henley, J.P., Tarrer A.R., and Guin, J.A., I&EC, Proc. Des. and Dev., 16 (3), 267 (1977).

Purnanik, S.S., and Vogelpohl, A., Chem. Eng. Science, 29, 501 (1974).

Rajagopalan, K., and Luss, D., Ind. Eng. Chem., Proc. Des. Dev., 18 (3), 459 (1979).

Renkin, E.M., J. of General Physiology, 38 (2), 225 (1954).

Richardson, R.L., and Alley, S.K., Div. of Pet. Chem., ACS Preprint, 20 (2), 554 (1975).

Riediger, B., International Chemical Engineering, 16 (2), 203 (1976).

Riley, K.L., Div. of Pet. Chem., ACS Preprint, 23 (1), 81 (1978).

Rosscup, R.J., Bowman, D.H., Preprint A-77, Div. of Pet. Chem., 153rd national Meeting of the ACS, Miami Beach, Fla., April, 1967.

Rosscup, R.J., and Pohlmann, H.P., Div. of Pet. Chem., ACS, Miami Beach Meeting, April 9-14 (1967).

Rovesti, W.C., and Wolk, R.H., U.S. Enviromental Protection agency, report no. EPA-650/2-73-041 (1973).

Ruckenstein, E., Vaidyanathan, A.S. and Youngquist, G.R., Chemical Engineering Science, 26, 1305 (1971).

Saraceno, A.J., Fanale, D.T., and Coggeshall, N.D., Analytical Chemistry, 33, 500 (1961).

Sato, M., Kwan, T., Shimizu, Y., Inoue, K., Koenuma, Y., Nishikata, H., Takenuma, Y., Aizawa, R., Kobayashi, S., Egi, K., and Matsumoto, K., Pollution Control, 5 (2), 121 (1970).

Sato, M., Takayoma, N., Kurita, S., and Kwan, T., Nippon Kagaku Zasshi, 92 (10), 834 (1971).

Satterfield, C.N., AIChE J., 21 (2), 209 (1975).

Satterfield, C.N., Colton, C.K. and Pitcher, W.H., Jr., AIChE Journal, 19 (3), 628 (1973).

Schuit, G.C.A., and Gates, B.C., AIChE J., 19 (3), 417 (1973).

Schwartz, J.G., Weger, E., and Dudukovic, M.P., AIChE J., 22 (5), 953 (1976).

Shah, Y.T., and Paraskos, J.A., Ind. Eng. Chem., Proc. Des. and Dev., 14 (4), 368 (1975).

Shah, Y.T., Stiegel, G.J., and Sharma, M.M., AIChE J., 24 (3), 369 (1978).

Simnick, J.J., Liu, K.D., Lin, H.M., and Chao, K.C., Ind. Eng. Chem., Proc. Des. Dev., 17 (2), 204 (1978).

Smith, A.J., Rice, O.J., Shaner, W.C., Jr., and Cerato, C.C., Div. of Pet. Chem., ACS Preprint, 18, 609 (1973).

Smith, H.M., Dunning, H.M., Rall, H.T., and Ball, J.S., Paper-24th Mid year Meeting of API Division of Refining, New York City, May 29, 1959.

Smith, K.M., Editor of "Porphyrins and Metalloporphyrins", Elsevier (1975).

Sohn, H.Y., and Szekely, J., Chemical Engineering Science, 27, 763 (1972).

Sohn, H.Y., and Szekely, J., Chemical Engineering Science, 29, 630 (1974).

Sokolov, V.I., and Polyakov, A.A., J. of Applied Chemistry of the USSR, JAPUAW 50 (6), 1347 (1977).

Specchia, V., Baldi, G., and Gianetto, A., Ind. Eng. Chem., Process Des. Dev., 17 (3), 362 (1978).

Spry, J.C., Jr., and Sawyer, W.H., Paper presented at Sixty-Eighth annual AIChE Meeting, Los Angeles, Calif., Nov. 16-20, 1975.

Steenbergen, C., "Chemical and Process Technology Encyclopedia", edited by D.M. Considine, McGraww Hill (1974).

Sugihara, J.M., Branthaver, J.F., Wu, G.Y., and Weatherbee, C., Div. of Pet. Chem., ACS Preprint, 15 (2), C5 (1970).

Sylvester, N.D., Kulkarni, A.A., and Carberry, J.J., The Canadian J. of Chem. Eng., 53, 313 (1975).

Szekely, J., Lin, C.I., and Sohn, H.Y., Chemical Engineering Science, 28 (11), 1975 (1973).

Tamm, P.W., Harnsberger, H.F., and Bridge, A.G., Paper presented at the 72nd annual meeting of AIChE, San Francisco, California (1979).

Todo, N., Kabe, T., Ogawa, K., Kurita, M., Sato, T., Sihmada, K., Kuriki, Y., Oshima, T., Takematsu, T., and Kotera, Y., Kogyo KagaKu Zasshi, 74 (4), 563 (1971).

Treibs, A., Ana. Chem., 49, 682 (1936).

Tremper, K.K. and Prausnitz, J.M., J. of Chem. & Eng. Data, 21 (3), 295 (1976).

Trent, D., and Slavin, W., Atomic Absorption Newsletter, 3 (10), 131 (1964).

Van Dongen, R.H., Chemical Engineering of Gas-Liquid-Solid Catalyst Reactions, Ch-9, Guy A.L'Homme Editor, CEBEDOC, Liège, Belgium (1979).

Weekman, V.W., Chemical Reaction Eng. Proc. Int. Symp., pp. 615-646, (1976).

Wei, J., J. of Catalysis, 1, 526 (1962-a).

Wei, J., J. of Catalysis, 1, 538 (1962-b).

Wei, J., and Prater, C.D., Adv. Catalysis, 13, 203 (1962).

Weisz, P.B., Doctoral Dissertation, Swiss Federal Institute of Technology, Zurich (1966).

Weisz, P.B., and Hicks, J.S., Chem. Eng. Sci, 17, 265 (1962).

Wheeler, A., Adv. in Cat., 3, 249 (1951).

Yen, T.F., Erdman, J.G., and Pollack, S.S., Analytical Chemistry, 33, 1587 (1961).

Yen, T.F., Boucher, L.J., Dickie, J.P., Tynan, E.C., and Vaughan, G.B., Div. of Pet. Chem., ACS Preprint, 13 (1), 59 (1968).

Yen, T.F., Boucher L.J., Dickie, J.P., Tynan, E.C. and Vaughan, G.B., J. of the Institute of Petroleum, 55 (542), 87 (1969).

Yen, T.F., The Role of Trace Metals in Petroleum, Ann Arbor Science Publishers Inc., Michigan (1975).

APPENDIX - I

ASSESSMENT OF POSSIBLE HEAT AND MASS TRANSFER LIMITATIONS IN THE REACTORS

Since some of the results of the microreactor will also provide the basis for the one inch reactor, we would first do calculations for the microreactor. The physical properties have been estimated by the help of Table III-2 and Chemical Engineer's Handbook (Perry and Chilton - 1973) and are listed below for the temperature range of 600-650^{o}F:

Viscosity = $\mu = 0.062 \times 10^{-2}$ g/sec. cm.

Density = $\rho = 0.70$ g/cm^3

Heat Capacity = $C_p = 0.7$ cal/gm^{o}C

Thermal conductivity = $k_T = 2.6 \times 10^{-4}$ cal/cm sec^{o}C

Prandtl No. = $Pr \equiv \frac{C_p \mu}{k_T} = 1.67$

All the following calculations are based on the work of Mears (1971).

A. Micro Reactor Calculations:

(1) Intraparticle Transport: The catalyst particles have to be small enough such that there are no intraparticle transport limitations. One can do the calculations based on the various criteria given by Mears. However for HDM, in the form of metal deposition, the history of the reaction is

imprinted on the catalyst. Hung (1979) studied the metal deposition profiles for the various sizes of the catalyst and found that in the size range of 170-200 mesh (.088 mm - .074 mm) fairly uniform profiles were obtained. Since under our reaction conditions the rates are even slower, the use of particles of the same sizes ensures the absence of intra-particle limitations.

(2) Interparticle Transport: Generally interparticle heat resistance becomes limiting and leads to radial temperature gradiant in the tube. Dilution of the catalyst with inert solids is helpful because it decreases the ratio of catalyst volume to wall area for heat transfer. In our case radial aspect ratio (D/d_p) is around 60-70 and we may be able to neglect the heat transfer resistance at the wall. For interparticle heat resistance to be not limiting first:

$$\frac{(1-\varepsilon_b)}{(1+b)} \left(\frac{hd_p}{k_e}\right) \frac{D}{d_p} < 5.3$$

Where ε_b = bed void fraction, b = ratio of diluent to catalyst volume, h = heat transfer coefficient between fluid and particle, d_p = diameter of catalyst in micro-reactor, k_e = effective thermal conductivity across reactor bed and D = reactor diameter.

For a flow rate of about 14 ml/hour the value of h is estimated from the following correlation

$$j_H \equiv \frac{h}{C_p \rho v}\Big) \, P_r^{2/3} = 1.15 \left(\frac{\rho v d_p}{\mu}\right)^{-1/2}$$

to be 0.116 cal/cm^2 sec ^{o}C. Thus for the required criterion

$$\frac{1-\varepsilon_b}{1+b} < 0.35$$

for $\varepsilon_b = 0.3$ we have b>1. Therefore minimum value of the ratio of diluent to catalyst volume is 1.

The upper bound value for b is due to by passing effects in the bed and is calculated by satisfying the following criterion:

$$\frac{L_b}{d_p} > 250\ \frac{b}{\delta}$$

where L_b = bed length including diluent, and δ = relative percent error in the conversion. For relative error of 1% and bed length of 12 cm, b should be less than 5.5. Thus for our case

1 <Ratio of diluent to catalyst volume < 5.5

Another important interparticle resistance may be in axial direction. The axial dispersion effects are minimized by increasing the bed length. For first order reaction the criterion is:

$$\frac{L_b}{d_p} > \frac{20}{Pe_a}\ \ln\ \frac{C_o}{C_f}$$

where Pe_a = axial Peclet number based on particle diameter, C_o = initial concentration of the reactant and C_f = effluent concentration of the reactant. For liquid at low Reynolds number $Pe_a \simeq 0.5$, and for C_o = 30 ppm and C_f = 1 ppm we get:

$$L_b > 1.2 \text{ cm.}$$

For this minimum value of bed length we have L_b/d_p = 136.4 which is greater than 30 and the flow is nearly a plug flow and we can neglect the axial heat conduction effects.

(3) Interphase Transport: Since, after catalyst dilution, interparticle heat resistance cannot be the limiting one, it is necessary to check the heat transfer resistance from the fluid to the catalyst particle. For interphase heat resistance to be negligible the following criterion should be satisfied:

$$\left|-\Delta H\right| \frac{(\text{Rate/particle volume})\ d_p}{h\ T_b} < 0.3\ \frac{R_g T_b}{E}$$

where ΔH = Heat of the reaction, R_g = Gas constant, and T_b = bulk solution temperature. For the highest value of observed rate at 30 ppm and $T_b \simeq 315^{\circ}C$ and E = 35 Kcal/g-mole it is required that

$|-\Delta H| < 630$ Kcal/g mole.

But 630 Kcal/g mole is very high heat of reaction and we anticipate that interphase heat transfer resistance is negligible.

For interphase mass transfer not to be limiting DamKöhler number should satisfy following criterion:

$$\text{DamKöhler number} = \frac{(\text{Rate/particle volume})\ d_p}{2C_b\ k_c} < 0.15$$

where C_b = concentration of reactant in bulk fluid, and k_c = mass transfer coefficient between fluid and the particle. From Stokes-Einstein equation it is estimated that the bulk diffusivity of a molecule of diameter 14.2 Å in Nujol at 315°C is 10^{-4} cm^2/sec. With this value of diffusivity it is estimated (Perry and Chilton - 1973) that k_c = 0.0078 cm/sec. By using the maximum reaction rate at 30 ppm concentration the value of Damköhler number calculated is about 0.004 which is much less than 0.15. Therefore, we definitely do not have interphase mass transfer resistance.

B. ONE INCH REACTOR CALCULATIONS:

(1) Intraparticle: As is clear from the experimental metal deposition profiles in the 1/16" catalyst extrudates, we do have severe intraparticle mass transfer limitation. In

order to estimate intraparticle heat resistance Weisz and Hicks (1962) criterion is used. The values of the effective diffusivity in the catalyst and the thermal conductivity of the catalyst used are 10^{-6} cm^2/sec and $0.51X10^{-3}$ cal/sec cm ^oC respectively. For intraparticle heat transfer resistance to be important the heat of the reaction should be greater than $6.3X10^4$ kcal/gmole. Since this is a very large number, we definitely do not have intraparticle heat limitation.

(2) Interparticle: As discussed in section III.D., we satisfy the radial and axial aspect ratio criteria of Doraiswamy and Tajble (1974), and therefore have plug flow situation. In order to see if any dilution of the catalyst bed to reduce radial temperature gradient is necessary, calculations similar to microreactor are made. For flow rate of 20 ml/hr it is estimated that the value of heat transfer coefficient between fluid and particle is 0.00103 cal/cm^2 sec^oC. Therefore the required criterion is:

$$6.92\left(\frac{1-\varepsilon_b}{1+b}\right) < 5.3$$

The above criterion for b=o requires that $\varepsilon_b > 0.23$. Since the normal value of bed void volume is 0.4, there is no need for catalyst dilution. However, in order to increase the bed length so that there are no axial dispersion effects the value of the ratio of diluent to catalyst volume used is 2.5. This value of b obviously satisfies the above criterion. Thus we do not have any interparticle limitations.

(3) Interphase: When calculations similar to the micro-reactor are done for the interphase heat transfer limitations it turns out that heat of the reaction should be lower than about 30 kcal/g mole. Since this number is not very large there exist a finite possibility that we might have some interphase heat transfer resistance. However, due to the uncertainity in the value of the heat of the reaction, we would neglect this resistance in our modelling.

Calculation of the Damköhler number, with the catalyst effectiveness factor of 0.1, gives its value of about 0.04 which is less than 0.15. Therefore we do not have any significant external fluid to solid surface mass transfer resistance.

APPENDIX-II

SOLUTION OF THE KINETIC MODEL RATE EQUATIONS

The proposed model is:

$$A \underset{k_2}{\overset{k_1}{\rightleftharpoons}} B \xrightarrow{k_3} \text{Metal Deposition on Catalyst}$$

The pertinent rate equations for the first order dependence on the metal concentrations in the solution are:

Total metal concentration $M = A+B$ A.II.1

$$\frac{dM}{dt} = -k_3 B \qquad \text{A.II.2}$$

$$\frac{dB}{dt} = k_1 M - (k_1 + k_2 + k_3) B \qquad \text{A.II.3}$$

Define:

$$\Sigma k = k_1 + k_2 + k_3 \qquad \text{A.II.4}$$

$$\underline{\underline{K}} \equiv \begin{bmatrix} 0 & -k_3 \\ k_1 & -\Sigma k \end{bmatrix} \qquad \text{A.II.5}$$

In Matrix notation:

$$\frac{d}{dt}\begin{bmatrix} M \\ B \end{bmatrix} = \underline{\underline{K}} \begin{bmatrix} M \\ B \end{bmatrix} \qquad \text{A.II.6}$$

The above equations are solved by the classical analysis of Wei and Prater (1962). The eigenvalues of the $\underline{\underline{K}}$ matrix are

$$\lambda_+, \lambda_- = \frac{-\Sigma k \pm [\Sigma k^2 - 4\, k_1 k_3]^{1/2}}{2} \qquad \text{A.II.7}$$

The eigenvectors corresponding to λ_+ and λ_- are:

$$\begin{bmatrix} -k_3 \\ \overline{\lambda_+} \\ 1 \end{bmatrix} \quad \text{and} \quad \begin{bmatrix} \lambda_- + \Sigma k \\ \overline{k_1} \\ 1 \end{bmatrix} \qquad \text{A.II.8}$$

For the initial condition that at $t = 0$, $M = M_o$ and $B = 0$ the solution is:

$$\begin{bmatrix} M \\ \\ B \end{bmatrix} = C_1 \begin{bmatrix} -k_3 \\ \overline{\lambda_+} \\ 1 \end{bmatrix} e^{\lambda_+ t} \quad -C_1 \begin{bmatrix} \lambda_- + \Sigma k \\ \overline{k_1} \\ 1 \end{bmatrix} e^{\lambda_- t} \qquad \text{A.II.9}$$

where

$$C_1 = - \frac{M_o}{\left[\frac{k_3}{\lambda_+} + \frac{\lambda_- + \Sigma k}{k_1}\right]} \qquad \text{A.II.10}$$

Method of nonlinear least squares can be used for equations A.II.7, A.II.9 and A.II.10 to evaluate the rate constants from the experimental data.

Since $\lambda_+ > \lambda_-$ (we are not considering the case when $\lambda_+ = \lambda_-$), it can be readily shown from the equation A.II.9 that:

$$\lim_{t \to \infty} \left[\frac{B}{M}\right]_1 = \frac{-\lambda_+}{k_3} \qquad \text{A.II.11}$$

If it is assumed that $\frac{dB}{dt} = 0$, then from equation A.II.3:

$$\left[\frac{B}{M}\right]_2 = \frac{k_1}{\Sigma k} \qquad \text{A.II.12}$$

For a thermodynamic equilibrium:

$$\left[\frac{B}{M}\right]_3 = \frac{k_1}{k_1 + k_2} \qquad \text{A.II.13}$$

It must be emphasized that no assumption was made for the equation A.II.11, and whether equation A.II.12 holds or not, at large contact times equation A.II.11 must agree with the experimental data. $\left[\frac{B}{M}\right]_1$ and $\left[\frac{B}{M}\right]_2$ both are the result of dynamic equilibrium considerations.

A. THE ADHOC MODEL: An attempt to explain the model in terms of adsorption on the catalyst sites is made. As discussed in section IV.B.2 the main assumptions involved are:

(i) All three, the metal Etioporphyrin, the chlorin and final product after the metal removal are adsorbed on the catalyst active sites. For each of these compounds, the surface concentration is in equilibrium with the concentration in the solution.

(ii) Hydrogen is either not adsorbed on the catalyst surface, or if adsorbed it does on the sites where none of the other porphyrin related compounds are adsorbed.

(iii) Kinetic steps are the rate controlling steps.

(IV) Sites where metal has deposited are either still active or the metal deposition does not change the total number of sites involved in the chemical reaction significantly.

If S stands for the empty reaction sites on the catalyst surface:

$$A + S \rightleftharpoons AS$$

$$B + S \rightleftharpoons BS$$

$$AS + H_2 \underset{k_{2s}}{\overset{k_{1s}}{\rightleftharpoons}} BS$$

$$BS + S \xrightarrow{k_{3s}+2H_2} \text{Metal.S.} + CS$$

$$CS \rightleftharpoons C + S$$

where C is the final metal free product; AS, BS and CS are the surface concentrations of A, B and C respectively, Metal.S. is the deposition of metal atom on the site S and k_{1s}, k_{2s} and k_{3s} are the first order rate constants in terms of surface concentrations. From assumption (i) it follows:

$$S_o = S + AS + BS + CS$$

$$[S] = \frac{S_o}{1+k_A A + k_B B + k_P C} \qquad \text{A.II.14}$$

where [S] is the number of empty active steps, S_o is the total number of active sites, k_A, k_B and k_p are the adsorption constants for A, B and C respectively. Since we always start with pure A, therefore at any given time:

$$C = M_o - A - B \qquad \text{A.II.15}$$

Substitution in eq. A.II.14 yields

$$[S] = \frac{S_o}{1+A\ [k_A-k_p] + B\ [k_B-k_p] + k_p\ M_o} \qquad \text{A.II.16}$$

In case of nickel runs, two possible assumptions can be made-(i) all the adsorption constants are approximately equal and it leads to:

$$[S] = \frac{S_o}{1+k_A M_o} \qquad \text{A.II.17}$$

or (ii) the concentration of B is so small that B $\left[k_B-k_p\right]$ can be neglected and $k_A \simeq k_p$. This assumption will also give equation A.II.17.

For nickel runs it can also be assumed that for our concentration range of M_o we have $k_A M_o >> 1$, then

$$[S] = \frac{S_o}{k_A M_o} \qquad \text{A.II.18}$$

For vanadium runs it is assumed that in the denominator of eq. A.II.16, all the terms other than 1 are negligible. This assumption implies that the total number of active sites basically remain unchanged due to the adsorption of A, B and C. Thus eq. A.II.16 reduces to:

$$[S] = S_o \qquad \text{A.II.19}$$

From assumption (iii), the kinetic rates r_A and r_B for A and B are:

$$r_A = -k_{1s} P_{H_2} k_A [S] A + k_{2s} k_B [S] B$$

$$r_B = k_{1s} P_{H_2} k_A [S] A - k_{2s} k_B [S] B - k_{3s} P_{H_2}^2 k_B [S] B$$

Thus the bulk rate constants expressed in terms of surface constants are:

$$\begin{aligned} k_1 &\equiv k_{1s} k_A [S] P_{H_2} \\ k_2 &\equiv k_{2s} k_B [S] \\ k_3 &\equiv k_{3s} k_B [S] P_{H_2}^2 \end{aligned} \qquad \text{A.II.20}$$

For nickel the value of [S] is given by eq. A.II.18 and for vanadium by eq. A.II.19.

B. <u>POSSIBLE EFFECT OF THE ADSORPTION ON THE RATE CONSTANTS EVALUATED FROM BATCH DATA</u>: If the adsorption effects are strong then the changes in the amount of the species on the catalyst surface have to be taken into account. Assuming instantaneous adsorption equilibrium between the catalyst surface and the bulk solution, we can develop the following expressions for our adhoc model.

Say W grams of catalyst are added to the V ml volume of the solution. Then change in the amount of A in the bulk solution in time T to T + ΔT is:

$$V\ (A\big|_{T+\Delta T} - A\big|_{T})$$

Amount of A lost from the catalyst surface to the bulk solution:

$$W\ [(AS\big|_{T} - AS\big|_{T+\Delta T}) - k_1 A + k_2 B]$$

where k_1 and k_2 are given by equation A.II.20. Equating the two expressions and substituting for the surface concentrations in terms of bulk concentrations and letting $\Delta T \rightarrow 0$:

$$-\frac{V}{W}\frac{dA}{dT} = \frac{1}{(1+\frac{W}{V}k_A[S])}\ (-k_1 A + k_2 B) \qquad \text{A.II.21}$$

The rate constants evaluated from the experiments would be the actual rate constants divided by $(1+\frac{W}{V}k_A\ [S]\ )$. The magnitude of the error would depend on the value of the adsorption constant. The best way to check the magnitude of the error is to change the catalyst loading term W/V and observe the value of the rate constant.

APPENDIX - III

EXPERIMENTAL DATA FROM SOME OF THE MICROREACTOR RUNS

In this appendix some of the kinetic data for the nickel and vanadyl Etioporphyrin (I) runs are tabulated. Some of the pertinent data for the one inch reactor are already summarized in the tables of Chapter V; however, for more details on these data and the metal deposition profiles, the author may be contacted.

For the tables of this appendix, the units of temperature, pressure, amount of catalyst in reactor, inlet concentration, flowrate Q and rate constants are ^{o}C, psig, gms, ppm by weight, ml/hr. and ml of solution/gm of cat.-hr respectively. M is the total metal concentration and is obtained by atomic absorption spectrophotometer, and B is the concentration of the reaction intermediate. These concentrations are in ppm by weight.

The first letter M of the run number MANE-3 (III) stands for microreactor, A for American Cynamid HDS-16A catalyst extrudates and NE for nickel etioporphyrin. Similarly for the run MAVE-2, letters VE stand for vanadyl etioporphyrin.

Section A has the data for the nickel runs and the section B for the vanadium runs.

A. Data for the Nickel Etioporphyrin (I) runs.

RUN NO.=MANE-3(III)

TEMPERATURE=343.0 PRESSURE=1400.0
AMOUNT OF CATALYST IN REACTOR=0.4311
INLET CONCENTRATION=27.0

Q	M	B
39	22.3	3.01
30	21.9	2.81
16	18.3	2.25
10	14.4	1.75
6	7.2	0.92
4	3.7	0.56
3	2.4	0.47

CALCULATED RATE CONSTANTS= 39.8,153.5,146.2,

RUN NO.=MANE-5(II)

TEMPERATURE=288.0 PRESSURE=1400.0
AMOUNT OF CATALYST IN REACTOR=0.8214
INLET CONCENTRATION=25.0

Q	M	B
34	24.4	4.69
16	22.4	4.76
10	20.9	4.35
4	16.6	3.10
3	14.2	2.54
2	12.7	2.22

CALCULATED RATE CONSTANTS= 9.0, 28.0, 10.0,

RUN NO.=MANE-5(III)

TEMPERATURE=302.0 PRESSURE=1400.0
AMOUNT OF CATALYST IN REACTOR=0.8214
INLET CONCENTRATION=25.0

Q	M	B
34	23.7	5.04
16	20.8	4.74
10	18.4	4.15
6	16.8	3.85
5	15.3	3.33
4	13.5	2.86
3	10.8	2.32
2	7.9	1.64

CALCULATED RATE CONSTANTS= 14.4, 37.2, 16.2,

RUN NO.=MANE-5(IV)

TEMPERATURE=315.0 PRESSURE=1400.0
AMOUNT OF CATALYST IN REACTOR=0.8214
INLET CONCENTRATION=25.0

Q	M	B
34	23.1	4.29
20	20.6	3.92
14	19.2	3.76
10	17.6	3.42
8	12.9	2.38
6	11.3	2.18
5	9.5	1.63

CALCULATED RATE CONSTANTS= 21.1, 60.0, 33.4,

RUN NO.=MANE-8(III)

TEMPERATURE=343.0 PRESSURE=1000.0
AMOUNT OF CATALYST IN REACTOR=0.5712
INLET CONCENTRATION=27.8

Q	M	B
39	22.7	2.80
24	20.4	2.50
16	17.1	2.10
10	15.4	1.80
6	10.2	1.20
5	6.6	0.80
3	3.2	0.40

CALCULATED RATE CONSTANTS= 25.4,118.0, 95.1,

RUN NO.=MANE-8(IV)

TEMPERATURE=329.0 PRESSURE=1000.0
AMOUNT OF CATALYST IN REACTOR=0.5712
INLET CONCENTRATION=26.0

Q	M	B
28	22.0	2.97
10	17.5	2.42
2	5.4	0.68

CALCULATED RATE CONSTANTS= 19.2, 76.3, 43.1,

RUN NO.=MANE-13(II)

TEMPERATURE=315.0 PRESSURE= 600.0
AMOUNT OF CATALYST IN REACTOR=1.1676
INLET CONCENTRATION=26.5

Q	M	B
24	25.4	3.00
10	23.4	2.85
4	19.3	2.43
2	14.5	1.85

CALCULATED RATE CONSTANTS= 9.0, 48.3, 8.0,

RUN NO.=MANE-13(III)

TEMPERATURE=343.0 PRESSURE= 600.0
AMOUNT OF CATALYST IN REACTOR=1.1676
INLET CONCENTRATION=27.0

Q	M	B
34	23.9	2.64
20	23.2	2.57
10	19.3	2.22
6	15.7	1.87
4	12.2	1.45
3	9.5	1.19

CALCULATED RATE CONSTANTS= 17.0,125.0, 27.1,

RUN NO.=MANE-13(IV)

TEMPERATURE=329.0 PRESSURE= 600.0
AMOUNT OF CATALYST IN REACTOR=1.1676
INLET CONCENTRATION=26.0

Q	M	B
34	24.3	2.57
16	21.9	2.53
10	20.3	2.32
6	16.8	2.14
2	9.1	1.30

CALCULATED RATE CONSTANTS= 13.6, 81.1, 15.9,

RUN NO.=MANE-14(III)

TEMPERATURE=343.0 PRESSURE=1000.0
AMOUNT OF CATALYST IN REACTOR=0.5710
INLET CONCENTRATION=16.3

Q	M	B
39	11.3	1.60
22	9.0	1.18
14	6.3	0.82
6	1.9	0.32
5	0.8	0.08

CALCULATED RATE CONSTANTS= 57.7,228.0,201.8,

RUN NO.=MANE-14(IV)

TEMPERATURE=329.0 PRESSURE=1000.0
AMOUNT OF CATALYST IN REACTOR=0.5710
INLET CONCENTRATION=15.0

Q	M	B
39	12.2	1.57
22	10.2	1.53
14	9.4	1.44
10	6.6	1.10
6	4.6	0.67
5	3.4	0.40
3	1.8	0.22

CALCULATED RATE CONSTANTS= 39.4,159.8, 99.7,

RUN NO.=MANE-14(V)

TEMPERATURE=315.0 PRESSURE=1000.0
AMOUNT OF CATALYST IN REACTOR=0.5710
INLET CONCENTRATION=14.5

Q	M	B
34	13.4	1.50
16	11.4	1.35
10	8.5	1.11
6	6.7	1.04
4	4.0	0.69
2	1.9	0.39

CALCULATED RATE CONSTANTS= 27.8, 91.9, 51.0,

B. Data for the Vanadyl Etioporphyrin (I) runs.

RUN NO.=MAVE-2

TEMPERATURE=343.0 PRESSURE=1400.0
AMOUNT OF CATALYST IN REACTOR=0.4300
INLET CONCENTRATION=25.0

Q	M	B
39	17.3	4.07
24	15.0	4.34
16	6.9	2.15
14	6.6	2.10
10	1.0	0 30

CALCULATED RATE CONSTANTS= 80.0, 81.0,170.0,

RUN NO.=MAVE-3(II)

TEMPERATURE=288.0 PRESSURE=1400.0
AMOUNT OF CATALYST IN REACTOR=0.7473
INLET CONCENTRATION=28.0

Q	M	B
39	26.4	5.93
14	22.0	6.06
10	18.9	5.71
6	15.7	4.74

CALCULATED RATE CONSTANTS= 16.0, 22.0, 20.2.

RUN NO.=MAVE-3(III)

TEMPERATURE=302.0 PRESSURE=1400.0
AMOUNT OF CATALYST IN REACTOR=0.7473
INLET CONCENTRATION=22.5

Q	M	B
39	21.6	5.56
20	16.6	4.97
10	10.1	3.04
8	8.7	2.92

CALCULATED RATE CONSTANTS= 25.7, 30.0, 37.0,

RUN NO.=MAVE-6(II)

TEMPERATURE=343.0 PRESSURE= 600.0
AMOUNT OF CATALYST IN REACTOR=0.9570
INLET CONCENTRATION=22.0

Q	M	B
30	19.8	3.12
22	17.2	3.39
12	12.3	2.83
10	10.8	2.73
8	9.3	2.09
4	4.4	1.75

CALCULATED RATE CONSTANTS= 30.0, 83.0, 33.0,

RUN NO.=MAVE-7(II)

TEMPERATURE=343.0 PRESSURE=1400.0
AMOUNT OF CATALYST IN REACTOR=0.3170
INLET CONCENTRATION=22.5

Q	M	B
39	17.7	4.06
26	16.4	3.98
20	14.9	3.72
14	9.8	2.72

CALCULATED RATE CONSTANTS= 71.6, 82.2,155.4,

RUN NO.=MAVE-8(III)

TEMPERATURE=288.0 PRESSURE=1400.0
AMOUNT OF CATALYST IN REACTOR=0.4943
INLET CONCENTRATION=15.9

Q	M	B
24	15.4	4.26
14	12.2	3.84
10	13.5	4.21
4	7.2	2.35
2	5.8	1.97

CALCULATED RATE CONSTANTS= 17.0, 20.0, 18.0,

RUN NO.=MAVE-9(III)

TEMPERATURE=315.0 PRESSURE=1400.0
AMOUNT OF CATALYST IN REACTOR=0.5019
INLET CONCENTRATION=24.0

Q	M	B
39	20.2	5.17
10	14.4	3.76
6	7.2	2.63
4	4.5	1.86
2	2.1	1.20

CALCULATED RATE CONSTANTS= 34.2, 41.7, 48.1,

RUN NO.=MAVE-9(V)

TEMPERATURE=343.0 PRESSURE=1000.0
AMOUNT OF CATALYST IN REACTOR=0.5019
INLET CONCENTRATION=25.0

Q	M	B
39	21.4	4.75
26	18.8	4.78
16	16.4	4.67
6	4.2	1.49
4	0.6	0.0

CALCULATED RATE CONSTANTS= 51.0, 81.5, 77.3,

APPENDIX - IV

LISTINGS OF THE PERTINENT COMPUTER PROGRAMS

In this appendix four computer programs, written in FORTRAN, are listed.

Section A is the listing of program BIS3. This program is used to calculate rate constants k_1, k_2 and k_3 for the kinetic data by Himmelbau-Jones-Bischoff (HJB - 1967) technique.

Section B is the program BEDCONC1 and is used to calculate, for the given values of the diffusivities, the exit solution concentration from the one inch reactor and also the metal deposition profiles in the catalyst at various reactor bed positions.

Sections C and D are the programs to do the poisoning calculations for the bimodal and unimodal catalysts respectively.

The input parameters for each of these programs are explained in the beginning of the respective programs.

A. Program to calculate rate constants k_1, k_2 and k_3 for the kinetic data by Himmelbau-Jones-Bischoff (HJB - 1967) technique.

```
FILE: BIS3     FORTRAN  A                    CONVERSATIONAL MONITOR SYSTEM

C THIS PROGRAM CALCULATES RATE CONSTANTS K1,K2,AND K3 BY                BIS00010
C HJB METHOD                                                            BIS00020
C                                                                       BIS00030
C  RAKESH AGRAWAL       CHEM. ENGG.       M.I.T.                       BIS00040
C                                                                       BIS00050
C ND=NO. OF DATA POINTS,WC=WT. OF CAT,IP=NO. OF TIME INTERVALS          BIS00060
C 1=TOTAL METAL,2=CHLORIN                                               BIS00070
C THIS PROGRAM USES BISCHOFS TECHNIQUE                                  BIS00080
C***************************************                                BIS00090
C PROGRAM USES ICSICU,DCSQDU,LINV2F AND VMULFF PROGRAMS.                BIS00100
C THESE ARE INTERNATIONAL MATHEMATICAL AND STATISTICAL                  BIS00110
C LIBRARIES,INC. (IMSL) PACKAGES.                                       BIS00120
C ICSICU=INTERPOLATORY APPROXIMATION BY CUBIC SPLINES WITH              BIS00130
C ARBITRARY SECOND DERIVATIVE END CONDITIONS.                           BIS00140
C DCSQDU=INTEGRATE A CUBIC SPLINE BETWEEN LIMITS A AND B                BIS00150
C LINV2F=INVERSION OF A MATRIX-FULL STORAGE MODE-HIGH                   BIS00160
C ACCURACY SOLUTION                                                     BIS00170
C VMULFF=MATRIX MULTIPLICATION-FULL STORAGE MODE                        BIS00180
C***************************************                                BIS00190
      DIMENSION T(50),C(50,2),Y(50,2),X(50,2,4),W(2),A(3,3),G(3,1),B(3,1BIS00200
     &),XI(2),YI(2),CI(1,3),BPAR(4),AINV(3,3),WKAREA(28),CI1(1,3),TITLE(BIS00210
     &20)                                                               BIS00220
      READ(5,1100)TITLE                                                 BIS00230
      READ(5,*)ND,WC                                                    BIS00240
      READ(5,*)T(1),C(1,1),C(1,2)                                       BIS00250
      Y1=0.0                                                            BIS00260
      Y2=0.0                                                            BIS00270
      IP=0                                                              BIS00280
      DO 10 I1=2,ND                                                     BIS00290
      READ(5,*)T(I1),C(I1,1),C(I1,2)                                    BIS00300
      IP=IP+1                                                           BIS00310
      Y(IP,1)=C(I1,1)-C(1,1)                                            BIS00320
      Y(IP,2)=C(I1,2)-C(1,2)                                            BIS00330
      Y1=Y1+Y(IP,1)                                                     BIS00340
 10    Y2=Y2+Y(IP,2)                                                    BIS00350
      WRITE(6,1100)TITLE                                                BIS00360
      DO 5 KWC=1,ND                                                     BIS00370
 5    T(KWC)=T(KWC)*WC                                                  BIS00380
      Y1=Y1/IP                                                          BIS00390
      Y2=Y2/IP                                                          BIS00400
      NX=2                                                              BIS00410
      IC=1                                                              BIS00420
      W(1)=0.0                                                          BIS00430
      W(2)=0.0                                                          BIS00440
      DO 20 I=1,IP                                                      BIS00450
      X(I,1,1)=0.0                                                      BIS00460
      X(I,1,2)=0.0                                                      BIS00470
      X(I,2,4)=0.0                                                      BIS00480
      XI(1)=T(I)                                                        BIS00490
      I1=I+1                                                            BIS00500
      XI(2)=T(I1)                                                       BIS00510
      YI(1)=C(I,2)                                                      BIS00520
      YI(2)=C(I1,2)                                                     BIS00530
      AL=XI(1)                                                          BIS00540
      AU=XI(2)                                                          BIS00550
```

FILE: BIS3 FORTRAN A CONVERSATICNAL MONITOR SYSTEM

```
      BPAR(1)=0.0                                                    BIS00560
      BPAR(2)=0.0                                                    BIS00570
      BPAR(3)=0.0                                                    BIS00580
      BPAR(4)=0.0                                                    BIS00590
      CALL ICSICU(XI,YI,NX,BPAR,CI,IC,E1)                            BIS00600
      CALL DCSQDU(XI,YI,NX,CI,IC,AL,AU,Q,E2)                         BIS00610
      X(I,1,3)=Q                                                     BIS00620
      YI(1)=C(I,1)-YI(1)                                             BIS00630
      YI(2)=C(I1,1)-YI(2)                                            BIS00640
      BPAR(1)=0.0                                                    BIS00650
      BPAR(2)=0.0                                                    BIS00660
      BPAR(3)=0.0                                                    BIS00670
      BPAR(4)=0.0                                                    BIS00680
      CALL ICSICU(XI,YI,NX,BPAR,CI1,IC,E3)                           BIS00690
      CALL DCSQDU(XI,YI,NX,CI1,IC,AL,AU,Q1,E4)                       BIS00700
      X(I,2,1)=Q1                                                    BIS00710
      W(1)=W(1)+(Y(I,1)-Y1)**2                                       BIS00720
      W(2)=W(2)+(Y(I,2)-Y2)**2                                       BIS00730
20     CONTINUE                                                      BIS00740
      W(1)=1.0/SQRT(W(1))                                            BIS00750
      W(2)=1.0/SQRT(W(2))                                            BIS00760
      DO 30 J=2,IP                                                   BIS00770
      J1=J-1                                                         BIS00780
      X(J,1,3)=X(J1,1,3)+X(J,1,3)                                    BIS00790
      X(J,2,1)=X(J1,2,1)+X(J,2,1)                                    BIS00800
      X(J,1,4)=0.0                                                   BIS00810
      X(J,2,2)=X(J,1,3)                                              BIS00820
30     X(J,2,3)=X(J,1,3)                                             BIS00830
      W(1)=W(1)**2                                                   BIS00840
      W(2)=W(2)**2                                                   BIS00850
      DO 50 K=1,3                                                    BIS00860
      DO 50 L=1,3                                                    BIS00870
      S=0.0                                                          BIS00880
      DO 40 I=1,IP                                                   BIS00890
40     S=S+W(1)*X(I,1,K)*X(I,1,L)+W(2)*X(I,2,K)*X(I,2,L)             BIS00900
50     A(K,L)=S                                                      BIS00910
      DO 70 K=1,3                                                    BIS00920
      S=0.0                                                          BIS00930
      DO 60 I=1,IP                                                   BIS00940
60    S=S+W(1)*Y(I,1)*X(I,1,K)+W(2)*Y(I,2)*X(I,2,K)                  BIS00950
70    G(K,1)=S                                                       BIS00960
      N=3                                                            BIS00970
      IA=3                                                           BIS00980
      IDGT=3                                                         BIS00990
      CALL LINV2F(A,N,IA,AINV,IDGT,WKAREA,E5)                        BIS01000
      L=3                                                            BIS01010
      M=3                                                            BIS01020
      N=1                                                            BIS01030
      IB=3                                                           BIS01040
      IC=3                                                           BIS01050
      CALL VMULFF(AINV,G,L,M,N,IA,IB,B,IC,E6)                        BIS01060
      WRITE(6,*)E1,E2,E3,E4,E5,E6                                    BIS01070
      B(2,1)=-B(2,1)                                                 BIS01080
      B(3,1)=-B(3,1)                                                 BIS01090
      AK4=0.0                                                        BIS01100
```

FILE: BIS3 FORTRAN A CONVERSATIONAL MONITOR SYSTEM

```
      WRITE(6,110)B(1,1),B(2,1),B(3,1),AK4                                  BIS01110
      SK=B(1,1)+B(2,1)+B(3,1)                                               BIS01120
      AL2=SK**2-4.0*B(1,1)*B(3,1)                                           BIS01130
      AL2=SQRT(AL2)                                                         BIS01140
      AL1=(-SK+AL2)*0.5                                                     BIS01150
      AL2=(-SK-AL2)*0.5                                                     BIS01160
      WRITE(6,120)AL1,AL2                                                   BIS01170
      WRITE(6,155)C(1,1)                                                    BIS01180
      C1=1.0/AL1                                                            BIS01190
      C2=1.0/AL2                                                            BIS01200
      C3=C1-C2                                                              BIS01210
      C3=C(1,1)/C3                                                          BIS01220
      C1=C1*C3                                                              BIS01230
      C2=C2*C3                                                              BIS01240
      C3=-C3/B(3,1)                                                         BIS01250
      WRITE(6,130)                                                          BIS01260
      WRITE(6,135)                                                          BIS01270
      EM=0.0                                                                BIS01280
      EC=0.0                                                                BIS01290
      DO 15 I=2,ND                                                          BIS01300
      E1=EXP(T(I)*AL1)                                                      BIS01310
      E2=EXP(T(I)*AL2)                                                      BIS01320
      AM=C1*E1-C2*E2                                                        BIS01330
      AC=C3*(E1-E2)                                                         BIS01340
      EM=(C(I,1)-AM)**2+EM                                                  BIS01350
      EC=(C(I,2)-AC)**2+EC                                                  BIS01360
      T1=T(I)/WC                                                            BIS01370
      WRITE(6,140)T1,C(I,1),AM,C(I,2),AC                                    BIS01380
 15   CONTINUE                                                              BIS01390
      EM=EM/IP                                                              BIS01400
      EC=EC/IP                                                              BIS01410
      EM=SQRT(EM)                                                           BIS01420
      EC=SQRT(EC)                                                           BIS01430
      WRITE(6,145)EM,EC                                                     BIS01440
 120  FORMAT(1H ,'LAMDA1=',E15.6,5X,'LAMDA2=',E15.6)                        BIS01450
 130  FORMAT(1H ,18X,'TOTAL METAL',23X,'CHLORIN')                           BIS01460
 135  FORMAT(1H ,5X,'TIME',7X,'EXP',5X,'CAL.',22X,'EXP.',5X,'CAL.',//)      BIS01470
 140  FORMAT(1H ,4X,F6.4,6X,F4.1,5X,F4.1,20X,F4.2,5X,F4.2)                  BIS01480
 110  FORMAT(1H ,'K1=',E15.7,//,'K2=',E15.7,//,'K3=',E15.7,//,'K4=',E15.   BIS01490
     &7)                                                                    BIS01500
 145  FORMAT(1H ,//,'EM=',E15.6,5X,'EC=',E15.6)                             BIS01510
 155   FORMAT(1H ,//,'INITIAL CONC.=',F6.2)                                 BIS01520
1100  FORMAT(20A4)                                                          BIS01530
      STOP                                                                  BIS01540
      END                                                                   BIS01550
```

B. Program to evaluate exit solution concentration from the one inch reactor and also the metal deposition profiles in the catalyst at various bed positions.

FILE: BEDCONC1 FORTRAN A CONVERSATIONAL MONITOR SYSTEM

```
C THIS PROGRAM CALCULATES OUTPUT CONC FOR INTEGRAL REACTOR AND          BED00010
C  ALSO CALCULATES METAL DEPOSITION PROFILES IN THE CATALYST           BED00020
C                                                                      BED00030
C  RAKESH AGRAWAL   CHEM. ENGG.   M.I.T.                              BED00040
C                                                                      BED00050
C  MODEL USED IS THE NEW HYDRODEMETALLATION MODEL                      BED00060
C  CK1,CK2,CK3 ARE THE RATE CONSTANTS K1,K2,K3 RESPECTIVELY            BED00070
C  AM0=INLET TOTAL METAL CONC. , Q=FLOW RATE(ML/HR)                    BED00080
C  TIME=TIME ON STREAM IN HOURS, N=NO. OF POINTS IN BED FOR METAL      BED00090
C  DEPOSITION CALCULATIONS, W(J)=CUMMULATIVE WEIGHT TILL J LOCATION    BED00100
C  IN BED FROM ENTRANCE,  DA,DB =DIFFUSIVITY OF PARENT COMPOUND        BED00110
C  AND INTERMEDIATE RESPECTIVELY(CM**2/SEC.),RHOC=DENSITY OF CATALYST  BED00120
C , R=RADIUS OF CATALYST IN CMS. , RHOS=DENSITY OF SOLUTION(G/CM**3)   BED00130
C                                                                      BED00140
C*********                                                             BED00150
      DIMENSION TITLE(20),AM(20),B(20),W(20)                           BED00160
      READ(5,100)TITLE                                                 BED00170
      READ(5,*)CK1,CK2,CK3                                             BED00180
       READ(5,*)AM0,Q,TIME,N                                           BED00190
      DO 10 J=1,N                                                      BED00200
 10    READ(5,*)W(J)                                                   BED00210
      READ(5,*)DA,DB,RHOC,R,RHOS                                       BED00220
      WRITE(6,100)TITLE                                                BED00230
      WRITE(6,90)DA,DB                                                 BED00240
       DA=DA/RHOC                                                      BED00250
      DB=DB/RHOC                                                       BED00260
      DA=3600.0*DA                                                     BED00270
      DB=3600.0*DB                                                     BED00280
      AK1=CK1/DA                                                       BED00290
      AK2=CK2/DA                                                       BED00300
      AK3=CK1/DB                                                       BED00310
      AK4=(CK2+CK3)/DB                                                 BED00320
      AL2=AK1+AK4                                                      BED00330
      AL3=AL2**2-4.0*(AK1*AK4-AK2*AK3)                                 BED00340
      AL3=SQRT(AL3)                                                    BED00350
      AL1=(AL2+AL3)*0.5                                                BED00360
      AL2=(AL2-AL3)*0.5                                                BED00370
      PHI1=SQRT(AL1)                                                   BED00380
      PHI2=SQRT(AL2)                                                   BED00390
      PHI1R=PHI1*R                                                     BED00400
      PHI2R=PHI2*R                                                     BED00410
      WRITE(6,80)PHI1R,PHI2R                                           BED00420
      AI1=BES(PHI1R)                                                   BED00430
      AI2=BES(PHI2R)                                                   BED00440
      DAI1=DBES(PHI1R)                                                 BED00450
      DAI2=DBES(PHI2R)                                                 BED00460
      DI1=(PHI1/AI1)*DAI1                                              BED00470
      DI2=(PHI2/AI2)*DAI2                                              BED00480
      ALPH1=DI1                                                        BED00490
      BITA1=-((AK1-AL1)/AK3)*DI2                                       BED00500
      GAMA1=((AK1-AL1)/AK2)*DI1                                        BED00510
      DELT1=DI2                                                        BED00520
      AKL1=AK1-AL1                                                     BED00530
      ALPH2=AK3*(ALPH1*AK2-BITA1*AKL1)                                 BED00540
      BITA2=AK2*(BITA1*AK3+ALPH1*AKL1)                                 BED00550
```

FILE: BEDCONC1 FORTRAN A CONVERSATIONAL MONITOR SYSTEM

```
      GAMA2=AK3*(AK2*GAMA1-AKL1*DELT1)                                  BED00560
      DELT2=AK2*(AK3*DELT1+AKL1*GAMA1)                                  BED00570
      SHI=AK3*AK2+AKL1**2                                               BED00580
      SHA=(2.0*DA)/(R*SHI)                                              BED00590
      SHB=(2.0*DB)/(R*SHI)                                              BED00600
      ALPH3=SHA*ALPH2                                                   BED00610
      BITA3=SHA*BITA2                                                   BED00620
      GAMA3=SHB*GAMA2                                                   BED00630
      DELT3=SHB*DELT2                                                   BED00640
      WRITE(6,110)ALPH3,BITA3,GAMA3,DELT3                               BED00650
      ALPH4=-ALPH3/Q                                                    BED00660
      BITA4=-BITA3/Q                                                    BED00670
      GAMA4=-GAMA3/Q                                                    BED00680
      DELT4=-DELT3/Q                                                    BED00690
      BL2=ALPH4+DELT4                                                   BED00700
      BL3=BL2**2-4.0*(ALPH4*DELT4-GAMA4*BITA4)                          BED00710
      BL3=SQRT(BL3)                                                     BED00720
      BL1=(BL2+BL3)*0.5                                                 BED00730
      BL2=(BL2-BL3)*0.5                                                 BED00740
      RBL1=BL1*Q                                                        BED00750
       RBL2=BL2*Q                                                       BED00760
      WRITE(6,140)RBL1,RBL2                                             BED00770
      WRITE(6,120)BL1,BL2                                               BED00780
      BL1A=BL1-ALPH4                                                    BED00790
      BL2D=BL2-DELT4                                                    BED00800
      C1=(AM0*BITA4*GAMA4)/(BITA4*GAMA4-BL1A*BL2D)                      BED00810
      C3=BL1A/BITA4                                                     BED00820
      C2=C3*BL2D/GAMA4                                                  BED00830
      P1=AK2/(SHI*AI1)                                                  BED00840
      P2=AKL1/(SHI*AI2)                                                 BED00850
      P3=AKL1/(SHI*AI1)                                                 BED00860
      P4=AK3/(SHI*AI2)                                                  BED00870
      P5=CK3*TIME*1.0E-4*RHOS                                           BED00880
      DO 20 L=1,N                                                       BED00890
      E1=EXP(BL1*W(L))                                                  BED00900
      E2=EXP(BL2*W(L))                                                  BED00910
      AM(L)=C1*(E1-C2*E2)                                               BED00920
      B(L)=C1*C3*(E1-E2)                                                BED00930
      AM(L)=AM(L)+B(L)                                                  BED00940
      WRITE(6,130)W(L),AM(L),B(L)                                       BED00950
      DEPMS=0.0                                                         BED00960
      DEPM1=0.0                                                         BED00970
      DEPM2=0.0                                                         BED00980
      Z=1.0                                                             BED00990
      S1=AK3*(AM(L)-B(L))+AKL1*B(L)                                     BED01000
      S2=AK2*B(L)-AKL1*(AM(L)-B(L))                                     BED01010
      PS1=P1*S1                                                         BED01020
      PS2=P2*S2                                                         BED01030
      PS3=P3*S1                                                         BED01040
      PS4=P4*S2                                                         BED01050
      WRITE(6,60)                                                       BED01060
      Z1=P5*B(L)                                                        BED01070
      DEPM1=Z1                                                          BED01080
      Z3=AM(L)-B(L)                                                     BED01090
      WRITE(6,70)Z,AM(L),Z3,B(L),Z1                                     BED01100
```

FILE: BEDCONC1 FORTRAN A CONVERSATIONAL MONITOR SYSTEM

```
      DO 40 M1=1,12                                                    BED01110
      Z=Z-0.025                                                        BED01120
      Z1=Z*PHI1R                                                       BED01130
      Z2=Z*PHI2R                                                       BED01140
      Z1=BES(Z1)                                                       BED01150
      Z2=BES(Z2)                                                       BED01160
      Z3=PS1*Z1-PS2*Z2                                                 BED01170
      Z4=PS3*Z1+PS4*Z2                                                 BED01180
      Z2=Z3+Z4                                                         BED01190
      Z1=P5*Z4                                                         BED01200
      DEPM2=Z1*Z                                                       BED01210
      DEPMS=DEPMS+0.025*(DEPM1+DEPM2)                                  BED01220
      DEPM1=DEPM2                                                      BED01230
      WRITE(6,70)Z,Z2,Z3,Z4,Z1                                         BED01240
 40    CONTINUE                                                        BED01250
      DO 30 M=1,14                                                     BED01260
      Z=Z-0.05                                                         BED01270
       Z1=Z*PHI1R                                                      BED01280
      Z2=Z*PHI2R                                                       BED01290
      Z1=BES(Z1)                                                       BED01300
      Z2=BES(Z2)                                                       BED01310
      Z3=PS1*Z1-PS2*Z2                                                 BED01320
      Z4=PS3*Z1+PS4*Z2                                                 BED01330
      Z2=Z3+Z4                                                         BED01340
      Z1=P5*Z4                                                         BED01350
      DEPM2=Z1*Z                                                       BED01360
      DEPMS=DEPMS+0.05*(DEPM1+DEPM2)                                   BED01370
      DEPM1=DEPM2                                                      BED01380
      WRITE(6,70)Z,Z2,Z3,Z4,Z1                                         BED01390
 30    CONTINUE                                                        BED01400
      WRITE(6,160)DEPMS                                                BED01410
 20    CONTINUE                                                        BED01420
 60    FORMAT(1H ,/,3X,'Z',7X,'M',6X,'A',6X,'B',9X,'M DEP.')           BED01430
 70    FORMAT(1H ,F5.3,3X,F4.1,3X,F4.1,4X,F4.2,6X,F6.2)                BED01440
 80    FORMAT(1H ,//,'PHI1*R=',E15.7,4X,'PHI2*R=',E15.7)               BED01450
 90    FORMAT(1H ,//,'DA=',E14.7,4X,'DB=',E14.7)                       BED01460
 100    FORMAT(20A4)                                                   BED01470
 110    FORMAT(1H ,'ALPHA3=',E15.7,/,'BITA3=',E15.7,/,'GAMA3=',E15.7,/, BED01480
     &'DELTA3=',E15.7)                                                 BED01490
 120    FORMAT(1H ,//,'LAMDA1=',E15.7,4X,'LAMDA2=',E15.7)               BED01500
 130    FORMAT(1H ,//,'AMT.CAT=',F7.4,4X,'TOTAL METAL=',F4.1,4X,'CHLORIN BED01510
     &=',F6.2)                                                         BED01520
 140    FORMAT(1H ,//,'DIFF.LAMDA1=',E14.7,4X,'DIFF.LAMDA2=',E14.7)     BED01530
 150   FORMAT(1H ,//,'KIN.LAMDA1=',E14.7,'KIN.LAMDA2=',E14.7)           BED01540
 160    FORMAT(1H ,//,'NET WT. PERCENT METAL IN CAT.=',F6.2)            BED01550
      STOP                                                             BED01560
      END                                                              BED01570
C************************                                             BED01580
C************************                                             BED01590
C                                                                      BED01600
C                                                                      BED01610
      FUNCTION BES(X)                                                  BED01620
      T=(X/2.0)**2                                                     BED01630
      BES=1.0+T                                                        BED01640
      SUM=T                                                            BED01650
```

```
      DO 71 I=2,200                                                    BED01660
      SUM=SUM*T/I**2                                                   BED01670
      IF(SUM.LE.1.0E-5) GO TO 72                                       BED01680
      BES=BES+SUM                                                      BED01690
 71    CONTINUE                                                        BED01700
 72    CONTINUE                                                        BED01710
      RETURN                                                           BED01720
      END                                                              BED01730
C*********************************                                    BED01740
C*********************************                                    BED01750
C                                                                      BED01760
C                                                                      BED01770
      FUNCTION DBES(X)                                                 BED01780
      SUM=X/2.0                                                        BED01790
      T=SUM**2                                                         BED01800
      DBES=SUM                                                         BED01810
      DO 74 I=1,200                                                    BED01820
      SUM=(SUM*T)/(I*(I+1))                                            BED01830
      IF(SUM.LE.1.0E-5)GO TO 75                                        BED01840
      DBES=DBES+SUM                                                    BED01850
 74     CONTINUE                                                      BED01860
 75    CONTINUE                                                        BED01870
      RETURN                                                           BED01880
      END                                                              BED01890
```

C. Program for the poisoning studies of the bimodal catalyst.

```
FILE: BIMODAL  FORTRAN  A                    CONVERSATIONAL MONITOR SYSTEM

C THEORETICAL POISONING STUDIES OF THE BIMODAL CATALYST                    BIM00010
C THIS PROGRAM CALCULATES METAL DEPOSITION HISTORY IN BIMODAL CAT.         BIM00020
C                                                                          BIM00030
C     RAKESH AGRAWAL     CHEM. ENGG.          M.I.T.                       BIM00040
C                                                                          BIM00050
C********                                                                  BIM00060
C DOUBLE PRECISION HAS BEEN USED                                           BIM00070
      IMPLICIT REAL*8 (A-H,O-Z)                                            BIM00080
      DIMENSION D1(99),D2(99),D3(99),D4(99),G(99,30),NI(99),AEQ(200,200)BIM00090
     &,BEQ(200,1),WKAREA(40600),RLOC(99),CMETL(99),TITLE(20)               BIM00100
      COMMON U1(99,30),U2(99,30),SHI(30),ALPHI(30),H(99,30),AI1,AI2,DELIBIM00110
     &2,PH1DL,PH2DL,NND,NSTRT,NCONT,JM                                     BIM00120
C RI=MICRO SPHERE RADII,EI=MICROPOROSITY,RP=MICRO PORE RADII,RA=           BIM00130
C      PELLET RADII,RPA=MACROPORE RADII,RM=MOLECULAR RADII,RHOM=           BIM00140
C     METAL DEPOSITION DENSITY,D=BULK DIFFUSIVITY, AS, BS =BULK SOL.       BIM00150
C    &CONC.,NND+1=NO. OF NODAL PTS IN MICRO SPHERE,M+1=NO. OF NODAL        BIM00160
C    PTS IN MACROSPHERE,AL=MICROPORE LENGTH,CNP=NO. OF PORES IN            BIM00170
C     MICRO SPHERES,CNM=NO. OF MICROSPHERE/VOLUME OF PELLET,               BIM00180
C EA=MACROPOROSITY. AK1,AK2,AK3=RATE CONSTANTS PER UNIT                    BIM00190
C SURFACE AREA (METER**2),                                                 BIM00200
C TAU=TORTUOSITY-THIS PROGRAM ASSUMES THAT THE TOTUOSITY OF MICRPSPHERE    BIM00210
C AND MACROPORES IN MACROSPHERES ARE SAME.HOWEVER,ONLY WITH MINOR          BIM00220
C MODIFICATION FOR THE EXPRESSION OF DA ,THIS ASSUMPTION CAN BE            BIM00230
C RELAXED.                                                                 BIM00240
C DELT=TIME INCREAMENTS FOR METAL DEPOSITION CALCULATIONS,                 BIM00250
C CRTRIA=FRACTION OF THE INITIAL RATE FOR WHICH CATALYST IS TAKEN AS       BIM00260
C INACTIVE.                                                                BIM00270
C DELINC=IN EACH CYCLE OF CALCULATION,THE VALUE OF DELT IS INCREASED BY    BIM00280
C DELINC .THIS IS DONE TILL THE VALUE OF DELT BECOMES EQUAL TO MAXIMUM     BIM00290
C ALLOWED TIME STEP SIZE DTMAX.IT IS DONE TO GET SMALLER TIME STEP         BIM00300
C SIZES INITIALLY AND THEN LARGER TIME STEPS TO SAVE COMPUTATION TIME      BIM00310
C MPRINT=NO. OF NODAL POINTS IN MACROSPHERE LEFT BETWEEN THE TWO           BIM00320
C SUCCESSIVE PRINTOUTS OF THE METAL DEPOSITIONS IN THE MICROSPHERES OF     BIM00330
C THE MACROSPHERE                                                          BIM00340
C******************************************                                BIM00350
C PROGRAM USES LEQT2F MATRIX SOLVER. AN IMSL PROGRAM                       BIM00360
C******************************************                                BIM00370
      READ(5,114)TITLE                                                     BIM00380
      READ(5,*)RI,EI,RP,RA,EA                                              BIM00390
      READ(5,*)RM,RHOM                                                     BIM00400
      READ(5,*)AK1,AK2,AK3                                                 BIM00410
      READ(5,*)D,TAU                                                       BIM00420
      READ(5,*)AS,BS                                                       BIM00430
      READ(5,*)NND,M,DELT,CRTI  A,DELINC,MPRINT,DTMAX                      BIM00440
      WRITE(6,91)                                                          BIM00450
      WRITE(6,114)TITLE                                                    BIM00460
      WRITE(6,92)RI,EI,RP,RA                                               BIM00470
      WRITE(6,93)RM,RHOM                                                   BIM00480
      WRITE(6,94)AK1,AK2,AK3,D                                             BIM00490
      WRITE(6,95)AS,BS                                                     BIM00500
      WRITE(6,96)NND,M,DELT                                                BIM00510
      RI=1.0D-4*RI                                                         BIM00520
      RP=1.0D-8*RP                                                         BIM00530
      RM=1.0D-8*RM                                                         BIM00540
      AK1=1.0D-4*AK1                                                       BIM00550
```

FILE: BIMODAL FORTRAN A CONVERSATIONAL MONITOR SYSTEM

```
      AK2=1.0D-4*AK2                                                    BIM00560
      AK3=1.0D-4*AK3                                                    BIM00570
      D=3600.0*D                                                        BIM00580
      WRITE(6,97)                                                       BIM00590
      PI=3.14159                                                        BIM00600
       TAUSQ=DSQRT(TAU)                                                 BIM00610
      AL=(RI*TAUSQ)/3.0                                                 BIM00620
      CNP=(4.0*EI*RI**2)/(TAUSQ*RP**2)                                  BIM00630
      RPA=(2.0*EA*RI)/(3.0*(1.0-EA))                                    BIM00640
      CNM=3.0*(1.0-EA)/(4.0*PI*RI**3)                                   BIM00650
      SUMK=AK1+AK2+AK3                                                  BIM00660
      AL2=SUMK**2-4.0*AK1*AK3                                           BIM00670
      AL2=DSQRT(AL2)                                                    BIM00680
      AL1=(SUMK+AL2)*0.5                                                BIM00690
      AL2=(SUMK-AL2)*0.5                                                BIM00700
      ALMI=RM/RP                                                        BIM00710
      ALMA=RM/RPA                                                       BIM00720
      DI=D*((1.0-ALMI)**4)                                              BIM00730
      DA=(D*((1.0-ALMA)**4)*EA)/TAU                                     BIM00740
      PHI2=(2.0*AL**2)/(RP*DI)                                          BIM00750
      PHI1=PHI2*AL1                                                     BIM00760
      PHI2=PHI2*AL2                                                     BIM00770
      M1=M+1                                                            BIM00780
      N1=NND+1                                                          BIM00790
      DO 10 J=1,M1                                                      BIM00800
      NI(J)=NND                                                         BIM00810
      DO 10 K=1,N1                                                      BIM00820
      H(J,K)=1.0                                                        BIM00830
10     G(J,K)=1.0                                                       BIM00840
      DELI=1.0/NND                                                      BIM00850
      DELI2=0.5*DELI                                                    BIM00860
      DELA=RA/M                                                         BIM00870
      PH1DL0=DELI*DELI*PHI1                                             BIM00880
      PH2DL0=DELI*DELI*PHI2                                             BIM00890
      AKL1=AK1-AL1                                                      BIM00900
      ALPH=AK1*AK2+AKL1**2                                              BIM00910
      ALINV=1.0/ALPH                                                    BIM00920
      ALPH1=ALINV*AK1*AK2                                               BIM00930
      BITA2=ALPH1                                                       BIM00940
      ALPH2=ALINV*AK2*AKL1                                              BIM00950
      BITA1=-ALINV*AK1*AKL1                                             BIM00960
      SHI1P=2.0*PI*CNP*RP*AL                                            BIM00970
      SHI2=AL1-AK1-AK2                                                  BIM00980
      ALPH5=SHI1P*AL1*ALPH1                                             BIM00990
      ALPH6=SHI1P*AL1*ALPH2                                             BIM01000
      BITA5=SHI1P*SHI2*BITA1                                            BIM01010
      BITA6=SHI1P*SHI2*BITA2                                            BIM01020
      DUMY1=SHI1P*AK3                                                   BIM01030
      ALPH7=(DUMY1*AKL1*ALPH1)/AK2                                      BIM01040
      ALPH8=(DUMY1*AKL1*ALPH2)/AK2                                      BIM01050
      BITA7=DUMY1*BITA1                                                 BIM01060
      BITA8=DUMY1*BITA2                                                 BIM01070
      ALPH9=ALPH7-ALPH5                                                 BIM01080
      BITA9=BITA7-BITA5                                                 BIM01090
      ALPH10=ALPH8-ALPH6                                                BIM01100
```

FILE: BIMODAL FORTRAN A CONVERSATIONAL MONITOR SYSTEM

```
      BITA10=BITA8-BITA6                                              BIM01110
      DUMY2=CNM/DA                                                    BIM01120
      ALPH5=DUMY2*ALPH5                                               BIM01130
      BITA5=DUMY2*BITA5                                               BIM01140
      ALPH6=DUMY2*ALPH6                                               BIM01150
      BITA6=DUMY2*BITA6                                               BIM01160
      ALPH9=DUMY2*ALPH9                                               BIM01170
      BITA9=DUMY2*BITA9                                               BIM01180
      ALPH10=DUMY2*ALPH10                                             BIM01190
      BITA10=DUMY2*BITA10                                             BIM01200
C **** VARIABLES FOR EQN SOLVING:LEQT1F                               BIM01210
      IA=200                                                          BIM01220
      NEQ=2*M1                                                        BIM01230
      MEQ=1                                                           BIM01240
      IDGT=4                                                          BIM01250
      M2=M1+1                                                         BIM01260
      M3=M2+1                                                         BIM01270
      DELASQ=DELA*DELA                                                BIM01280
      AM01=(-1.0D-6*AK3)/(RHOM*RP)                                    BIM01290
      ALPH1P=(AM01*AKL1*ALPH1)/AK2                                    BIM01300
      ALPH2P=(AM01*AKL1*ALPH2)/AK2                                    BIM01310
      BITA1P=AM01*BITA1                                               BIM01320
      BITA2P=AM01*BITA2                                               BIM01330
      T=0.0                                                           BIM01340
      FABP=4.0*PI*DA*RA**2                                            BIM01350
      NEQ1N=NEQ-1                                                     BIM01360
      N2=N1+1                                                         BIM01370
      DO 80 IRLOC=1,M1                                                BIM01380
 80     RLOC(IRLOC)=(IRLOC-1.0)/M                                     BIM01390
      ALMID=1.0/((1.0-ALMI)**4)                                       BIM01400
      RPAAA=RPA*1.0D8                                                 BIM01410
      WRITE(6,98)EA,CNM,RPAAA                                         BIM01420
      WRITE(6,99)AL1,AL2                                              BIM01430
      CMETL1=AL*CNP*RHOM*PI*RP**2                                     BIM01440
      CMETL2=4.0*PI*CNM                                               BIM01450
      VOLMIC=(4.0*PI*RA**3)*(1.0-EA)/3.0                              BIM01460
      KTYPE=0                                                         BIM01470
C*** NOW CONC. PROFILE IN MICRO SPHERES ARE CALCULATED                BIM01480
 190    CONTINUE                                                       BIM01490
      DO 30 J=2,M                                                     BIM01500
      N=NI(J)                                                         BIM01510
      NSTRT=NND-N+1                                                   BIM01520
      IF(NSTRT.GE.NND) GO TO 40                                       BIM01530
      PRATIO=(1.0*N/NND)**2.0                                         BIM01540
      PH1DL=PH1DL0*PRATIO                                             BIM01550
      PH2DL=PH2DL0*PRATIO                                             BIM01560
      NCONT=NSTRT+1                                                   BIM01570
      DO 20 K=NCONT,NND                                               BIM01580
      HDEL=H(J,K+1)-H(J,K)                                            BIM01590
      GDEL=G(J,K+1)-G(J,K)                                            BIM01600
      SHI(K)=H(J,K)*G(J,K)                                            BIM01610
 20     ALPHI(K)=2.0*G(J,K)*HDEL+H(J,K)*GDEL+SHI(K)                   BIM01620
      JM=J                                                            BIM01630
      CALL TDM                                                        BIM01640
      D1(J)=ALPH5*AI1+BITA5*AI2                                       BIM01650
```

```
      D2(J)=ALPH6*AI1+BITA6*AI2                                          BIM01660
      D3(J)=ALPH9*AI1+BITA9*AI2                                          BIM01670
      D4(J)=ALPH10*AI1+BITA10*AI2                                        BIM01680
      GO TO 30                                                           BIM01690
 40    D1(J)=0.0                                                         BIM01700
      D2(J)=0.0                                                          BIM01710
      D3(J)=0.0                                                          BIM01720
      D4(J)=0.0                                                          BIM01730
 30    CONTINUE                                                          BIM01740
C*** NOW CONC. IN THE WHOLE PELLET IS SOLVED:                            BIM01750
      DO 60 K1=1,NEQ                                                     BIM01760
      BEQ(K1,1)=0.0                                                      BIM01770
      DO 50 K2=1,NEQ                                                     BIM01780
 50    AEQ(K1,K2)=0.0                                                    BIM01790
 60    CONTINUE                                                          BIM01800
      BEQ(M1,1)=AS                                                       BIM01810
      BEQ(NEQ,1)=BS                                                      BIM01820
      AEQ(1,1)=1.0                                                       BIM01830
      AEQ(1,2)=-1.0                                                      BIM01840
      AEQ(M1,M1)=1.0                                                     BIM01850
      AEQ(M2,M2)=1.0                                                     BIM01860
      AEQ(M2,M3)=-1.0                                                    BIM01870
      AEQ(NEQ,NEQ)=1.0                                                   BIM01880
      DO 70 I=2,M                                                        BIM01890
      I1=I+1                                                             BIM01900
      I1N=I-1                                                            BIM01910
      IM1=I+M1                                                           BIM01920
      IM=I+M                                                             BIM01930
      IM2=IM1+1                                                          BIM01940
      AEQ(I,I1N)=1.0                                                     BIM01950
      AEQ(IM1,IM)=1.0                                                    BIM01960
      DUMY3=1.0+(2.0/(I-1))                                              BIM01970
      AEQ(I,I1)=DUMY3                                                    BIM01980
      AEQ(IM1,IM2)=DUMY3                                                 BIM01990
      AEQ(I,I)=-1.0-DUMY3-DELASQ*D1(I)                                   BIM02000
      AEQ(IM1,IM1)=-1.0-DUMY3-DELASQ*D4(I)                               BIM02010
      AEQ(I,IM1)=-DELASQ*D2(I)                                           BIM02020
 70    AEQ(IM1,I)=-DELASQ*D3(I)                                          BIM02030
      CALL LEQT2F(AEQ,MEQ,NEQ,IA,BEQ,IDGT,WKAREA,IER)                    BIM02040
      WRITE(6,*)IER                                                      BIM02050
      FA=((AS-BEQ(M,1))/DELA)*FABP                                       BIM02060
      FB=(FABP*(BS-BEQ(NEQ1N,1)))/DELA                                   BIM02070
      FNET=FA+FB                                                         BIM02080
      IF(T.EQ.0.0)F0=FNET                                                BIM02090
      FACTON=FNET/F0                                                     BIM02100
      WRITE(6,101)T,FA,FB,FNET,FACTON                                    BIM02110
      WRITE(6,102)                                                       BIM02120
      N4A=M/MPRINT                                                       BIM02130
      KDUMY=M1+MPRINT                                                    BIM02140
      DO 90 K3=1,N4A                                                     BIM02150
      KDUMY=KDUMY-MPRINT                                                 BIM02160
      K3M=KDUMY+M1                                                       BIM02170
 90    WRITE(6,103)RLOC(KDUMY),BEQ(KDUMY,1),BEQ(K3M,1)                   BIM02180
      WRITE(6,103)RLOC(1),BEQ(1,1),BEQ(M2,1)                             BIM02190
      IF(FACTON.LE.CRTRIA) GO TO 200                                     BIM02200
```

```
FILE: BIMODAL  FORTRAN  A                    CONVERSATIONAL MONITOR SYSTEM

C*** NOW TIME DIMENSION OF THE PROBLEM IS INTRODUCED                    BIM02210
      DO 100 K4=1,M1                                                    BIM02220
      K4M3=K4+M1                                                        BIM02230
      NPLUG=N2                                                          BIM02240
      IF(H(K4,N1).LE.ALMI) GO TO 100                                    BIM02250
      DO 110 K5=1,N1                                                    BIM02260
      NPLUG=NPLUG-1                                                     BIM02270
      H(K4,NPLUG)=DELT*((ALPH1P*BEQ(K4,1)+ALPH2P*BEQ(K4M3,1))*U1(K4,NPLUBIM02280
     &G)+(BITA1P*BEQ(K4,1)+BITA2P*BEQ(K4M3,1))*U2(K4,NPLUG))+H(K4,NPLUG)BIM02290
      G(K4,NPLUG)=ALMID*((1.0-ALMI/H(K4,NPLUG))**4)                     BIM02300
      IF(H(K4,NPLUG).LE.ALMI)GO TO 100                                  BIM02310
  110  CONTINUE                                                         BIM02320
  100   NI(K4)=N1-NPLUG                                                 BIM02330
      T=T+DELT                                                          BIM02340
      IF(DELT.GE.DTMAX)GO TO 401                                        BIM02350
      DELT=DELT+DELINC                                                  BIM02360
  401   CONTINUE                                                        BIM02370
      KTYPE=KTYPE+1                                                     BIM02380
      IF(KTYPE.EQ.4)GO TO 201                                           BIM02390
      GO TO 190                                                         BIM02400
  200  WRITE(6,104)                                                     BIM02410
  201   CONTINUE                                                        BIM02420
      WRITE(6,105)ALMI                                                  BIM02430
      WRITE(6,106)                                                      BIM02440
      N4A=M/MPRINT                                                      BIM02450
      MDUMY=M1+MPRINT                                                   BIM02460
      DO 120 K5=1,N4A                                                   BIM02470
      MDUMY=MDUMY-MPRINT                                                BIM02480
  120  WRITE(6,107)(H(MDUMY,K6),K6=1,N1)                                BIM02490
      MDUMY=M1+1                                                        BIM02500
      DO 130 K7=1,M1                                                    BIM02510
      MDUMY=MDUMY-1                                                     BIM02520
      HDUMY1=H(MDUMY,1)**2                                              BIM02530
      H2INTG=0.0                                                        BIM02540
      DO 140 K8=2,N1                                                    BIM02550
      HDUMY2=H(MDUMY,K8)**2                                             BIM02560
      H2INTG=H2INTG+DELI2*(HDUMY1+HDUMY2)                               BIM02570
  140  HDUMY1=HDUMY2                                                    BIM02580
  130  CMETL(MDUMY)=CMETL1-CMETL1*H2INTG                                BIM02590
      WRITE(6,108)                                                      BIM02600
      TOTLM=0.0                                                         BIM02610
      DELA2=DELA*0.5                                                    BIM02620
      MDUMY=M1                                                          BIM02630
      PROFM=CNM*CMETL(M1)                                               BIM02640
      WRITE(6,109)RLOC(M1),CMETL(M1),PROFM                              BIM02650
      TOTLM1=CMETL(M1)*RA**2                                            BIM02660
      DO 150 K9=1,M                                                     BIM02670
      MDUMY=MDUMY-1                                                     BIM02680
      RASQ=(RA-K9*DELA)**2                                              BIM02690
      TOTLM2=CMETL(MDUMY)*RASQ                                          BIM02700
      TOTLM=TOTLM+DELA2*(TOTLM1+TOTLM2)                                 BIM02710
      TOTLM1=TOTLM2                                                     BIM02720
      PROFM=CNM*CMETL(MDUMY)                                            BIM02730
      WRITE(6,109)RLOC(MDUMY),CMETL(MDUMY),PROFM                        BIM02740
  150  CONTINUE                                                         BIM02750
```

```
FILE: BIMODAL  FORTRAN  A                    CONVERSATIONAL MONITOR SYSTEM

      TOTLM=TOTLM*CMETL2                                                BIM02760
      WRITE(6,111)TOTLM                                                 BIM02770
      TOTLM=TOTLM/VOLMIC                                                BIM02780
      WRITE(6,112)TOTLM                                                 BIM02790
      IF(FACTON.LE.CRTRIA)GO TO 202                                     BIM02800
      KTYPE=0                                                           BIM02810
      GO TO 190                                                         BIM02820
  202  CONTINUE                                                         BIM02830
   91   FORMAT(1H ,' B I M O D A L  P O R E  P L U G G I N G  C A L C U LBIM02840
     & A T I O N S',///)                                                BIM02850
   92   FORMAT(1H ,'MICRO SPHERE RADII=',F6.1,'MICRON',3X,'MICRO POROSITYBIM02860
     &=',F5.3,3X,'MICRO PORE RADII=',F6.1,'A',//,2X,'PELLET RADII=',F7.5BIM02870
     &,'CM',3X,'MACRO PORE RADII=',F10.2,'A')                           BIM02880
   93   FORMAT(1H ,'MOLECULAR RADII=',F7.2,'A',3X,'DENSITY OF METAL DEPOSBIM02890
     &IT=',F6.3,'GMS/CM**3')                                            BIM02900
   94   FORMAT(1H ,'K1=',E14.7,2X,'K2=',E14.7,2X,'K3=',E14.7,2X,'RATE/METBIM02910
     &ER**3',//,'DIFFUSIVITY=',E14.7,'CM**2/SEC')                       BIM02920
   95   FORMAT(///,'BULK POR. CONC.=',F7.3,'BULK CHLO. CONC.=',F7.3,'PPM'BIM02930
     &),                                                                BIM02940
   96   FORMAT(1H ,'NO.OF DIV IN MICROSPHERE=',I3,'NO. OF DIV IN PELLET='BIM02950
     &,I3,//,'TIME STEPS=',F6.2,'HRS')                                  BIM02960
   97   FORMAT(///,'  C A L C U L A T I O N  B E G I N S',//)           BIM02970
   98   FORMAT(1H ,'MACRO POROSITY=',F6.4,2X,'NO. OF MICROSPHERES/CM**3='BIM02980
     &,E14.7,2X,'MACROPORE RADII=',E14.7,'A')                           BIM02990
   99   FORMAT(1H ,'FIRST EIG. VAL.=',E14.7,2X,'SECOND EIG VAL=',E14.7)  BIM03000
  101   FORMAT(1H ,//,'TIME=',F9.2,'HRS',//,'FLUX A=',E14.7,'FLUX B=',E14 BIM03010
     &.7,'NET FLUX=',E14.7,'FRACTIONAL RATE=',F8.6)                     BIM03020
  102    FORMAT(1H ,2X,'RA',9X,'PORPHYRIN',5X,'CHLORIN')                 BIM03030
  103   FORMAT(1H ,3X,F6.4,5X,F6.3,7X,F6.3)                              BIM03040
  104   FORMAT(1H1,//,3X,'P E L L E T  I S  P R A C T I C A L L Y  P L U BIM03050
     &G G E D',///)                                                     BIM03060
  105   FORMAT(1H ,3X,'MOLECULAR RADII/MICROPORE RADII=',F8.6,//)        BIM03070
  106   FORMAT(1H ,3X,' T H E  H  M A T R I X')                          BIM03080
  107   FORMAT(1H ,30F4.2)                                               BIM03090
  108   FORMAT(1H1,//,4X,'RA',8X,'M IN MICROSPHERE',4X,'DEPOSIT M PROFILEBIM03100
     &')                                                                BIM03110
  109   FORMAT(1H ,3X,F6.4,5X,E14.7,5X,E14.7)                            BIM03120
  111   FORMAT(1H ,//,'TOTAL DEPOSITED METAL IN PELLET=',E14.7,'GMS')    BIM03130
  112   FORMAT(1H ,//,'TOTAL METAL DEPOSITED/VOLUME OF CAT MATERIAL=',E14BIM03140
     &.7)                                                               BIM03150
  114   FORMAT(20A4)                                                     BIM03160
      STOP                                                             BIM03170
      END                                                              BIM03180
C*********************************************************           BIM03190
C*********************************************************           BIM03200
            SUBROUTINE TDM                                             BIM03210
C*********************************************************           BIM03220
      IMPLICIT REAL*8 (A-H,O-Z)                                        BIM03230
      COMMON U1(99,30),U2(99,30),SHI(30),ALPHI(30),H(99,30),AI1,AI2,DELIBIM03240
     &2,PH1DL,PH2DL,NND,NSTRT,NCONT,JM                                 BIM03250
      DIMENSION Q1(30),Q2(30)                                          BIM03260
      Q1(NSTRT)=-1.0                                                   BIM03270
      Q2(NSTRT)=-1.0                                                   BIM03280
      NID1=NND+1                                                       BIM03290
      U1(JM,NID1)=1.0                                                  BIM03300
```

FILE: BIMODAL FORTRAN A CONVERSATIONAL MONITOR SYSTEM

```
      U2(JM,NID1)=1.0                                                          BIM03310
      DO 500 I=NCONT,NND                                                       BIM03320
      DUMY=ALPHI(I)+SHI(I)                                                     BIM03330
      Q1(I)=-ALPHI(I)/(DUMY+SHI(I)*Q1(I-1)+PH1DL)                              BIM03340
500    Q2(I)=-ALPHI(I)/(DUMY+SHI(I)*Q2(I-1)+PH2DL)                             BIM03350
      AI1=0.0                                                                  BIM03360
      AI2=0.0                                                                  BIM03370
      NRUN=NID1                                                                BIM03380
      DO 550 I=NSTRT,NND                                                       BIM03390
      NRUN1=NRUN                                                               BIM03400
      NRUN=NRUN-1                                                              BIM03410
      U1(JM,NRUN)=-Q1(NRUN)*U1(JM,NRUN1)                                       BIM03420
      U2(JM,NRUN)=-Q2(NRUN)*U2(JM,NRUN1)                                       BIM03430
      AI1=AI1+DELI2*U1(JM,NRUN1)*(H(JM,NRUN1)-Q1(NRUN)*H(JM,NRUN))             BIM03440
550    AI2=AI2+DELI2*U2(JM,NRUN1)*(H(JM,NRUN1)-Q2(NRUN)*H(JM,NRUN))            BIM03450
      RETURN                                                                   BIM03460
      END                                                                      BIM03470
```

D. Program for the poisoning studies of the unimodal catalyst.

```
FILE: UNIMODAL FORTRAN  A                    CONVERSATIONAL MONITOR SYSTEM

C THEORETICAL POISONING STUDIES OF THE UNIMODAL CATALYST                    UNI00010
C THIS PROGRAM CALCULATES METAL DEPOSITION HISTORY IN UNIMODAL CAT.         UNI00020
C                                                                           UNI00030
C     RAKESH AGRAWAL        CHEM. ENGG.        M.I.T.                       UNI00040
C                                                                           UNI00050
C********                                                                   UNI00060
C  DOUBLE PRECISION HAS BEEN USED                                           UNI00070
      IMPLICIT REAL*8 (A-H,O-Z)                                             UNI00080
      DIMENSION G(200),RLOC(200),B(200),TITLE(20)                           UNI00090
      COMMON U1(200),U2(200),SHI(200),ALPHI(200),H(200),AI1,AI2,DELI2,PHUNI00100
     &1DL,PH2DL,NND,NSTRT,NCONT                                             UNI00110
C RI= SPHERE RADII,EI=POROSITY,RP= PORE RADII,                              UNI00120
C     RM=MOLECULAR RADII,       RHOM=                                       UNI00130
C     METAL DEPOSITION DENSITY,D=BULK DIFFUSIVITY, AS, BS =BULK SOL.        UNI00140
C    CONC.,NND+1=NO. OF NODAL PTS IN  SPHERE,                               UNI00150
C    AL=PORE LENGTH,CNP=NO. OF PORES IN CATALYST SPHERE                     UNI00160
C   AK1,AK2,AK3=RATE CONSTANTS PER UNIT SURFACE AREA(METER**2)              UNI00170
C  DELT=TIME INCREAMENTS FOR METAL DEPOSITION CALCULATIONS                  UNI00180
C  CRTRIA=FRACTION OF INITIAL RATE FOR WHICH CATALYST IS TAKEN AS           UNI00190
C  INACTIVE.                                                                UNI00200
C  DELINC=IN EACH CYCLE OF CALCULATION,THE VALUE OF DELT IS INCREASED       UNI00210
C  BY DELINC. NORMALLY ITS VALUE IS ZERO.                                   UNI00220
C  NPRINT=NO. OF NODAL POINTS IN CATALYST SPHERE LEFT BETWEEN TWO           UNI00230
C  SUCCESSIVE PRINTOUTS OF THE METAL DEPOSITIONS IN THE SPHERE.             UNI00240
C*****************************************                                  UNI00250
      READ(5,98)TITLE                                                       UNI00260
      READ(5,*)RI,EI,RP                                                     UNI00270
      READ(5,*)RM,RHOM                                                      UNI00280
      READ(5,*)AK1,AK2,AK3                                                  UNI00290
      READ(5,*)D                                                            UNI00300
      READ(5,*)AS,BS                                                        UNI00310
      READ(5,*)NND,DELT,CRTRIA,DELINC,NPRINT                                UNI00320
      WRITE(6,91)                                                           UNI00330
      WRITE(6,98)TITLE                                                      UNI00340
      WRITE(6,92)RI,EI,RP                                                   UNI00350
      WRITE(6,93)RM,RHOM                                                    UNI00360
      WRITE(6,94)AK1,AK2,AK3,D                                              UNI00370
      WRITE(6,95)AS,BS                                                      UNI00380
      WRITE(6,96)NND,DELT                                                   UNI00390
      RP=1.0D-8*RP                                                          UNI00400
      RM=1.0D-8*RM                                                          UNI00410
      AK1=1.0D-4*AK1                                                        UNI00420
      AK2=1.0D-4*AK2                                                        UNI00430
      AK3=1.0D-4*AK3                                                        UNI00440
      D=3600.0*D                                                            UNI00450
      WRITE(6,97)                                                           UNI00460
      PI=3.14159                                                            UNI00470
      AL=(RI*(2.0**0.5))/3.0                                                UNI00480
      CNP=(4.0*EI*RI**2)/((2.0**0.5)*RP**2)                                 UNI00490
      SUMK=AK1+AK2+AK3                                                      UNI00500
      AL2=SUMK**2-4.0*AK1*AK3                                               UNI00510
      AL2=DSQRT(AL2)                                                        UNI00520
      AL1=(SUMK+AL2)*0.5                                                    UNI00530
      AL2=(SUMK-AL2)*0.5                                                    UNI00540
      ALMI=RM/RP                                                            UNI00550
```

```
      DI=D*((1.0-ALMI)**4)                                              UNI00560
      PHI2=(2.0*AL**2)/(RP*DI)                                          UNI00570
      PHI1=PHI2*AL1                                                     UNI00580
      PHI2=PHI2*AL2                                                     UNI00590
      N1=NND+1                                                          UNI00600
      NI=NND                                                            UNI00610
      DO 10 K=1,N1                                                      UNI00620
      H(K)=1.0                                                          UNI00630
 10    G(K)=1.0                                                         UNI00640
      DELI=1.0/NND                                                      UNI00650
      DELI2=0.5*DELI                                                    UNI00660
      PH1DL0=DELI*DELI*PHI1                                             UNI00670
      PH2DL0=DELI*DELI*PHI2                                             UNI00680
      AKL1=AK1-AL1                                                      UNI00690
      ALPH=AK1*AK2+AKL1**2                                              UNI00700
      ALINV=1.0/ALPH                                                    UNI00710
      ALPH1=ALINV*AK1*AK2                                               UNI00720
      BITA2=ALPH1                                                       UNI00730
      ALPH2=ALINV*AK2*AKL1                                              UNI00740
      BITA1=-ALINV*AK1*AKL1                                             UNI00750
      SHI1P=2.0*PI*CNP*RP*AL                                            UNI00760
      SHI2=AL1-AK1-AK2                                                  UNI00770
      ALPH5=SHI1P*AL1*ALPH1                                             UNI00780
      ALPH6=SHI1P*AL1*ALPH2                                             UNI00790
      BITA5=SHI1P*SHI2*BITA1                                            UNI00800
      BITA6=SHI1P*SHI2*BITA2                                            UNI00810
      DUMY1=SHI1P*AK3                                                   UNI00820
      ALPH7=(DUMY1*AKL1*ALPH1)/AK2                                      UNI00830
      ALPH8=(DUMY1*AKL1*ALPH2)/AK2                                      UNI00840
      BITA7=DUMY1*BITA1                                                 UNI00850
      BITA8=DUMY1*BITA2                                                 UNI00860
      ALPH9=ALPH7-ALPH5                                                 UNI00870
      BITA9=BITA7-BITA5                                                 UNI00880
      ALPH10=ALPH8-ALPH6                                                UNI00890
      BITA10=BITA8-BITA6                                                UNI00900
      B10=ALPH1*AS+ALPH2*BS                                             UNI00910
      B20=BITA1*AS+BITA2*BS                                             UNI00920
      B10KL=(B10*AKL1)/AK2                                              UNI00930
      B20KL=(B20*AKL1)/AK1                                              UNI00940
      AM01=(-1.0D-6*AK3)/(RHOM*RP)                                      UNI00950
      T=0.0                                                             UNI00960
      N2=N1+1                                                           UNI00970
      DO 80 IRLOC=1,N1                                                  UNI00980
 80    RLOC(IRLOC)=(IRLOC-1.0)/NND                                      UNI00990
      ALMID=1.0/((1.0-ALMI)**4)                                         UNI01000
      WRITE(6,99)AL1,AL2                                                UNI01010
      WRITE(6,113)PHI1,PHI2                                             UNI01020
      CMETL1=AL*CNP*RHOM*PI*RP**2                                       UNI01030
      RUMETL=CMETL1/AL                                                  UNI01040
      KTYPE=0                                                           UNI01050
      VOLMIC=(4.0*PI*RI**3)/3.0                                         UNI01060
      AI1=0.0                                                           UNI01070
      AI2=0.0                                                           UNI01080
C*** NOW CONC. PROFILE IN  SPHERE IS CALCULATED                         UNI01090
 190   CONTINUE                                                         UNI01100
```

FILE: UNIMODAL FORTRAN A CONVERSATIONAL MONITOR SYSTEM

```
      N=NI                                                              UNI01110
      NSTRT=NND-N+1                                                     UNI01120
      IF(NSTRT.GE.NND) GO TO 40                                         UNI01130
      PRATIO=(1.0*N/NND)**2.0                                           UNI01140
      PH1DL=PH1DL0*PRATIO                                               UNI01150
      PH2DL=PH2DL0*PRATIO                                               UNI01160
      NCONT=NSTRT+1                                                     UNI01170
      DO 20 K=NCONT,NND                                                 UNI01180
      HDEL=H(K+1)-H(K)                                                  UNI01190
      GDEL=G(K+1)-G(K)                                                  UNI01200
      SHI(K)=H(K)*G(K)                                                  UNI01210
 20    ALPHI(K)=2.0*G(K)*HDEL+H(K)*GDEL+SHI(K)                          UNI01220
      CALL TDM                                                          UNI01230
      E1=ALPH5*AI1+BITA5*AI2                                            UNI01240
      E2=ALPH6*AI1+BITA6*AI2                                            UNI01250
      E3=ALPH9*AI1+BITA9*AI2                                            UNI01260
      E4=ALPH10*AI1+BITA10*AI2                                          UNI01270
      GO TO 60                                                          UNI01280
 40    E1=0.0                                                           UNI01290
      E2=0.0                                                            UNI01300
      E3=0.0                                                            UNI01310
      E4=0.0                                                            UNI01320
 60    CONTINUE                                                         UNI01330
      FA=E1*AS+E2*BS                                                    UNI01340
      FB=E3*AS+E4*BS                                                    UNI01350
      FNET=FA+FB                                                        UNI01360
      IF(T.EQ.0.0)F0=FNET                                               UNI01370
      FACTON=FNET/F0                                                    UNI01380
      WRITE(6,101)T,FA,FB,FNET,FACTON                                   UNI01390
      WRITE(6,102)                                                      UNI01400
      KDUMY=N2                                                          UNI01410
      DO 90 K3=1,N1                                                     UNI01420
      KDUMY=KDUMY-1                                                     UNI01430
 90    B(KDUMY)=B10KL*U1(KDUMY)+B20*U2(KDUMY)                           UNI01440
      N4A=NND/NPRINT                                                    UNI01450
      KDUMY=N1+NPRINT                                                   UNI01460
      DO 710 K4A=1,N4A                                                  UNI01470
      KDUMY=KDUMY-NPRINT                                                UNI01480
      A=B10*U1(KDUMY)-B20KL*U2(KDUMY)                                   UNI01490
 710    WRITE(6,103)RLOC(KDUMY),A,B(KDUMY)                             UNI01500
      A=B10*U1(1)-B20KL*U2(1)                                           UNI01510
      WRITE(6,103)RLOC(1),A,B(1)                                        UNI01520
      IF(FACTON.LE.CRTRIA) GO TO 200                                    UNI01530
C*** NOW TIME DIMENSION OF THE PROBLEM IS INTRODUCED                    UNI01540
      NPLUG=N2                                                          UNI01550
      IF(H(N1).LE.ALMI) GO TO 200                                       UNI01560
      DO 110 K5=1,N1                                                    UNI01570
      NPLUG=NPLUG-1                                                     UNI01580
      H(NPLUG)=AM01*DELT*B(NPLUG)+H(NPLUG)                              UNI01590
      G(NPLUG)=ALMID*((1.0-ALMI/H(NPLUG))**4)                           UNI01600
      IF(H(NPLUG).LE.ALMI)GO TO 100                                     UNI01610
 110   CONTINUE                                                         UNI01620
 100    NI=N1-NPLUG                                                     UNI01630
      T=T+DELT                                                          UNI01640
      DELT=DELT+DELINC                                                  UNI01650
```

FILE: UNIMODAL FORTRAN A CONVERSATIONAL MONITOR SYSTEM

```
      KTYPE=KTYPE+1                                                     UNI01660
      IF(KTYPE.EQ.4)GO TO 201                                           UNI01670
      GO TO 190                                                         UNI01680
200    WRITE(6,104)                                                     UNI01690
201    CONTINUE                                                         UNI01700
      WRITE(6,105)ALMI                                                  UNI01710
      WRITE(6,106)                                                      UNI01720
      N4A=NND/NPRINT                                                    UNI01730
      IRUSH=N1+NPRINT                                                   UNI01740
      DO 700 K5A=1,N4A                                                  UNI01750
      IRUSH=IRUSH-NPRINT                                                UNI01760
      POINTM=RUMETL*(1.0-H(IRUSH)**2)                                   UNI01770
700    WRITE(6,107)RLOC(IRUSH),H(IRUSH),POINTM                          UNI01780
      HDUMY1=H(1)**2                                                    UNI01790
      H2INTG=0.0                                                        UNI01800
      DO 140 K8=2,N1                                                    UNI01810
      HDUMY2=H(K8)**2                                                   UNI01820
      H2INTG=H2INTG+DELI2*(HDUMY1+HDUMY2)                               UNI01830
140    HDUMY1=HDUMY2                                                    UNI01840
      TOTLM=CMETL1-CMETL1*H2INTG                                        UNI01850
      WRITE(6,111)TOTLM                                                 UNI01860
      TOTLM=TOTLM/VOLMIC                                                UNI01870
      WRITE(6,112)TOTLM                                                 UNI01880
      IF(FACTON.LE.CRTRIA)GO TO 202                                     UNI01890
      KTYPE=0                                                           UNI01900
      GO TO 190                                                         UNI01910
202    CONTINUE                                                         UNI01920
91     FORMAT(1H ,' U N I M O D A L  P O R E  P L U G G I N G  C A L C UUNI01930
     & L A T I O N S',///)                                              UNI01940
92     FORMAT(1H ,' SPHERE RADII=',F7.5,'CM',3X,' POROSITY',            UNI01950
     &'=',F5.3,3X,' PORE RADII=',F6.1,'A')                              UNI01960
93     FORMAT(1H ,'MOLECULAR RADII=',F7.2,'A',3X,'DENSITY OF METAL DEPOSUNI01970
     &IT=',F6.3,'GMS/CM**3')                                            UNI01980
94     FORMAT(1H ,'K1=',E14.7,2X,'K2=',E14.7,2X,'K3=',E14.7,2X,'RATE/METUNI01990
     &ER**3',//,'DIFFUSIVITY=',E14.7,'CM**2/SEC')                       UNI02000
95     FORMAT(///,'BULK POR. CONC.=',F7.3,'BULK CHLO. CONC.=',F7.3,'PPM'UNI02010
     &)                                                                 UNI02020
96     FORMAT(1H ,'NO.OF DIV IN SPHERE=',I3,                            UNI02030
     &//,'TIME STEPS=',F6.2,'HRS')                                      UNI02040
97     FORMAT(///,'  C A L C U L A T I O N  B E G I N S',//)            UNI02050
98     FORMAT(20A4)                                                     UNI02060
99     FORMAT(1H ,'FIRST EIG. VAL.=',E14.7,2X,'SECOND EIG VAL=',E14.7)  UNI02070
101   FORMAT(1H ,//,'TIME=',F9.2,'HRS',//,'FLUX A=',E14.7,'FLUX B=',E14 UNI02080
     &.7,'NET FLUX=',E14.7,'FRACTIONAL RATE=',F8.6)                     UNI02090
102     FORMAT(1H ,2X,'RA',9X,'PORPHYRIN',5X,'CHLORIN')                 UNI02100
103    FORMAT(1H ,3X,F6.4,5X,F6.3,7X,F6.3)                              UNI02110
104    FORMAT(1H1,//,3X,'P E L L E T  I S  P R A C T I C A L L Y  P L U UNI02120
     &G G E D',///)                                                     UNI02130
105    FORMAT(1H ,3X,'MOLECULAR RADII/PORE RADII=',F8.6,//)             UNI02140
106    FORMAT(1H ,3X,' T H E  H  M A T R I X')                          UNI02150
107    FORMAT(1H ,3X,F6.4,5X,F4.2,5X,E14.7)                             UNI02160
111    FORMAT(1H ,//,'TOTAL DEPOSITED METAL IN PELLET=',E14.7,'GMS')    UNI02170
112    FORMAT(1H ,//,'TOTAL METAL DEPOSITED/VOLUME OF CAT MATERIAL=',E14UNI02180
     &.7)                                                               UNI02190
113    FORMAT(1H ,'PHI1SQ=',E14.7,3X,'PHI2SQ=',E14.7)                   UNI02200
```

FILE: UNIMODAL FORTRAN A CONVERSATIONAL MONITOR SYSTEM

```
      STOP                                                                  UNI02210
      END                                                                   UNI02220
C*****************************************************                    UNI02230
C*****************************************************                    UNI02240
            SUBROUTINE TDM                                                  UNI02250
C*****************************************************                    UNI02260
      IMPLICIT REAL*8 (A-H,O-Z)                                             UNI02270
      COMMON U1(200),U2(200),SHI(200),ALPHI(200),H(200),AI1,AI2,DELI2,PHUNI02280
     &1DL,PH2DL,NND,NSTRT,NCONT                                             UNI02290
      DIMENSION Q1(200),Q2(200)                                             UNI02300
      Q1(NSTRT)=-1.0                                                        UNI02310
      Q2(NSTRT)=-1.0                                                        UNI02320
      NID1=NND+1                                                            UNI02330
      U1(NID1)=1.0                                                          UNI02340
      U2(NID1)=1.0                                                          UNI02350
      DO 500 I=NCONT,NND                                                    UNI02360
      DUMY=ALPHI(I)+SHI(I)                                                  UNI02370
      Q1(I)=-ALPHI(I)/(DUMY+SHI(I)*Q1(I-1)+PH1DL)                           UNI02380
500    Q2(I)=-ALPHI(I)/(DUMY+SHI(I)*Q2(I-1)+PH2DL)                          UNI02390
      AI1=0.0                                                               UNI02400
      AI2=0.0                                                               UNI02410
      NRUN=NID1                                                             UNI02420
      DO 550 I=NSTRT,NND                                                    UNI02430
      NRUN1=NRUN                                                            UNI02440
      NRUN=NRUN-1                                                           UNI02450
      U1(NRUN)=-Q1(NRUN)*U1(NRUN1)                                          UNI02460
      U2(NRUN)=-Q2(NRUN)*U2(NRUN1)                                          UNI02470
      AI1=AI1+DELI2*U1(NRUN1)*(H(NRUN1)-Q1(NRUN)*H(NRUN))                   UNI02480
550    AI2=AI2+DELI2*U2(NRUN1)*(H(NRUN1)-Q2(NRUN)*H(NRUN))                  UNI02490
      RETURN                                                                UNI02500
      END                                                                   UNI02510
```